



Sustrato morfológico y molecular de las alteraciones auditivas implicadas en la susceptibilidad a crisis audiogénas del modelo GASH/Sal

Tesis doctoral de

David Sánchez Benito

Directores

M^a Dolores E. López García

Ricardo Gómez-Nieto

Laboratorio de Trastornos Audiomotores

Instituto de Neurociencias de Castilla y León (INCyL)

Universidad de Salamanca

Salamanca, 2020

FINANCIACIÓN

Este trabajo ha sido realizado gracias a los proyectos cofinanciados con fondos FEDER de la Unión Europea: #SA070P17 (Junta de Castilla y León) y #PI19/01364 (Instituto de Salud Carlos III); la Universidad de Salamanca (Programa XIII- 2014-2020) y el proyecto de colaboración internacional USAL/FAPESP (#2019/16574-2).

El autor disfrutó durante cuatro años de un contrato predoctoral financiado por la Junta de Castilla y León (#EDU/346/2013).

AGRADECIMIENTOS

En primer lugar, quiero agradecer a mis directores, la **Dra. López “Lita”** y al **Dr. Gómez-Nieto “Richard”**, su dedicación y esfuerzo por intentar hacer de mí un mejor científico, pero sobre todo por hacer que el laboratorio sea mi segunda familia.

A todas mis compañeras del laboratorio: **Laura, Sandra, Sandra “Burgos”, Samara y Gisel** por los llantos y carcajadas compartidos.

A **Luis**, por regalarnos a sus “hijos” que con tanto cariño trajo a Salamanca hace más de 15 años.

A **Orlando y Consuelo**, por prestarme siempre su ayuda desinteresada.

A **Lymarye**, por la acogida en el que era “su” laboratorio.

A todas las personas que han pasado alguna vez por nuestro laboratorio, pues todos han aportado su granito de arena en este trabajo: **Nicole, Belén, Rubén, Estela, Ana...**

A **Marianny**, por su ayuda en la medición de los ABR.

A **Rosa**, por su excelente habilidad técnica.

A **Nati**, por acogerme en su laboratorio en pleno verano.

A **Daniel, Javier, Mª Dolores, Adriana, José Antonio, Norberto, Hyppolito y Antonio**, por la colaboración en los trabajos que componen esta tesis; y especialmente a **Elena**, por traer la biología molecular a nuestro laboratorio.

Al **baloncesto**, por ser mi otra pasión y mi vía de escape en los momentos más duros y por darme a tanta gente como **Alberto, Espe, Saúl, Pablo, Juan o Mariano**, que me acompañan en “mi otra vida”.

Por supuesto, a mis **padres** y a mi **hermana**, por ayudarme a ser quien soy y acompañarme en todos mis años de estudio.

A **Carla**, por “obligarme” a escribir esta Tesis, pero sobre todo por ser mi compañera de vida y la persona por la que me esfuerzo día a día para que se sienta orgullosa de mí.

Y para terminar, he querido dejar un hueco especial para **Sonia**, por tantas y tantas cosas que requerirían de otra Tesis... por traerme al laboratorio 12, por su generosidad infinita, por su alegría, por ser mi “editora en jefe” etc., pero sobre todo por ser mi amiga, y es que contigo a mi lado puedo decir que me tocó la lotería.

LISTA DE PUBLICACIONES

Esta tesis corresponde a un compendio de tres artículos científicos publicados en revistas indexadas en Journal Citation Reports.

1. **Sánchez-Benito, D.**^{1,2,5}, Hyppolito, M. A.³, Alvarez-Morujo, A. J.^{1,2,4}, López, D. E.^{1,2,5}, & Gómez-Nieto, R.^{1,2,5} (2020). Morphological and molecular correlates of altered hearing sensitivity in the genetically audiogenic seizure-prone hamster GASH/Sal. *Hearing Research*, 107973. doi: [10.1016/j.heares.2020.107973](https://doi.org/10.1016/j.heares.2020.107973). FI: 3,639. Q1 (open access)
2. **Sánchez-Benito, D.**^{1,2,5}, Gómez-Nieto, R.^{1,2,5}, Hernández-Noriega, S.^{1,2}, Murashima, A. A. B.³, de Oliveira, J. A. C.⁶, García-Cairasco, N.⁶, López, D. E.^{1,2,5}, & Hyppolito, M. A.³ (2017). Morphofunctional alterations in the olivocochlear efferent system of the genetic audiogenic seizure-prone hamster GASH:Sal. *Epilepsy & Behavior*, 71, 193-206. doi: [10.1016/j.yebeh.2016.05.040](https://doi.org/10.1016/j.yebeh.2016.05.040). FI: 2,335. Q2
3. López-López, D.^{1,2}, Gómez-Nieto, R.^{1,2,5}, Herrero-Turrión, M. J.¹, García-Cairasco, N.⁶, **Sánchez-Benito, D.**^{1,2,5}, Ludeña, M. D.⁵, & López, D. E^{1,2,5}. (2017). Overexpression of the immediate-early genes *Egr1*, *Egr2*, and *Egr3* in two strains of rodents susceptible to audiogenic seizures. *Epilepsy & Behavior*, 71, 226-237. doi: [10.1016/j.yebeh.2015.12.020](https://doi.org/10.1016/j.yebeh.2015.12.020). FI: 2,60. Q2

¹ Instituto de Neurociencias de Castilla y León (INCYL), Universidad de Salamanca, Salamanca, España.

² Instituto de Investigación Biomédica de Salamanca (IBSAL), Universidad de Salamanca, Salamanca, España.

³ Laboratorio de Neurobiología de la Audición, Departamento de Oftalmología, Otorrinolaringología, Cirugía de Cabeza y Cuello, Facultad de Medicina de Ribeirão Preto, Universidad de São Paulo, São Paulo, Brasil.

⁴ Departamento de Anatomía e Histología Humana, Facultad de Medicina, Universidad de Salamanca, Salamanca, España.

⁵ Departamento de Biología Celular y Patología, Facultad de Medicina, Universidad de Salamanca, Salamanca, España.

⁶ Laboratorio de Neurofisiología y Neuroetología Experimental, Facultad de Medicina de Ribeirão Preto, Universidad de São Paulo, São Paulo, Brasil.



Los abajo firmantes, Dra. Dña M^a Dolores E. López García y Dr. D. Ricardo Gómez Nieto, miembros del Instituto de Neurociencias de Castilla y León

CERTIFICAN:

Que la tesis doctoral titulada "**Sustrato morfológico y molecular de las alteraciones auditivas implicadas en la susceptibilidad a crisis audiogénas del modelo GASH/Sal**", ha sido realizada bajo su dirección por D. David Sánchez Benito. La tesis presenta un compendio de tres artículos científicos redactados en inglés, y publicados en prestigiosas revistas especializadas de investigación. Con el fin de cumplir con la normativa vigente, la tesis incluye, además, una introducción que refleja la relación entre las tres publicaciones, la hipótesis de trabajo, los objetivos, una discusión general y las principales conclusiones.

Se trata de una obra original que reúne las condiciones necesarias de calidad y rigor científico para su exposición pública y defensa con el fin de optar al título de Doctor por la Universidad de Salamanca.

En Salamanca, 24 de noviembre de 2020

Dra. Dña. M^a Dolores E. López García

Dr. D. Ricardo Gómez Nieto

RESUMEN

La epilepsia es una enfermedad neurológica que afecta aproximadamente a 400.000 personas en España y se caracteriza por una predisposición continuada a la generación de crisis convulsivas. Estas crisis se definen por la aparición de signos y/o síntomas debido a una actividad neuronal excesiva o asincrónica en el cerebro. El uso de modelos animales con epilepsia es esencial para entender los mecanismos subyacentes a esta enfermedad, así como para elaborar tratamientos adecuados para su control.

En nuestro laboratorio, contamos con un modelo de hámster que sufre epilepsia audiogénica de origen genético, un tipo de epilepsia refleja caracterizada por la aparición de crisis convulsivas generalizadas cuando es expuesto a un estímulo sonoro intenso.

Esta tesis doctoral está compuesta por tres artículos científicos publicados en revistas indexadas en el *Journal Citation Reports*, en los que nos adentramos en la búsqueda de anomalías en la vía auditiva del GASH/Sal que puedan explicar la predisposición a sufrir este tipo de crisis. En ellos, estudiamos la vía auditiva con un abordaje multitécnico: técnicas histológicas (tinción de Nissl, inyección de trazadores, inmunohistoquímica, microscopía óptica y electrónica), reconstrucción tridimensional, técnicas biomoleculares y de evaluación de la funcionalidad de la propia vía.

En primer lugar, encontramos que el hámster GASH/Sal presenta déficits auditivos muy acentuados, incluyendo incremento de los umbrales auditivos y otoemisiones acústicas anormales. Para el correcto funcionamiento del sistema auditivo, la onda sonora debe ser captada y transformada en una señal eléctrica que es interpretada por el sistema nervioso, función acometida por el órgano de Corti. El hámster GASH/Sal presenta serias anomalías a nivel coclear. Hemos descrito alteraciones morfológicas en los estereocilios de las células ciliadas internas y externas encargadas del proceso de mecanotransducción, que pueden ser debidas a déficits en la expresión de proteínas estructurales imprescindibles para su organización y función. Además, presentan cambios en las células de soporte que las acompañan y en la estría vascular, elementos muy importantes en el mantenimiento de la homeostasis necesaria para la generación del impulso nervioso en las neuronas del ganglio espiral que constituyen el nervio auditivo. Al comparar estas neuronas del GASH/Sal con las del hámster control, observamos una drástica reducción en el número de células así como

también reducción en el tamaño de sus somas. Pero no sólo existen alteraciones en el receptor coclear, sino que encontramos anomalías en el mecanismo encargado de la modulación del proceso de mecanotransducción: el sistema eferente olivococlear. Este sistema es capaz de realizar ajustes en el órgano de Corti para mejorar la captación del sonido, proteger el sistema de ruidos extremos o dirigir la atención a estímulos concretos. El sistema eferente se origina en el complejo olivar superior, un conjunto de núcleos situados en el tronco del encéfalo. Está formado por una serie de neuronas conocidas como neuronas olivococleares mediales y laterales, que envían sus proyecciones a las células ciliadas externas e internas respectivamente. En el hámster GASH/Sal, hemos encontrado que estas neuronas tienen un tamaño menor que las presentes en el hámster control, además de una reducción de la oliva lateral superior donde se ubican las neuronas olivococleares laterales.

La información auditiva codificada por la cóclea es transmitida en forma de impulsos nerviosos hasta los núcleos cocleares (primer relevo en el tronco cerebral) que reciben las proyecciones glutamatérgicas del nervio auditivo . En el GASH/Sal, hemos detectado una disminución en la expresión de genes codificantes de proteínas transportadoras de glutamato tipo 1 y 2, tanto en la cóclea como en los núcleos cocleares, indicando una disminución de señales aferentes excitatorias en el núcleo coclear. No obstante, los núcleos cocleares no sólo reciben proyecciones auditivas, sino también proyecciones de tipo somatosensorial, principalmente a través terminales nerviosos que contienen el transportador de glutamato tipo 2. El análisis de la distribución de esta proteína en los núcleos cocleares mostró un aumento del número de eferencias somatosensoriales en algunas de las subdivisiones de los núcleos cocleares, que puede ser debido a un mecanismo compensatorio por la falta de actividad auditiva. Este desbalance de señales glutamatérgicas de uno y otro origen, genera un flujo de información aberrante que finalmente alcanza los colículos inferiores y provoca una respuesta anómala de los mismos y la predisposición a desencadenar crisis convulsivas audiogénas.

Finalmente, hemos encontrado que genes de respuesta temprana se encuentran sobreexpresados en el núcleo epileptógeno tras la estimulación auditiva. Estos genes están implicados en numerosas cascadas de señalización que podrían participar en el comienzo de las crisis convulsivas audiogénas.

En conjunto, esta tesis doctoral incluye un análisis detallado a nivel funcional, morfológico y molecular de la cóclea y los núcleos subcoliculares de la vía auditiva del GASH/Sal, permitiendo desvelar las alteraciones innatas de origen genético del modelo que le hacen tener predisposición a desarrollar crisis convulsivas audiogénas. Los resultados indican la existencia de una reorganización de vías nerviosas glutamatérgicas que podrían contribuir a originar las crisis convulsivas audiogénas en el colículo inferior. Este trabajo es clave para entender etiopatogenia del GASH/Sal y para su caracterización como modelo de crisis epilépticas.

ÍNDICE

1. INTRODUCCIÓN	17
1.1. La epilepsia	19
1.2. Modelos animales con crisis convulsivas audiogénas	23
1.2.1. El hámster como modelo experimental: el modelo GASH/Sal	24
1.3. La vía auditiva	28
1.3.1. El órgano de Corti	28
1.3.2. El nervio auditivo	29
1.3.3. Los núcleos cocleares	30
1.3.4. El complejo olivar superior	31
1.3.5. Núcleos del lemnisco lateral	31
1.3.6. El colículo inferior	32
1.3.7. Estaciones auditivas superiores	33
2. HIPÓTESIS Y OBJETIVOS	35
3. RESÚMENES DE LOS ARTÍCULOS	39
3.1. Correlato morfológico y molecular de la sensibilidad auditiva alterada en el hámster GASH/Sal	41
3.2. Alteraciones morfofuncionales en el sistema eferente olivoclear del modelo de epilepsia audiogénica GASH/Sal	47
3.3. Correlato morfológico y molecular de la sensibilidad auditiva alterada en el hámster GASH/Sal	53
4. DISCUSIÓN	59
5. CONCLUSIONES	69
6. BIBLIOGRAFÍA	73
7. ANEXOS	85
7.1. Tabla de abreviaturas	87
7.2. Comunicaciones a congresos	89
8. COMPENDIO DE PUBLICACIONES	99

1. INTRODUCCIÓN

Maestro, traje a ti mi hijo que tiene un espíritu mudo, el cual dondequiera le toma, le sacude y echa espumajos por la boca y crujen los dientes (...) Jesús preguntó al padre: ¿cuánto tiempo hace que le sucede eso? Y él dijo: desde niño y muchas veces lo echa al fuego y al agua para matarlo...".

Marcos Cap. 9 (17-27).

1.1. La epilepsia

Desde que los seres humanos tomamos conciencia de nuestro propio cuerpo, hemos intentado comprender la fisiología de todos los sistemas del organismo. En parte, para satisfacer la curiosidad innata que nos ha hecho evolucionar y, en parte, como un mecanismo de supervivencia. Conocer el funcionamiento de cada uno de los órganos ha permitido a la humanidad elaborar remedios y curas cada vez más desarrolladas que han mejorado la calidad de vida y alargado enormemente la supervivencia.

No obstante, nuestro conocimiento ha avanzado de manera desigual en el entendimiento de todos los órganos y, aún hoy, el funcionamiento del cerebro humano sigue siendo un gran misterio en muchos aspectos. Esto hace que el tratamiento de muchas enfermedades del sistema nervioso siga suponiendo un reto enorme por el desconocimiento sobre su etiología.

Debido a la espectacularidad de algunos de sus síntomas, una de las enfermedades que más curiosidad e incluso miedo ha suscitado a lo largo de la historia ha sido la epilepsia. Las primeras referencias a esta dolencia aparecen en el *Sakikku*, una talla en piedra de origen babilónico (Wilson & Reynolds, 1990), pero podemos encontrar rastros de la enfermedad en la cultura griega, egipcia e india. De hecho, el término epilepsia proviene del vocablo “epilepsia”, del verbo griego *Epilambanein* (ἐπιλαμβάνειν), que significa poseer, atacar, ser cogido por sorpresa. Para los helenos, las convulsiones clásicas de la enfermedad eran provocadas por los mismísimos dioses; aunque ya algunos pensadores como Hipócrates o Galeno de Pérgamo defendían una explicación más racional de la enfermedad. El pensamiento mágico-religioso se mantiene en auge hasta el siglo XVIII, y no es hasta el siglo XIX cuando empieza a considerarse una enfermedad psiquiátrica (Magiorkinis et al., 2010).

Uno de los hitos que más ha influido en los avances en el estudio de esta enfermedad fue la creación de la “Liga Internacional Contra la Epilepsia” (ILAE) en 1909 en Budapest. Uno de sus cometidos es el de recabar toda la información disponible y elaborar informes en los que actualizan periódicamente la definición de la enfermedad a la vista de la nueva información recopilada en las distintas investigaciones.

Actualmente, tras varias revisiones e informes de la ILAE, se considera epilepsia como “un trastorno caracterizado por una predisposición continuada a la generación de crisis epilépticas” (Scheffer et al., 2017). Estas crisis se definen por la aparición de signos y/o síntomas debido a una actividad neuronal excesiva o asincrónica en el cerebro. La definición actualizada se divide en tres puntos:

1. Aparición de al menos dos crisis no provocadas o reflejas con una separación de más de 24 horas. Esta es la definición tradicional y la que aún muchos investigadores consideran como única válida, excluyendo incluso a las epilepsias reflejas (aquellas provocadas por un estímulo externo).
2. Aparición de una crisis no provocada (o refleja) y probabilidad de que aparezcan más crisis durante los 10 años siguientes similar al riesgo de recurrencia general (al menos el 60 %) después de dos crisis no provocadas.
3. Diagnóstico de un síndrome epiléptico, es decir, una condición epiléptica específica con unos síntomas y signos perfectamente definidos.

Existen unos seis millones de pacientes en Europa (entre 300.000-400.000 en España) que responden a estos requisitos, con una tasa de incidencia mundial de 61,44 nuevos enfermos anuales por cada 100.000 habitantes. Esta enfermedad puede llegar a reducir la esperanza de vida de los pacientes entre 2 y 10 años, multiplicando la tasa de mortalidad hasta por dos y tres veces. Dichas características hacen que sea la segunda enfermedad neurológica en años de vida potencialmente perdidos o vividos con discapacidad según la Organización Mundial de la Salud (López-González et al., 2019).

Se considera que la epilepsia está resuelta en los sujetos que presentan un síndrome epiléptico dependiente de la edad y han superado la edad correspondiente y en los que se han mantenido sin crisis durante los 10 últimos años sin haber tomado medicación antiepileptica desde hace al menos 5 años (Fisher et al., 2014).

Ahora bien, la epilepsia en realidad no es una única enfermedad. Las crisis epilépticas pueden sobrevenir debido a distintas causas y manifestarse de infinidad de maneras. Inicialmente, las crisis se clasificaron según sus características externas visibles, pero la ILAE en 2017 elabora una clasificación basándose en su origen, la presencia/ausencia de síntomas motores y afectación o no del nivel de conciencia,

siendo el primer signo el que marca la clasificación de la misma (Tabla 1) (Fisher et al., 2017):

- Según el origen:
 - Crisis focales: a las que clásicamente se denominaban parciales. La descarga comienza en redes limitadas a un hemisferio cerebral.
 - Crisis generalizadas: surgen e involucran rápidamente a redes bilaterales.
 - Crisis de inicio desconocido: aquellas para las que no existe información suficiente para incluirlas en uno de los dos grupos.
 - Crisis focales con evolución a una crisis tónico-clónica bilateral: sustituye al término “crisis parcial con generalización secundaria”.
- Según la presencia o no de signos motores: aplicable tanto a las crisis focales como a las generalizadas. Existen muchos subtipos:
 - Inicio motor: tónico-clónicas, mioclónicas, atonías, automatismos, etc.
 - Inicio no motor: ausencias, cognitivas, emocionales, sensoriales, etc.
- Según la afectación de conciencias: solo aplicable a crisis focales:
 - Nivel de conciencia preservado: conocidas antiguamente como “crisis simples”.
 - Nivel de conciencia alterado: conocida anteriormente como “crisis complejas”.

Tabla 1

Clasificación de las epilepsias según su origen, la presencia/ausencia de síntomas motores y afectación o no del nivel de conciencia.

Tipo de crisis epilépticas según la ILAE 2017			
Inicio focal		Inicio generalizado	Inicio desconocido
Conciencia preservada	Conciencia alterada		
Inicio motor: <ul style="list-style-type: none"> • Automatismos • Atónica • Clónica • Espasmos epilépticos • Hipercinética • Mioclónica • Tónica 	Motores: <ul style="list-style-type: none"> • Tónico-clónica • Clónica • Tónica • Mioclónica • Mioclónica-tónico-clónica • Atónica • Espasmos epilépticos 	Motoras: <ul style="list-style-type: none"> • Tónico-clónica • Espasmos epilépticos 	
Inicio no motor: <ul style="list-style-type: none"> • Automatismos • Interrupción de actividad • Cognitivo • Emocional • Sensorial 	No motoras (ausencias): <ul style="list-style-type: none"> • Típica • Atípica • Mioclónica • Mioclónia parpebral 	No motora: <ul style="list-style-type: none"> • Interrupción de actividad 	
Inicio focal con evolución a bilateral			Inclasificable

Nota: recuperado de “Manual de práctica clínica en epilepsia. Recomendaciones diagnóstico-terapéuticas de la SEN 2019”, López-González et al., 2019.

Además, se pueden clasificar según la etiología:

- Estructural: si existe una lesión observable por neuroimagen.
- Genética: si existe una anomalía genética conocida o un patrón de herencia familiar. Hasta hace unos años se conocían como epilepsias idiopáticas.
- Infecciosa: si existe una infección que determine una lesión cerebral.
- Metabólica: provocada por una alteración metabólica genética o adquirida permanente.
- Inmune: debido a una enfermedad autoinmune.

En esta tesis doctoral, nos centraremos en un grupo especial de epilepsias, las epilepsias reflejas. Son aquéllas desencadenadas por la exposición a un estímulo interno o externo generalmente bien definido, y que afecta aproximadamente al 6% de los pacientes epilépticos (Salas Puig et al., 2000). Existen multitud de desencadenantes, ya sean simples (táctiles, luminosos, sonoros) o complejos (lectura, toma de decisiones, etc.) (Szűcs et al., 2019). En concreto, se tratará de forma exclusiva la epilepsia audiogénica, es decir, aquélla cuyas crisis son desencadenadas por un estímulo sonoro. En humanos, se suele conocer como musicogénica y es muy poco frecuente. Sin embargo, existen numerosos modelos animales con este tipo de epilepsia que abren un amplio abanico de posibilidades para el estudio del origen y tratamiento de la epilepsia (García-Cairasco et al., 2017; Muñoz et al., 2017; Ross & Coleman, 2000).

1.2. Modelos animales con crisis convulsivas audiogénicas

El uso de modelos animales con convulsiones y/o epilepsia es esencial para entender los mecanismos subyacentes a esta enfermedad. Sólo conociendo cómo se originan y los sustratos anatómicos y fisiológicos de las crisis, podremos mejorar la prevención, tratamiento y, por qué no, la curación de esta patología.

En la actualidad, hay multitud de modelos animales de crisis convulsivas y de epilepsia, casi todos roedores, pero también hay moscas, peces e incluso lombrices (Kandratavicius et al., 2014; Fuentes-Santamaría et al., 2005). Sin embargo, ningún modelo refleja la totalidad de la clínica de la epilepsia en humanos y además existen infinidad de tipos de epilepsias como hemos visto.

El origen de dichos modelos es muy variado. Existen algunos inducidos por agentes químicos como el kainato o la pilocarpina; físicos, como descargas eléctricas o estímulos repetitivos (*kindling*) o animales con epilepsia de origen genético. Se cree que el primer roedor con crisis convulsivas audiogénicas (AGS) fue observado por Studenov en 1924 cuando estudiaba el condicionamiento por sonidos en ratones (Poletaeva et al., 2017; Ross & Coleman, 2000). Desde entonces se han desarrollado y descrito muchos modelos, algunos de los más importantes son:

- Ratas KM (*Krushinsky-Molodkina*): ratas con AGS de origen genético originadas en 1940 por el cruce de ratas Wistar que sufrían crisis convulsivas al ser expuestas a un estímulo sonoro. Su peculiaridad es que son vulnerables a sufrir hemorragias cerebrales, por lo que no solo sirven como modelo genético de síndromes epilépticos, sino que además se utilizan para estudiar anomalías en el riego sanguíneo del cerebro (Poletaeva et al., 2017). Sus crisis se caracterizan por una o dos carreras salvajes, seguidas por convulsiones tónico-clónicas y un periodo de catalepsia.
- Ratas GEPR (*Genetically Epilepsy-Prone Rats*): originadas en la Universidad de Arizona a finales de los años 50 seleccionando ratas *Sprague-Dawley* que presentaban AGS. Estas AGS no sólo son debidas a un estímulo auditivo, sino que también pueden sufrirlas por hipertermia o incluso surgir de forma espontánea (Dailey & Jobe, 1985).
- Ratón DBA/2 (*Dilute Brown Agouti coat color*): posiblemente el modelo más estudiado. Su susceptibilidad comienza a los 12 días y dura hasta los 42. La gravedad de sus crisis puede llevar a la muerte por fallo respiratorio (Ross & Coleman, 2000). Estos ratones sufren una pérdida auditiva progresiva a partir de las 3-4 semanas, que se hace severa a los 3 meses de edad.
- WAR (*Wistar Audiogenic Rat*): al igual que las ratas KM, fueron seleccionadas ratas Wistar susceptibles de sufrir AGS en la Facultad de Medicina de Ribeirão Preto de la Universidad de São Paulo en Brasil (Garcia-Cairasco et al., 1993).

1.2.1. El hámster como modelo experimental: el modelo GASH/Sal

Los animales más utilizados en investigaciones biomédicas han sido los roedores. Dentro de este orden, existen más de dos mil especies, siendo las más utilizadas la rata, el ratón y la cobaya. No obstante, cada vez es más frecuente la utilización de hámsteres (*Mesocricetus*). Su uso se ha extendido gracias a sus múltiples ventajas (Muñoz de la Pascua, 2004):

- Fácil reproducción: pueden llegar a tener seis crías por parto, unas seis veces al año, lo que les hace ser un modelo ideal para estudiar enfermedades genéticas hereditarias.
- Ausencia de infecciones específicas y susceptibilidad a infecciones experimentales. Esto último ha permitido utilizarlos para estudiar multitud de enfermedades.
- Características anatómicas únicas:
 - Abazones en la pared bucal con glándulas y vías de drenaje linfático que permiten aceptar exotrasplantes.
 - Hibernación, característica interesante para estudios del metabolismo de la grasa.

En 1982, aparece descrita una cepa de hámster dorado (*Mesocricetus auratus*) que sufre AGS en una tesis doctoral en la Universidad de Valladolid (Aparicio, 1982), se trataba del modelo GPG/Vall. Esta línea sufría crisis de origen troncoencefálico y de transmisión hereditaria, desencadenadas por estímulos acústicos de 1-20Khz. Eran crisis convulsivas generalizadas tónico-clónicas, semejantes a las humanas tipo Gran Mal. A partir de esta cepa, se desarrolló en la Universidad de Salamanca la línea sobre la que se trabaja en este estudio: el hámster GASH/Sal (*Genetic Audiogenic Seizure Hamster, Universidad de Salamanca*).

Esta nueva línea surgió a partir de cruzamientos de la línea GPG/Vall con hámsteres sirios normales. Este estudio descrito en la tesis doctoral de Muñoz de la Pascua en 2004, tenía como objetivo estudiar el patrón de transmisión de la susceptibilidad audiogena, así como establecer un nuevo modelo estandarizado de hámsteres para el estudio de las epilepsias reflejas.

Se describió que la susceptibilidad audiogena se transmite de forma autosómica recesiva. Sus crisis son provocadas por estímulos auditivos de 0 a 18 kHz y una intensidad de 115-120 dB. Constan de varias fases comunes a casi todos los modelos experimentales de etiología genética (Ross & Coleman, 2000) y están presentes desde los 30 días hasta los 4-6 meses. Estas fases son:

- Carrera salvaje: tras el sobresalto inicial provocado por el comienzo del estímulo, el animal corre rápidamente de manera descontrolada.
- Fase tónico-clónica: aparece inicialmente una fase tónica en opistótono, con rigidez en todo el cuerpo, seguida de convulsiones clónicas en los miembros anteriores y espasmos tónicos en los posteriores.
- Fase tónica: se produce una hiperextensión sostenida del dorso, cuello y extremidades anteriores, pudiendo darse también en las posteriores según la gravedad.
- Periodo post-ictal: el hámster entra en un estado catatónico de mayor o menor duración y del cual se recuperan pasados unos minutos, volviendo a su actividad normal previa a la crisis.

Desde la publicación de la tesis doctoral de Muñoz de la Pascua, se han realizado numerosos trabajos con el GASH/Sal como protagonista, con el objetivo de caracterizar en profundidad esta cepa (Barrera Bailón, 2013; Barrera-Bailón et al., 2017, 2017; Damasceno et al., 2020; Díaz-Casado et al., 2020; Díaz-Rodríguez et al., 2020) habiendo validado sus crisis como verdaderas crisis epilépticas (Carballosa-Gonzalez et al., 2013).

Evaluación de la función auditiva

Como las crisis epilépticas de estos animales están desencadenadas por estímulos auditivos, es de vital importancia valorar la función auditiva del hámster GASH/Sal. Para este fin, se recurre al análisis de respuestas troncoencefálicas evocadas por estímulos auditivos (ABR). Esta técnica mide la respuesta eléctrica y su propagación a lo largo de la vía auditiva tras la estimulación sonora. Gracias a ella, se ha observado un aumento del umbral auditivo del hámster GASH/Sal en comparación con animales control (Carballosa González, 2008; Muñoz et al., 2017), lo que se traduce en una pérdida auditiva severa de la cepa epiléptica.

Respuesta a fármacos antiepilepticos

Una de las fases para determinar si el hámster GASH/Sal es un modelo válido de epilepsia era comprobar la eficacia de los fármacos antiepilepticos clásicos. Se ha demostrado que la administración aguda de retigabina, lamotrigina, fenobarbital, levetiracetam y ácido valproico tiene efecto anticonvulsivo en nuestro hámster. No obstante, no todos tienen la misma eficacia y depende, en gran parte, de la dosis, la vía y la frecuencia de administración (Barrera-Bailón et al., 2013, 2017).

Alteraciones genéticas y moleculares

Otros de los trabajos realizados con el fin de caracterizar al hámster GASH/Sal y realizar una descripción exhaustiva de sus crisis convulsivas se basan en estudiar los cambios genéticos a nivel de expresión del núcleo epileptógeno tras las crisis convulsivas.

En estudios previos de nuestro grupo de investigación se detectaron hasta 58 genes con una expresión inequívocamente alterada en el hámster GASH/Sal al compararlo con un hámster control (López-López et al., 2017). Estos genes están implicados en funciones muy diversas: moleculares (catalizadores o transportadores entre otros), componentes celulares (de membrana y de orgánulos), procesos biológicos, rutas metabólicas, etc. Además, algunos de ellos estaban directamente relacionados con procesos epileptógenos.

Por otro lado, se ha descrito una disminución en la expresión del cotransportador de K^+/Cl^- KCC2 en varias áreas cerebrales. Este transportador está íntimamente relacionado con la neurotransmisión GABAérgica. Esto, unido a alteraciones en la expresión de las subunidades β del receptor GABA_A, estaría provocando un estado de hiperexcitabilidad generalizado que podría subyacer a la susceptibilidad epiléptica (Prieto-Martín et al., 2017).

Recientemente se ha visto que esta línea exhibe variantes génicas en homocigosis, 7 de alto impacto y 17 de impacto moderado (Díaz-Casado et al., 2020).

1.3. La vía auditiva

Debido a la naturaleza sonora del estímulo desencadenante de las crisis epilépticas en el modelo de epilepsia que ocupa este estudio, es necesario tener una visión general de la estructura y funcionamiento de la vía auditiva.

Lo primero que hay que tener presente es que el sonido es una onda de presión que debe ser transformada en una señal eléctrica. Este proceso se lleva a cabo en el receptor auditivo, el órgano de Corti, situado en el oído interno. A partir de aquí, la señal eléctrica es transportada por el nervio auditivo hasta los núcleos cocleares (CN), y desde éstos se generan una serie de canales de información ascendente hasta la corteza auditiva, situada en el lóbulo temporal. En este recorrido, existen una serie de estaciones intermedias en las que se va procesando la información: complejo olivar superior (SOC), núcleos del lemnisco lateral (LLN), colículo inferior (IC) y núcleo geniculado medial del tálamo.

1.3.1. El órgano de Corti

El sonido es captado por los pabellones auriculares y dirigido por el conducto auditivo externo hasta la membrana timpánica. Las vibraciones sonoras se transmiten y se amplifican hasta el oído interno que se encuentra dentro del laberinto óseo, conocido comúnmente como cóclea. En su interior se localiza el laberinto membranoso y está lleno por la límpida líquido coclear. Se compone de dos membranas, la membrana de Reissner o tectoria y la membrana basilar, que dividen el espacio en tres escalas: escala vestibular, escala media y la escala timpánica.

Sobre la membrana basilar, se asienta el órgano de Corti, que es el verdadero epitelio sensorial. Se compone de células de soporte (células de Deiters y pilares o arcos de Corti) y de las células sensoriales propiamente dichas: las células ciliadas internas (IHC) y externas (OHC). En el hamster, las primeras se disponen en una única hilera de células, mientras que las segundas se organizan en tres filas y tienen forma de V. En la parte más apical de estas células, se localizan los estereocilios sobre los que se asienta

la membrana tectoria. Cuando llega la onda sonora, vibra toda la membrana basilar, haciendo que estos estereocilios se deformen al chocar contra la membrana tectoria y así comienza el mecanismo de transducción (Hasko & Richardson, 1988). Los estereocilios están unidos por puentes proteicos, y al desplazarse lateralmente, se abren canales de potasio, generándose la despolarización de las IHC y OHC. Esto hace que las primeras acabén liberando glutamato sobre las neuronas ganglionares, cuyas prolongaciones forman el nervio auditivo. En cambio, las OHC responden a estos potenciales generados y se encargan de regular la captación de los sonidos mediante su acortamiento o estiramiento (Pickles & Corey, 1992). La membrana basilar es capaz de responder a distintas frecuencias sonoras a lo largo de su superficie, iniciándose en este punto el procesamiento del sonido.

Existe una técnica para evaluar el correcto funcionamiento de la estructura coclear, que se utiliza en uno de los estudios de los que consta este trabajo: las emisiones otoacústicas producto de distorsión (DPOAEs). Consiste en captar y analizar los sonidos producidos por la contracción de las OHC en la cóclea después de estimularla con tonos puros y aporta información relevante sobre posibles daños cocleares (Nobili et al., 1998).

Existen diversos estudios de la cóclea en modelos animales con susceptibilidad a sufrir AGS; muchos de ellos comparten anomalías congénitas o lesiones (Pierson & Li, 1996). Se han descrito cambios estructurales y en el número de IHC y OHC en las ratas GEPR (Penny et al., 1986).

1.3.2. El nervio auditivo

A lo largo de todo el eje central de la cóclea, conocido como modiolo, se disponen una serie de neuronas primarias denominadas células ganglionares (SGNs) que constituyen el ganglio espiral, encargado de recoger la información procedente del órgano de Corti y transportarla hasta la siguiente estación de la vía a través de la rama auditiva del VIII par craneal.

Este órgano de Corti posee dos tipos de neuronas: tipo I (95% del total) y tipo II (5%). Las de tipo I son de gran tamaño, bipolares y mielinizadas y son las encargadas de

inervar las IHC. Las de tipo II inervan las OHC y son pseudomonopolares y su axón es amielínico (Liberman, 1980; Romand & Romand, 1987).

1.3.3. Los núcleos cocleares

Los CN reciben todos los terminales provenientes de las fibras del ganglio espiral, además de un amplio espectro de proyecciones descendentes de otras regiones auditivas y no auditivas (Yin et al., 2019). Estas proyecciones entran al núcleo a través de la raíz del nervio coclear. En esa zona, en algunos roedores como el hámster, existen unas células de gran tamaño muy grandes conocidas como neuronas de la raíz (Gómez-Nieto et al., 2008; Hormigo et al., 2017; López et al., 1999).

Anatómicamente, en los CN podemos diferenciar el núcleo coclear anteroventral (AVCN) y núcleo coclear posteroventral (PVCN), por encima de los cuales se sitúa el núcleo coclear dorsal (DCN) (Malmierca, 2015).

El núcleo coclear ventral (VCN) contiene cinco tipos neuronales: esféricas y globulares (*Bushy cells*), multipolares, pulpo y células grano. Se pueden observar estructuras muy características en este núcleo. Cada neurona esférica está inervada por una fibra del nervio auditivo en forma de cáliz de *Held* rodeando al soma (Gómez-Nieto & Rubio, 2009; 2011).

En el VCN se mantiene la distribución de frecuencias y, además, este núcleo se ocupa de la localización horizontal del sonido, analizando las diferencias interaurales de tiempo e intensidad. Por otro lado, el AVCN está implicado en el reflejo de atenuación del oído medio que protege el sistema auditivo ante sonidos de alta intensidad (Musiek & Chermak, 2015).

El DCN, en los roedores, se estructura en forma de capas o láminas. Está formado principalmente por neuronas piramidales, con unas prolongaciones dendríticas muy características dando lugar a tres capas: capa molecular, capa de las células piramidales y capa profunda, que además posee neuronas gigantes. En esta última descargan las proyecciones de los núcleos cocleares (Mugnaini et al., 1980).

Los CN se han relacionado con las AGS, puesto que la destrucción electrolítica del VCN causa la eliminación de las crisis, aunque reaparecen pasados varios días (Browning, 1986).

1.3.4. El complejo olivar superior

El SOC está formado por varios núcleos densamente agrupados, entre los que destacan: la oliva superior lateral (LSO), la oliva superior medial (MSO), el núcleo medial del cuerpo trapezoide (MNTB) y núcleo ventral del cuerpo trapezoide (VNTB).

EL SOC está directamente implicado en localización del sonido en el espacio, gracias a un sistema muy coordinado de integración de la información excitatoria e inhibitoria proveniente de ambos oídos en cada uno de los núcleos del complejo (Tollin, 2003).

Una de las características del SOC, que facilita su estudio, es que la proteína de unión al calcio calbindina (CaBP) marca de forma selectiva los núcleos que lo conforman (Matsubara, 1990). Por tanto, mediante técnicas inmunohistoquímicas, es muy sencillo identificar estos núcleos. La LSO por ejemplo, tiene forma de "S" en roedores, aunque en hámster tiene una forma peculiar, más semejante a la silueta de un pato (Fuentes-Santamaría et al., 2005). Desde este núcleo, la información auditiva viaja al lemnisco, al colículo inferior, al tálamo o incluso directamente a la corteza.

Además de su función aferente auditiva, el SOC está implicado en la regulación de la captación del sonido a través de fibras olivococleares, formando los conocidos como sistemas eferentes lateral y medial. El lateral parte de la LSO y de las neuronas que la rodean (denominadas *Shell*) y modula el funcionamiento de las IHC de su mismo lado. El sistema medial se origina en neuronas del VNTB y termina en las OHC de ambas cócleas. Este sistema modula la contractibilidad de las OHC, disminuyendo o aumentando la sensibilidad de las IHC (Sánchez-González et al., 2003; Warr, 1980).

1.3.5. Núcleos del lemnisco lateral

El lemnisco lateral es un tracto de fibras situado en los laterales del tronco del encéfalo y discurre desde la zona del SOC hasta el IC. Los LLN son agrupaciones neuronales situadas entre las fibras. Clásicamente, se han diferenciado dos

subdivisiones funcionales: el complejo ventral del lemnisco lateral, que recibe aferencias de los CN contralaterales y del NMTB y envían sus axones mayoritariamente al IC del mismo lado, al cuerpo geniculado medial y al colículo superior; y el núcleo dorsal del lemnisco lateral que está inervado por células biaurales del SOC y proyecta bilateralmente a ambos colículos.

1.3.6. El colículo inferior

El IC está formado por un núcleo central y unas cortezas externa y dorsal. El núcleo central se caracteriza por una organización laminar tonotópica. En él se produce el relevo de los axones procedentes del lemnisco y que ascienden hasta el núcleo geniculado medial. Además, recibe información desde su homólogo contralateral. En este núcleo se afina el procesamiento biaural ya iniciado en el SOC (Yin et al., 2019). En la corteza se procesan principalmente proyecciones descendentes desde la propia corteza cerebral (Malmierca, 2004).

En modelos animales de epilepsia audiogénica, se acepta que el IC es el núcleo crucial en el que tiene lugar la conversión del estímulo auditivo en una respuesta motora que da lugar a las convulsiones clónicas (Gale, 1992). Su estimulación eléctrica en ratas o la aplicación local de drogas que provocan la liberación de neurotransmisores excitatorios desencadenan las crisis (Faingold et al., 1989). Además, si se bloquea la transmisión de GABA, se produce el mismo efecto convulsivo (Frye et al., 1983). Utilizando ratas GEPR, se observa que la lesión o inhibición del IC elimina total o parcialmente la generación de las crisis evocadas por un estímulo auditivo (Browning, 1986; Kesner, 1966; Wada et al., 1970).

En nuestro modelo animal GASH/Sal, se ha probado la implicación del IC en las crisis convulsivas, demostrando que existe una mayor activación de este núcleo medido por la inmunotinción frente a c-Fos tras la estimulación acústica, sobre todo en ambas cortezas (Carballosa González, 2008; Hernández-Noriega, 2017; Muñoz et al., 2017), y un incremento en la expresión de la óxido nítrico sintasa (Prieto-Martín et al., 2012), enzima relacionada con la actividad epiléptica.

1.3.7. Estaciones auditivas superiores

Desde el IC, la información auditiva continua hacia los centros auditivos superiores. Estos centros son el colículo superior, cuerpo geniculado medial y la corteza auditiva. Estas estaciones son de vital importancia en la recepción y procesamiento de la onda sonora, pero no son protagonistas en este trabajo.

El cuerpo geniculado medial está dividido en tres partes: ventral, medial y dorsal, conectadas con el núcleo central y las cortezas dorsal y externa del IC respectivamente, y manda la información auditiva a la corteza. Mientras que el núcleo ventral mantiene la organización tonotópica, las subdivisiones dorsal y medial carecen de esta distribución, y se cree que están más implicadas a las respuestas emocionales a los sonidos (Malmierca, 2015).

Finalmente, la señal eléctrica generada tras la captación de la onda sonora alcanza la corteza auditiva, localizada en el lóbulo temporal y que se divide en corteza auditiva primaria y secundaria (Malmierca & Merchán, 2007).

En este punto, y de forma resumida, termina la vía ascendente auditiva. Aquí, las señales acústicas se convierten en una percepción consciente. Resulta de vital importancia el conocimiento de la organización, estructura y funcionamiento de la vía auditiva en el GASH/Sal para poder encontrar las anomalías que expliquen la predisposición a sufrir crisis convulsivas en respuesta a un estímulo sonoro.

2. HIPÓTESIS Y OBJETIVOS

Mi hijo es endemoniado, y no hay día que tres o cuatro veces no le atormenten los malignos espíritus; y de haber caído una vez en el fuego, tiene el rostro arrugado como pergamino, y los ojos algo llorosos y manantiales; pero tiene una condición de un ángel, y si no es que se aporrea y se da de puñadas él mismo a sí mismo, fuera un bendito.

Labrador, El Quijote, Miguel de Cervantes

La investigación en epilepsia se nutre de modelos animales que reproducen de la forma más fidedigna posible la genética, fisiopatología y etiología de los diferentes síndromes epilépticos. En nuestro laboratorio, contamos con el modelo GASH/Sal, un hámster susceptible a sufrir AGS de origen genético. Estas crisis se desencadenan por un estímulo sonoro de alta intensidad lo que implica que la vía auditiva esté alterada. Se ha constatado que el IC es el núcleo epileptógeno, sin embargo, se desconoce si los núcleos y las vías auditivas subcoliculares también están alterados. La hipótesis de partida es que el modelo GASH/Sal debe presentar alteraciones en la vía auditiva, desde el receptor coclear hasta el IC, que contribuyan al inicio y propagación de las crisis audiogénas.

Objetivo general:

El objetivo principal de esta tesis doctoral es determinar las bases morfológicas y moleculares de las alteraciones auditivas implicadas en la susceptibilidad a sufrir crisis audiogénas en el modelo GASH/Sal.

Objetivos específicos:

1. Evaluar la sensibilidad auditiva del GASH/Sal y la funcionalidad de su sistema eferente.
2. Describir las alteraciones morfológicas existentes en el órgano de Corti del modelo GASH/Sal.
3. Determinar posibles alteraciones en los niveles de expresión génica de proteínas implicadas en la organización y funcionalidad del órgano de Corti del GASH/Sal.
4. Analizar las posibles alteraciones en los niveles de expresión génica de los trasportadores vesiculares de glutamato en la cóclea y en los núcleos cocleares del GASH/Sal.
5. Determinar la distribución del trasportador vesicular de glutamato tipo 2 en los núcleos cocleares del hámster GASH/Sal.

6. Analizar posibles alteraciones en la distribución y morfología de las neuronas olivococleares del hámster GASH/Sal.
7. Estudiar los genes de expresión temprana *Egr1*, *Egr2* y *Egr3* en el núcleo epileptógeno tras las crisis convulsivas, y su papel en la predisposición genética a la epilepsia.

3. RESÚMENES DE LOS ARTÍCULOS

“Durante breves momentos siento tal felicidad difícil de describir. Siento una completa armonía conmigo y el mundo, y esto es tan fuerte y placentero que por un segundo de esta sensación cambiaría años o toda mi vida”.

Príncipe Mishkin, El Idiota, Fiódor Mijailovich Dostoyevski

3.1. Correlato morfológico y molecular de la sensibilidad auditiva alterada en el hámster GASH/Sal

Sánchez-Benito, D., Hyppolito, M. A., Alvarez-Morujo, A. J., López, D. E., & Gómez-Nieto, R. (2020). Morphological and molecular correlates of altered hearing sensitivity in the genetically audiogenic seizure-prone hamster GASH/Sal. *Hearing Research*, 107973.

<https://doi.org/10.1016/j.heares.2020.107973>. FI: 3,639. Q1 (Open access)

Introducción: Los modelos animales de epilepsia son cruciales para investigar los procesos que subyacen a los episodios ictales así como para desarrollar nuevas estrategias terapéuticas para el tratamiento de esta enfermedad. La epilepsia audiogena es una enfermedad caracterizada por la susceptibilidad a sufrir convulsiones tónico-clónicas en respuesta a una estimulación sonora intensa. Es típica de roedores, pero hay modelos de muchas especies diferentes, tanto inducidos por sustancias químicas o daños cocleares en etapas tempranas del desarrollo, como de origen genético. Uno de estos modelos genéticos disponibles es el hámster GASH/Sal. Se han realizado hasta ahora numerosos estudios sobre la epilepsia utilizando este modelo: neuroetológicos, electrofisiológicos, neuroquímicos, moleculares, farmacológico etc. Al ser un sonido el que provoca las crisis (epilepsia audiogena), está clara la implicación de la vía auditiva, pero a pesar de que se conoce que el núcleo epileptógeno es el IC, poco se sabe acerca del papel de las estaciones anteriores de la vía auditiva.

Es por ello que, en este estudio, nos planteamos estudiar las posibles alteraciones estructurales y moleculares de la cóclea y de los núcleos cocleares del hámster GASH/Sal, en comparación con hámsteres sirios controles sanos.

Métodos: para llevar a cabo este objetivo, se utilizaron 15 animales controles (*Mesocricetus auratus*) y 14 hámsteres GASH/Sal, todos machos de 4 meses de edad, empleando una amplia batería de técnicas histológicas y moleculares.

El primer paso, fue estudiar la función del oído interno a través del test de ABR. Este test proporciona un perfil de ondas eléctricas generadas por el paso del impulso eléctrico por cada una de las estaciones de la vía auditiva.

A continuación, se buscaron anomalías en el receptor auditivo. Se obtuvieron y analizaron cortes de 6 µm del órgano de Corti incluido en parafina y teñidos con violeta de cresilo. Con este material, se contaron y midieron las SGNs cuyas prolongaciones forman el nervio auditivo, y se analizó la estría vascular, epitelio encargado de asegurar el aporte de oxígeno y todo tipo de moléculas necesarias para mantener la homeostasis coclear.

A través de la microscopía electrónica de barrido, se obtuvo una visión pormenorizada de la ultraestructura del epitelio neurosensorial. Esto permitió medir y contar los estereocilios de las IHC y OHC, así como analizar otros elementos acompañantes, como las células de Deiters. Tras las observaciones realizadas, se decidió abordar el estudio a nivel molecular, mediante un análisis de expresión por la reacción en cadena de la polimerasa en tiempo real (RT-qPCR) de genes que codifican proteínas implicadas en la función y mantenimiento de la estructura de los estereocilios, como la prestina, la cadherina23 (*Cdh23*) y la protocadherina15 (*Pcdh15*). El estudio de expresión se completó con la medición de los transportadores vesiculares de glutamato 1 y 2 (*Vglut1* y *Vglut2*) en la cóclea y en los núcleos cocleares. El glutamato es el neurotransmisor excitatorio de las neuronas ganglionares del órgano de Corti, por lo que analizar su expresión permitió discernir cómo se estaba transmitiendo el impulso nervioso.

Finalmente, se avanzó a la siguiente estación de la vía auditiva: los núcleos cocleares. Mediante la tinción con violeta de cresilo y técnicas inmunohistoquímicas, se determinó el perfil de distribución de los terminales VGLUT2, ya que cambios en su inmunorreactividad están íntimamente relacionados con desórdenes caracterizados por hiperexcitabilidad, como la epilepsia y el tinnitus.

Resultados: al igual que en el estudio del punto siguiente 3.2 (Sánchez-Benito et al., 2017) los test ABR de los hámsteres GASH/Sal mostraron un aumento del umbral auditivo de casi el 40% respecto a los controles, así como una reducción significativa de

la amplitud de la onda I. Esta disminución de la respuesta estaba acompañada por alteraciones en el órgano de Corti, las SGNs y la estría vascular encontradas en el análisis histológico de la cóclea de estos animales. En las células ciliadas de los hámsteres GASH/Sal, se describió la ausencia de algunos estereocilios tanto en las internas como en las externas, así como malformaciones en las células de sostén. A estas alteraciones se suma una reducción en el tamaño y la densidad de las SGNs y una estría vascular que, aunque conservaba su organización característica, se encontraba estrechada en las porciones basal y medial de la cóclea y tenía un menor número de capilares en toda su extensión. Para hacer una descripción más precisa del epitelio neurosensorial del órgano de Corti, se recurrió a la microscopía electrónica de barrido. En primer lugar, se confirmó la desorganización de los estereocilios descrita en Sánchez-Benito et al. (2017). En las IHC, en vez de formar una línea de apéndices alineados, se encontraban cada uno orientados en una dirección. En el caso de las OHC, el patrón de estereocilios característico con forma de "V" se encontraba enormemente alterado. En muchos casos, las agrupaciones estaban colapsadas y se veía que faltaban algunos estereocilios. Las mediciones realizadas demostraron que, los que quedaban, eran significativamente mayores en el animal epiléptico. Debido al papel fundamental que tienen las células de soporte en la regeneración y mantenimiento de los estereocilios, se estudiaron las células de Deiters que se intercalan entre las OHC. En el GASH/Sal, aparecían expandidas y con unas granulosidades muy peculiares. Para intentar dilucidar a qué se debían estos cambios en la disposición de los estereocilios, se recurrió al análisis de la expresión de tres genes estructurales: *prestina*, *Cdh23* y *Pcdh15*. La RT-qPCR mostraba que los tres genes estaban infraexpresados en el GASH/Sal. Esto iba acompañado de bajos niveles de expresión de *Vglut1* y *Vglut2* en la cóclea, lo que denotaba una transmisión sináptica deficitaria desde el nervio auditivo, y que, además, este déficit se mantenía al hacer el análisis de expresión de receptores glutamatérgicos en los núcleos cocleares. La inmunohistoquímica (visualizada con el microscopio óptico convencional y de fluorescencia) en esta estación de la vía auditiva permitió observar que, además, existía una distribución anómala de la proteína VGLUT2 en el hámster GASH/Sal que no se correspondía con la descrita en otros roedores ni con lo observado en los controles. Los animales GASH/Sal presentaban un intenso marcaje en las zonas magnocelulares del

VCN, (tanto en su división anterior como posterior), mientras que la capa granular aparecía tímidamente teñida, patrón justamente opuesto al que presentan los roedores sanos. Esta distribución quedó confirmada con los análisis cuantitativos de los terminales marcados con immunofluorescencia para la detección de VGLUT2.

Discusión y conclusiones: Este estudio aporta nuevos datos morfológicos y moleculares del oído interno y de los núcleos cocleares del hámster dorado sirio *Mesocricetus auratus* poco estudiado hasta el momento. Esta especie sirve como referencia de la cepa GASH/Sal y permite determinar qué alteraciones morfológicas y moleculares podrían explicar las convulsiones audiogénas que sufre.

En este trabajo, se han descrito anomalías en el epitelio neurosensorial, degeneración de las SGNs y atrofia de la estría vascular; alteraciones que sugieren problemas en el procesamiento y la propagación de la información auditiva. Estos datos están respaldados por una infraexpresión de los genes que mantienen la unión de los estereocilios del receptor auditivo, de los receptores glutamatérgicos en la cóclea y en los núcleos cocleares, y por una redistribución de la proteína VGLUT2 en estos últimos. Existen, por tanto, cambios en la transmisión de información auditiva ascendente desde la cóclea hasta el IC. En gran parte de la bibliografía existente, se considera que el IC es el núcleo de iniciación de los episodios convulsivos en los modelos de roedores con epilepsia audiogénica, pero apenas han sido estudiados los núcleos auditivos subcoliculares.

Desde el inicio de la transmisión del impulso nervioso, ya se observa que existe una alteración. Los resultados de los ABR, con el aumento del umbral de respuesta y la reducción de la amplitud de la onda I, denotan algún tipo de neuropatía coclear. Estos resultados se relacionan normalmente con daños cocleares debidos a la edad o la exposición a un ruido fuerte, y suele ir acompañada de patologías auditivas como hiperacusia o tinnitus. A nivel histológico, la pérdida de SGNs descrita en el GASH/Sal demuestra una desafección del nervio auditivo que se une a una mecanotransducción deficiente derivada de todos los cambios descritos en la cóclea. Por un lado, la atrofia de la estría vascular puede estar condicionando el mantenimiento de la diferencia de potencial en la endolinfa para la generación del impulso nervioso.

Además, a la hora de producirse la transducción de la onda sonora, es indispensable un movimiento coordinado de los estereocilios de las IHCs y la regulación por parte de las OHCs. La no alineación de los estereocilios en las IHCs posiblemente guarde una estrecha relación con la baja expresión de los genes *Cdh23* y *Pcdh 15*, ya que las proteínas que transcriben están implicadas en las uniones entre estos apéndices. Esta disposición anárquica es incompatible con la deflexión sincrónica de todos los estereocilios que determina la apertura y cierre de canales. Por su parte, la reducción en la expresión de la prestina ocasiona una pérdida de movilidad de las OHC, lo que puede afectar a la regulación de la captación del estímulo sonoro y se relaciona directamente con las alteraciones en el sistema eferente que se describen en el estudio del punto siguiente 3.2 (Sánchez-Benito et al., 2017).

Todos estos datos pueden indicar una reducción de las señales en el origen del impulso nervioso y provocaría una disminución de las señales glutamatérgicas que se originan en la cóclea y alcanzan los núcleos cocleares. No obstante, este punto de la vía también recibe sinapsis glutamatérgicas intrínsecas de los propios núcleos y otras de origen somatosensoriales desde otras localizaciones del sistema nervioso. Ante la falta de señales auditivas podría existir un mecanismo compensatorio proveniente de señales somatosensoriales, provocando la distribución anómala de terminales marcados con VGLUT2. Se ha demostrado que los receptores glutamatérgicos están implicados en los mecanismos de iniciación y propagación de las crisis epilépticas desde el IC, por lo que estas modificaciones de los patrones presinápticos podrían alterar los circuitos neuronales en el colículo y explicar así la susceptibilidad a padecer crisis audiogénas.

Por tanto, todas las alteraciones morfológicas y moleculares descritas podrían derivar en una liberación anómala de glutamato en el núcleo epileptógeno que generaría señales discordantes y provocarían las descargas asincrónicas responsables de las crisis convulsivas.

3.2. Alteraciones morfológicas en el sistema eferente olivoclear del modelo de epilepsia audiogénica GASH/Sal

Sánchez-Benito, D., Gómez-Nieto, R., Hernández-Noriega, S., Murashima, A. A. B., de Oliveira, J. A. C., García-Cairasco, N., López, D. E., & Hyppolito, M. A. (2017). Morphofunctional alterations in the olivocochlear efferent system of the genetic audiogenic seizure-prone hamster GASH:Sal. *Epilepsy & Behavior*, 71, 193-206. <https://doi.org/10.1016/j.yebeh.2016.05.040>. FI: 2,335. Q2

Introducción: el hámster GASH/Sal es un modelo de epilepsia desarrollado en el bioterio de la Universidad de Salamanca que sufre convulsiones audiogénas generalizadas cuando es expuesto a un sonido de alta intensidad. En otros modelos animales con esta enfermedad se han descrito una serie de alteraciones en distintas estructuras troncoencefálicas que podrían estar relacionadas con dicha susceptibilidad.

Hasta ahora, no se había realizado ningún estudio morfológico de la vía auditiva del GASH/Sal que intentase dilucidar las bases anatómicas subyacentes a las crisis audiogénas. El SOC es un conjunto de núcleos que intervienen en múltiples aspectos de la audición, y contiene las neuronas del conocido como sistema olivoclear que inerva la cóclea. Se divide a su vez en dos, en función del origen de las proyecciones que inervan el órgano de Corti: 1) Sistema olivoclear lateral (LOC): se origina en la LSO y termina en el arranque axónico de la base de las IHC de la cóclea ipsilateral; y 2) Sistema olivoclear medial (MOC): se origina en el VNTB y termina en la base de las OHC de la cóclea contralateral predominantemente. Este segundo sistema es más complejo, e incluye también proyecciones a los CN y fibras descendentes desde el IC y la corteza auditiva. Además, existe una tercera clase de neuronas olivocleares rodeando la LSO, las neuronas *shell*. La función de esta vía descendente es, de forma general, modular la sensibilidad del receptor auditivo.

El objetivo de este estudio es determinar si el sistema olivoclear eferente del GASH/Sal presenta alteraciones funcionales y/o morfológicas que puedan explicar la susceptibilidad a sufrir crisis convulsivas audiogénas.

Métodos: la realización de los experimentos requirió de 9 animales controles (*Mesocricetus auratus*) y de 16 hámsteres GASH/Sal todos machos de 4 meses de edad. Para evaluar la función auditiva, se analizaron las DPOAEs y los ABR. Las DPOAEs son sonidos fisiológicos de baja intensidad producidos por la contracción de las células ciliadas externas de la cóclea en respuesta a estímulos auditivos de un amplio rango de frecuencias. Los ABR miden la señal bioeléctrica que se transmite a través del tronco del encéfalo cuando la cóclea detecta un sonido. Esta señal eléctrica puede ser captada por una serie de electrodos y está representada por entre 5 y 7 ondas que se corresponden con cada una de las estaciones de la vía auditiva por las que viaja este impulso: nervio auditivo, CN, SOC, lemnisco lateral e IC, núcleo geniculado medial y núcleos auditivos tálamocorticales. Los resultados obtenidos con estas dos pruebas se correlacionaron con un análisis de la estructura del órgano de Corti, realizado con microscopía electrónica de barrido.

Para el estudio morfológico de las neuronas olivococleares, se realizaron inyecciones en la cóclea izquierda de un trazador retrógrado, Fluoro-Gold (FG). Este trazador difunde hasta los somas de las neuronas olivococleares presentes en el SOC. Una vez perfundidos los cerebros de los animales, este trazador se visualizó mediante marcaje inmunohistoquímico. Esto permitió realizar análisis morfométricos de las neuronas MOC y LOC utilizando el programa ImageJ (versión 1.42; Rasband, N.S., National Institutes of Health, Bethesda, Maryland, USA). Además, el estudio se completó con la reconstrucción tridimensional de la LSO mediante el software Neurolucida (versión 10) y NeuroExplorer (version 3) de MicroBrightField Bioscience, (Williston, VT, USA), lo que nos permitió evaluar el volumen de la LSO. Para ello, se utilizaron secciones cerebrales seriadas inmunoteñidas de forma alternativa con anticuerpos para visualizar la CaBP, una proteína específica de la LSO, y contrastadas con violeta de cresilo.

Resultados: el análisis de los ABR mostró un aumento de los umbrales auditivos de los hámsteres GASH/Sal en comparación con los controles, acompañado de una ampliación de la latencia de cada una de las ondas en el oído izquierdo frente al derecho, aspecto que no era visible en los controles. Además, el GASH/Sal mostraba unas latencias entre los picos III-V y I-V significativamente superiores a las obtenidas en el control. Por otra parte, se observó una asimetría entre ambos oídos que se hacía

evidente a partir de la onda III, es decir, más rostral a los núcleos cocleares, lo que motivó parte del diseño de nuestro artículo Sánchez-Benito et al. (2020).

Por otro lado, no se detectaron otoemisiones ante estímulos de frecuencias de entre 500 y 6000 Hz en los animales epilépticos. A partir de esa frecuencia, sí se recogieron, pero con una mayor amplitud en el oído izquierdo.

Para intentar encontrar una explicación a esta falta de respuesta, se analizó la estructura del órgano de Corti mediante microscopía electrónica de barrido. Los hámsteres controles mostraban la estructura característica del receptor sensitivo, con las células ciliadas perfectamente dispuestas y acompañadas por las células de soporte formando tres filas de OHC separadas de una única fila IHC. Las primeras presentaban sus estereocilios dispuestos en forma de “V”, mientras que las internas formaban una fila recta o ligeramente curvada. Sin embargo, en los GASH/Sal, pese a disponer de ambos tipos celulares distribuidos de forma más o menos similar, la organización de los estereocilios resultaba ser mucho más anárquica, que se percibía de manera más evidente en la espira basal de la cóclea. La mayoría de las células ciliadas mostraba una desorganización de los cilios propiciada por una aparente pérdida de unión entre ellos.

El estudio continuó con el análisis de las neuronas olivococleares marcadas retrógradamente tras la inyección de FG en la cóclea. En el VNTB, encontramos neuronas MOC características, grandes y multipolares, prevalentemente en el lado contralateral a la inyección del trazador en una proporción 4:1.

Dentro y alrededor de la LSO, localizamos neuronas LOC marcadas retrógradamente intrínsecas y extrínsecas. Las intrínsecas tenían forma oval, con tres dendritas primarias; mientras que las *shell* eran mayores, con un soma poligonal, globular o alargado y dos o más dendritas que se extendían a lo largo de los ejes medio-lateral y rostro-caudal de la LSO. En este caso, aproximadamente el 90% de las neuronas se encontraban predominantemente en el lado ipsilateral a la inyección. No se observaron alteraciones en la distribución rostrocaudal de estas neuronas al comparar el animal epiléptico con el control, pero sí se reportaron diferencias en la ratio ipsi-contralateral de las neuronas MOC y LOC. Las variaciones más evidentes fueron descritas al comparar los tamaños celulares, ya que los tres tipos neuronales en los hámsteres

GASH/Sal tienen somas más pequeños. Para comprobar si estos tamaños neuronales afectaban al tamaño global de la LSO, se llevó a cabo la reconstrucción tridimensional de este núcleo, concluyendo que existe una reducción aproximada del 30% del volumen total.

Discusión y conclusiones: este estudio muestra alteraciones funcionales y morfológicas existentes en el sistema eferente olivoclear del GASH/Sal. El aumento del umbral auditivo concuerda con los trabajos previos publicados en nuestro laboratorio, lo que confirma una pérdida de sensibilidad auditiva en el hámster GASH/Sal. Esta disfunción sensitiva puede estar relacionada con la pérdida de organización y, posiblemente, de funcionalidad de los estereocilios de las IHC observada en las microfotografías electrónicas.

Además, la ausencia de DPOAEs en un amplio espectro de frecuencias implica alguna alteración en la función del sistema olivoclear medial. Este sistema es el encargado de modular la ganancia del amplificador coclear, interfiriendo en la contractibilidad de las OHC y en el movimiento de los estereocilios.

Las observaciones de la distribución y apariencia de estos estereocilios, tanto de las IHC como de las OHC, no se traduce en una reducción significativa en el número de neuronas LOC y MOC encargadas de su regulación, pero sí en el tamaño del soma neuronal, así como del tamaño total de la LSO.

Existen proyecciones ascendentes y descendentes entre la LSO y el VNTB y el IC, estructura que se ha demostrado que es clave en el comienzo de las crisis audiogénas. La falta de estas interconexiones podría estar afectando al sistema eferente olivoclear, contribuyendo a una reorganización de las vías neuronales y al desbalance responsable de provocar la susceptibilidad y comienzo de las crisis en el IC ante la llegada de un estímulo sonoro intenso.

Todas estas anomalías funcionales y estructurales se han descrito en animales que no habían sido expuestos previamente a ningún estímulo y no habían sufrido, por lo tanto, ningún episodio epileptógeno. Esto hace suponer que en relación con el órgano

de Corti y su modulación, tanto la base fisiológica como anatómica del GASH/Sal tienen un origen genético y no se produce por las crisis convulsivas.

De este modo, se puede concluir que nuestro modelo animal de crisis convulsivas audiógenas presenta, de forma inherente, alteraciones funcionales en el receptor auditivo que se encuentran íntimamente relacionadas con variaciones estructurales y morfológicas del receptor coclear y del sistema eferente olivococlear. Este sistema es el encargado de modular la ganancia de la cóclea mejorando la audición; su mal funcionamiento podría estar implicado en una sobreestimulación que llevaría a la iniciación y propagación de las crisis audiógenas en el GASH/Sal.

3.3. Correlato morfológico y molecular de la sensibilidad auditiva alterada en el hámster GASH/Sal

López-López, D., Gómez-Nieto, R., Herrero-Turrión, M. J., García-Cairasco, N., Sánchez-Benito, D., Ludeña, M. D., & López, D. E. (2017). Overexpression of the immediate-early genes Egr1, Egr2, and Egr3 in two strains of rodents susceptible to audiogenic seizures. *Epilepsy & Behavior*, 71, 226-237.
<https://doi.org/10.1016/j.yebeh.2015.12.020>. FI: 2,60. Q2

Introducción: la epilepsia es un desorden neurológico muy complejo que se puede abordar desde diversas perspectivas. A pesar de los grandes avances realizados, sigue siendo necesario profundizar en el conocimiento de esta enfermedad y, para ello, se disponen de una gran variedad de modelos para estudios *in silico*, *in vivo* e *in vitro*. Los modelos *in vivo* de origen genético más utilizados son aquellos que sufren crisis convulsivas tras ser expuestos a un sonido de alta intensidad. Este estudio se centra en la comparación y caracterización de dos cepas con epilepsia audiogénica de origen genético: las ratas WAR y los hámsteres GASH/Sal. La primera se trata de una cepa genéticamente seleccionada a principios de los años 90 en la Escuela de Medicina de Ribeirão Preto en Brasil. El hámster GASH/Sal, por su parte, fue desarrollado en la Universidad de Salamanca.

De forma similar a lo que les ocurre a otros modelos con epilepsia audiogénica, la activación de la vía auditiva es crucial y, en concreto, el IC juega un papel fundamental en la génesis de las crisis. Por ello, con el fin de encontrar procesos moleculares similares entre ambas cepas, se ha llevado a cabo un análisis comparativo de los perfiles de expresión genética en el IC.

Este estudio pretende contribuir a la comprensión los mecanismos moleculares asociados a la predisposición genética a la epilepsia y así reconocer nuevas dianas que podrían ser útiles en el desarrollo de nuevos fármacos antiepilepticos.

Métodos: para la consecución de los objetivos de este experimento se necesitaron 17 ratas WAR, 6 ratas controles (*Rattus norvegicus*), 16 GASH/Sal y 12 hámster sirios controles (*Mesocricetus auratus*). Todos estos animales fueron expuestos a estimulación acústica intensa (115-120dB) y 60 minutos después, fueron perfundidos transcardialmente para los estudios inmunohistoquímicos o eutanasiados rápidamente para la obtención del IC, del que se extrajo el mRNA para los análisis moleculares. Además, se tomaron muestras de tejido de los linfomas que desarrollan algunos de los hámsteres GASH/Sal.

Los estudios de biología molecular consistieron en análisis de expresión por *microarray* (Rat Gene 1.0 ST y MicroarrayMoGene 1.0 ST para rata y hámster respectivamente), análisis del transcriptoma del núcleo epileptógeno y RT-qPCR de determinados genes.

Los *microarrays* se realizaron en el Centro de Investigación del Cáncer de Salamanca y se comparó cada modelo animal con su control, seleccionando aquellos genes cuya expresión estaba aumentada o disminuida 2 veces o más respecto al control (Fold change, $|FC| \geq 2$). Los datos obtenidos en este estudio han sido anotados en la base de datos Gene Expression Omnibus (*accession numbers* GSE74150 y GSE74043 para las líneas WAR y GASH/Sal respectivamente).

Para la realización del transcriptoma, tras una crisis convulsiva, se obtuvo un pool de RNA del núcleo epileptógeno de tres animales de cada grupo, con los que se crearon librerías que fueron secuenciadas. Así, se obtuvieron una ingente cantidad de mRNA correspondiente a genes expresados tras una estimulación sonora, datos que también han sido anotados en el NCBI Bio Project (*accession number* 230618).

Para corroborar los resultados obtenidos en el transcriptoma, se realizaron RT-qPCR de los genes cuya expresión estaba alterada en ambas cepas, utilizando la β -actina como gen de referencia. Además, se llevaron a cabo inmunotinciones para detectar las proteínas codificadas por estos genes sobre secciones de cerebro de 40 μm y sobre secciones de 3 μm de tejido extraído de los linfomas del GASH/Sal.

Resultados: los microarrays realizados en ambos modelos animales proporcionaron una amplia lista de genes, de los que se seleccionaron aquellos que presentaban un $|FC| \geq 2$ y se obtuvieron 15 genes al comparar el GASH/Sal con su control y 71 al hacer lo propio con la rata WAR. Estos genes no guardaban relación aparente entre ellos y estaban implicados en muy diversas funciones. Al comparar los dos modelos, solo se encontró un gen común: el *Egr3*, sobreexpresado en ambos modelos. Se trata de un gen de respuesta temprana que actúa como factor de transcripción en muchos procesos. Para comprobar este resultado, se realizaron análisis RT-qPCR de éste y de otros dos genes de la misma familia: *Egr1* y *Egr2*. Los tres genes estaban muy sobreexpresados tanto en las ratas WAR como en el GASH/Sal estimulados al compararlas con sus respectivos controles. También, se evaluó el efecto de la estimulación sonora sobre la expresión génica, analizando la expresión del núcleo epileptógeno de ambas cepas epilépticas con y sin estimulación acústica. El resultado fue una expresión muy superior de los tres genes cuando ambas cepas eran expuestas a un sonido.

Los análisis inmunohistoquímicos mostraron un patrón de distribución similar de la proteína EGR3 en las dos especies. Se detectó inmureactividad en toda la vía auditiva, tanto en animales estimulados como en los no estimulados. En el IC, se encuentran neuronas inmunoteñidas en las tres divisiones del núcleo, aunque con mayor prevalencia en las cortezas dorsal y externa. También, aparecen inmunoteñidos los núcleos cocleares y, fuera de la vía auditiva, el hipocampo. Como este factor de transcripción está implicado en la proliferación de linfocitos B y T, se examinó la presencia de esta proteína en los linfomas que desarrolla la cepa GASH/Sal, encontrando que esta proteína se localiza en el citoplasma de células linfoideas del tejido neoplásico.

Por último, el análisis del transcriptoma realizado en el hámster GASH/Sal estimulado y en controles, muestra la sobreexpresión de los genes *Egr2*, *Egr3* y *Egr1*, este último no se había observado en los *microarrays*.

Discusión y conclusiones: la comparación de la expresión génica entre el hámster GASH/Sal y su control y la rata WAR y su control mediante el empleo sondas predichas y bien anotadas de mensajeros (*microarrays* específicos) permite detectar la

sobreexpresión de un gen común a ambas especies: el *Egr3*. Este dato pudo confirmarse a través de la RT-qPCR, donde además se mostró que *Egr1* y -2 estaban sobreexpresados. La diferencia de resultados entre ambas metodologías puede ser debida a las distintas sondas utilizadas, ya que el microarray empleado para los hámsteres era de ratón (en el momento de realizar los experimentos no había disponible ninguno para hámster) o a los distintos métodos de normalización.

Egr1, *Egr2* y *Egr3* son genes de respuesta temprana, cuya expresión es rápidamente inducida por una gran cantidad de estímulos celulares. Pertenecen a la familia EGR que presenta motivos estructurales en dedos de Zinc capaces de unirse a DNA, RNA o proteínas. Los factores que suscitan su transcripción incluyen el estrés externo, tanto físico como químico, o estresores internos. Esto provoca la expresión de *Egr* en sitios tan diversos como las glándulas adrenales o el hipocampo. Se ha descrito que *Egr1* está implicado en procesos de aprendizaje y memoria y *Egr3* en plasticidad neuronal. *Egr1*, *Egr2* y *Egr3* intervienen en la adaptación a nuevos estímulos, lo que explicaría su presencia en núcleos auditivos en este experimento.

Muchos procesos relacionados con la hiperexcitabilidad neuronal provocan la sobreexpresión de estos genes de la familia *Egr*. Se ha observado, por ejemplo, en las convulsiones inducidas por ácido kaínico.

La sobreexpresión de *Egr3* puede estar alterando diversos procesos fisiológicos relacionados con la epilepsia como son: 1) la regulación de la expresión de genes implicados en la actividad motora; 2) la alteración en la expresión de la subunidad $\alpha 4$ del receptor GABA_A, que media la inhibición en el sistema nervioso central; y 3) la formación de dendritas y axones durante el desarrollo del sistema nervioso central, que junto con *Egr2* interviene en la mielinización del sistema nervioso periférico. Además, *Egr2* y *Egr3* están implicados en el control de procesos inflamatorios y en la proliferación de linfocitos B y T, lo cual concuerda con la inmunorreactividad descrita en los linfomas del GASH/Sal. *Egr3* también se sobreexpresa en otros tipos de cáncer como en el de próstata o el de pecho.

Como conclusión, los eventos ictales de los modelos con epilepsia audiogena WAR y GASH/Sal provocan desregulación génica en el colículo inferior.

Las limitaciones técnicas de los análisis por *microarray* requieren la validación mediante RT-qPCR. Ambos modelos presentan sobreexpresión de los genes de respuesta temprana *Egr1*, *Egr2* y *Egr3*, presumiblemente debido al estrés asociado a las crisis convulsivas. Estos genes son factores de transcripción que están relacionados con procesos de mielinización, crecimiento celular, apoptosis y activación de otros genes reguladores.

4. DISCUSIÓN

*La desdichada Isabela
de improviso mide el suelo
con un espantoso grito
con un desmayo violento.
¿No ve que brama y patea?*

*—Ay
¡Habló!
—No hay mal que sea
tan semejante a morir*

La difunta pleiteada, Lope de Vega

En los tres trabajos que componen esta tesis doctoral, hemos reportado anomalías morfológicas y moleculares del órgano de Corti como epitelio sensorial auditivo, así como de los primeros núcleos de la vía auditiva del GASH/Sal en comparación con el hámster dorado control. Hemos encontrado alteraciones morfológicas en la cóclea que concuerdan con la disminución de los niveles de expresión de genes relacionados con la organización de los estereocilios descrita en los dos últimos estudios. Estas alteraciones morfológicas, concuerdan con el aumento del umbral auditivo y la disminución de la amplitud de la onda I detectada por los ABR. Todos estos datos, unidos a la degeneración de las SGNs y la atrofia de la estría vascular, nos llevan a pensar que el hámster GASH/Sal tiene problemas en la captación, procesamiento y propagación de la información auditiva. Esto queda plasmado en la reducción de la expresión de genes relacionados con la señalización del glutamato, neurotransmisor principal en el inicio de la vía auditiva. Además, hemos demostrado que existe una deficiencia en la regulación del receptor llevada a cabo por parte del sistema olivococlear. Por lo tanto, las señales de entrada aberrantes, unidas a un déficit en la regulación de la captación de sonidos puede conllevar a la llegada de estímulos discordantes al IC, comenzando en este núcleo una cascada de señalización a través de distintos factores de transcripción, como *Egr3*, que podría traducirse en el comienzo de las crisis convulsivas.

Antes de la publicación de estos trabajos, ya había sido descrito un déficit auditivo en nuestro modelo animal GASH/Sal (Muñoz et al., 2017). Además, los ABR muestran una reducción de la amplitud de la onda I y la onda IV. La onda I, capta las despolarizaciones sincronizadas de las fibras que componen el nervio auditivo, mientras que la onda IV hace lo propio con la actividad neuronal del IC (Church & Kaltenbach, 1993). Por tanto, estos resultados indican algún tipo de neuropatía coclear, así como actividad neuronal aberrante en el núcleo epileptógeno. La reducción de la onda I se ha relacionado con pérdida de células ciliadas ocurrida tras la exposición a un ruido intenso o la edad, y puede venir acompañado con deficiencias auditivas, tinnitus e hiperacusia (Liberman & Kujawa, 2017). La histología de las cócleas del GASH/Sal concuerda con esta afirmación. La desorganización de los estereocilios de las IHC, provocada seguramente por la menor presencia de las proteínas CDH23 y PCDH15 que se les unen, indican una

mala mecanotransducción y, por lo tanto, una reducción en la señal enviada (Alagramam et al., 2011; Jeng et al., 2020). Además, la degeneración de la estría vascular, directamente implicada en el mantenimiento del potencial endococlear (Patuzzi, 2011), podría estar también contribuyendo a esta transducción sonora deficiente reflejada en la menor amplitud de la onda I.

Por otro lado, la menor expresión de la prestina en el GASH/Sal sugiere una menor electromotilidad de las OHC, afectando a la amplificación coclear (Liberman et al., 2002). En línea con esto, hemos descrito cambios en las células de Deiters, con un incremento en las microvellosidades que se ha asociado a también a la pérdida de sensibilidad auditiva (Flock et al., 1999). Todas estas alteraciones, incluidas las descritas para las células de soporte, son comunes a otros modelos con epilepsia audiogena de origen genético como las ratas GEPR (Penny et al., 1983) y los ratones *Black Swiss* (Charizopoulou et al., 2011).

El hámster GASH/Sal presenta, según lo descrito anteriormente, modificaciones estructurales asociadas a la captación y amplificación del sonido. Además, la ausencias de DPOAEs indican alteraciones en el sistema eferente olivococlear que puede estar modificando sustancialmente el proceso de audición. Las funciones de estas proyecciones olivococleares se relacionan con protección ante ruidos de alta intensidad (Maison & Liberman, 2000), detección selectiva de ruidos en ambientes ruidosos (Kawase & Liberman, 1993) y modulación de la sensibilidad coclear (Ryugo, 2011). Hemos descrito una lateralización del sistema eferente, con predominancia del oído izquierdo en el GASH/Sal. Esta predominancia de uno de los lados de la vía auditiva no es de extrañar, pues ya ha sido descrita con anterioridad en humanos (Khalfa & Collet, 1996), aunque en nuestro caso llama la atención que no ocurre en los hámsteres controles. En consonancia con esto, se ha descrito una reducción significativa de la amplitud de las DPOAEs en pacientes con epilepsia del lóbulo temporal (Brodtkorb et al., 2005). Este autor hipotetiza que son las propias crisis las que provocan este daño en la función auditiva, pero nuestro modelo animal presenta las anomalías descritas sin haber sufrido crisis desde su nacimiento, por lo que las tiene de forma innata, y son más causa que consecuencia de la susceptibilidad a sufrir crisis epilépticas.

La ausencia de DPOAEs, compatible con un sistema eferente dañado, tiene su correlato anatómico tal y como mostramos en el trabajo de 2017. El sistema olivococlear, descrito en la introducción, parte de las conocidas como neuronas MOC y LOC situadas en el VNTB y LSO respectivamente. Los datos aportados por nuestro estudio no indican degeneración de estas neuronas. De hecho, el número de neuronas olivococleares, tanto MOC como LOC, en el GASH/Sal no fue significativamente inferior al contabilizado en el hámster control. No obstante, los déficits de ABR y DPOAES no implican necesariamente la degeneración de las neuronas olivococleares (Reuss et al., 2016). Sí encontramos, en cambio, variaciones en el tamaño de los somas neuronales. Las neuronas MOC (ipsi y contralaterales) y LOC ipsilaterales son más pequeñas que sus homónimas en el hámster GASH/Sal. También, describimos diferencias entre el tamaño de las neuronas ipsi y contralaterales, pero no podemos relacionarlo directamente con la asimetría funcional previamente descrita ya que el número de neuronas LOC contralaterales y MOC ipsilaterales es tan reducido, que la estadística no es fiable. Para poder validar este resultado, deberemos diseñar un nuevo experimento con inyecciones de FG en la cóclea en ambos lados.

Para verificar si la disminución del tamaño neuronal podría conllevar a la reducción del tamaño del núcleo, llevamos a cabo la reconstrucción tridimensional de la LSO. De este modo, determinamos que la LSO del hámster GASH/Sal es más pequeña que la del hámster control, por lo que el menor tamaño de los somas está provocando una disminución en el volumen total del núcleo. Otros estudios, como el de Loftus en el año 2000, ya apoyan esta idea de que el colapso de las neuronas que conforman un núcleo provoca una disminución del tamaño del mismo (Loftus et al., 2000). Realizamos este experimento solo en la LSO gracias a la especificidad de marcaje de esta estructura con CaBP, pero ya estamos analizando el tamaño del VNTB, así como de otros núcleos auditivos mediante su reconstrucción tridimensional en secciones seriadas contrastadas con la tinción de Nissl.

La LSO y el VNTB están implicadas en el envío de señales ascendentes al IC (Warr & Beck, 1996) y éste a su vez envía de vuelta órdenes descendentes (Faye-Lund, 1986; Gómez-Nieto et al., 2008) a través del sistema eferente. Hemos descrito numerosas alteraciones de esta retroalimentación tanto a nivel estructural como funcional. Por

tanto, el sistema eferente del GASH/Sal no es capaz de regular la respuesta de la cóclea ante un ruido de alta intensidad y como el IC es el núcleo clave en la iniciación de las AGS (Wada et al., 1970), déficits en estas conexiones recíprocas podrían contribuir a la epileptogénesis en el GASH/Sal.

Todas las alteraciones morfológicas y moleculares en el órgano de Corti son consistentes con la pérdida de SGNs y la desaferenciación del nervio auditivo. Normalmente, se utiliza la presencia VGLUT1 y VGLUT2 como marcadores de la liberación de glutamato en el nervio auditivo (Takamori, 2006), ya que se expresa en las SGNs pero no en las células ciliadas (Seal et al., 2008). Nuestras RT-qPCR muestran una reducción de ambos transportadores en la cóclea del GASH/Sal, lo que confirma una menor transducción de estímulos auditivos. El nervio auditivo es la mayor fuente excitatoria de los CN, y nuestros resultados implican una disminución de la concentración de glutamato en los mismos. Además de esta fuente glutamatérgica, los CN reciben proyecciones intrínsecas de los núcleos cocleares contralaterales, así como información somatosensorial diversa (Rubio, 2019), por lo que los resultados obtenidos no sólo dependen de los aferentes auditivos primarios, sino de todas aquellas aferencias que les llegan. En los núcleos cocleares, VGLUT1 se asocia sobre todo a los terminales auditivos, mientras VGLUT2 lo hace con todos aquellos terminales somatosensoriales (Gómez-Nieto & Rubio, 2009; Zhou et al., 2007). Para evaluar el papel de estas proyecciones extrínsecas a la vía auditiva en los núcleos cocleares, realizamos un análisis de la distribución de VGLUT2 en el GASH/Sal. Encontramos una mayor densidad de VGLUT2 tanto en el PVCN como en el AVCN del hámster epiléptico en comparación con los controles. Este aumento puede deberse a un mecanismo de compensación de señales somatosensoriales por la falta de señales glutamatérgicas del nervio auditivo, y supondría un foco más de generación de señales aberrantes que llegarían al IC. Un alto número de terminales VGLUT2 en las células *bushy* podría tener un efecto adverso en las aferencias del VCN. Hay varios estudios que relacionan el tinnitus y la hiperacusia con desaferenciación coclear o la neuropatía y una elevada hiperactividad debido a un desbalance entre las señales auditivas y somatosensoriales que llegan al VCN (Heeringa et al., 2018; Liberman & Kujawa, 2017; Vogler et al., 2011; Zeng et al., 2009). Animales con tinnitus tienen una sobreexpresión de VGLUT2 en varias subdivisiones de los CN

(Heeringa et al., 2018). Esto concuerda con el aumento de densidad de VGLUT2 descrito tras un daño coclear (Heeringa et al., 2016; Zeng et al., 2009).

Por otro lado, en la región de las células grano de los CN encontramos que la densidad de VGLUT2 en el GASH/Sal es menor que en la misma región del hámster control, y no apreciamos diferencias significativas en el DCN. Esto indica que las anomalías estructurales y moleculares en la cóclea de los GASH/Sal afecta de forma diferente a la señalización glutamatérgica en cada subdivisión de los núcleos cocleares del GASH/Sal, y, por tanto, cada una de las vías aferentes que alcanzan el IC podrían estar afectadas en distinta medida. En relación con esta hipótesis, nuestros estudios mostraron menores niveles de transcripción de *Vglut1* y *2* en el IC, sugiriendo una desregulación presináptica de la liberación de glutamato en este núcleo. Los patrones de liberación de VGLUT1 y VGLUT2 en el IC constituyen la base estructural de la organización tonotópica del IC (Malmierca, 2003), por lo que la posible desregulación existente en el GASH/Sal podría alterar este mapa de frecuencias y desencadenar la hiperexcitabilidad en el IC. Hay varios estudios de inmunoreactividad por c-Fos en el IC de modelos de roedores con AGS tanto genéticos como inducidos que aportan evidencias claras que un deterioro en la organización tonotópica del IC está detrás de la susceptibilidad a sufrir AGS (Klein et al., 2004; Pierson & Snyder-Keller, 1994). Parece contradictorio pensar que si el GASH/Sal tiene una mecanosensibilidad limitada en la cóclea, esto pueda provocar la hiperexcitabilidad necesaria para el desencadenamiento de las crisis epilépticas. La pérdida auditiva y la susceptibilidad a sufrir AGS podrían ser dos patologías dependientes o independientes que comparten el mismo correlato morfológico y molecular. No obstante, al igual que en otros modelos que sufren AGS, la susceptibilidad del GASH/Sal a sufrir estas crisis, está muy ligada a una edad muy concreta por lo que desaparecerían con el avance de la pérdida auditiva (Henry, 1985; Henry & Buzzone, 1986). Tal como se indica anteriormente, hay estudios que afirman que la susceptibilidad audiogena provocada por un trauma sonoro en neonatos depende de alteraciones en la representación tonotópica en el IC, el cual se debe seguramente a un desarrollo anormal de la cóclea (Garcia-Cairasco, 2002; Pierson & Snyder-Keller, 1994). Las imágenes de microscopía electrónica muestran alteraciones en la parte más basal de la cóclea (altas frecuencias) del GASH/Sal, lo que apoyaría esta hipótesis. Sin

embargo, la pérdida de SGNs descrita afecta por igual a toda la extensión del órgano de Corti.

Hemos descrito alteraciones morfológicas y moleculares en el receptor auditivo, así como en el sistema eferente encargado de su regulación que conllevan cambios en la señalización de la vía auditiva y la llegada de información aberrante en el IC. Al estudiar el perfil de expresión génico en el IC del GASH/Sal respecto el control, encontramos una desregulación génica, con genes sobreexpresados y otros infraexpresados. Destacamos el incremento en la expresión del gen *Egr3*, aspecto que comparten el GASH/Sal y las ratas WAR, que también presenta epilepsia audiogena. Este gen, junto a otros de la misma familia, pertenece a una familia de genes de respuesta temprana inducida por una gran variedad de factores (Beckmann & Wilce, 1997; Patwardhan et al., 1991). *Egr3* se ha relacionado con plasticidad neuronal en respuesta a estrés y a estímulos novedosos (Gallitano-Mendel et al., 2007). Hemos observado un aumento de la expresión de este factor de transcripción en distintas situaciones en las que existe hiperexcitabilidad neuronal, como la producida por la abstinencia alcohólica (Beckmann et al., 2002) o las convulsiones inducidas por ácido kaínico (Honkaniemi & Sharp, 1999). Además, se puede observar un aumento de la expresión de *Egr3* en el hipocampo de humanos con epilepsia del lóbulo temporal (Roberts et al., 2006). Este gen, tras las convulsiones epilépticas, también induce la expresión de una subunidad aberrante del receptor GABRA4, haciéndolo disfuncional (Grabenstatter et al., 2012). Este receptor GABA está implicado en procesos inhibitorios dentro del sistema nervioso central muy importante en el control de las crisis epilépticas.

Este estudio ha supuesto la descripción por primera vez de un gen sobreexpresado en el foco epileptogénico del hámster GASH/Sal.

Finalmente, hay que destacar en modelos animales de AGS, siempre se ha puesto el foco en el IC, núcleo epileptógeno (Faingold et al., 1992; García-Cairasco, 2002), pero apenas se había prestado atención a las estaciones subcoliculares y su posible implicación en la generación de las crisis convulsivas.

Los trabajos aquí expuestos suponen una primera aproximación al conocimiento sobre los eventos que preceden al inicio de las crisis convulsivas en el IC. Obviamente, aún queda mucho por estudiar para entender completamente el proceso, pero podemos suponer que debido a las alteraciones estructurales descritas y a los cambios en la expresión de algunos genes, se generan una serie de señales aberrantes que se magnifican por la falta de regulación. Estas señales alcanzan el IC en donde no pueden ser procesadas correctamente y se produce la hiperexcitación por parte de este centro integrador troncoencefálico. En cualquier caso, debemos continuar abordando el estudio de la vía auditiva en animales con epilepsia audiogénica para desenmarañar el sustrato morfológico y molecular de las alteraciones auditivas implicadas en la susceptibilidad a padecer AGS, y el hámster GASH/Sal se ha erigido como una herramienta tremadamente útil para este fin.

5. CONCLUSIONES

Cuando desperté tuve un vago recuerdo de lo ocurrido, sin poder identificar el lugar donde me encontraba. Un estremecimiento se agitó en mi pecho. (...) Sentía ansiedad, miedo, un endurecimiento en los brazos y un desgarrón en la corteza cerebral. (...) De pronto caí en un sueño profundo, como si dormir fuera una forma de alejarme de la soledad de la epilepsia.

La piel del miedo, Javier Vásconez

Primera

El modelo de epilepsia audiogénica GASH/Sal presenta un déficit auditivo acentuado, con umbrales auditivos más elevados que los detectados para los hámsteres controles.

Segunda

En el órgano de Corti del GASH/Sal, se observan alteraciones morfológicas en los estereocilios de las células ciliadas internas y externas, déficits en la expresión de proteínas implicadas en la organización de los estereocilios, degeneración de las células ganglionares y atrofia de la estría vascular, lo que pudiera ser responsable de problemas en la captación, procesamiento y propagación de la información auditiva

Tercera

El hámster GASH/Sal exhibe atrofia en las neuronas olivococleares y déficits en las emisiones otoacústicas, indicando alteraciones en el sistema eferente olivoclear.

Cuarta

Hay disminución en la expresión de genes codificantes de proteínas transportadoras de glutamato tipo 1 y 2, tanto en la cóclea como en los núcleos cocleares del GASH/Sal, denotando una falta de señales excitatorias.

Quinta

El patrón de distribución de la proteína VGLUT2 en los núcleos cocleares del GASH/Sal, indica la existencia de algún tipo de mecanismo compensatorio de las vías somatosensoriales para subsanar la falta de estímulos auditivos.

Sexta

Todas las alteraciones de las estaciones subcoliculares descritas aparecen de forma inherente a la cepa GASH/Sal, y no son consecuencia de la severidad de las crisis epilépticas, ya que todos los animales utilizados en este trabajo, excepto los de expresión del colículo inferior, son animales que no han sufrido estimulación auditiva.

Séptima

La estimulación sonora genera un patrón de respuesta alterado que llevan a la sobreexpresión de genes de expresión temprana asociados al estrés en el núcleo epileptógeno, el colículo inferior, implicados en rutas de señalización relacionadas con plasticidad neuronal, procesos de mielinización y apoptosis.

Octava

El presente estudio pone de manifiesto que existen alteraciones subcoliculares implicadas en el inicio de las crisis convulsivas audiogénas en el modelo de epilepsia GASH/Sal.

6. BIBLIOGRAFÍA

- Alagramam, K. N., Goodyear, R. J., Geng, R., Furness, D. N., van Aken, A. F. J., Marcotti, W., Kros, C. J., & Richardson, G. P. (2011). Mutations in Protocadherin 15 and Cadherin 23 Affect Tip Links and Mechanotransduction in Mammalian Sensory Hair Cells. *PLoS ONE*, 6(4), e19183. <https://doi.org/10.1371/journal.pone.0019183>
- Barrera Bailón, B. (2013). Validación del hámster GASH:Sal como modelo de epilepsia: Estudio farmacológico y neuroetológico. Universidad de Salamanca.
- Barrera-Bailón, B., Oliveira, J. A. C., López, D. E., Muñoz, L. J., Garcia-Cairasco, N., & Sancho, C. (2013). Pharmacological and neuroethological studies of three antiepileptic drugs in the Genetic Audiogenic Seizure Hamster (GASH:Sal). *Epilepsy & Behavior*, 28(3), 413-425. <https://doi.org/10.1016/j.yebeh.2013.05.028>
- Barrera-Bailón, B., Oliveira, J. A. C., López, D. E., Muñoz, L. J., Garcia-Cairasco, N., & Sancho, C. (2017). Pharmacological and neuroethological study of the acute and chronic effects of lamotrigine in the genetic audiogenic seizure hamster (GASH:Sal). *Epilepsy & Behavior*, 71, 207-217. <https://doi.org/10.1016/j.yebeh.2015.11.005>
- Beckmann, A. M., Matsumoto, I., & Wilce, P. A. (2002). AP-1 and Egr DNA-Binding Activities Are Increased in Rat Brain During Ethanol Withdrawal. *Journal of Neurochemistry*, 69(1), 306-314. <https://doi.org/10.1046/j.1471-4159.1997.69010306.x>
- Beckmann, A. M., & Wilce, P. A. (1997). Egr transcription factors in the nervous system. *Neurochemistry International*, 31(4), 477-510. [https://doi.org/10.1016/S0197-0186\(96\)00136-2](https://doi.org/10.1016/S0197-0186(96)00136-2)
- Brodtkorb, E., Steinlein, O. K., & Sand, T. (2005). Asymmetry of Long-latency Auditory Evoked Potentials in LGI1-related Autosomal Dominant Lateral Temporal Lobe Epilepsy. *Epilepsia*, 46(10), 1692-1694. <https://doi.org/10.1111/j.1528-1167.2005.00271.x>
- Browning, R. A. (1986). VII. Neuroanatomical localization of structures responsible for seizures in the GEPR: Lesion studies. *Life Sciences*, 39(10), 857-867. [https://doi.org/10.1016/0024-3205\(86\)90367-X](https://doi.org/10.1016/0024-3205(86)90367-X)
- Carballosa González, M. M. (2008). Hacia un nuevo modelo de epilepsia: El hámster GASH:Sal. Universidad de Salamanca.
- Carballosa-Gonzalez, M. M., Muñoz, L. J., López-Alburquerque, T., Pardal-Fernández, J. M., Nava, E., de Cabo, C., Sancho, C., & López, D. E. (2013). EEG characterization of audiogenic seizures in the hamster strain GASH:Sal. *Epilepsy Research*, 106(3), 318-325. <https://doi.org/10.1016/j.eplepsyres.2013.07.001>
- Charizopoulou, N., Lelli, A., Schraders, M., Ray, K., Hildebrand, M. S., Ramesh, A., Srisailapathy, C. R. S., Oostrik, J., Admiraal, R. J. C., Neely, H. R., Latoche, J. R., Smith, R. J. H., Northup, J. K., Kremer, H., Holt, J. R., & Noben-Trauth, K. (2011). Gipc3 mutations associated with audiogenic seizures and sensorineural hearing loss in mouse and human. *Nature Communications*, 2(1), 201. <https://doi.org/10.1038/ncomms1200>
- Church, M. W., & Kaltenbach, J. A. (1993). The Hamster's Auditory Brain Stem Response as a

- Function of Stimulus Intensity, Tone Burst Frequency, and Hearing Loss: Ear and Hearing, 14(4), 249-257. <https://doi.org/10.1097/00003446-199308000-00004>
- Dailey, J. W., & Jobe, P. C. (1985). Anticonvulsant drugs and the genetically epilepsy-prone rat. Federation Proceedings, 44(10), 2640-2644.
- Damasceno, S., Gómez-Nieto, R., García-Cairasco, N., Herrero-Turrión, M. J., Marín, F., & Lopéz, D. E. (2020). Top Common Differentially Expressed Genes in the Epileptogenic Nucleus of Two Strains of Rodents Susceptible to Audiogenic Seizures: WAR and GASH/Sal. Frontiers in Neurology, 11, 33. <https://doi.org/10.3389/fneur.2020.00033>
- Díaz-Casado, E., Gómez-Nieto, R., de Pereda, J. M., Muñoz, L. J., Jara-Acevedo, M., & López, D. E. (2020). Analysis of gene variants in the GASH/Sal model of epilepsy. PLOS ONE, 15(3), e0229953. <https://doi.org/10.1371/journal.pone.0229953>
- Díaz-Rodríguez, S. M., López-López, D., Herrero-Turrión, M. J., Gómez-Nieto, R., Canal-Alonso, A., & Lopéz, D. E. (2020). Inferior Colliculus Transcriptome After Status Epilepticus in the Genetically Audiogenic Seizure-Prone Hamster GASH/Sal. Frontiers in Neuroscience, 14, 508. <https://doi.org/10.3389/fnins.2020.00508>
- Faingold, C. L., Millan, M. H., Anderson, C. A. B., & Meldrum, B. S. (1989). Induction of audiogenic seizures in normal and genetically epilepsy-prone rats following focal microinjection of an excitant amino acid into reticular formation and auditory nuclei. Epilepsy Research, 3(3), 199-205. [https://doi.org/10.1016/0920-1211\(89\)90024-7](https://doi.org/10.1016/0920-1211(89)90024-7)
- Faye-Lund, H. (1986). Projection from the inferior colliculus to the superior olfactory complex in the albino rat. Anatomy and Embryology, 175(1), 35-52. <https://doi.org/10.1007/BF00315454>
- Fisher, R. S., Acevedo, C., Arzimanoglou, A., Bogacz, A., Cross, J. H., Elger, C. E., Engel, J., Forsgren, L., French, J. A., Glynn, M., Hesdorffer, D. C., Lee, B. I., Mathern, G. W., Moshé, S. L., Perucca, E., Scheffer, I. E., Tomson, T., Watanabe, M., & Wiebe, S. (2014). ILAE Official Report: A practical clinical definition of epilepsy. Epilepsia, 55(4), 475-482. <https://doi.org/10.1111/epi.12550>
- Fisher, R. S., Cross, J. H., French, J. A., Higurashi, N., Hirsch, E., Jansen, F. E., Lagae, L., Moshé, S. L., Peltola, J., Roulet Perez, E., Scheffer, I. E., & Zuberi, S. M. (2017). Operational classification of seizure types by the International League Against Epilepsy: Position Paper of the ILAE Commission for Classification and Terminology. Epilepsia, 58(4), 522-530. <https://doi.org/10.1111/epi.13670>
- Flock, Å., Flock, B., Fridberger, A., Scarfone, E., & Ulfendahl, M. (1999). Supporting Cells Contribute to Control of Hearing Sensitivity. The Journal of Neuroscience, 19(11), 4498-4507. <https://doi.org/10.1523/JNEUROSCI.19-11-04498.1999>
- Frye, G. D., McCown, T. J., & Breese, G. R. (1983). Characterization of susceptibility to audiogenic seizures in ethanol-dependent rats after microinjection of gamma-aminobutyric acid (GABA) agonists into the inferior colliculus, substantia nigra or medial septum. The Journal of Pharmacology and Experimental Therapeutics, 227(3), 663-670.
- Fuentes-Santamaría, V., Cantos, R., Alvarado, J. C., García-Atares, N., & Lopez, D. E. (2005).

- Morphologic and Neurochemical Abnormalities in the Auditory Brainstem of the Genetically Epilepsy-prone Hamster (GPG/Vall). *Epilepsia*, 46(7), 1027-1045. <https://doi.org/10.1111/j.1528-1167.2005.68104.x>
- Gale, K. (1992). Subcortical Structures and Pathways Involved in Convulsive Seizure Generation: *Journal of Clinical Neurophysiology*, 9(2), 264-277. <https://doi.org/10.1097/00004691-199204010-00007>
- Gallitano-Mendel, A., Izumi, Y., Tokuda, K., Zorumski, C. F., Howell, M. P., Muglia, L. J., Wozniak, D. F., & Milbrandt, J. (2007). The immediate early gene early growth response gene 3 mediates adaptation to stress and novelty. *Neuroscience*, 148(3), 633-643. <https://doi.org/10.1016/j.neuroscience.2007.05.050>
- Garcia-Cairasco, N., Terra, V. C., & Doretto, M. C. (1993). Midbrain substrates of audiogenic seizures in rats. *Behavioural Brain Research*, 58(1-2), 57-67. [https://doi.org/10.1016/0166-4328\(93\)90090-D](https://doi.org/10.1016/0166-4328(93)90090-D)
- Garcia-Cairasco, N. (2002). A critical review on the participation of inferior colliculus in acoustic-motor and acoustic-limbic networks involved in the expression of acute and kindled audiogenic seizures. *Hearing Research*, 168(1-2), 208-222. [https://doi.org/10.1016/S0378-5955\(02\)00371-4](https://doi.org/10.1016/S0378-5955(02)00371-4)
- Garcia-Cairasco, N., Umeoka, E. H. L., & Cortes de Oliveira, J. A. (2017). The Wistar Audiogenic Rat (WAR) strain and its contributions to epileptology and related comorbidities: History and perspectives. *Epilepsy & Behavior*, 71, 250-273. <https://doi.org/10.1016/j.yebeh.2017.04.001>
- Gómez-Nieto, R., Horta-Junior, J. A. C., Castellano, O., Herrero-Turrión, M. J., Rubio, M. E., & López, D. E. (2008). Neurochemistry of the afferents to the rat cochlear root nucleus: Possible synaptic modulation of the acoustic startle. *Neuroscience*, 154(1), 51-64. <https://doi.org/10.1016/j.neuroscience.2008.01.079>
- Gómez-Nieto, R., & Rubio, M. E. (2011). Ultrastructure, synaptic organization, and molecular components of bushy cell networks in the anteroventral cochlear nucleus of the rhesus monkey. *Neuroscience*, 179, 188-207. <https://doi.org/10.1016/j.neuroscience.2011.01.058>
- Gómez-Nieto, R., & Rubio, M. E. (2009). A bushy cell network in the rat ventral cochlear nucleus. *The Journal of Comparative Neurology*, 516(4), 241-263. <https://doi.org/10.1002/cne.22139>
- Gómez-Nieto, R., Rubio, M. E., & López, D. E. (2008). Cholinergic input from the ventral nucleus of the trapezoid body to cochlear root neurons in rats. *The Journal of Comparative Neurology*, 506(3), 452-468. <https://doi.org/10.1002/cne.21554>
- Grabenstatter, H. L., Russek, S. J., & Brooks-Kayal, A. R. (2012). Molecular pathways controlling inhibitory receptor expression: Molecular Pathways Controlling Inhibitory Receptor Expression. *Epilepsia*, 53, 71-78. <https://doi.org/10.1111/epi.12036>
- Hasko, J. A., & Richardson, G. P. (1988). The ultrastructural organization and properties of the mouse tectorial membrane matrix. *Hearing Research*, 35(1), 21-38.

[https://doi.org/10.1016/0378-5955\(88\)90037-8](https://doi.org/10.1016/0378-5955(88)90037-8)

Heeringa, N., Wu, C., Chung, C., West, M., Martel, D., Liberman, L., Liberman, M. C., & Shore, S. E. (2018). Glutamatergic Projections to the Cochlear Nucleus are Redistributed in Tinnitus. *Neuroscience*, 391, 91-103. <https://doi.org/10.1016/j.neuroscience.2018.09.008>

Heeringa, A.N., Stefanescu, R. A., Raphael, Y., & Shore, S. E. (2016). Altered vesicular glutamate transporter distributions in the mouse cochlear nucleus following cochlear insult. *Neuroscience*, 315, 114-124. <https://doi.org/10.1016/j.neuroscience.2015.12.009>

Henry, K. R. (1985). Cochlear function and audiogenic seizures: Developmental covariance in the LP/J mouse. *Developmental Psychobiology*, 18(6), 461-466. <https://doi.org/10.1002/dev.420180603>

Henry, K. R., & Buzzone, R. (1986). Auditory physiology and behavior in RB/1bg, RB/3bg, and their F₁ hybrid mice (*Mus musculus*): Influence of genetics, age, and acoustic variables on audiogenic seizure thresholds and cochlear functions. *Journal of Comparative Psychology*, 100(1), 46-51. <https://doi.org/10.1037/0735-7036.100.1.46>

Hernández-Noriega, S. (2017). Efecto de las crisis repetitivas en el modelo experimental de epilepsia GASH Sal. Universidad de Salamanca.

Honkaniemi, J., & Sharp, F. R. (1999). Prolonged expression of zinc finger immediate-early gene mRNAs and decreased protein synthesis following kainic acid induced seizures: Zinc finger IEGs after kainic acid seizures. *European Journal of Neuroscience*, 11(1), 10-17. <https://doi.org/10.1046/j.1460-9568.1999.00401.x>

Hormigo, S., Gómez-Nieto, R., Sancho, C., Herrero-Turrión, J., Carro, J., López, D. E., & Horta-Júnior, J. de A. de C. e. (2017). Morphological correlates of sex differences in acoustic startle response and prepulse inhibition through projections from locus coeruleus to cochlear root neurons. *Brain Structure and Function*, 222(8), 3491-3508. <https://doi.org/10.1007/s00429-017-1415-1>

Jeng, J., Carlton, A. J., Johnson, S. L., Brown, S. D. M., Holley, M. C., Bowl, M. R., & Marcotti, W. (2020). Biophysical and morphological changes in inner hair cells and their efferent innervation in the ageing mouse cochlea. *The Journal of Physiology*, JP280256. <https://doi.org/10.1113/JP280256>

Kawase, T., & Liberman, M. C. (1993). Antimasking effects of the olivocochlear reflex. I. Enhancement of compound action potentials to masked tones. *Journal of Neurophysiology*, 70(6), 2519-2532. <https://doi.org/10.1152/jn.1993.70.6.2519>

Kesner, R. P. (1966). Subcortical mechanisms of audiogenic seizures. *Experimental Neurology*, 15(2), 192-205. [https://doi.org/10.1016/0014-4886\(66\)90045-8](https://doi.org/10.1016/0014-4886(66)90045-8)

Khalfa, S., & Collet, L. (1996). Functional asymmetry of medial olivocochlear system in humans. Towards a peripheral auditory lateralization: *NeuroReport*, 7(5), 993-996. <https://doi.org/10.1097/00001756-199604100-00008>

Klein, B. D., Fu, Y.-H., Ptacek, L. J., & White, H. S. (2004). C-Fos immunohistochemical mapping

- of the audiogenic seizure network and tonotopic neuronal hyperexcitability in the inferior colliculus of the Frings mouse. *Epilepsy Research*, 62(1), 13-25. <https://doi.org/10.1016/j.eplepsyres.2004.06.007>
- Liberman, M. C., Gao, J., He, D. Z. Z., Wu, X., Jia, S., & Zuo, J. (2002). Prestin is required for electromotility of the outer hair cell and for the cochlear amplifier. *Nature*, 419(6904), 300-304. <https://doi.org/10.1038/nature01059>
- Liberman, M. C., & Kujawa, S. G. (2017). Cochlear synaptopathy in acquired sensorineural hearing loss: Manifestations and mechanisms. *Hearing Research*, 349, 138-147. <https://doi.org/10.1016/j.heares.2017.01.003>
- Liberman, M.C. (1980). Morphological differences among radial afferent fibers in the cat cochlea: An electron-microscopic study of serial sections. *Hearing Research*, 3(1), 45-63. [https://doi.org/10.1016/0378-5955\(80\)90007-6](https://doi.org/10.1016/0378-5955(80)90007-6)
- Loftus, M., Knight, R. T., & Amaral, D. G. (2000). An Analysis of Atrophy in the Medial Mammillary Nucleus Following Hippocampal and Fornix Lesions in Humans and Nonhuman Primates. *Experimental Neurology*, 163(1), 180-190. <https://doi.org/10.1006/exnr.2000.7361>
- López, D. E., Saldaña, E., Nodal, F. R., Merchán, M. A., & Warr, W. B. (1999). Projections of cochlear root neurons, sentinels of the rat auditory pathway. *The Journal of Comparative Neurology*, 415(2), 160-174.
- López-González, F. J., Villanueva, V., Falip, M., Toledo, M., Campos, D., & Serratosa, J. (Eds.). (2019). *Manual de Práctica Clínica en Epilepsia. Recomendaciones diagnóstico-terapéuticas de la SEN 2019* (Sociedad Española de Neurología). <http://epilepsia.sen.es/wp-content/uploads/2020/GuiaEpilepsia2019.pdf>
- López-López, D., Gómez-Nieto, R., Herrero-Turrión, M. J., García-Cairasco, N., Sánchez-Benito, D., Ludeña, M. D., & López, D. E. (2017). Overexpression of the immediate-early genes Egr1, Egr2, and Egr3 in two strains of rodents susceptible to audiogenic seizures. *Epilepsy & Behavior*, 71, 226-237. <https://doi.org/10.1016/j.yebeh.2015.12.020>
- Maison, S. F., & Liberman, M. C. (2000). Predicting Vulnerability to Acoustic Injury with a Noninvasive Assay of Olivocochlear Reflex Strength. *The Journal of Neuroscience*, 20(12), 4701-4707. <https://doi.org/10.1523/JNEUROSCI.20-12-04701.2000>
- Malmierca, M. S. (2003). The structure and physiology of the rat auditory system: An overview. En *International Review of Neurobiology* (Vol. 56, pp. 147-211). Elsevier. [https://doi.org/10.1016/S0074-7742\(03\)56005-6](https://doi.org/10.1016/S0074-7742(03)56005-6)
- Malmierca, M. S. (2004). The Inferior Colliculus: A Center for Convergence of Ascending and Descending Auditory Information. *Neuroembryology and Aging*, 3(4), 215-229. <https://doi.org/10.1159/000096799>
- Malmierca, M. S. (2015). Auditory System. En *The Rat Nervous System* (pp. 865-946). Elsevier. <https://doi.org/10.1016/B978-0-12-374245-2.00029-2>
- Malmierca, M. S., & Merchán, M. Á. (2007). Estructura y función del cerebro auditivo. En

- Tratado de Otorrinolaringología y Cirugía de Cabeza y Cuello (2a Edición, Vol. 2, pp. 969-996). Médica Panamericana.
- Matsubara, J. A. (1990). Calbindin D-28K immunoreactivity in the cat's superior olfactory complex. *Brain Research*, 508(2), 353-357. [https://doi.org/10.1016/0006-8993\(90\)90424-A](https://doi.org/10.1016/0006-8993(90)90424-A)
- Mugnaini, E., Osen, K. K., Dahl, A.-L., Friedrich, V. L., & Korte, G. (1980). Fine structure of granule cells and related interneurons (termed Golgi cells) in the cochlear nuclear complex of cat, rat and mouse. *Journal of Neurocytology*, 9(4), 537-570. <https://doi.org/10.1007/BF01204841>
- Muñoz de la Pascua, L. (2004). Establecimiento y caracterización de una línea de hámsters sirios propensos a padecer convulsiones audiogénas. Universidad de Salamanca.
- Muñoz, L. J., Carballosa-Gautam, M. M., Yanowsky, K., García-Atarés, N., & López, D. E. (2017). The genetic audiogenic seizure hamster from Salamanca: The GASH:Sal. *Epilepsy & Behavior*, 71, 181-192. <https://doi.org/10.1016/j.yebeh.2016.03.002>
- Musiek, F. E., & Chermak, G. D. (2015). Psychophysical and behavioral peripheral and central auditory tests. En *Handbook of Clinical Neurology* (Vol. 129, pp. 313-332). Elsevier. <https://doi.org/10.1016/B978-0-444-62630-1.00018-4>
- Nobili, R., Mammano, F., & Ashmore, J. (1998). How well do we understand the cochlea? *Trends in Neurosciences*, 21(4), 159-167. [https://doi.org/10.1016/S0166-2236\(97\)01192-2](https://doi.org/10.1016/S0166-2236(97)01192-2)
- Patuzzi, R. (2011). Ion flow in stria vascularis and the production and regulation of cochlear endolymph and the endolymphatic potential. *Hearing Research*, 277(1-2), 4-19. <https://doi.org/10.1016/j.heares.2011.01.010>
- Patwardhan, S., Gashler, A., Siegel, M. G., Chang, L. C., Joseph, L. J., Shows, T. B., Le Beau, M. M., & Sukhatme, V. P. (1991). EGR3, a novel member of the Egr family of genes encoding immediate-early transcription factors. *Oncogene*, 6(6), 917-928.
- Penny, J. E., Brown, R. D., Hodges, K. B., Kupetz, S. A., Glenn, D. W., & Jobe, P. C. (1983). Cochlear Morphology of the Audiogenic-Seizure Susceptible (Ags) Or Genetically Epilepsy Prone Rat (Gepr). *Acta Oto-Laryngologica*, 95(1-4), 1-12. <https://doi.org/10.3109/00016488309130909>
- Penny, J. E., Don Brown, R., Wallace, M. S., & Henley, C. M. (1986). X. Auditory aspects of seizure in the genetically epilepsy prone rat. *Life Sciences*, 39(10), 887-895. [https://doi.org/10.1016/0024-3205\(86\)90370-X](https://doi.org/10.1016/0024-3205(86)90370-X)
- Pickles, J. O., & Corey, D. P. (1992). Mechanoelectrical transduction by hair cells. *Trends in Neurosciences*, 15(7), 254-259. [https://doi.org/10.1016/0166-2236\(92\)90066-H](https://doi.org/10.1016/0166-2236(92)90066-H)
- Pierson, M., & Li, D. (1996). Cochlear integrity in rats with experimentally induced audiogenic seizure susceptibility. *Hearing Research*, 101(1-2), 7-13. [https://doi.org/10.1016/S0378-5955\(96\)00125-6](https://doi.org/10.1016/S0378-5955(96)00125-6)
- Pierson, M., & Snyder-Keller, A. (1994). Development of frequency-selective domains in inferior colliculus of normal and neonatally noise-exposed rats. *Brain Research*, 636(1), 55-67.

[https://doi.org/10.1016/0006-8993\(94\)90175-9](https://doi.org/10.1016/0006-8993(94)90175-9)

Poletaeva, I. I., Surina, N. M., Kostina, Z. A., Perepelkina, O. V., & Fedotova, I. B. (2017). The Krushinsky-Molodkina rat strain: The study of audiogenic epilepsy for 65 years. *Epilepsy & Behavior*, 71, 130-141. <https://doi.org/10.1016/j.yebeh.2015.04.072>

Prieto-Martín, A. I., Aroca-Aguilar, J. D., Sánchez-Sánchez, F., Muñoz, L. J., López, D. E., Escribano, J., & de Cabo, C. (2017). Molecular and neurochemical substrates of the audiogenic seizure strains: The GASH:Sal model. *Epilepsy & Behavior*, 71, 218-225. <https://doi.org/10.1016/j.yebeh.2015.05.025>

Prieto-Martín, A. I., Llorens, S., Pardal-Fernández, J. M., Muñoz, L. J., López, D. E., Escribano, J., Nava, E., & de Cabo, C. (2012). Opposite caudal versus rostral brain nitric oxide synthase response to generalized seizures in a novel rodent model of reflex epilepsy. *Life Sciences*, 90(13-14), 531-537. <https://doi.org/10.1016/j.lfs.2012.01.010>

Reuss, S., Closhen, C., Riemann, R., Jaumann, M., Knipper, M., Rüttiger, L., & Wolpert, S. (2016). Absence of Early Neuronal Death in the Olivocochlear System Following Acoustic Overstimulation: OC NEURONS AND NOISE-INDUCED HEARING LOSS. *The Anatomical Record*, 299(1), 103-110. <https://doi.org/10.1002/ar.23277>

Roberts, D. S., Hu, Y., Lund, I. V., Brooks-Kayal, A. R., & Russek, S. J. (2006). Brain-derived Neurotrophic Factor (BDNF)-induced Synthesis of Early Growth Response Factor 3 (Egr3) Controls the Levels of Type A GABA Receptor α 4 Subunits in Hippocampal Neurons. *Journal of Biological Chemistry*, 281(40), 29431-29435. <https://doi.org/10.1074/jbc.C600167200>

Romand, M. R., & Romand, R. (1987). The Ultrastructure of Spiral Ganglion Cells in the Mouse. *Acta Oto-Laryngologica*, 104(1-2), 29-39. <https://doi.org/10.3109/00016488709109044>

Ross, K. C., & Coleman, J. R. (2000). Developmental and genetic audiogenic seizure models: Behavior and biological substrates. *Neuroscience & Biobehavioral Reviews*, 24(6), 639-653. [https://doi.org/10.1016/S0149-7634\(00\)00029-4](https://doi.org/10.1016/S0149-7634(00)00029-4)

Rubio, M. E. (2019). Molecular and Structural Changes in the Cochlear Nucleus in Response to Hearing Loss. En K. Kandler (Ed.), *The Oxford Handbook of the Auditory Brainstem* (pp. 142-162). Oxford University Press. <https://doi.org/10.1093/oxfordhb/9780190849061.013.7>

Ryugo, D. K. (2011). Introduction to Efferent Systems. En D. K. Ryugo & R. R. Fay (Eds.), *Auditory and Vestibular Efferents* (Vol. 38, pp. 1-15). Springer New York. https://doi.org/10.1007/978-1-4419-7070-1_1

Salas Puig, J., Mateos Marcos, V., Amorín Díaz, M., Calleja, S., & Jiménez Blanco, L. (2000). Epilepsias reflejas. *Revista de Neurología*, 30(S1), 85. <https://doi.org/10.33588/rn.30S1.2000227>

Sánchez-Benito, D., Gómez-Nieto, R., Hernández-Noriega, S., Murashima, A. A. B., de Oliveira, J. A. C., García-Cairasco, N., López, D. E., & Hyppolito, M. A. (2017). Morphofunctional alterations in the olivocochlear efferent system of the genetic audiogenic seizure-prone hamster GASH:Sal. *Epilepsy & Behavior*, 71, 193-206.

<https://doi.org/10.1016/j.yebeh.2016.05.040>

Sánchez-González, M. A., Warr, W. B., & López, D. E. (2003). Anatomy of olivocochlear neurons in the hamster studied with FluoroGold. *Hearing Research*, 185(1-2), 65-76. [https://doi.org/10.1016/S0378-5955\(03\)00213-2](https://doi.org/10.1016/S0378-5955(03)00213-2)

Scheffer, I. E., Berkovic, S., Capovilla, G., Connolly, M. B., French, J., Guilhoto, L., Hirsch, E., Jain, S., Mathern, G. W., Moshé, S. L., Nordli, D. R., Perucca, E., Tomson, T., Wiebe, S., Zhang, Y.-H., & Zuberi, S. M. (2017). ILAE classification of the epilepsies: Position paper of the ILAE Commission for Classification and Terminology. *Epilepsia*, 58(4), 512-521. <https://doi.org/10.1111/epi.13709>

Seal, R. P., Akil, O., Yi, E., Weber, C. M., Grant, L., Yoo, J., Clause, A., Kandler, K., Noebels, J. L., Glowatzki, E., Lustig, L. R., & Edwards, R. H. (2008). Sensorineural Deafness and Seizures in Mice Lacking Vesicular Glutamate Transporter 3. *Neuron*, 57(2), 263-275. <https://doi.org/10.1016/j.neuron.2007.11.032>

Szűcs, A., Rosdy, B., Kelemen, A., Horváth, A., & Halász, P. (2019). Reflex seizure triggering: Learning about seizure producing systems. *Seizure*, 69, 25-30. <https://doi.org/10.1016/j.seizure.2019.03.019>

Takamori, S. (2006). VGLUTs: 'Exciting' times for glutamatergic research? *Neuroscience Research*, 55(4), 343-351. <https://doi.org/10.1016/j.neures.2006.04.016>

Tollin, D. J. (2003). The Lateral Superior Olive: A Functional Role in Sound Source Localization. *The Neuroscientist*, 9(2), 127-143. <https://doi.org/10.1177/1073858403252228>

Vogler, D. P., Robertson, D., & Mulders, W. H. A. M. (2011). Hyperactivity in the Ventral Cochlear Nucleus after Cochlear Trauma. *Journal of Neuroscience*, 31(18), 6639-6645. <https://doi.org/10.1523/JNEUROSCI.6538-10.2011>

Wada, J. A., Terao, A., White, B., & Jung, E. (1970). Inferior colliculus lesion and audiogenic seizure susceptibility. *Experimental Neurology*, 28(2), 326-332. [https://doi.org/10.1016/0014-4886\(70\)90240-2](https://doi.org/10.1016/0014-4886(70)90240-2)

Warr, W. B. (1980). Efferent Components of the Auditory System. *Annals of Otology, Rhinology & Laryngology*, 89(5_suppl), 114-120. <https://doi.org/10.1177/00034894800890S527>

Warr, W. B., & Beck, J. E. (1996). Multiple projections from the ventral nucleus of the trapezoid body in the rat. *Hearing Research*, 93(1-2), 83-101. [https://doi.org/10.1016/0378-5955\(95\)00198-0](https://doi.org/10.1016/0378-5955(95)00198-0)

Wilson, J. V. K., & Reynolds, E. H. (1990). Translation and analysis of a cuneiform text forming part of a Babylonian treatise on epilepsy. *Medical History*, 34(2), 185-198. <https://doi.org/10.1017/S0025727300050651>

Yin, T. C. T., Smith, P. H., & Joris, P. X. (2019). Neural Mechanisms of Binaural Processing in the Auditory Brainstem. *Comprehensive Physiology*, 9(4), 1503-1575. <https://doi.org/10.1002/cphy.c180036>

Zeng, C., Nannapaneni, N., Zhou, J., Hughes, L. F., & Shore, S. (2009). Cochlear Damage Changes

the Distribution of Vesicular Glutamate Transporters Associated with Auditory and Nonauditory Inputs to the Cochlear Nucleus. *Journal of Neuroscience*, 29(13), 4210-4217. <https://doi.org/10.1523/JNEUROSCI.0208-09.2009>

Zhou, J., Nannapaneni, N., & Shore, S. (2007). Vesicular glutamate transporters 1 and 2 are differentially associated with auditory nerve and spinal trigeminal inputs to the cochlear nucleus. *The Journal of Comparative Neurology*, 500(4), 777-787. <https://doi.org/10.1002/cne.21208>

7. ANEXOS

7.1. Tabla de abreviaturas

Todas las abreviaturas incluidas en esta tesis doctoral están referidas por sus siglas en inglés para facilitar la comprensión del texto y los artículos que lo acompañan.

ABR	<i>Auditory Brainstem Response</i>	Potenciales auditivos evocados
AGS	<i>Audiogenic Seizures</i>	Crisis convulsivas audiogénas
AVCN	<i>Anteroventral Cochlear Nucleus</i>	Núcleo coclear anteroventral
CaBP	<i>Calcium Binding Protein, Calbindin</i>	Proteína de unión al calcio, calbindina
Cdh23	<i>Cadherin23</i>	Cadherina23
CN	<i>Cochlear Nucleus</i>	Núcleo coclear
DBA/2	<i>Dilute Brown Agouti coat color (mouse)</i>	
DCN	<i>Dorsal Cochlear Nucleus</i>	Núcleo coclear dorsal
DPOAE	<i>Distortion Product Otoacoustic Emissions</i>	Emisiones otoacústicas por productos de distorsión
FG	<i>Fluorogold</i>	
GABA	<i>Gamma Aminobutyric Acid</i>	Ácido gamma aminobutírico
GASH/Sal	<i>Genetic Audiogenic Seizure Hamster from Salamanca</i>	Hámster con epilepsia audiogénica de origen genético de Salamanca
GEPR	<i>Genetically Epilepsy-Prone Rats</i>	
IC	<i>Inferior Colliculus</i>	Colículo inferior
IHC	<i>Inner Hair Cells</i>	Células ciliadas internas
ILAE	<i>International League Against Epilepsy</i>	Liga internacional contra la epilepsia
KM	<i>Krushinsky-Molodkina (rats)</i>	
LLN	<i>Lateral Lemniscus Nucleus</i>	Núcleo del lemnisco lateral
LOC	<i>Lateral Olivocochlear</i>	Lateral olivococlear
LSO	<i>Lateral Superior Olive</i>	Oliva superior lateral
MNTB	<i>Medial Nucleus of the Trapezoid Body</i>	Núcleo medial del cuerpo trapezoide
MOC	<i>Medial Olivocochlear</i>	Medial olivococlear
MSO	<i>Medial Superior Olive</i>	Oliva superior medial
OHC	<i>Outer Hair Cells</i>	Células ciliadas externas
Pcdh15	<i>Protocadherin15</i>	Protocadherina15

PVCN	<i>Posteroventral Cochlear Nucleus</i>	Núcleo coclear posteroventral
RT-qPCR	<i>Real Time quantitative Polymerase Chain Reaction</i>	Reacción en cadena de la polimerasa cuantitativa en tiempo real
SGN	<i>Spiral Ganglion Neuron</i>	Neurona del ganglio espiral
SOC	<i>Superior Olivary Complex</i>	Complejo olivar superior
VCN	<i>Ventral Cochlear Nucleus</i>	Núcleo coclear ventral
Vglut	<i>Vesicular Glutamate Transporter</i>	Transportador vesicular de glutamato
VNTB	<i>Ventral Nucleus of the Trapezoid Body</i>	Núcleo ventral del cuerpo trapecioide
WAR	<i>Wistar Audiogenic Rats</i>	

7.2. Comunicaciones a congresos

50 Inner Ear Biology Workshop (IEB 2013). Alcalá de Henares. 10-13 Septiembre 2013

AUTORES: Sonia Hernández Noriega, David Sánchez Benito, Miguel Angelo Hyppolito, Ricardo Gómez Nieto, Orlando Castellano Benítez, Luis J Muñoz, Adriana de Andrade Batista Murashima, Norberto Garcia Cairasco and Dolores E. López García

TÍTULO: Changes of the olivocochlear efferent system in the hamster GASH:Sal

TIPO DE PARTICIPACIÓN: póster

XXXVII Reunião Anual da sociedade Brasileira de Neurociências e Comportamento-SBNeC. UFMG.Belo Horizonte. 11-14 Septiembre 2013

AUTORES: Beduschi R, Barioni NO, da Silva AV, Martins MG, Ferreira MS, Gómez-Nieto R, Lópezde DE.

TÍTULO: Distribuição e caracterização morfométrica dos neurônios do núcleo ventral do corpo trapezóide aferentes aos neurônios da raiz coclear.

TIPO DE PARTICIPACIÓN: póster

15º Congreso Nacional SENC 2013, Oviedo, 25 al 27 septiembre

AUTORES: O. Castellano , D. Sánchez-Benito, S. Hernández-Noriega, R. Gómez-Nieto, L.J. Muñoz , N. Garcia-Cairasco, J.A. Oliveira, C. Sancho, DE.López

TÍTULO: Estudio anatómico y conductual del hámster epiléptico GASH:sal en reposo y tras estimulación audiogénica repetitiva.

TIPO DE PARTICIPACIÓN: póster

I Congress audiogenic epilepsy: from models to the clinic. Salamanca, 9-12 de Septiembre 2014

AUTORES: AA Batista Murashima, D. Sánchez-Benito, S. Hernández-Noriega, R.Gomez-Nieto, JA Cortes de Oliveira, DE. López, N.Garcia- Cairasco, MA. Hyppolito

TÍTULO: Changes in ABR after Audiogenic Kindling in Hamsters of the GASH-Sal strain.

TIPO DE PARTICIPACIÓN: póster

AUTORES: S. Hernández-Noriega, D. Sánchez-Benito, JA Côrtes de Oliveira, N Garcia-Cairasco, DE López, C Sánchez and O Castellano

TÍTULO: Morphofunctional alterations in The GASH:Sal induced by Audiogenic Kindling.

TIPO DE PARTICIPACIÓN: póster

AUTORES: D. López-López, LJ. Herrero-Turrión, LJ Muñoz, C Sancho, S Hernández-Noriega, D Sánchez Benito, R Gómez-Nieto, T López-Alburquerque, O Castellano, L. Millian Morell, DE López

TÍTULO: Sequencing of the complete transcriptome of two strains of Mesocricetus auratus, bioinformatic analysis and SRA and TSA online submission.

TIPO DE PARTICIPACIÓN: póster

AUTORES: D Sánchez Benito, S Hernández Noriega, LJ. Muñoz, DE López, L. Millian Morell, R. Gómez-Nieto

TÍTULO: Morfological changes of auditory nuclei in the hamster GASH:Sal.

TIPO DE PARTICIPACIÓN: póster

Inner Ear Biology workshop 2014. Kyoto University.Kyoto. 1-4 de Noviembre 2014

AUTORES: Sánchez-Benito D, Hernández-Noriega S, Hyppolito MA, Gómez-Nieto R, Castellano O, Muñoz LJ, Batista A, García-Cairasco N, Morujo A, López D
TÍTULO: Pro David Alterations in the Olivocochlear Efferent System of the Epileptic Hamster GASH:Sal

TIPO DE PARTICIPACIÓN: póster

16 Congreso SENC, Granada, 23-25 de Septiembre 2015

AUTORES: D. Sánchez-Benito, E. García-Calzado, JR. del Bosque, R. Gómez-Nieto, C. Sancho, D. López-López, D.E. López

TÍTULO: Variations in gene and protein expression in the inferior colliculus of the GASH:Sal hamster

TIPO DE PARTICIPACIÓN: póster

AUTORES: D. Sánchez-Benito, D. López-López, S. Hernández-Noriega, M.J. Herrero-Turrión, R. Gómez-Nieto, C. Sancho, O. Castellano, L.J. Muñoz, D.E. López

TÍTULO: The transcriptome of the inferior colliculus after acoustic induced seizure in the GASH:Sal hamster.

TIPO DE PARTICIPACIÓN: póster

Sesión científica-Exhibición de pósters, INCyL., 2015. 6 noviembre

AUTORES: D. Sánchez-Benito, D. López-López, S. Hernández-Noriega*, M.J. Herrero-Turrión, R. Gómez-Nieto, C. Sancho, O. Castellano, L.J. Muñoz, D.E. López.

TÍTULO: The transcriptome of the inferior colliculus after acoustic induced seizure in the GASH:SAL hamster

TIPO DE PARTICIPACIÓN: póster

AUTORES: D. Sánchez-Benito*, E. García-Calzado, JR. del Bosque, R. Gómez-Nieto, C. Sancho, D. López-López, D. E. López.

TÍTULO: Variations in gene and protein expression in the inferior colliculus of the GASH:SAL hamster

TIPO DE PARTICIPACIÓN: póster

3rd Symposium on Biomedical Research IIBM. "Advances and Perspectives in Neuroscience" Facultad de Medicina. Madrid, 22-04-2016

AUTORES: Sánchez-Benito D, López-López D, del Bosque JR, Herrero-Turrión, López DE

TÍTULO: A portrait of the transcriptome of the Inferior Colliculus of the GASH:Sal strain after one audiogenic seizure“.

TIPO DE PARTICIPACIÓN: póster

AUTORES: Hernández-Noriega S, Pereira-Figueiredo I, Sánchez-Benito D, Calvo-Rodríguez B, López DE, Muñoz L, Castellano O, Sancho C

TÍTULO: Characterization of the stress response induced by audiogenic seizures in the GASH:Sal“.

TIPO DE PARTICIPACIÓN: póster

XXXV Congreso Panamericano de Otorrinolaringología y cirugía de cabeza y cuello. La Habana, Cuba, 13-16 de Junio de 2016

AUTORES: Castellano Benítez O, Hernández S, Pereira I, Sánchez-Benito D, Calvo-Rodríguez B, López DE, Sancho C

TÍTULO: Stress response induced by audiogenic seizures in the GASH:Sal

TIPO DE PARTICIPACIÓN: póster

53rd Inner Ear Biology Workshop (IEB 2016). Montpellier. 17-21 Septiembre 2016

AUTORES: Alvarez-Morujo D, López-López D, Herrero-Turrión MJ, Sánchez-Benito D, Hernández-Noriega S, Gómez-Nieto R, Alvarez-Morujo AJ, López DE.

TÍTULO: The ADGRV1 gene is under expressed in the GASH:Sal model of epilepsy

TIPO DE PARTICIPACIÓN: póster

Sesión científica-Exhibición de pósters, INCyL., 2016. 4 noviembre

AUTORES: Sánchez-Benito D, López-López D, del Bosque JR, Herrero-Turrión, López DE.

TÍTULO: A portrait of the transcriptome of the Inferior Colliculus of the GASH:Sal strain after one audiogenic seizure.

TIPO DE PARTICIPACIÓN: póster

AUTORES: Hernández-Noriega S, Pereira-Figueiredo I, Sánchez-Benito D, Calvo-Rodríguez B, López DE, Muñoz L, Castellano O, Sancho C.

TÍTULO: Characterization of the stress response induced by audiogenic seizures in the GASH:Sal

TIPO DE PARTICIPACIÓN: póster

AUTORES: Sánchez-Benito D, Calvo-Rodríguez B, López DE, Gómez-Nieto R.

TÍTULO: Efferent projections from the inferior colliculus to brainstem motor nuclei in the Genetic Audiogenic Seizure Hamster (GASH:Sal).

TIPO DE PARTICIPACIÓN: póster

AUTORES: Álvarez- Morujo D, López-López D, Herrero-Turrión MJ, Sánchez-Benito D, Hernández-Noriega S, Gómez-Nieto R, Antonio J. Alvarez-Morujo AJ, López DE

TÍTULO: The ADGRV1 gene is under expressed in the GASH:Sal model of epilepsy

TIPO DE PARTICIPACIÓN: póster

32nd International Epilepsy Congress. Barcelona 2-6 Septiembre 2017

AUTORES: Sánchez-Benito D, Hernández-Noriega S, Hyppolito MA, Castellano O, Sancho C, Muñoz LJ, Batista Murashima AD, García-Cairasco N, Álvarez-Morujo AJ, Gómez-Nieto R, López DE

TÍTULO: Alterations in the olivocochlear efferent system of the epileptic hamster GASH:Sal

TIPO DE PARTICIPACIÓN: póster

AUTORES: Fuerte A, Masa R, Sánchez-Benito D, Hernández-Noriega S, Gómez-Nieto R, López DE

TÍTULO: Distribution of CB1 cannabinoid receptors in the model of epilepsy GASH: Sal

TIPO DE PARTICIPACIÓN: póster

AUTORES: López DE, Herrero-Turrión MJ; López-López D, Sánchez-Benito D, Sancho C, Hernández-Noriega S, Castellano O, Muñoz LJ, GarcíaCairasco N, Gómez-Nieto R.

TÍTULO: Audiogenic seizures induce changes in the gene expression in the inferior colliculus of two animal models of epilepsy, the WAR and GASH:Sal strains

TIPO DE PARTICIPACIÓN: póster

AUTORES: Alvarez-Morujo de Sande D, López-López D, Herrero-Turrión MJ, Sánchez-Benito D, Hernández-Noriega S, Gómez-Nieto R, Álvarez-Morujo AJ, López DE

TÍTULO: Downregulation of ADGRV1 gene expression in the inferior colliculus of the genetic audiogenic seizure-prone hamster GASH:Sal

TIPO DE PARTICIPACIÓN: póster

AUTORES: Hernández-Noriega S, Sánchez-Benito D, Gómez-Nieto R, Cortes de Oliveira JA, Domínguez-Hernández N, García-Cairasco N, Muñoz LJ, Castellano O, López DE, Sancho C

TÍTULO: Repetitive epileptic seizures induce behavioral and activation changes in the hamster GASH:Sal

TIPO DE PARTICIPACIÓN: póster

17 Congreso SENC, Alicante, 27-30 de Septiembre 2017

AUTORES: Masa R, Fuerte A, Sánchez-Benito D, Hernández-Noriega S, Sancho C, Castellanos O, Gómez-Nieto R, López DE

TÍTULO: Study of the CB1 cannabinoid receptors in the genetic audiogenic seizure hamster (GASH:Sal)

TIPO DE PARTICIPACIÓN: póster

AUTORES: López DE, Herrero-Turrión MJ, López-López D, Sánchez-Benito D, Sancho C, Hernández-Noriega S, Castellano O, Muñoz LJ, GarcíaCairasco N, Gómez-Nieto R.

TÍTULO: Overexpression of common genes in two strains of rodents susceptible to audiogenic seizures after ictal crises

TIPO DE PARTICIPACIÓN: póster

XIV Congreso SECAL 2017 – Las Palmas de Gran Canaria, 13 -16 Junio

AUTORES: Hernández-Noriega S, Pereira-Figueiredo I, Sánchez-Benito D, Gómez-Nieto R, Castellano O, Sancho C, Lopez DE, Muñoz LJ

TÍTULO: Stress induced by audiogenic kindling causes physiological and behavioral changes in the GASH-Sal model of epilepsy

TIPO DE PARTICIPACIÓN: Póster

Sesión científica-Exhibición de pósters, INCyL., 2017. 10 noviembre

AUTORES: Gómez-Nieto, R., Sánchez-Benito, D, Hernández-Noriega, S., Hyppolito, M.A.,Castellano, O, Muñoz, L J.,Batista Murashima, A. ,Garcia-Cairasco, N., Morujo,A. and López, D. E

TÍTULO: Alterations In The Efferent System In The Epileptic Hamster GASH:Sal

TIPO DE PARTICIPACIÓN: póster

AUTORES: López DE, Herrero-Turrión MJ, López-López D, Sancho C, Sánchez-Benito D, Hernández-Noriega S, Castellano O, Muñoz LJ, García-Cairasco N, Gómez-Nieto R.

TÍTULO: Overexpression of common genes in two strains of rodents susceptible to audiogenic seizures after ictal crises

TIPO DE PARTICIPACIÓN: póster

AUTORES: Sancho C, Hernández-Noriega S, Sánchez-Benito D, Gómez-Nieto R, Cortes de Oliveira JA, Domínguez-Hernández N, García-Cairasco N, Muñoz LJ, López DE, Castellano

TÍTULO: Repetitive epileptic seizures induce behavioral and activation changes in the hamster GASH:Sal

TIPO DE PARTICIPACIÓN: póster

**International Symposium NEWroscience 2018. September 18 th to 21 st.
Ribeirão Preto -São Paulo - Brasil**

AUTORES: Samara Damasceno, Dalia Álvarez-Morujo, David Sánchez-Benito, Mª Elena Díaz-Casado, Rosa Mª García-Aparicio, Daniel de Castro Medeiros, Antonio J. Álvarez-Morujo, Dolores E. López, Ricardo Gómez-Nieto.

TÍTULO “Morphofunctional and molecular defects of hearing sensitivity in the genetic audiogenic seizure-prone hamster GASH/Sal”.

TIPO DE PARTICIPACIÓN: póster

XXVIII de la sociedad anatómica española . Badajoz. Febrero 1-3, 2018

AUTORES: Álvarez-Morujo de Sande D; Sánchez-Benito D Gómez-Nieto R; García-Aparicio, RM; López DE; Álvarez-Morujo AJ.

TÍTULO: Posibles consecuencias de la baja expresión del gen GPR98 en la línea de hámsteres GASH:Sal

TIPO DE PARTICIPACIÓN: póster

AUTORES: David Sánchez-Benito, Ricardo Gómez-Nieto, Sonia Hernández-Noriega, Orlando Castellano, Luis J. Muñoz, Dolores E. López, Antonio J. Álvarez-Morujo

TÍTULO: Alteraciones del sistema olivoclear eferente en el hámster epiléptico GASH/Sal

TIPO DE PARTICIPACIÓN: póster

V Congreso de la Sociedad Española de Epilepsia. Málaga 25-27 de Octubre de 2018

AUTORES: David Sánchez Benito, M^a Elena Díaz Casado, Dolores E. López, Rosa M^a García -Aparicio,. Antonio J. Álvarez-Morujo, Ricardo Gómez-Nieto

TÍTULO:. El correlato neuroanatómico y funcional de la alteración en la sensibilidad auditiva del modelo de epilepsia audiogena GASH/Sal

TIPO DE PARTICIPACIÓN: Póster

AUTORES: Alejandro Fuerte, Jaime Gonçalves Sánchez, María Victoria Barbado González, Daniel de Castro Medeiros, David Sánchez-Benito, Dolores E. López

TÍTULO:. FDG-PETITC en el modelo de epilepsia GASH:SAL

TIPO DE PARTICIPACIÓN: Póster

AUTORES: Dalia Álvarez-Morujo, Samara Damasceno, David Sánchez-Benito, Ricardo Gómez-Nieto, Dolores E. López,

TÍTULO:. Modificación de la expresión de genes relacionados con el síndrome de usher en la cóclea del hámster modelo de epilepsia GASH/Sal

TIPO DE PARTICIPACIÓN: póster

Sesión científica-Exhibición de pósters, INCyL., 2018. 26 octubre

AUTORES: David Sánchez Benito, M^a Elena Díaz Casado, Dolores E. López, Rosa M^a García García-Aparicio, Antonio J. Álvarez-Morujo, Ricardo Gómez-Nieto.

TÍTULO: El correlato neuroanatómico y funcional de la alteración en la sensibilidad auditiva del modelo de epilepsia audiogena GASH:Sal

TIPO DE PARTICIPACIÓN: póster

AUTORES: Dalia Alvarez-Morujo, Samara Damasceno, David Sánchez-Benito, Ricardo Gómez-Nieto, Dolores E. López, Antonio J. Alvarez-Morujo

TÍTULO: modificación de la expresión de genes relacionados con el síndrome de Usher en la cóclea del hámster modelo de epilepsia GASH/Sal

TIPO DE PARTICIPACIÓN: póster

18 Congreso SENC, Santiago de Compostela, 4 al 6 de septiembre de 2019

AUTORES: D. Sánchez-Benito, C. Sancho, S. Vicente González, L.J. Muñoz, R. Gómez-Nieto, DE. López,

TÍTULO: Cannabidiol for epilepsy treatment: pharmacokinetics and effects in the genetic audiogenic seizure hamster GASH/Sal

TIPO DE PARTICIPACIÓN: póster

V Congreso de la Sociedad Española de Epilepsia. Málaga 24-26 de Octubre de 2019

AUTORES: Dalia Álvarez-Morujo, David Sánchez-Benito, Rosa Mª García-Aparicio, Antonio J. Álvarez-Morujo, Dolores E. López, Ricardo Gómez-Nieto.

TÍTULO: Alteraciones moleculares y morfológicas en la cóclea del modelo de epilepsia audiogénica GASH/Sal

TIPO DE PARTICIPACIÓN: póster

Sesión científica-Exhibición de pósters, INCyL, 2019. 29 noviembre

AUTORES: Samara Damasceno, Dalia Álvarez-Morujo, David Sánchez-Benito, Rosa Mª García-Aparicio, Antonio J. Álvarez-Morujo, Dolores E. López, Ricardo Gómez-Nieto

TÍTULO: Alteraciones moleculares y morfológicas en la cóclea del modelo de epilepsia audiogénica GASH/Sal

TIPO DE PARTICIPACIÓN: póster

8. COMPENDIO DE PUBLICACIONES



Research Paper

Morphological and molecular correlates of altered hearing sensitivity in the genetically audiogenic seizure-prone hamster GASH/Sal



David Sánchez-Benito ^{a, b}, Miguel A. Hyppolito ^c, Antonio J. Alvarez-Morujo ^{a, b, d}, Dolores E. López ^{a, b, e}, Ricardo Gómez-Nieto ^{a, b, e,*}

^a Institute of Neuroscience of Castilla y León (INCYL), University of Salamanca, Salamanca, Spain

^b Institute of Biomedical Research of Salamanca (IBSAL), University of Salamanca, Salamanca, Spain

^c Laboratory of Neurobiology of Hearing, Department of Ophthalmology, Otorhinolaryngology, Head and Neck Surgery, Ribeirão Preto Medical School, University of São Paulo, São Paulo, Brazil

^d Department of Human Anatomy and Histology, Faculty of Medicine, University of Salamanca, Salamanca, Spain

^e Department of Cell Biology and Pathology, Faculty of Medicine, University of Salamanca, Salamanca, Spain

ARTICLE INFO

Article history:

Received 8 January 2020

Received in revised form

30 March 2020

Accepted 7 April 2020

Available online 26 April 2020

Keywords:

Animal models of epilepsy
Cochlear neuropathy
Cochlear nucleus
VGLUT
Audiogenic seizures
Spiral ganglion neurons

ABSTRACT

Rodent models of audiogenic seizures, in which seizures are precipitated by an abnormal response of the brain to auditory stimuli, are crucial to investigate the neural bases underlying ictogenesis. Despite significant advances in understanding seizure generation in the inferior colliculus, namely the epileptogenic nucleus, little is known about the contribution of lower auditory stations to the seizure-prone network. Here, we examined the cochlea and cochlear nucleus of the genetic audiogenic seizure hamster from Salamanca (GASH/Sal), a model of reflex epilepsy that exhibits generalized tonic-clonic seizures in response to loud sound. GASH/Sal animals under seizure-free conditions were compared with matched control hamsters in a multi-technical approach that includes auditory brainstem responses (ABR) testing, histology, scanning electron microscopy analysis, immunohistochemistry, quantitative morphometry and gene expression analysis (RT-qPCR). The cochlear histopathology of the GASH/Sal showed preservation of the sensory hair cells, but a significant loss of spiral ganglion neurons and mild atrophy of the stria vascularis. At the electron microscopy level, the reticular lamina exhibited disarray of stereociliary tufts with blebs, loss or elongated stereocilia as well as non-parallel rows of outer hair cells due to protrusions of Deiters' cells. At the molecular level, the abnormal gene expression patterns of *prestin*, *cadherin 23*, *protocadherin 15*, *vesicular glutamate transporters 1* (*Vglut1*) and -2 (*Vglut2*) indicated that the hair-cell mechanotransduction and cochlear amplification were markedly altered. These were manifestations of a cochlear neuropathy that correlated to ABR waveform I alterations and elevated auditory thresholds. In the cochlear nucleus, the distribution of VGLUT2-immunolabeled puncta was differently affected in each subdivision, showing significant increases in magnocellular regions of the ventral cochlear nucleus and drastic reductions in the granule cell domain. This modified inputs lead to disruption of *Vglut1* and *Vglut2* gene expression in the cochlear nucleus. In sum, our study provides insight into the morphological and molecular traits associated with audiogenic seizure susceptibility in the GASH/Sal, suggesting an upward spread of abnormal glutamatergic transmission throughout the primary acoustic pathway to the epileptogenic region.

© 2020 The Authors. Published by Elsevier B.V. This is an open access article under the CC BY-NC-ND license (<http://creativecommons.org/licenses/by-nc-nd/4.0/>).

1. Introduction

Epilepsy research has made significant progress thanks to a wide range of animal models that, to a greater or lesser extent, mimics the variety of clinical, electrophysiological, and behavioral manifestations that comprise epilepsy syndromes. A comparative approach using animal models of epilepsies uncovered many of the deficits associated with the epileptic brain, providing unique insights into

* Corresponding author. Institute of Neuroscience of Castilla y León (INCYL), Laboratory of Audiomotor Disorders, C/ Pintor Fernando Gallego, 1, 37007, Salamanca, Spain.

E-mail address: richard@usal.es (R. Gómez-Nieto).

aspects of ictogenesis (Grone and Baraban, 2015), and leading to discovery of anti-seizure treatment strategies (Loscher, 2011). Audiogenic seizure (AGS) is a type of generalized clonic or tonic-clonic convulsive muscle contractions caused by excessive or abnormal neuronal firing in response to intense sound stimulation. AGS is frequent in rodents, in which susceptibility can occur genetically or be induced by a large variety of experimental treatments such as priming procedures (Ross and Coleman, 2000; Garcia-Cairasco, 2002). Using acoustic priming, several rodent strains not initially AGS-susceptible become seizure prone by exposure to an acoustic insult during a critical period of postnatal development (e.g. Pierson and Snyder-Keller, 1994). For genetically prone strains of rodents, the priming procedure is not required and seizures are elicited by high-intensity acoustic stimulation just a few weeks after birth (Ross and Coleman, 2000). In contrast to traditional models of epilepsy induced by chemical or electrical means or primed models, the AGS rodents of genetic origin offer several advantages. Firstly, the AGS susceptibility is inherited and does not require any experimental procedure to become susceptible, avoiding thus incompatibilities with experimental designs that require anti-seizure drugs administration or the possibility of chemically or electrically modulating seizures (Kandratavicius et al., 2014). In addition, the innate occurring seizures can be elicited at will by an investigator, as the specific trigger is a sound. A further advantage lies in the substantial characterization of behavioral, cellular, and molecular alterations available of genetically AGS models that potentiates their usefulness in elucidating mechanisms and neuronal substrates underlying the seizure genesis and propagation (Ross and Coleman, 2000; Kandratavicius et al., 2014). Examples of genetically seizure-prone strains of rodents include mainly rats and mice such as the genetically epilepsy-prone rat (GEPR; Reigel et al., 1986), the Wistar audiogenic rat (WAR; Doretto et al., 2003), the DBA/2 mouse (De Sarro et al., 2017), the Black Swiss mouse (BLSW, Charizopoulou et al., 2011) and the Frings mouse (Skradzki et al., 2001). The only available hamster strain that exhibits susceptibility to sound-induced seizures is the genetic audiogenic seizure hamster from Salamanca (GASH/Sal) that presents an autosomal recessive inheritance pattern (Muñoz et al., 2017). The GASH/Sal has recently gathered attention as a model for sensory-evoked reflex seizures precisely for the amount of interesting data related to the neuroethological (Barrera-Bailón et al., 2013, 2017), electrophysiological (Carballosa-Gonzalez et al., 2013), neurochemical (Prieto-Martín et al., 2017), molecular (López-López et al., 2017; Díaz-Casado et al., 2020) and morphological (Sánchez-Benito et al., 2017) substrates underlying AGS. Nearly 100% of the GASH/Sal strain, from 2 to 4 months of age at which susceptibility reached its maximum, undergoes generalized tonic–clonic seizures that are characterized by a short latency period after loud acoustic stimulation, followed by phases of wild running, convulsions, and stupor, with origin in the brainstem (Muñoz et al., 2017). Anticonvulsant drugs are very effective in suppressing sound-induced seizures in the GASH/Sal (Barrera-Bailón et al., 2013, 2017; Werner and Coveñas, 2017), and hence clarification of molecular and neuronal mechanisms leading to susceptibility of AGS could have important implications for the use of the GASH/Sal model in development of new anti-seizure agents. Activation of auditory pathways is required for seizure development in all AGS models, and many studies pointed out the inferior colliculus, a critical integration center in the auditory midbrain pathway, as the epileptogenic focus (reviewed in Garcia-Cairasco, 2002). This implies that defects in lower auditory structures might be common among AGS models, thereby causing alterations of bottom-up auditory inputs to the inferior colliculus. In this regard, cochlear abnormalities have been identified in the GEPR model (Penny et al., 1983), and electrolytic destruction of the ventral cochlear nucleus was reported to cause a blockade of audiogenic convulsions in rats

(Browning, 1986). In the GASH/Sal, auditory-evoked brainstem responses (ABR) and distortion-product of otoacoustic emissions analyses revealed an altered hearing sensitivity with increased ABR thresholds and absence of otoacoustic emissions in a wide range of frequencies (Muñoz et al., 2017; Sánchez-Benito et al., 2017). Consequently, such hearing impairments were correlated with morphological alterations in the olivocochlear efferent system that reflexively modulates the sensitivity of receptor mechanisms operating in the cochlear hair cells (Sánchez-Benito et al., 2017). In the current study, we used histology, scanning electron microscopy analysis and quantitative morphometry to examine in detail the major sites of the cochlear pathology in the GASH/Sal. These elements include: 1) the two anatomically and functionally distinct types of mechanosensitive receptor cells within the organ of Corti, the inner and outer hair cells (IHCs and OHCs, respectively); 2) the spiral ganglion neurons (SGNs) that relay auditory inputs from the cochlear hair cells to the cochlear nucleus; and 3) the stria vascularis (SV) that is essential for transporting oxygen and nutrients into the cochlea. We further sought to determine the possible molecular defects associated to the cochlear histopathology of the GASH/Sal. By using the reverse transcription-quantitative polymerase chain reaction (RT-qPCR), we analyzed mRNA expression levels of key cochlear genes such as *prestin* (*Slc26a5*), *cadherin 23* (*Cdh23*), and *proto-cadherin 15* (*Pcdh15*) that are involved in the function and integrity of the sensory hair cells (Kazmierczak et al., 2007; Xia et al., 2013). Given that cochlear neuropathy is associated with damage at the cochlear synapse without loss of sensory hair cells, and is often accompanied by adaptive responses and hyperexcitability in auditory brainstem nuclei (Salvi et al., 2000; Rachel et al., 2002; Mulders et al., 2011; Liberman and Kujawa, 2017), we also determine whether the cochlea and cochlear nucleus of the GASH/Sal exhibit altered gene expression of vesicular glutamate transporters 1 (*Vglut1*) and -2 (*Vglut2*). VGLUT1 and -2, encoded by two separate genes, are primarily localized in axon terminals and define two distinct classes of excitatory synapsis with a non-overlapping distribution (Takamori et al., 2001; Fremeau et al., 2001). In the cochlear nucleus, these two VGLUT isoforms have been used to differentiate glutamate signaling inputs as auditory nerve terminals preferentially colabeled with VGLUT1 and somatosensory terminals with VGLUT2 (Furness and Lawton, 2003; Zhou et al., 2007; Gómez-Nieto and Rubio, 2009). In addition, several studies showed correlations between changes in VGLUT2-immunoreactivity and disorders characterized by hyperexcitability such as epilepsy (Wallen-Mackenzie et al., 2010) and tinnitus (Heeringa et al., 2018). Thus, we analyzed the distribution of VGLUT2 axon terminals in the cochlear nucleus subdivisions of the GASH/Sal model. The overall goal of this study was to present a comprehensive picture of a cochlear neuropathy that may generate hyperexcitability in central auditory pathways and therefore bring about an upstream seizure-prone circuitry. In particular, we show a link of functional, molecular and morphological correlations between the peripheral pathologies and glutamatergic imbalance in the cochlear nucleus that might underlie the innate audiogenic seizure susceptibility of the GASH/Sal model. Since the outcomes of the present study were based on the comparisons with age-matched wild-type Syrian hamsters, our study also provides valuable information of the auditory peripheral system and the cochlear nucleus of the *Mesocricetus auratus*.

2. Material and methods

2.1. Experimental animals

In total, 15 control hamsters (*Mesocricetus auratus*) from Janvier Labs (Le Genest-Saint-Isle, France) and 14 hamsters of the GASH/Sal strain from the animal's facility of the University of Salamanca

(Salamanca, Spain), with 4 months of age, were used in this study. We selected animals of that age because the GASH/Sal exhibits the maximum susceptibility to seizures from 2 to 4 months of age (Muñoz et al., 2017). All the GASH/Sal were males and naïve without receiving any acoustic stimulation to trigger audiogenic seizures. The experiments were conducted in compliance with the guidelines for the use and care of laboratory animals of the European Communities Council Directive (2010/63/EU), the current Spanish legislation (RD 1201/05), and with those established by the Institutional Bioethics Committee (approval number 300). All efforts were made to minimize the number of animals and their suffering. The animals were maintained under normal conditions of lighting (12 h light/dark cycle) and constant temperature with *ad libitum* access to food and water.

2.2. ABR recordings and analysis

The ABR testing followed a similar procedure previously described by Colmenárez-Raga et al. (2019). 4 control and 4 GASH/Sal hamsters were anesthetized using a mixture of ketamine hydrochloride (40 mg/kg) and xylazine hydrochloride (10 mg/kg) via intramuscular administration. A heating pad was used to maintain a constant body temperature of 37 °C. ABR recordings were performed for both ears using a real-time signal processing system (Tucker-Davis Technologies [TDT], System RZ-6, Alachua, FL, USA, 195,312-Hz sampling rate). The system output was calibrated before the recordings, using a one-quarter inch microphone (Bruél and Kjaer). Three subcutaneous needle electrodes placed at the vertex (reference electrode), the mastoid ipsilateral to the stimulated ear (active electrode), and the mastoid contralateral to the stimulated ear (ground electrode) were used for the recordings. Sound stimuli consisted of a 5 milliseconds (ms) window, with 1 ms pre-stimuli period, and a 0.1 ms alternating polarity click, with a repetition rate of 21 bursts/s, delivered in 10 dB ascending steps from 10 to 90 dB (Sound Pressure Level, SPL). The stimuli were delivered in close field using a magnetic speaker (TDT, MF1 Multi-Field Magnetic Speakers) connected to the external auditory meatus of a single ear through a 10 cm long plastic tube. This approach resulted in a total delay of 1.4 ms in stimulus arrival at the tympanic membrane. An ABR was obtained by averaging 1000 EEG responses to 1000 click stimuli. Evoked potentials were amplified and digitized using a Medusa RA16PA preamplifier and RA4LI headstage. The final signal was filtered with a 500 Hz high-pass filter and a 3000 Hz low-pass filter.

The ABR analysis was done using a custom-made script developed in MATLAB software (version R2014a, The MathWorks, Inc.). The quality of each recording was assessed measuring the mean background voltage of the 1 ms period before the stimulus onset. The ABR threshold was defined as the stimulus level that evoked a mean voltage value greater than 2 times the standard deviation above the mean background activity. These auditory thresholds were confirmed by blind visual inspections at the lowest intensity at which waves I and II were detectable above noise within the 5 ms response window immediately before the stimulus onset. The amplitude and latency of click ABR waves were measured at the suprathreshold hearing level of 90 dB SPL, analyzing positive and negative peaks of each wave with the MATLAB program. Wave amplitude was defined as the sum of the positive and negative peak values of each wave. The absolute wave I latency was defined as the time in ms from the stimulus onset to the positive peak of the wave. The inter-peak latencies were defined as the time in ms between the positive peaks of the different ABRs waves. All animals used for ABR measurements were processed for cochlear histology and immunohistochemistry.

2.3. Cochlear histology

After the ABR hearing measurements, animals were perfused through the aorta with aldehydes following the procedures described by Sánchez-Benito et al. (2017). The temporal bones of 2 control and 2 GASH/Sal hamsters were removed from the head. The bulla was opened, and the cochlea was dissected under the microscope and perfused through the round window with a fixative containing 4% paraformaldehyde in 0.1 M phosphate buffered saline (PBS), pH 7.4 solution, and subsequently immersed in the same fixative solution for 1 day. The cochleae were then decalcified in 10% ethylenediaminetetraacetic acid (EDTA) for 1 week, and embedded in paraffin. The paraffin-embedded cochleae were sliced along the mid-modiolar axis into sections of 6 µm thick, mounted on silane-coated slides and stained with cresyl-violet (Nissl stained). The serial sections were studied using a Leitz DMRB (Leica) light microscope equipped with digital camera, and the cochlear turns were divided into three regions: apical, middle and basal for histology image analysis, SGNs quantification and SV thickness measurements.

2.4. Quantification and morphometric analyses of SGNs and SV

Quantification and morphometry of spiral ganglion neurons (SGNs) and stria vascularis (SV) were carried out in light microscope images of 4 cochleae (corresponding to 2 control and 2 GASH/Sal animals), using the open source software ImageJ (v1.51g-v1.51n; Fiji package). Spiral ganglion cells were counted using a 20x objective lens. The corresponding area of the Rosenthal's canal was measured in digital photomicrographs of each canal profile (apical, middle and basal). The perimeter of the canal was traced with a cursor using ImageJ program. The computer then calculated the area within the outline. Density was calculated as the number of SGNs per mm³ as described elsewhere (Keithley and Feldman, 1979; Nadol, 1988) in every two sections of the entire cochlea. SGNs were included in the counts if their nuclei were visible in the section. Since the heterochromatin visible in the nucleus was sometimes mistaken for the nucleolus, nuclei were counted instead of nucleoli (Berglund and Ryugo, 1991). Type I and type II SGNs were not differentiated and all counts were corrected for split-cell error by the Abercrombie formula, with the assumption that the nuclei were spherical [corrected count = (nuclei counts x section thickness)/(section thickness + nuclear diameter); Abercrombie, 1946]. The nuclear diameter was determined by morphometric analyses of 486 nuclear cross-sections at 40x objective lens. The mean nuclear diameter was $7.1 \pm 0.71 \mu\text{m}$ ($n = 255$) for controls and $6.9 \pm 0.68 \mu\text{m}$ ($n = 231$) for GASH/Sal hamsters and these values were the same for all regions of the cochlea. In addition, cross-sectional areas, perimeter and roundness of SGNs somata were measured using the ImageJ software as described by Sánchez-Benito et al. (2017). A total of 834 SGNs (417 in each animal group) corresponding to different region of the cochlea were imaged at 40x objective lens and their somata measured while taking care not to include the satellite glial cells. The number of stria blood vessels and SV thickness were analyzed in digital images of Nissl-stained cochlear tissues acquired with a 20x objective lens. A total of 304 stria vascularis (134 for controls and 170 for GASH/Sal animals) corresponding to the apical, middle, and basal turns of the cochlea were evaluated with the ImageJ software. Capillaries in the SV that included endothelial cells were considered as a count. The measurement of SV thickness was made by using a cursor to draw a line from the margin of the SV to the junction of the basal cells with the spiral ligament half-way between the attachment of Reissner's membrane and the spiral prominence (Keithley et al., 2005). This measured line corresponding to the SV

thickness matched the perpendicular bisector of the reference structures. All quantification analyses were carried out in a single-blind assessment by two different investigators.

2.5. Scanning electron microscopy analyses and stereocilia counts

For the scanning electron microscopy study, the cochleae of 2 control and 2 GASH/Sal hamsters were processed following the procedure described by Sánchez-Benito et al. (2017). The animals were anaesthetized with sodium thiopental (Abbott) (69 mg/kg) and perfused transcardially with 0.1M phosphate buffer solution, followed by 4% paraformaldehyde and 0.1% glutaraldehyde in 0.1 M of phosphate buffer (pH = 7.4), using a speed-controlled pump perfusion Masterflex® (Paste, Parmer). Each temporal bone with its tympanic cavity was removed by exposing the tympanic bulla and then opened for cochlear exposure. The two cochleae of each animal were dissected under the microscope and gently perfused in 4% paraformaldehyde solution and subsequently maintained in the same fixative solution for 4 h. Cochleae were placed in 1% OsO₄, dehydrated with increasing concentrations of ethanol and critical point dried from CO₂. Dried samples were mounted on metal support stubs and then sputter coated with gold. The observation and analysis of the cochlear hair cells were carried out with an Electron Microscope JEOL SCANNING MICROSCOPE — JSM 5200. To map the results of our analysis, we divided the cochlea into several regions, with the base of the cochlea closest to the stapes and the apex or apical region at the tip of the spiral. Digital images of the basal, middle and apical cochlear turns were obtained at a magnification that ranged from 2,000x to 5,000x. The total number of stereocilia per hair cell was obtained by counting the number of stereocilia tips present in the tallest row of a given tuft. Hair cells that lose all or almost their entire stereocilia tuft were not included in the stereocilia analysis. A total of 27 IHCs and 57 OHCs were counted in each group of animals (n = 168). In addition, morphometric data of stereocilia and blebs (length in microns) was obtained from images taken with the same angle to the apical surface of the hair cell at a magnification of 5,000x using the ImageJ program.

2.6. Real-time quantitative PCR (RT-qPCR)

The cochlea of 6 control and 6 GASH/Sal hamsters were collected to study the differential expression of the following cochlear genes: *Prestin*, *Cdh23*, *Pcdh15*, *Vglut1*, and *Vglut2*. Tissue samples containing the entire cochlear nucleus of those animals were also used to perform differential gene expression analysis of *Vglut1* and *Vglut2*. The cochleae and the cochlear nuclei of each animal were obtained following euthanasia by deep anaesthesia and rapid decapitation. Each cochlear nucleus was frozen immediately in liquid nitrogen and each cochlea was transferred into the Trizol reagent (Gibco BRL, Gaithersburg, MD, USA). The oval window and the apex of the cochlea were opened immediately to let the Trizol reagent enter the cochlea as soon as possible. The samples were stored at -80 °C until RNA extraction. The RT-qPCR approach was identical to that used previously by our group (e.g. Damasceno et al., 2020). Total cellular RNA from frozen tissue was extracted from the individual tissue samples using the Trizol reagent in accordance with the manufacturer's procedure. The quantity and quality of total RNA were verified by optical density using the NanoPhotometer® spectrophotometer (Implen GmbH), taking into account the absorbances ratios 260/280 and 260/230 nm, and the RNA integrity was checked by electrophoresis in agarose gel (1.5%).

Complementary DNA (cDNA) was synthesized from 800 ng of total RNA using the ImProm-II™ Reverse Transcription System Kit

(Promega Corporation, Madison, WI, USA) according to the manufacturer's instructions. The RT-qPCR analysis was performed using the QuantStudio 7 Flex System (Applied Biosystems by Life Technology, Europe) with the Power SYBR Green PCR Master Mix (Applied Biosystems by Life Technologies, Europe). 20 µl PCR mixture contained 80 ng of cDNA template, 400 nMol of each primer and 10 µl of Power SYBR Green PCR Master Mix. Table 1 shows the specific primers for the genes examined in the present study, which were designed in such a way that RT-qPCR products spanned two identified introns (for more details on the primer design methodology, see Damasceno et al., 2020). PCR amplification was as follows: 10 min at 95 °C before 40 thermal cycles, each consisting of denaturation at 95 °C for 15 s and annealing/extending at 60 °C for 30 s, followed by melting curve. Output data were analyzed with QuantStudio™ Real-Time PCR software (v. 1.3; Applied Biosystems by Thermo Fisher Scientific) and were normalized by beta-actin (β-actin) expression. The relative gene expression value of each transcript was calculated following the comparative 2^{-ΔΔCt} method as used previously (Damasceno et al., 2020). Finally, a negative template-free (water) control reaction was used in all RT-qPCRs and the control group was used as the calibration sample.

2.7. Antibody characterization

In this study, we used immunohistochemistry to determine the distribution of the vesicular glutamate transporter 2 (VGLUT2) in the cochlear nucleus of control and GASH/Sal hamsters. We used polyclonal antibodies generated in rabbits against Strep-Tag fusion protein containing amino acid residues 510–582 of rat VGLUT2 (catalog No. 135 402; Synaptic Systems). This recombinant protein from rat VGLUT2 has been tested in preadsorption experiments that blocked efficiently and specifically the corresponding signals (manufacturer's technical information). In Western blots analysis of cerebellum and cochlear nucleus, the rabbit polyclonal antibodies for VGLUT2 recognize a single band migrating at ~65 kDa, respectively (Zhou et al., 2007). This primary antibody has been successfully used in previous studies to immunolabel VGLUT2 axon terminals in the cochlear nucleus of guinea pig (Zhou et al., 2007), rat (Gómez-Nieto and Rubio, 2009) and monkey (Gómez-Nieto and Rubio, 2011). According to the manufacturer's technical information, the reactivity has not been tested yet in hamster brain tissue. Thus, a multisequence alignment analysis was developed firstly to determine the variability or conservation of epitopes in the hamster. To do this, the VGLUT2 protein sequences corresponding to the Slc17a6 gene were retrieved from the NCBI protein database (<http://www.ncbi.nlm.nih.gov/protein/>), and then analyzed using the EBI-Clustal Omega program (<http://www.ebi.ac.uk/Tools/msa/clustalo/>) (Sievers and Higgins, 2018). The multiple sequence alignment showed that the epitope sequence, antigenic region, is highly conserved for all VGLUT2 isoforms in the hamster (Supplemental Material 1).

2.8. Brain tissue processing and immunostaining

Brain tissue used for immunohistochemical analysis was obtained from the animals previously tested for ABR (4 control and 4 GASH/Sal hamsters). After injection of a lethal dose of sodium pentobarbital (60 mg/kg) and the subsequent perfusion through the heart with 4% paraformaldehyde in 0.1 M PBS, brains were removed from the skull, cryoprotected by immersion in 30% sucrose, and coronal sections were cut with a freezing sliding microtome at 40 µm thickness (Sánchez-Benito et al., 2017). Serial sections were collected in PBS and divided into series of 6, 3 of which were for light microscope immunohistochemistry and the

Table 1

List of primers used for RT-qPCRs.

Target gen	Primer Forward	Primer Reverse	Size of products (pb)	Temp (°C)
Vglut1 (<i>Slc17a7</i>)	ACCTGTTCTGGTGCTCGTC	CGTAGACTGGCATGGATGTG	184	60
Vglut2 (<i>Slc17a6</i>)	CTTGGCATGGCTGGTACA	ACGGGGTCTGAATTTC	155	60
Prestin (<i>Slc26a5</i>)	TCGCCATGTCTGACCTTA	CCCACTGTACCGCTTGT	185	60
Cadherin 23 (<i>Cdh23</i>)	ATCCAAGTGGAGATGTGAATGAC	GTTGACGATGAAGATGGGTGTC	108	60
Protocadherin 15 (<i>Pcdh15</i>)	AGTTCTGGATAGAGACCCACCA	ATAACTGTGCCACCTTCTGT	84	60
β-actin	AGCCATGTACGTAGCCATCC	ACCCCTCATAGATGGGCACAG	115	60

other 3 for immunofluorescence. The VGLUT2 was visualized following the indirect method of immunohistochemical staining described by Gómez-Nieto et al. (2008b). All immunostaining steps were performed at room temperature (~22 °C), unless otherwise stated. Washes were made in Tris-buffered saline (TBS), pH 7.4 and dilutions of antisera in TBS containing 0.2% Triton X-100 (catalog No. T9284; Sigma). For light microscopy analysis, free-floating sections were blocked for 1 h with 5% normal goat serum (catalog No. S-1000, Vector Labs.) in TBS-Tx and were incubated with primary antibodies, rabbit anti-VGLUT2, at 1:1000 dilution for 72 h at 4 °C. Sections were then washed and followed an incubation with the biotinylated secondary antibodies, goat anti-rabbit (catalog No. BA-1000, Vector Laboratories), at 1:200 dilution for 2 h. After removal of secondary antisera, the visualization of epitope-antibody interactions was developed with the avidin-biotin-peroxidase complex procedure (catalog No. PK-4000, Vectastain, Vector Labs.), and diaminobenzidine histochemistry for peroxidase without heavy-metal intensification (DAB Kit, catalog No. SK-4100, Vector Labs.). All sections were mounted on slides, dehydrated and coverslipped with Entellan® Neu (catalog No. 107961, Merck). For immunofluorescence analysis, brain sections followed the blocking with 5% fetal calf serum (Sigma) and incubation with primary antibodies as described above. Thereafter, the sections were rinsed extensively and reacted for 2 h with secondary antibody (Cy2 donkey anti-rabbit, catalog No. 711-225-152, Jackson Immunoresearch) at 1:200 dilution for 2 h. Finally, sections were mounted on slides and coverslipped with VECTASHIELD® mounting medium for preserving fluorescence, containing the DAPI counterstain (4',6-diamidino-2-phenylindole, catalog No. H-1200, Vector Labs.).

An additional control hamster was processed to study the morphology of the hamster cochlear nucleus to distinguish its subdivisions. Brain tissue of this animal was processed as described above to obtain coronal and parasagittal sections of 40 μm thickness. Brain sections containing the cochlear nucleus were collected in PBS and divided into 2 series. The first series was processed following the Nissl-staining method to reveal the cytoarchitecture of different cochlear nucleus regions. The second series was stained with the fluorescent DAPI dye that labels the nuclear DNA of cells to precisely identify cytoarchitectonic borders of the cochlear nucleus subdivisions.

In another set of experiments, we studied the morphometric features of VGLUT2-immunolabeled terminals in the cochlear nucleus. For this purpose, 2 control and 2 GASH/Sal hamsters were used. The brain tissue was obtained as described above and embedded in paraffin wax before being cut into coronal sections of 6 μm thickness. Then, sections were mounted onto slides and followed the immunohistological staining procedure to visualize the VGLUT2 protein using the EnVision FLEX Mini Kit, High pH (catalog No. K8023, Dako). After deparaffinization and rehydration, endogenous peroxidase activity was blocked using EnVision FLEX peroxidase-blocking reagent (catalog No. SM801, Dako) for 6 min. Sections were blocked with 5% normal goat serum in TBS-Tx for 1 h, and incubated with primary antibodies, rabbit anti-VGLUT2, at 1:1000 dilution for 24 h. After washing, sections were then

incubated with EnVision Flex linked with horseradish peroxidase (catalog No. SM802, Dako) for 30 min, and the staining was visualized by using the substrate DAB chromogen mix (catalog No. SM803/DM827, Dako). Finally, the sections were counterstained with Carazzi's hematoxylin, dehydrated and cover slipped with DPX Mountant (Sigma). In all immunohistochemical experiments, omission of primary antibody resulted in no positive staining of the preparations. Because VGLUT2-immunoreactivity is well documented in the cerebellar cortex (Hioki et al., 2003; Miyazaki et al., 2003; Zhou et al., 2007), we used the cerebellum as the positive control. The staining patterns for immunohistochemistry and immunofluorescence using VGLUT2 antibody in the cerebellar cortex of the hamster were almost the same as those described in other rodent species (Supplemental Material 2).

2.9. Image acquisition and VGLUT2 analysis

Digital images used for illustration and VGLUT2 analysis were taken from well-defined cytoarchitectonic subdivisions of the cochlear nucleus in control and GASH/Sal animals. All microscope parameters and settings for digitizing the photomicrographs remained constant across both experimental groups and for each animal. The sections processed for light microscopy were studied using a Leitz DMRB (Leica) light microscope coupled with digital camera. Low-magnification images were taken with the 4x or 20x objective lens, and high magnification images were taken with a 40x or 100x objective lens (oil immersion). Images of 6-μm coronal sections at 100x magnification were analyzed through the cochlear nucleus subdivisions to measure the size (area in μm^2) of 482 labeled puncta by tracing their contours using ImageJ software as described elsewhere (Gómez-Nieto et al., 2008a). The sections processed for immunofluorescence were studied on a Zeiss Axio Observer.Z1-Inverted Microscope with ApoTome optical sectioning system (Zeiss) using the appropriate filters for Cy2 and DAPI fluorochromes. Quantification of VGLUT2-immunolabeled puncta was carried out in fluorescence microscopy images that were taken in a single optical plane with a plan-apochromat 63x objective (NA-1.4) using the Multicolor module of AxioVision (Zeiss) with identical image acquisition settings and exposure times. The total number of fluorescence images analyzed was 542, ranging from 16 to 28 in each case (3 control and 3 GASH/Sal hamsters) and each cochlear nucleus subdivision. The analyzed areas had an average of 0.015 mm^2 and included caudal to rostral regions for each of the cochlear nucleus subdivisions. The procedure to count VGLUT2-immunolabeled puncta in fluorescence images using the ImageJ software is shown in the supplemental material 3. To ensure reliable counting, visual inspections were conducted after each automated count (Supplemental Material 3). This procedure was performed by two independent investigators in a single-blind assessment of the samples. The number of puncta was divided by the chosen area to yield the density of puncta per unit area (in mm^2) and corrected for double-counting errors with the Abercrombie formula. Representative images for illustration were collected as stacks with a z-step of 0.25 μm slices with 5x and 63x

objective lenses, and were showed as the maximum intensity projection images of 5 μm thick.

2.10. Image editing and statistical analysis

Representative images shown in the figures were processed by minor modifications with regard to brightness and contrast using ImageJ software and the final figures were composed with Canvas 14. Statistical analyses of ABR amplitudes and latencies, relative gene expression values, morphometric features such as area, perimeter, length and roundness as well as quantification of hair cell stereocilia, SGNs and VGLUT2-puncta were performed using the SPSS-IBM software, version 20 (SPSS Inc., Chicago, IL, USA). All quantitative data were expressed as mean value ± standard error of the mean (SEM). For each statistical analysis, comparisons between control and GASH/Sal animals were performed with analysis of variance (post-hoc analysis with Fisher's test) and Student's *t*-test. The differences were considered statistically significant with a *p* value < 0.05 (*), *p* value < 0.01 (**) and *p* value < 0.001 (***)�.

3. Results

3.1. Evaluation of hearing function

To estimate hearing sensitivity and to identify neurological abnormalities of the auditory nerve and the auditory pathway up through the brainstem of the GASH/Sal, we compared ABR differences between control and GASH/Sal hamsters with respect to ABR thresholds as well as waves amplitudes and latencies. The two animal groups showed five clear peaks of ABR (waves I to V) in response to clicks of the maximum testing intensity (90 dB SPL) after stimulation of the left and right ears. Examples of ABRs are shown in Fig. 1A. The means ± SEM of the ABR threshold in control and GASH/Sal hamsters were 28.7 ± 3.5 dB SPL and 75 ± 9.3 dB SPL, respectively. Statistical comparisons showed that the average ABR thresholds of GASH/Sal hamsters were significantly higher than ABR thresholds of age-matched control animals for left and right ears (*p* < 0.001; Fig. 1B). Differences in amplitudes of the ABR waves were also found between the control and GASH/Sal hamsters (Fig. 1A, C and 2A). The statistical analysis of ABR amplitudes (peak to peak) at 90 dB SPL showed that wave I and IV were significantly lower in the GASH/Sal than in the control hamster (*p* < 0.01; Fig. 1C). However, there were no significant differences in ABR amplitudes for waves II, III and V between the two animal groups (Fig. 1C). The GASH/Sal showed absolute latencies of all waveform components, waves I through V, very similar to those in control animals, and no statistically significant differences were found (Fig. 1D). The inter-peak latency of ABR waves did not show any statistically significant differences between the two animal groups (Fig. 1E). The ABR analysis showed that the auditory function of GASH/Sal animals is impaired at 4 months old, exhibiting very high auditory thresholds with a pronounced decrease in the amplitude of wave I, which was accompanied by an equivalent significant decline of wave IV.

3.2. Cochlear histopathology

The elevated ABR threshold and reduced wave I amplitude in the GASH/Sal might be associated with auditory nerve fibers reductions, reflecting possible pathological alterations in the cochlea. In order to investigate whether these ABR abnormalities in the GASH/Sal correlated with morphological defects in the cochlea, a histological study was performed after ABR testing (Fig. 2A). Same as in the control group, the cochlear microscopic structure of the GASH/Sal animals in a cross section from the base to the apex

showed preservation of the Reissner's, basilar and tectorial membranes as well as normal appearance of cochlear turns without apparent loss of sensory hair cells (Fig. 2B–G). However, alterations in the organ of Corti, the spiral ganglion cells and stria vascularis were found in all GASH/Sal animals that exhibited a decline of ABR wave I amplitude (Figs. 2–4). In the organ of Corti of control animals, the supporting cells and hair cells with stereocilia bundles were identified with clear cell definition (Fig. 2D and F). In contrast, GASH/Sal animals showed complete absence of stereocilia bundles in the IHCs and OHCs as well as morphological alterations in supporting cells (see Fig. 2F and G for comparison). Since the major site of cochlear pathology frequently includes auditory neurons in the spiral ganglion, we also assessed the number of SGNs in the basal, middle and apical regions of the cochlea from the same animal groups (Fig. 3). A generalized reduction of SGNs was observed in Nissl-stained sections of the GASH/Sal cochlea. In contrast to the control spiral ganglion (in which SGNs were tightly packed), the SGNs in the GASH/Sal were scattered in the entire cochlear modiolus (Fig. 3A). These qualitative differences of neuronal loss in the GASH/Sal animals were confirmed by counting the SGNs in each profile of the Rosenthal's canal. The mean SGN density of GASH/Sal animals was significantly lower than that of control animals for each cochlear region of the spiral ganglion (*p* < 0.001; Fig. 3B). Compared to controls, the following regional percent decreases were obtained in the GASH/Sal: apex (37.8%), middle (43.3%), and base (41.4%), indicating that these losses are occurring uniformly along the length of the spiral ganglion. The mean total density of SGNs per mm³ was 189.4 × 10³ (SEM = ± 33.9) for control animals and 112.1 × 10³ (SEM = ± 24.9) for GASH/Sal animals. These decreases in density might be caused by either a decrease in the number of SGNs or by an increase in the volume of the canal, thus we analyzed the canal volume measurements in both animal groups. The mean total volume of the canal measured in controls and GASH/Sal animals was 0.0083 mm³ (SEM = ± 0.0015) and 0.0084 mm³ (SEM = ± 0.0011), respectively, and the mean volume of the canal in each cochlear region was not significantly different in the two groups of animals (Supplemental Material 4). This indicates that the density differences between controls and GASH/Sal animals were due to changes in number of SGNs, rather than in the volume of the Rosenthal's canal. Another feature that might contribute to the differences observed in the ABR waveforms is the cell size and shape of SGNs. In controls animals, Nissl-stained sections of the spiral ganglion allowed to distinguish between the both types of SGNs (Supplemental Material 5). Type I neurons had a larger cell body with prominent Nissl bodies in their cytoplasm, and a pale staining nucleus. Type II neurons were distinguished by their small somatic size and pale cytoplasm. In the GASH/Sal, SGNs occasionally exhibited pyknotic nuclei and shrunken cell somata, and hence, distinguishing between the two types of SGNs was not possible (Supplemental Material 5). In both animal groups, a satellite glial cell was frequently observed in the side of the cell bodies of SGNs (Fig. 3A and Supplemental Material 5). Thus, in order to quantify changes in neuronal size, the cross-sectional areas of SGNs were measured along the length of the spiral ganglion, regardless of the cell type and without including the satellite glial cell. The differences in the area and perimeter of spiral ganglion cell bodies were statistically significant when compared control and GASH/Sal hamsters (*p* < 0.001; Fig. 3C). Relative to controls (mean area of 91.9 ± 16.3 μm² and perimeter of 34.8 ± 3.1 μm), the cross-sectional area and perimeter of SGNs in the GASH/Sal exhibited a percentage reduction of 20.4% and 10.6%, respectively. Furthermore, we measured the roundness of SGNs in the control and GASH/Sal hamsters. Although the mean values of soma roundness were slightly reduced in the GASH/Sal, we found no statistically significant difference (Fig. 3D). Since atrophy of the SV is a common cause

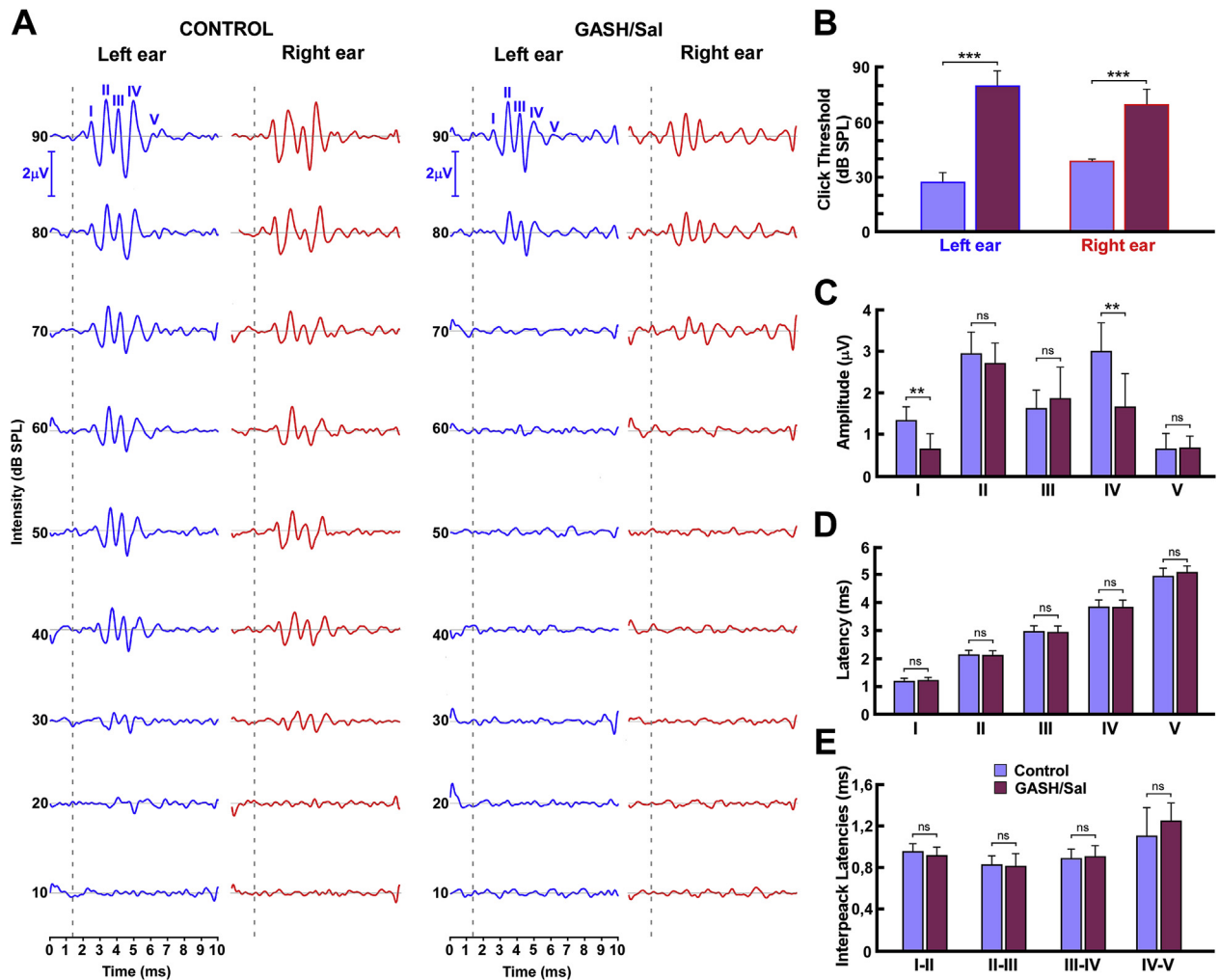


Fig. 1. ABRs differences between the control and GASH/Sal hamsters. **A**, Plots show a representative example of the ABR waveforms obtained from control and GASH/Sal hamsters after click stimulation on the left (in blue) and right (in red) ears. ABR waveforms (amplitude in μ V) were recorded from 10 to 90 dB SPL along the first 10 ms. The stimulus onset starts at 1.4 ms. Notice that waves were visible at 30 dB SPL for the control animal, whereas the GASH/Sal's waveforms were visible at 70 and 80 dB SPL for the right and left ears, respectively. Note that waves amplitudes in the GASH/Sal animal were smaller than in the control hamster at suprathreshold levels. **B**, Plot shows ABR thresholds to clicks for the two animal groups (control and GASH/Sal) after stimulation on the left and right ears. Note that ABR thresholds were significantly lower in GASH/Sal hamsters. **C**, Plot shows ABR amplitudes in microvolts (μ V) for each waveform responses (I, II, III, IV and V) measured at 90 dB SPL in the two animal groups. Notice that mean values of waves I and IV were significantly lower in the GASH/Sal. **D**, Plot displays latencies for each waveform responses in the two animal groups. Notice that there were no significant differences between the control and GASH/Sal hamsters. **E**, ABR mean inter-peak latencies in ms for the control group compared to GASH/Sal. There were no significant differences between the two animal groups. For histograms B-C-D-E, controls are displayed in blue and GASH/Sal in purple. Graphs display the mean with SEM error bars. *** = p value ≤ 0.01 ; **** = p value ≤ 0.001 ; ns = non-significant. (For interpretation of the references to color in this figure legend, the reader is referred to the Web version of this article).

for alterations in hearing sensitivity (Schuknecht et al., 1974), we analyzed the cytoarchitecture, the number of blood vessels and the thickness of SV in the apical, middle, and basal regions of the cochlea (Fig. 4). In the control hamster, the SV showed a normal histological organization consisting of three layers of distinct cell types (marginal, intermediate and basal cells) that were highly vascularized by intraepithelial capillaries (Fig. 4A). Although the gross morphology of the SV was apparently conserved in the GASH/Sal, we found traits of mild stria atrophy that included changes in the capillary network and SV thickness as well as absence of stria cells, particularly in the basal and middle cochlear turns (Fig. 4A). Accordingly, the quantitative analyses showed significantly fewer capillaries in all regions of the GASH/Sal cochlea compared with controls (Fig. 4B). In addition, the morphometric measurements indicated a significant reduction in SV thickness in the basal and middle regions of the GASH/Sal cochlea, whereas no significant differences were found in the apical regions (Fig. 4C). Together,

these results indicated a reduction of the microvasculature and thickness of the SV in the GASH/Sal cochlea that correlated with abnormalities in the spiral ganglion and cochlear function.

3.3. Scanning microscope study of the reticular lamina

Our histological results suggested defects in the cytoarchitecture of the organ of Corti of the GASH/Sal, including loss of stereocilia in the hair cells and changes in the morphology of cochlear supporting cells. This led us to investigate further the surface of the organ of Corti (the so-called "reticular lamina") along the longitudinal direction of the cochlea using scanning electron microscopy. Control hamsters exhibited the typical ordered cellular pattern of hair cells and supporting cells (Fig. 5 and Supplemental Material 6). The three rows of OHCs were separated from the single row of IHCs by the inner pillar cells (Fig. 5A and Supplemental Material 6A). Both IHC and OHC stereocilia had normal morphology and were observed as

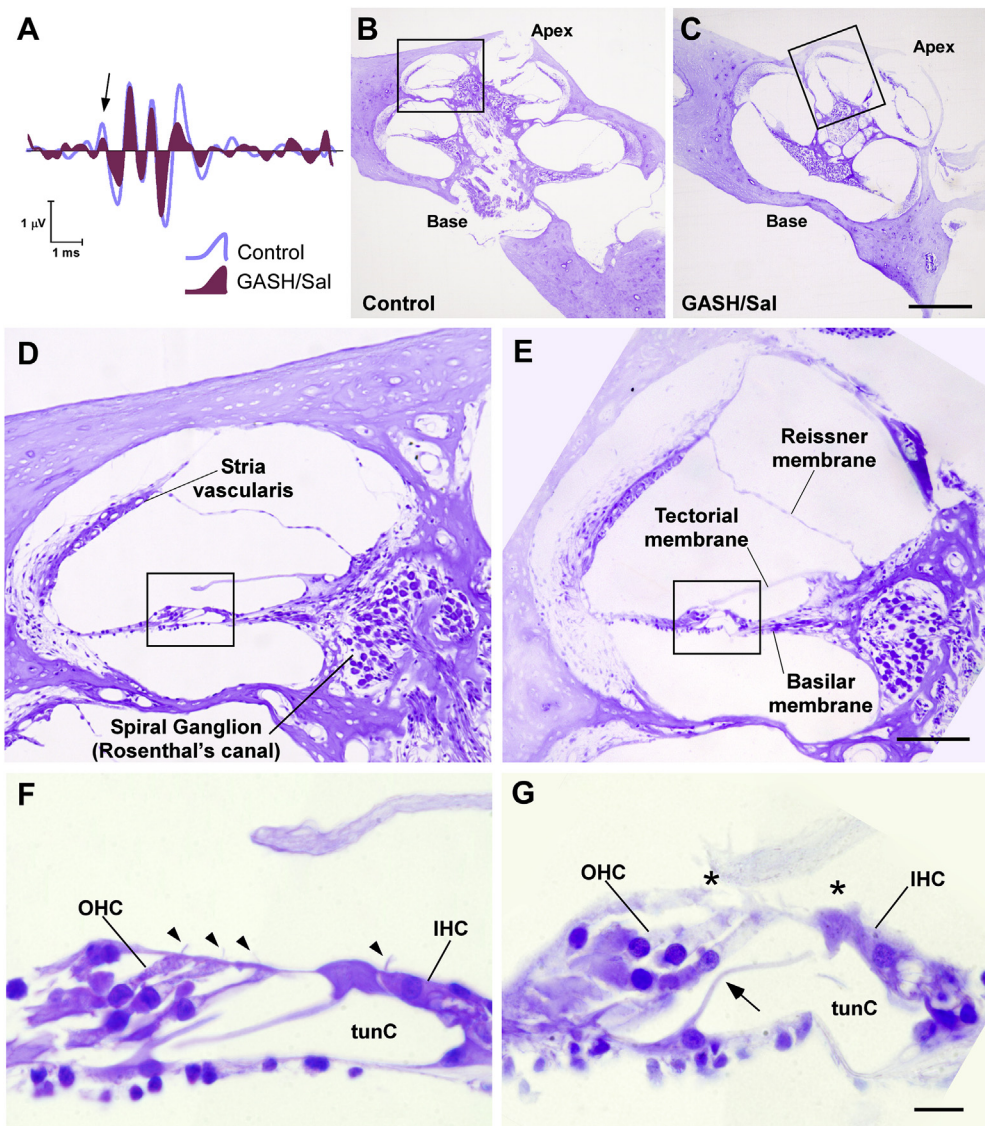


Fig. 2. Cochlea overview of the control and GASH/Sal hamsters. **A.** Representative ABRs in response of click stimulation at 90 dB SPL, corresponding to the cochleas showed in Fig. 2B and C. Notice the reduction in the amplitude of the ABR waveform I (arrow) in the GASH/Sal compared to the control. **B–C.** Light micrographs of mid-modiolar Nissl-stained cochlear sections in the control (B) and GASH/Sal (C) hamsters. **D–E.** Higher magnifications corresponding to the frame in B and C show the organ of Corti. Note the Reissner's, basilar and tectorial membranes are preserved in the GASH/Sal. **F–G.** Higher magnifications corresponding to the frame in D and E show inner and outer hair cells (IHC and OHC) in the control and GASH/Sal hamsters. Note that the control animal shows stereocilia (arrowheads) in both IHC and OHC, whereas the GASH/Sal shows missing stereocilia (asterisks). Also, notice the different appearance of the tonofilaments in pillar cells (arrow) enclosing the tunnel of Corti (tunC) in the GASH/Sal. Scale bars = 500 μ m in B, C; 100 μ m in D, E; 10 μ m in F, G.

cylindrical protrusions characterized by highly-organized rows of stereocilia with precise height and width. The stereocilia of IHCs formed a straight or slightly curved bundles (Fig. 5E and Supplemental Material 6A) and the OHC stereocilia formed a V-shaped pattern with a well-defined gradient in height across the stereocilia rows (Fig. 5C and E and Supplemental Material 6B). The reticular lamina of GASH/Sal animals also consisted of a single row of IHCs and three rows of OHCs, however in contrast to controls, a disarray of regular arrangement in three rows of the OHCs were frequently found (Fig. 5B and Supplemental Material 6C). The most noticeable difference compared to control hamsters was the disorganization of stereociliary tufts (Figs. 5 and 6). Such a severe disruption in the regular arrangement of stereocilia was found in both types of hair cells along the entire length of the cochlea (Fig. 6). This stereocilia distortion was frequent in all three rows of the OHCs, and included bents and separations from each other with loss of stereocilia links

(Fig. 5D, E and 6). The typical V-shaped pattern of stereociliary tufts was absent in the OHCs of the GASH/Sal (Figs. 5D and 6 and Supplemental Material 6C), and occasionally, their stereocilia appeared to be collapsed (Fig. 6A2–B2–C2). In addition, we frequently found blebs of various size (diameter 0.6–2.1 μ m) arising from the cuticular plates of IHCs in all regions of the reticular lamina (Fig. 6A1–B1–C1). Shortening and complete loss of stereociliary tufts were more prevalent in the OHCs than the IHCs, and was particularly more pronounced in the basal turn of the cochlea (Figs. 5D and 6C). To assess changes in stereociliary height and number of stereocilia in the preserved bundles, we measured the length of the tallest stereocilia row and counted their number for each IHC and OHC. Morphometric measurements showed elongated stereocilia in both hair cell types of the GASH/Sal, especially in OHCs with distorted bundle configuration (Fig. 5E and F). Thus, the stereocilia length of IHCs and OHCs in the GASH/Sal were significant greater than in

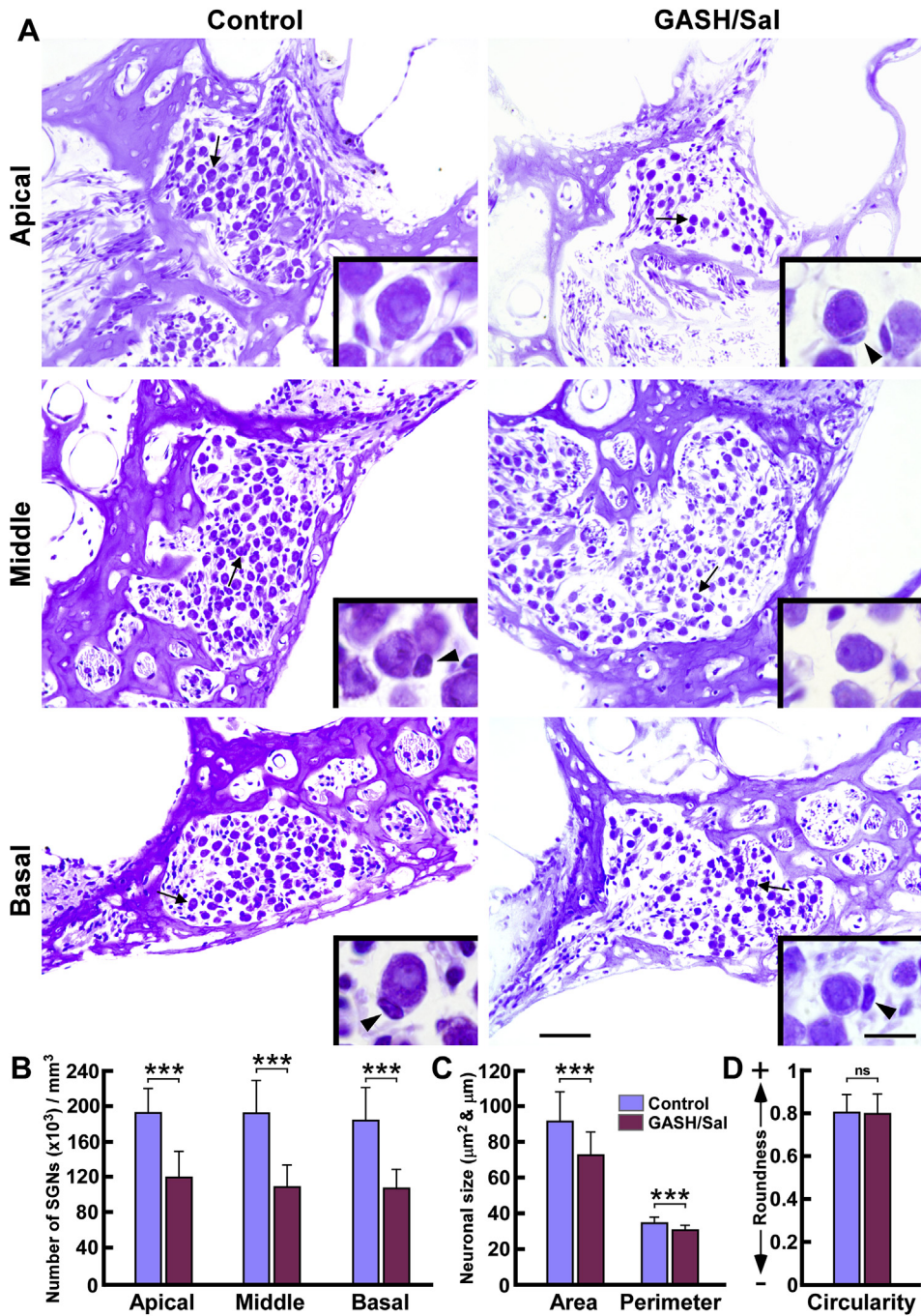


Fig. 3. Quantification and morphometric analyses of spiral ganglion neurons (SGNs) in the control and GASH/Sal hamsters. **A.** Photomicrographs of Nissl-stained sections corresponding to the basal, middle, and apical turns of the cochlea in the control and GASH/Sal hamsters. Insets show details of SGNs somata (corresponding to the arrows in each panel) and the neighboring satellite glial cells (arrowheads). Notice qualitative differences of neuronal loss and somata size in each different region of the GASH/Sal cochlea compared to control hamsters. Scale bars = 50 µm for all panels and 10 µm for insets. **B.** Plot shows the number of SGNs in each different region (apical, middle, and basal) of cochlea tissue. Notice significant loss of SGNs in the GASH/Sal compared to controls. **C.** Histogram shows the area (μm^2) and perimeter (μm) of the cross-sectional areas of SGNs in the control and GASH/Sal hamsters. Notice significant differences in somata size between the control and GASH/Sal hamsters. **D.** Histogram shows the cell roundness of SGNs, where 0 is an infinitely elongated polygon and 1 is a perfect sphere. There was no statistically significant difference in cell roundness between the control and GASH/Sal hamsters. For histograms B-C-D, controls are displayed in blue and GASH/Sal in purple. *** = p value ≤ 0.001 ; ns = non-significant. (For interpretation of the references to color in this figure legend, the reader is referred to the Web version of this article).

controls, with average increase of a quarter for IHCs and twice the length for OHCs ($p < 0.001$; Fig. 5F). We also found that the stereocilia number for both cell types was significantly lower in the GASH/Sal than in control animals ($p < 0.001$; Fig. 5G). Compared to control animals, the IHCs and OHCs in the GASH/Sal showed a percentage decrease of 24% and 38.3%, respectively. Therefore, changes in

morphology and number of stereocilia were more pronounced in OHCs than in IHCs. As a result of such abnormalities in the stereociliary bundles, and because supporting cochlear cells have an important role in degenerative and regenerative events of the hair cells, we also examined the Deiters' cells. In control animals, the cell apex of Deiters' cells extended upward to the reticular lamina in an

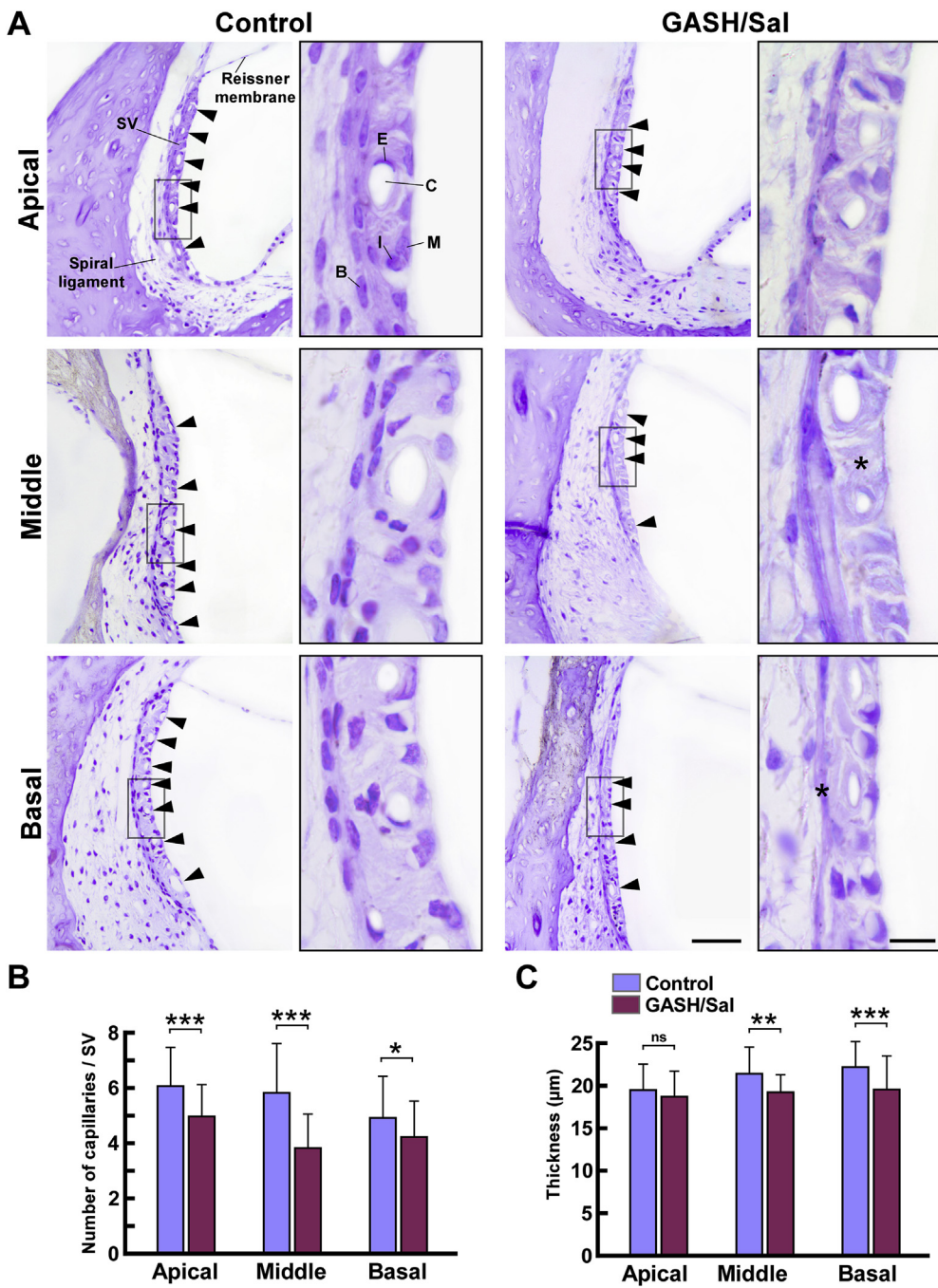


Fig. 4. Comparison of the stria vascularis (SV) in the control and GASH/Sal hamsters. **A.** Photomicrographs of Nissl-stained sections, corresponding to the scala media of basal, middle, and apical turns of the cochlea show representative examples of the SV in control and GASH/Sal hamsters. The area marked by a black square is presented in an adjacent panel with higher magnification to show details of the three layers of cells and capillaries in the SV. Notice lower number of stria capillaries (arrowheads) and lesser SV thickness as well as absence of stria cells (asterisks) in the GASH/Sal when compared to control hamsters. **B.** Plot shows the number of capillaries per SV in each cochlear region (apical, middle, and basal). Note there is a significant loss of vessels in the GASH/Sal compared to controls. **C.** Histogram shows the thickness (in μm) of the SV in each cochlear turn. Notice significant differences in the SV thickness of middle and basal turns between the control and GASH/Sal hamsters. For histograms B and C, controls are displayed in blue and GASH/Sal in purple. $^{**} = p \text{ value} \leq 0.05$; $^{***} = p \text{ value} \leq 0.01$; $^{****} = p \text{ value} \leq 0.001$; ns = non-significant. B, basal cell; C, capillary; E, endothelial cell; I, intermediate cell; M, marginal cell; SV, stria vascularis. Scale bars = 50 μm in low-magnification panels and 10 μm in high-magnification panels. (For interpretation of the references to color in this figure legend, the reader is referred to the Web version of this article).

orderly pattern that distributed in between neighboring OHCs (Fig. 5C and Supplemental Material 6A-B). In contrast to this, Deiters' cells in the GASH/Sal were observed extruding from the apical surface and encroaching into the space of neighboring cells (Fig. 6A and Supplemental Material 6C). These expansions of Deiters' cells were found with increased surface granularity that, at high magnification,

appeared as short microvilli (Fig. 6A2-B2 and Supplemental Material 6C). Also, the heads of Deiters' cells ended up merging areas of the reticular lamina that showed disarray in three rows of OHCs as well as areas with complete loss of OHC stereocilia (Fig. 6A-B-C and Supplemental Material 6C). Cell bodies of Deiters' cells were preserved in the GASH/Sal as in controls and their phalangeal processes

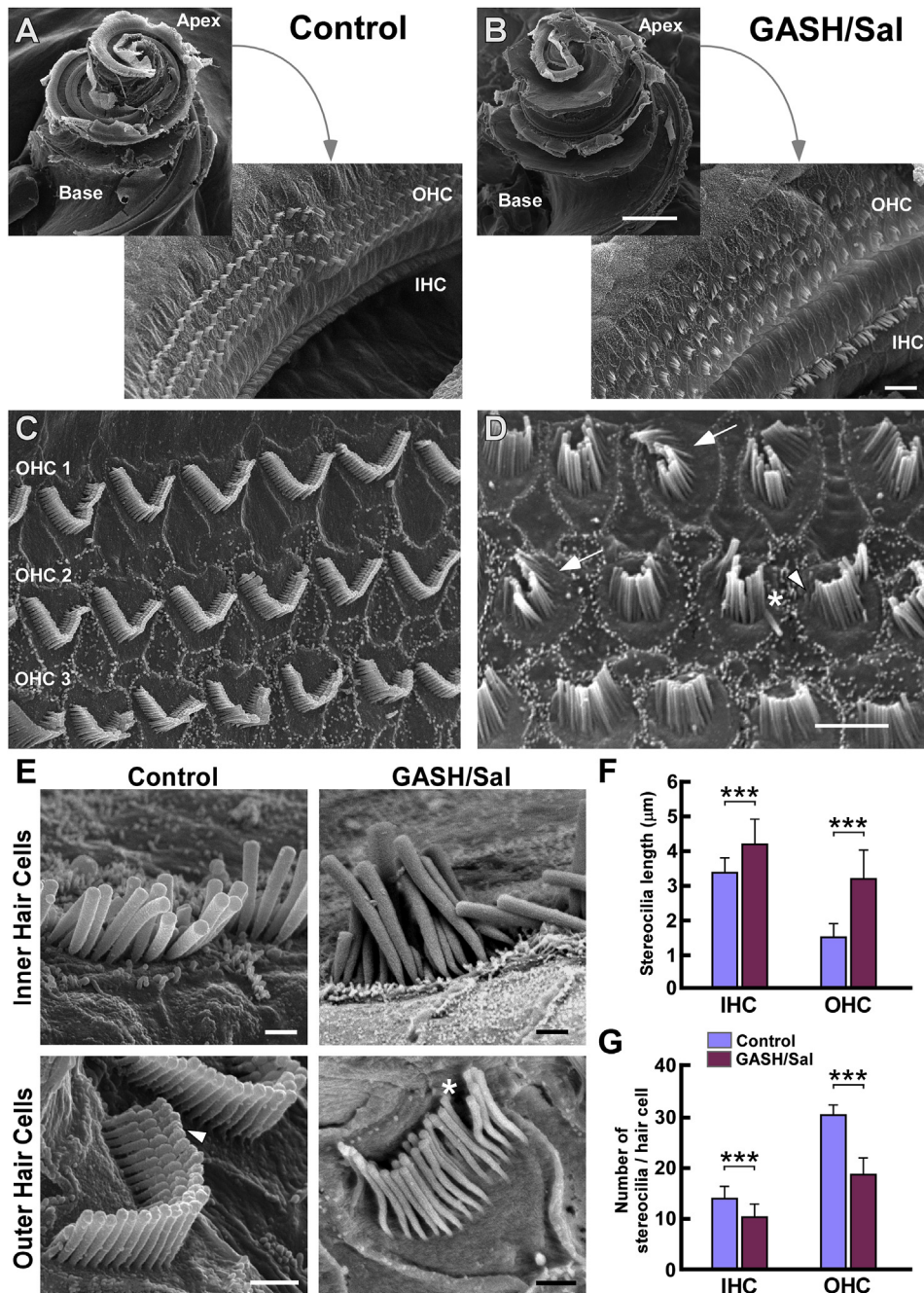


Fig. 5. Scanning electron microscopy (SEM) of the surface of the organ of Corti (reticular lamina) in the control and GASH/Sal hamsters. **A-B.** Low magnification SEM images show the 3 turns of the spiralling basilar membrane supporting the organ of Corti of the control (A) and GASH/Sal (B) hamsters. Higher magnifications of part of the mid-turn of the cochlea showing the orderly rows of inner (IHC) and outer hair cells (OHC). Compare the arrangement of stereocilia in the IHCs and OHCs of the control hamster with that observed in the GASH/Sal. **C-D.** SEM images of the reticular lamina show the three rows of outer hair cells (OHC 1–3) in the control (C) and GASH/Sal (D) hamsters. Compare the V-shape regular pattern of stereociliary tufts in the control cochlea with the disarray of the stereociliary bundles (arrows) in the GASH/Sal. Also, note collapse of stereocilia (asterisk) and shortened stereocilia (arrowhead) in the GASH/Sal. **E.** Higher magnification SEM images show details of stereocilia protruding from the apices of IHC and OHC in the control and GASH/Sal cochleae. Compare the straight or slightly curved bundles of stereocilia in the control IHC with the altered distribution in the GASH/Sal. The control OHC shows linear stereociliary bundles arranged in three rows of graded heights and the links between the stereocilia (arrowhead), whereas the stereocilia of the GASH/Sal OHC are thinner, bent and separated from each other with loss of their links (asterisk). **F.** Histogram shows the mean lengths of stereocilia from the tallest row of the bundle. Notice significant differences in stereocilia length of IHC and OHC between control and GASH/Sal hamsters. Each bar is an average \pm S.E.M. of stereocilia from 44 IHC and 62 OHC per animal group. **G.** Histogram shows the number of the tallest stereocilia row per hair cell. Notice significant differences in the number of IHC and OHC stereocilia between the control and GASH/Sal hamsters. Each bar is an average \pm S.E.M. of 27 IHCs and 57 OHCs per animal group. For histograms F and G, controls are displayed in blue and GASH/Sal in purple. “***” = p value ≤ 0.001 . Scale bars = 500 μ m in A and B (10 μ m for higher magnifications); 5 μ m in C and D; 1 μ m in E. (For interpretation of the references to color in this figure legend, the reader is referred to the Web version of this article).

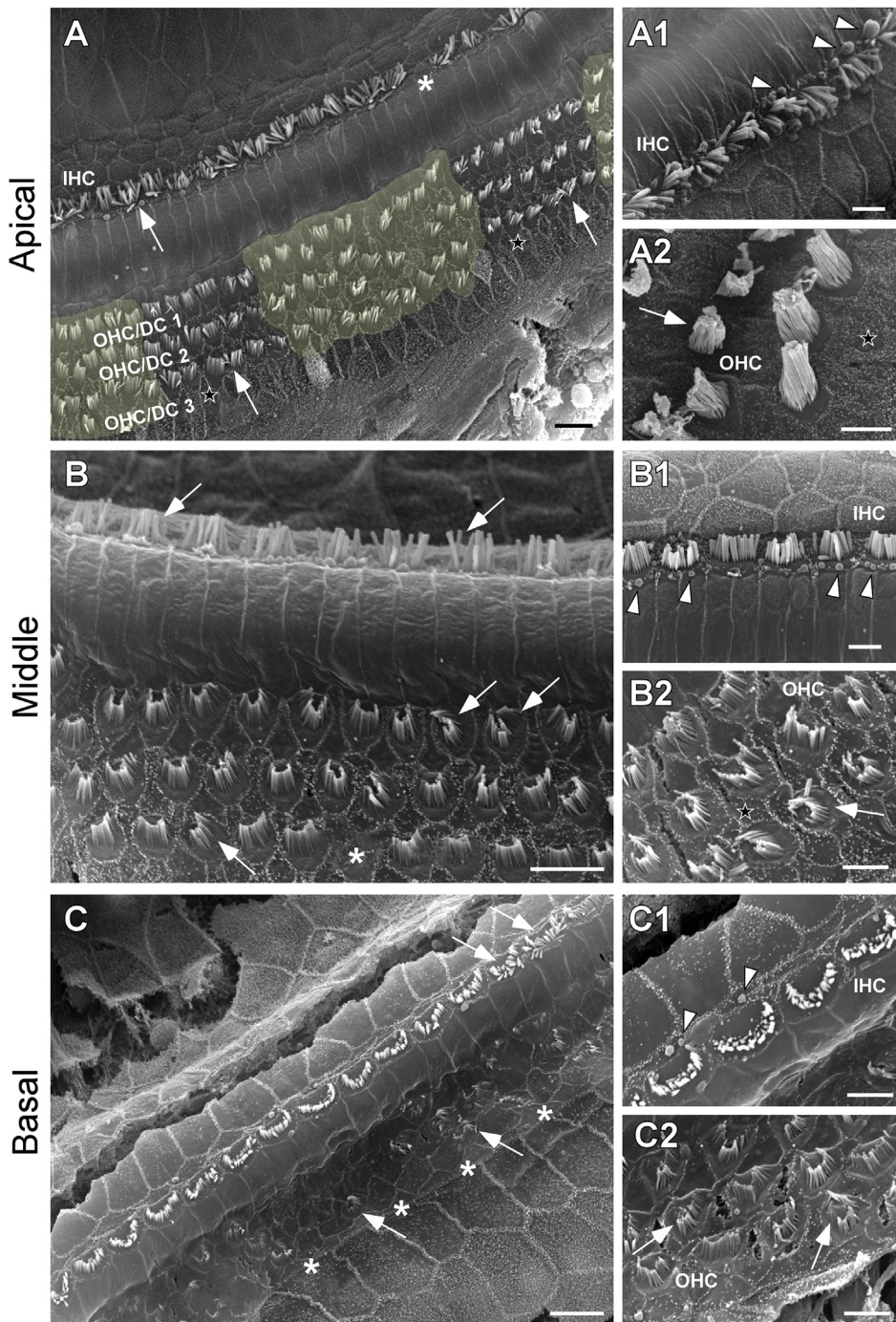


Fig. 6. Scanning electron microscopy of the apical (A), middle (B), and basal (C) turns of the reticular lamina in the GASH/Sal. Notice disarray of regular arrangement in three rows of outer hair cells and Deiters' cells (OHC/DC 1–3, depicted in yellow). Stereocilia distortion (arrows), including bends and separations from each other with loss of stereocilia links are frequent in the three rows of the OHC and in the inner hair cells (IHC). Also, notice the loss of stereociliary tufts and bundles (asterisks), particularly in the basal turn of the cochlea. Higher magnification SEM images show details of the OHC and IHC at the apical (A1–2), middle (B1–2), and basal (C1–2) turns of the GASH/Sal cochlea. Notice frequent blebs (arrowheads) arising from the cuticular plates of IHC. Also, note the increased surface granularity in form of short microvilli (black stars) in the cell apex of supporting cochlear cells. The "V" and "staircase"-like pattern of OHC stereocilia was absent, showing instead shortening, distortion and collapse of the stereociliary tufts (arrows). Scale bars = 10 µm in A, B and C; 5 µm in A1–2, B1–2 and C1–2. (For interpretation of the references to color in this figure legend, the reader is referred to the Web version of this article).

extended obliquely to the reticular lamina (Supplemental Material 6D). Together, these analyses showed an abnormal reticular lamina with peculiar stereociliary defects in the hair cells, thereby confirming our light microscopy observations and suggesting a clear correlation with the loss of functional hearing in the GASH/Sal.

3.4. Disruption in the expression of cochlear genes

To gain further knowledge of the gene expression patterns that underlie the alterations in the cochlear morphology and function of the GASH/Sal, we analyzed mRNA expression levels of the following cochlear genes: *Prestin*, *Cdh23*, *Pcdh15*, *Vglut1*, and *Vglut2*. We

selected these genes, as the proteins they encoded, are essential for the mechanoelectrical transduction and stereocilia integrity in hair cells as well as for the synaptic connection with the cochlear nuclei in the brainstem (Fig. 7A). Whole cochlear tissue containing the sensory epithelium and spiral ganglia were freshly dissected from control and GASH/Sal animals, and a total RNA was extracted immediately. Quantitative gene expression data were normalized using β -actin as internal reference gene. There were no significant differences in the number of cycles to reach the amplification threshold for β -actin with any of the animal groups, indicating that our sample preparation was consistent. Comparison of gene expression/ β -actin ratios showed that expression of the all five genes in the GASH/Sal cochleae was significantly lower than in the control cochleae (Fig. 7B). *Prestin* that is responsible of the OHC electromotility showed a marked reduction of mRNA levels in the GASH/Sal compared to controls ($p < 0.001$), a result that correlates to the increased ABR thresholds and the abnormal or absent OHC stereocilia bundles in the GASH/Sal. Expression levels of *Cdh23* and *Pcdh15* genes, the tip link constituents that connect stereocilia of a hair cell into a bundle, were also found significantly decreased in GASH/Sal animals versus control hamsters ($p < 0.05$; Fig. 7B). These results were associated with the stereocilia disorganization and loss of tip links observed in the electron microscopy analysis of the reticular lamina. Compared to controls, mRNA levels of *Vglut1* and *Vglut2* genes were severely underexpressed in the GASH/Sal ($p < 0.001$, Fig. 7B). Such a disruption in the expression of genes encoding vesicular glutamate transporters, which are essential for the auditory nerve fibers synaptic connections with the cochlear nuclei, were positively correlated with reductions of ABR wave I amplitudes and the neuronal loss in the spiral ganglion of the GASH/Sal.

3.5. Altered VGLUT2 puncta distribution and *Vglut1-2* mRNA expression in the cochlear nucleus

The reduced number of SGNs within the Rosenthal's canal of the GASH/Sal together with the expression imbalance of VGLUTs genes in the cochlea of the GASH/Sal, led us to analyze the distribution VGLUT2-immunolabeling in the cochlear nucleus of the GASH/Sal and compare with that of control animals. As shown in sagittal and coronal sections, the DAPI and Nissl staining allowed us to visualize the morphology of the hamster cochlear nucleus and identify its

subdivisions based on cellular characteristics (Fig. 8). The DCN capped the ventral cochlear nucleus, which in turn was divided into two subnuclei, the PVCN and AVCN, at the level of the cochlear nerve root. The granule cell domain (GCD) contained small ovoid cells that formed a continuous layer that covered most of the cochlear nucleus complex along the rostrocaudal axis. Thus, the GCD included granular regions of the DCN layers, PVCN, and AVCN that were clearly differentiated from magnocellular cell areas in each of those subdivisions (Fig. 8). Based on this cytoarchitectural features, we conducted the immunohistochemistry analysis in the following subdivisions of the cochlear nucleus: the DCN (deep and fusiform cell layer), the magnocellular cell areas of the PVCN and AVCN as well as the GCD (Fig. 8C–G). In control animals, VGLUT2-immunolabeling was found differentially distributed throughout the subdivisions of the cochlear nucleus complex. Thus, qualitative light microscope observations of 6- μ m coronal sections showed moderate immunolabeling in the DCN, weak immunolabeling in the magnocellular cell areas of PVCN and AVCN, and intense immunolabeling in the GCD (Fig. 9A). In contrast, the GASH/Sal hamsters exhibited strong and intense VGLUT2-immunolabeling in the magnocellular cell areas of PVCN and AVCN, whereas the GCD was weakly immunolabeled (Fig. 9B). VGLUT2-immunolabeling was observed as puncta around neuronal cell bodies counterstained with Carazzi's hematoxylin (Fig. 9). At higher magnification, VGLUT2-immunolabeled puncta was found to vary in shape and size throughout the cochlear nucleus subdivisions (Fig. 9). Small-to medium-size *en-passant* endings and large mossy-like endings were found in all subdivisions of the cochlear nucleus complex, with predominance of mossy-like puncta in the GCD (Fig. 9). There were slight differences in the size of VGLUT2-immunopositive puncta between both animal groups. Morphometric measurements revealed that the size (mean area \pm SEM) of VGLUT2 *en-passant* endings were $2 \pm 0.9 \mu\text{m}^2$ (ranging from 0.4 to $4 \mu\text{m}^2$) for control hamsters, and $2.2 \pm 1 \mu\text{m}^2$ (ranging from 0.4 to $4.4 \mu\text{m}^2$) for GASH/Sal animals. On the other hand, the size of VGLUT2 mossy-like endings were $8.4 \pm 3.6 \mu\text{m}^2$ (ranging from 4 to $21.8 \mu\text{m}^2$) for controls and $7.1 \pm 3.1 \mu\text{m}^2$ (ranging from 4.2 to $17.1 \mu\text{m}^2$) for GASH/Sal animals. Changes in the distribution of VGLUT2-immunolabeling were also evident in sections of 40- μ m thick (Fig. 10). When compared to controls, GASH/Sal animals exhibited a very dense, patchy and disorganized VGLUT2-immunolabeling composed of numerous varicosities, particularly noticeable in the

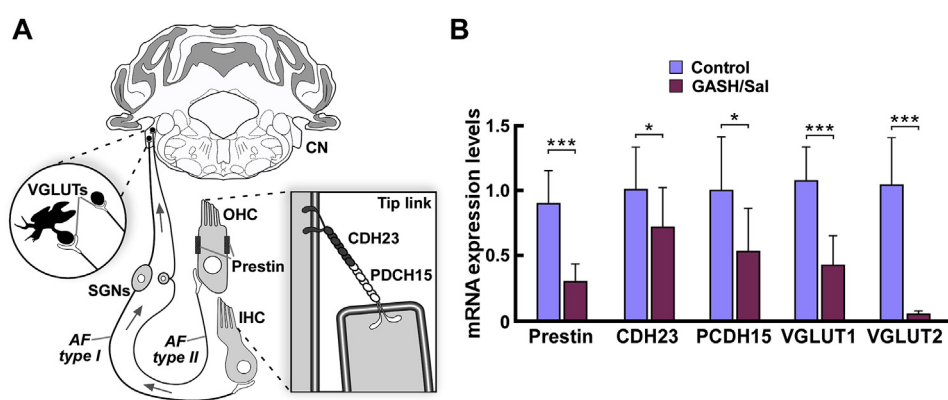


Fig. 7. mRNA expression levels of cochlear genes in the GASH/Sal. **A.** Sketch shows the molecular components of the mechanotransduction machinery that were subjected to gene expression analysis. Notice the location of the corresponding proteins: Prestin, cadherin 23 (CDH23), protocadherin 15 (PCDH15), and vesicular glutamate transporters (VGLUTs: VGLUT1 and 2). Arrows indicate direction of the signal transmission from the inner and outer hair cell (IHC and OHC, respectively) to the cochlear nuclei (CN), via afferent fibers of spiral ganglion neurons (AF type I and type II). **B.** Histogram shows relative quantities of transcripts of the cochlear genes in the control and GASH/Sal animals. The relative mRNA expression of each gene of interest was normalized to β -actin. ΔCt values were normalized to the average ΔCt of the control cochlear tissue. Asterisks indicate significance of the difference in expression of each gene in the GASH/Sal cochleae as compared to the control cochleae. “*” = p value ≤ 0.05 ; “**” = p value ≤ 0.01 ; “***” = p value ≤ 0.001 ; ns = non-significant.

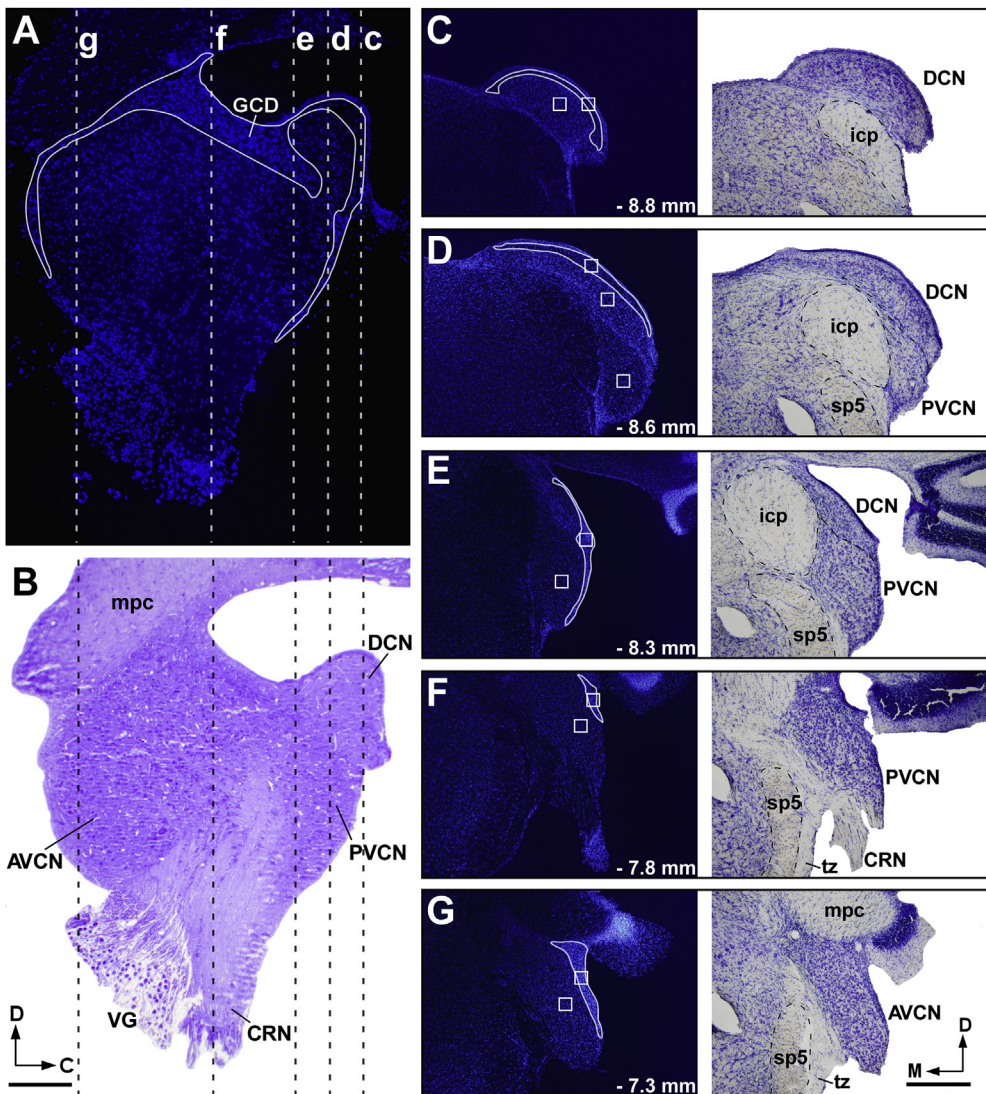


Fig. 8. Overview of the cochlear nucleus in the hamster and the slice planes used in this study. **A-B.** Sagittal sections of the hamster cochlear nucleus, stained with DAPI (A) and cresyl violet (B), show five representative levels (dashed lines) through the cochlear nucleus that were used for VGLUT2-immunoreactivity analysis. The GCD comprises the summed granular regions of the DCN layers, PVCN and AVCN. Notice the GCD outlined with a white line in A. **C-G.** Coronal sections corresponding to the slice planes depicted in A and B show representative locations where photomicrographs were taken for VGLUT2 analysis (indicated with squares in the DAPI stained sections). The regions of interest from caudal to rostral ends of cochlear nucleus, include the DCN (C, D, E), PVCN (D, E, and F), AVCN (G), and the granule cell domain (outlined with a white line in the DAPI stained sections). Each panel shows DAPI-stained sections and adjacent Nissl-staining sections, which allowed precise delineation of the cochlear nucleus subdivisions, and served as cytoarchitectural reference. The number at the bottom of each panel indicates the corresponding location in millimeters relative to Bregma. AVCN, anteroventral cochlear nucleus; CRN, cochlear root nucleus; DCN, dorsal cochlear nucleus; GCD, granule cell domain; icp, inferior cerebellar peduncle; mpc, middle cerebellar peduncle; PVCN, posteroventral cochlear nucleus; sp5, spinal trigeminal tract; tz, trapezoid body; VG, vestibular or Scarpa ganglion. Scale bars = 250 μ m in A and B; 500 μ m in C-G. (For interpretation of the references to color in this figure legend, the reader is referred to the Web version of this article).

magnocellular core of the PVCN and AVCN, whereas immunolabeling was sparser in the GCD (Fig. 10A). VGLUT2-immunolabeled puncta appeared to have a similar pattern and appearance in the DCN in both animal groups (Fig. 10A). In the cochlear root nucleus, we also observed qualitatively differences between control and GASH/Sal hamsters. VGLUT2-immunolabeling was also found in form of puncta surrounding dendrites and cell bodies of cochlear root neurons, with a much stronger immunolabeling in the GASH/Sal than in controls (Fig. 10B). In GASH/Sal animals, VGLUT2 immunohistochemistry gave so intense immunolabeling signal on the cell bodies of the cochlear root neurons that puncta were no clearly definable (Fig. 10B). In both animal groups, *en-passant* and mossy-like VGLUT2-immunolabeled puncta were found outlining neuronal clusters in magnocellular regions of the ventral cochlear

nucleus, preferentially in the AVCN (Fig. 10C). These neuronal clusters were identified as cells with ovoid shape, presumed to be bushy cells, with dendritic processes oriented toward adjacent cell bodies, which were frequently found next to each other (Fig. 10C). The observations based on qualitative assessment under light microscope were subjected to verification by a quantitative immunofluorescence analyses (Supplemental Material 3). Fig. 11A shows representative fluorescence microscopy images of all examined cochlear nucleus subdivisions and confirmed the altered distribution of VGLUT2-immunolabeling observed in the light microscopy analysis (for comparison see Figs. 9 and 11A). Quantitative immunofluorescence analysis showed that VGLUT2-puncta density was significantly increased in the PVCN and AVCN of the GASH/Sal as compared to controls ($p < 0.001$; Fig. 11B). By contrast, VGLUT2-

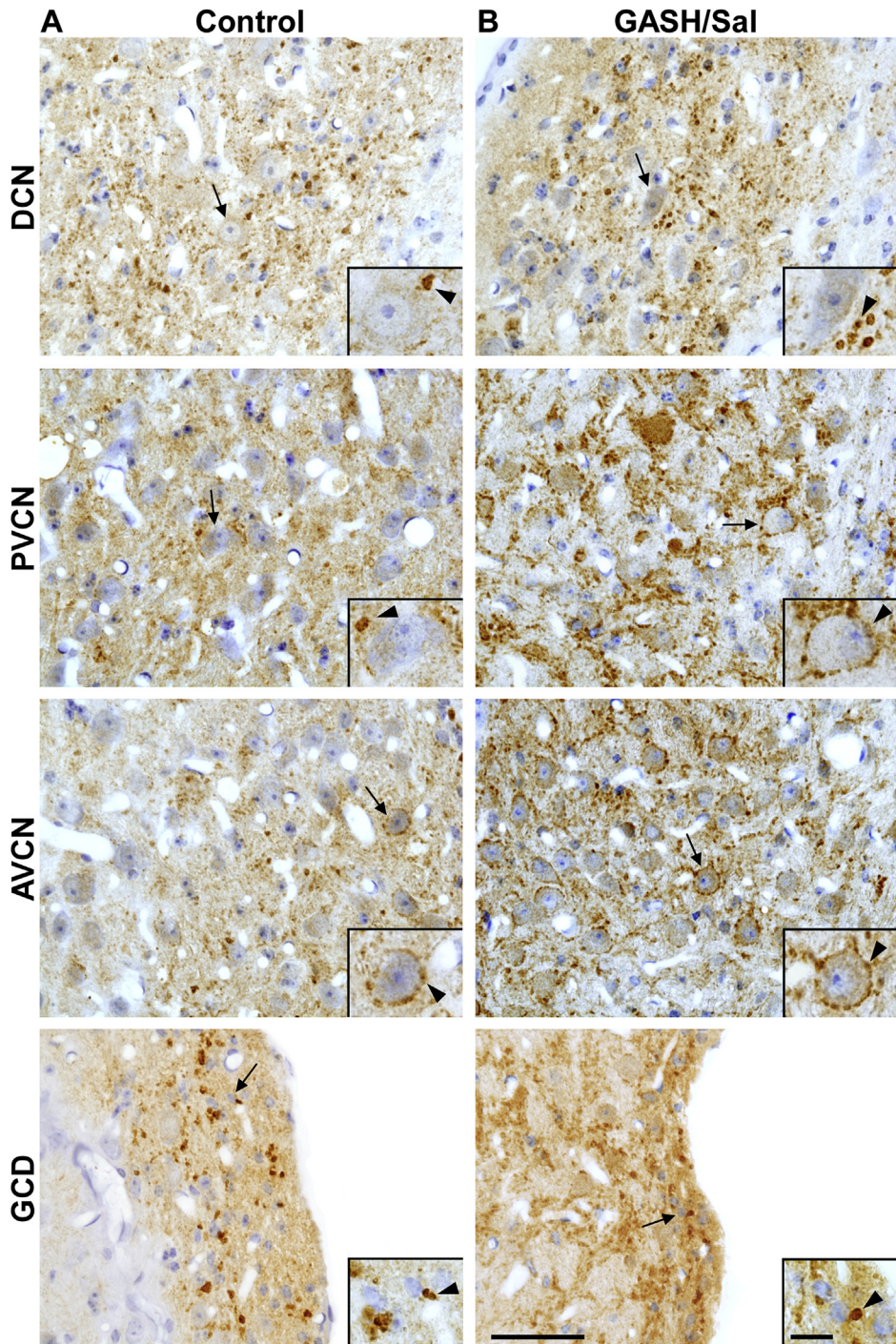


Fig. 9. VGLUT2-immunolabeling in the cochlear nucleus of the control (A) and GASH/Sal (B) hamsters. Light photomicrographs of 6- μ m coronal sections counterstained with Carazzi's hematoxylin show VGLUT2-immunolabeling in the cochlear nucleus regions indicated in Fig. 8. The normal distribution pattern of VGLUT2-immunolabeling in the control animal (A) is characterized by moderate immunolabeling in the DCN, weak immunolabeling in the magnocellular cell areas of PVCN and AVCN, and intense immunolabeling in the granule cell domain. Note the qualitative differences of VGLUT2-immunolabeling in the GASH/Sal cochlear nucleus (B) compared to control hamsters (A). An evident increase in the VGLUT2-immunolabeling in the magnocellular cell areas of PVCN and AVCN of the GASH/Sal is observed in comparison to controls, whereas VGLUT2-immunolabeling in the GCD of the GASH/Sal is weakly immunolabeled. The insets show higher magnifications of VGLUT2-immunolabeled puncta (arrowheads) in close apposition to the cell bodies depicted with arrows in each panel. Notice the heterogeneity of the shape and size of VGLUT2-immunolabeled puncta in each of the cochlear nucleus subdivisions. AVCN, anteroventral cochlear nucleus; DCN, dorsal cochlear nucleus; GCD, granule cell domain; PVCN, posteroventral cochlear nucleus. Scale bars = 50 μ m for all panels and 10 μ m for insets.

puncta density was significantly reduced in the GCD of GASH/Sal animals ($p < 0.001$; Fig. 11B). No significant changes in the density of VGLUT2-immunolabeled puncta were seen in the DCN ($p < 0.001$; Fig. 11B). Differences in VGLUT2-puncta density across cochlear nucleus subdivisions of the GASH/Sal relative to control

hamsters were highlighted as density ratios in Fig. 11C. VGLUT2 density were elevated above normal in the magnocellular areas of PVCN and AVCN as well as drastically reduced in GCD (Fig. 11C), suggesting an important reorganization of glutamatergic projections from auditory nerve and non-auditory sources to the

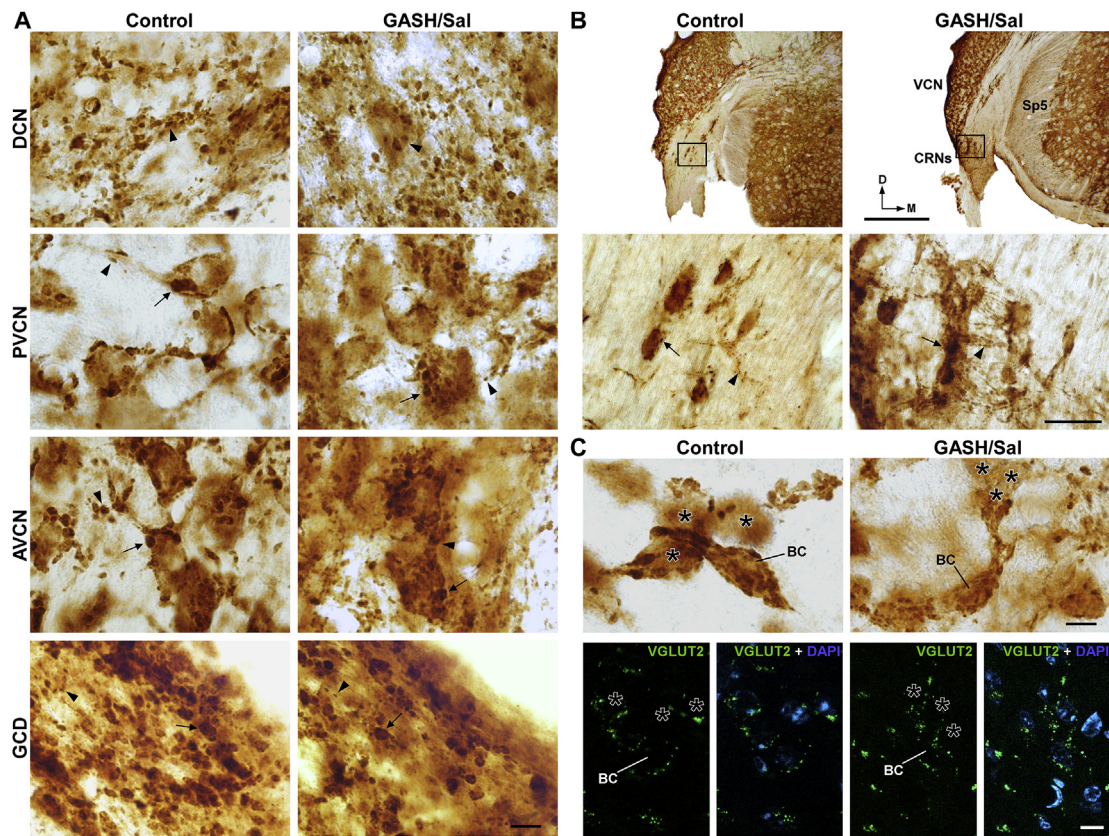


Fig. 10. Details of VGLUT2-immunolabeled puncta and neuronal clusters in the cochlear nucleus of the control and GASH/Sal hamsters. **A.** High magnification photomicrographs of 40- μ m coronal sections show VGLUT2-immunolabeling in the cochlear nucleus regions indicated in Fig. 8. These sections correspond to the animals with ABR waveforms shown in Fig. 1. Notice the heterogeneity of the shape and size of VGLUT2-immunolabeled puncta in each of the cochlear nucleus subdivisions. Small-to medium-size *en-passant* endings (arrowheads) are observed in the deep layer of the DCN, magnocellular regions of the PVCN and AVCN as well as the GCD. Large VGLUT2-immunopositive mossy-like endings (arrows) are found in the magnocellular core of the PVCN and AVCN as well as the GCD. Notice that both *en-passant* (arrowheads) and mossy-like (arrows) endings decorated clusters of unlabeled cell somata and dendrites in magnocellular regions of the PVCN and AVCN. In comparison to controls, note that GASH/Sal animals had a very dense, patchy and disorganized VGLUT2-immunolabeling composed of varicosities in the magnocellular core of the PVCN and AVCN, whereas immunolabeling was sparser in the GCD. **B.** Low magnification photomicrographs of 40- μ m coronal sections (upper panels) show VGLUT2-immunolabeling in the cochlear root nucleus of the control and GASH/Sal hamsters. Lower panels show high magnification photomicrographs corresponding to the frame depicted in the upper panels. Notice details of VGLUT2-immunolabeled puncta outlining unlabeled cell somata (arrows) and dendrites (arrowheads) of cochlear root neurons (CRNs). Also, note an increased number of VGLUT2-immunolabeled puncta in the CRNs of the GASH/Sal compared to controls. **C.** VGLUT2-immunostaining shows that cells with ovoid shape, presumed to be bushy cells, form neuronal clusters in the AVCN of control and GASH/Sal hamsters. Upper panels show high magnification photomicrographs of VGLUT2-immunopositive puncta outlining a presumably bushy cell (BC) that oriented their dendrites towards adjacent neuronal somata (asterisks), which were frequently found next to each other. Lower panels show fluorescent microscopy images of VGLUT2-positive terminals (in green) distributed around unlabeled cell bodies and dendrites of adjacent bushy cells (asterisks). DAPI (in blue) was used for nuclear staining to show cell position. AVCN, anteroventral cochlear nucleus; BC, bushy cell; CRNs, cochlear root neurons; DCN, dorsal cochlear nucleus; GCD, granule cell domain; PVCN, posteroventral cochlear nucleus; VCN, ventral cochlear nucleus; sp5, spinal trigeminal tract. Scale bars = 10 μ m for all panels in A and C; 500 μ m for upper panels and 50 μ m for lower panels in B. (For interpretation of the references to color in this figure legend, the reader is referred to the Web version of this article).

cochlear nucleus. Thus, cochlear nucleus regions in the GASH/Sal that should receive abundant auditory nerve terminals were dominated by non-auditory glutamatergic terminals, whereas regions preferentially innervated by non-auditory inputs reduce somatosensory cues. To determine whether this abnormal distribution of VGLUT2 inputs may lead to alterations in presynaptic glutamate release of cochlear nucleus efferents, we analyzed mRNA expression levels of *Vglut1* and *Vglut2* in the cochlear nucleus of the GASH/Sal. Cochlear nucleus tissue containing all the cochlear nucleus subdivisions were freshly dissected from control and GASH/Sal animals, and total RNA was extracted immediately. Quantitative gene expression data were normalized using β -actin as internal reference gene. Comparison of gene expression/ β -actin ratios showed that gene expression of *Vglut1* and *Vglut2* in the GASH/Sal cochlear nucleus was significantly lower than in control animals ($p < 0.001$; Fig. 11D). These results indicated aberrant glutamatergic transmission in the flow of sound processing from the inner ear to the cochlear nucleus to the inferior colliculus.

4. Discussion

In the current study, we provided new morphological and molecular data of the auditory sensory epithelium and cochlear nucleus of the GASH/Sal and its counterpart wild-type Syrian golden hamster. We reported marked morphological alterations of the GASH/Sal cochlea as well as a significantly decreased mRNA expression of cochlear genes that correlate with drastically elevated auditory thresholds and reduced ABR wave I amplitudes. Despite preservation of IHCs and OHCs, the GASH/Sal exhibited a hearing loss that is displayed by specific cochlear abnormalities such as disruption of the reticular lamina with severe disarray of stereociliary tufts, a significant degeneration of SGNs as well as mild atrophy of the SV. These are manifestations of cochlear neuropathy that are compatible with auditory perceptual abnormalities and alterations in the auditory information processing and propagation. Indeed, our study also showed changes in the distribution of somatosensory VGLUT2 puncta as well as alteration of mRNA

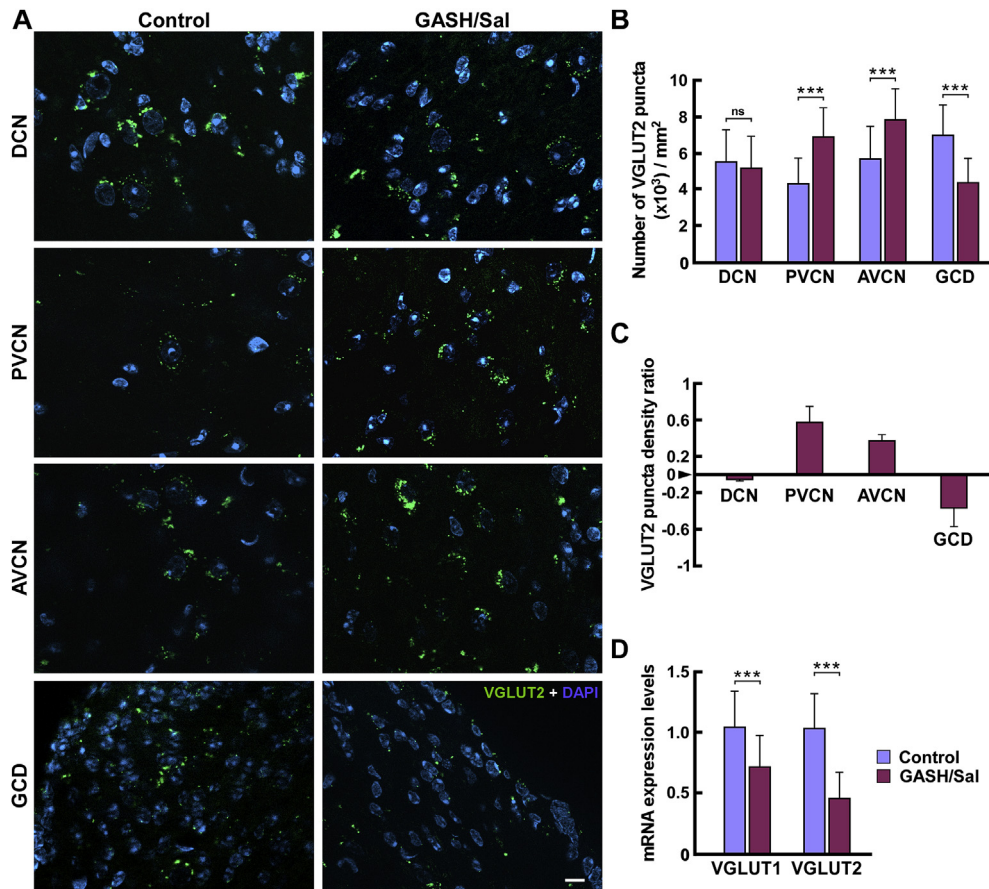


Fig. 11. Altered distribution of VGLUT2 axon terminals and mRNA expression of *Vglut1* and *Vglut2* genes in the cochlear nucleus of the GASH/Sal. **A.** Fluorescent microscopy images show VGLUT2-immunolabeled puncta (in green) across the cochlear nucleus subdivisions (depicted in Fig. 8) of control and GASH/Sal hamsters. DAPI (in blue) was used for nuclear staining to show cell position. Note the increase of VGLUT2 puncta in the PVCN and AVCN of the GASH/Sal compared to controls. Also, notice that VGLUT2 puncta are sparse in the GCD of the GASH/Sal. **B.** Histogram shows mean VGLUT2-puncta density (number of immunolabeled terminals per mm^2) in the cochlear nucleus subdivisions. VGLUT2-puncta densities are significantly increased in the magnocellular core of the PVCN and AVCN, but significantly decreased in the GCD of the GASH/Sal hamsters (compared to control hamsters). **C.** Plot shows the VGLUT2-puncta density ratio in the cochlear nucleus subdivisions of the GASH/Sal relative to controls, where 0 indicates no difference between GASH/Sal and control hamsters. Note VGLUT2 density is elevated above normal in the magnocellular core of the PVCN and AVCN as well as drastically reduced in GCD. Notice that DCN regions show normal VGLUT2 density values. **D.** Histogram shows relative quantities of transcripts of *Vglut1* and *Vglut2* genes in the cochlear nucleus of control and GASH/Sal animals. The relative mRNA expression of each gene was normalized to β -actin. ΔCt values were normalized to the average ΔCt of the cochlear nucleus tissues of control animals. For histograms B and D, controls are displayed in blue and GASH/Sal in purple. Each bar in the histograms is an average \pm S.E.M. Asterisks indicate significance differences between control and GASH/Sal hamsters ("***" = p value ≤ 0.001 ; ns = non-significant). AVCN, anteroventral cochlear nucleus; DCN, dorsal cochlear nucleus; GCD, granule cell domain; PVCN, posteroverentral cochlear nucleus. Scale bar = 10 μm for all panels in A. (For interpretation of the references to color in this figure legend, the reader is referred to the Web version of this article).

expression of *Vglut1* and *Vglut2* genes in the GASH/Sal cochlear nucleus. Together, these results indicated that the seizure-prone neural network of the GASH/Sal displays morphological and molecular abnormalities in the cochlea and cochlear nucleus, suggesting bottom-up modifications in glutamatergic transmission along the primary acoustic pathway, from the inner ear to the epileptogenic focus.

4.1. Methodological considerations: the wild-type golden hamster

The experimental design of the current study was based on comparisons with wild-type Syrian golden hamsters that were used as a control group. Thus, it was essential to characterize a strong control group that allow us to test the extent to which the morphological and molecular alterations are present in the GASH/Sal. The control hamsters used in our experiments exhibited an ABR waveform morphology as well as ABR thresholds, peak amplitudes and latencies in response to click stimuli very similar to those previously published (Church and Kaltenbach, 1993; Muñoz

et al., 2017; Sánchez-Benito et al., 2017). Consistently with normal hearing function, our morphological study revealed normal appearance of the main cochlear structures, including the sensory hair cells in the organ of Corti, the SGNs and the stria vascularis. The anatomical development of the hamster cochlea has been studied extensively at light and electron microscopic level, but the data available in adult hamsters still remains incomplete (Pujol and Abonnenc, 1977; Simmons et al., 1991; Kaltenbach and Falzarano, 1994; Kaltenbach et al., 1994). At light microscopy, our morphometrically analyses of normal SGNs yielded similar, but slightly smaller, values in cell size than those previously reported for the golden hamster (Simmons et al., 1994; Fuentes-Santamaría et al., 2005). This difference might be explained due to variations in the total number of SGNs and regions of the spiral ganglion included in each study, possible shrinkage during the tissue processing, and whether or not type I and II SGNs were assessed together. As shown in rats (Berglund and Ryugo, 1986), the Nissl technique not only stained the entire population of SGNs, but also allowed us distinction and identification of type I and II neurons

based on their staining properties and different cell body size. However, our morphometric and quantification analyses were performed regardless of the neuron type as those cytological features were not clearly distinguishable in the GASH/Sal. Our study further quantifies the number of SGNs within the Rosenthal's canal, showing that densities per mm³ were slightly higher in the golden hamster than in albino rats (Keithley and Feldman, 1979). Our morphological observations also indicated that the normal stria consisted of three layers of cells and a dense capillary network, with measures of SV thickness similar to those reported in other rodent species (Carlisle and Forge, 1989). At electron microscopy level, our analysis of the normal reticular lamina, including organization of hair cells, stereociliary bundles and supporting cochlear cells, as well as the measurements of stereocilia also coincides with previous reports (Kaltenbach and Falzarano, 1994; Kaltenbach et al., 1994). For the analysis of VGLUT2 puncta in the cochlear nucleus, it was necessary to determine the boundaries of the cochlear nucleus subdivisions based on histological characteristics. DCN, PVCN, AVCN and GCD were readily visible with Nissl and DAPI staining, and hence were considered separately in our analysis. These subdivisions in the cochlear nucleus hamster were also defined in other rodent species, in which similar relative volumes and basic structural features are found (Godfrey et al., 2016). Neither the reactivity of the VGLUT2 antibody used in our study nor the distribution of VGLUT2-immunolabeling in the cochlear nucleus subdivisions has been previously tested in the golden hamster. Our study provides several evidences that indicate this VGLUT2 antibody can be used as a marker of glutamatergic terminals in brain tissue of the golden hamster as efficiently as reported in other mammal species (Zhou et al., 2007; Gómez-Nieto and Rubio, 2009, 2011). First, the multiple sequence alignment showed that the specific target epitope is highly conserved for all VGLUT2 isoforms in the golden hamster. Second, the pattern of VGLUT2-immunolabeling in the cerebellar cortex of the hamster was consistent with that described in other rodent species (Hioki et al., 2003; Miyazaki et al., 2003). In addition, the distribution and morphology of VGLUT2 axon terminals in the hamster cochlear nucleus resembled to those reported in the guinea pig (Zhou et al., 2007), rat (Gómez-Nieto et al., 2009) and mouse (Heeringa et al., 2016). Finally, the VGLUT2-immunolabeled pattern in all regions of the hamster cochlear nucleus was consistently obtained using different cutting or immunodetection methods. Our immunostaining analysis in the hamster cochlear nucleus further showed VGLUT2 axon terminals outlining clusters of cell somata and dendrites in the magnocellular core of the PVCN and AVCN. These neuronal clusters resembled to those described in the ventral cochlear nucleus of the rat (Gómez-Nieto and Rubio, 2009) and monkey (Gómez-Nieto and Rubio, 2011), suggesting that a bushy cell network is also present in the hamster, and hence conserved across mammal species. It is also important to note in our comparative analysis that all control and GASH/Sal animals matched age, gender, housing, handling and care, therefore these characteristics can be ruled out as alternative explanations of any observed defects. Tissue samples for each set of experiments were obtained and processed in parallel for both animal groups, therefore the observed differences were not due to the passage of time, or any other experimental protocol variables such as incubation periods, temperature or sample manipulations. Our data analysis methods included single-blind assessments and quantification methods previously used by our research group (Gómez-Nieto et al., 2014; Sánchez-Benito et al., 2017), so experimental biases that arise from the observer effect were eliminated.

4.2. Morphological and molecular defects in the GASH/Sal cochlea: relevance to audiogenic seizure susceptibility

The inferior colliculus is considered the area of seizure initiation in rodent models of AGS susceptibility (Faingold et al., 1992; Garcia-Cairasco, 2002). This implies that the inferior colliculus is embedded in a web of pathologic connections that constitute a seizure-prone network to finally drive the AGS. Despite significant advances in understanding the seizure generation and propagation in the inferior colliculus (Garcia-Cairasco, 2002; N'Gouemo et al., 2009; Pinto et al., 2019), much less is known about the defects in lower auditory brainstem nuclei and the cochlea that might contribute to the seizure-prone network in AGS models. In this regard, recent studies from our research group reported that the GASH/Sal has an altered hearing sensitivity, showing high elevation of ABR thresholds and alterations in otoacoustic emissions (Muñoz et al., 2017; Sánchez-Benito et al., 2017). Our hearing evaluation of the GASH/Sal confirmed the increased hearing thresholds and further showed significant reductions of wave I and IV amplitudes, but normal latencies. The ABR wave I captures the synchronous firing of numerous auditory nerve fibers of the SGNs and wave IV is generated by the neuronal activity of the inferior colliculus (Church and Kaltenbach, 1993). Thus, our ABR results might be indicative of cochlear neuropathy, auditory nerve fiber reductions, decrease of synchronization of auditory nerve discharges and aberrant neuronal activity in the epileptogenic focus. The cochlear neuropathy, characterized by reduced ABR wave I amplitudes, is associated with damage at the cochlear synapse without loss of sensory hair cells and occurs after noise exposure, aging and may accompany several forms of hearing impairments, including tinnitus and hyperacusis (reviewed in Liberman and Kujawa, 2017; Milloy et al., 2017). Consistent with this, the cochlear histology of the GASH/Sal showed loss of SGNs and preservation of cochlear hair cells, indicating an auditory nerve deafferentation associated to a particular form of neuropathy that is no related with noise exposure. The normal or slightly elevated ABR waveforms II, III, and V in the GASH/Sal might reflect compensation mechanisms such as higher increased neural synchrony in central auditory regions. Something similar occurs in tinnitus, in which the normal wave V amplitude, despite a reduction in wave I, is evidence of an increased neural responsiveness in the central auditory system to compensate for the reduced activity of the auditory nerve (Schaette and McAlpine, 2011; Milloy et al., 2017). The normal latency of wave I in the GASH/Sal points to a defect in the receptor potential, instead of in the conduction velocities. Indeed, our electron microscopic study of the reticular lamina further showed marked disorganization of stereociliary tufts with loss, shortened or elongation of stereocilia. The compromised structure of the stereocilia bundle suggested an improper mechanoelectrical transduction in the GASH/Sal hair cells that correlates with the ABR results. In addition, the GASH/Sal exhibited disarray of regular arrangement in the cochlear hair cells, expansion of the surrounding supporting cochlear cells and blebs. Such abnormalities in the reticular lamina and stereocilia bundles were also observed in the GEPR rats (Penn et al., 1983) and BLSW mice (Charizopoulou et al., 2011), indicating that these cochlear defects are common among genetically AGS models, regardless of the animal species. Our study also revealed an important auditory hallmark of hearing impairment in the GASH/Sal that exhibited mild atrophy of the SV. Since strial dysfunction is associated to age-related hearing loss and alteration of cochlear homeostasis (Schuknecht et al., 1974; Gratton and Schulte, 1995; Patuzzi, 2011), the reduced SV thickness and fewer strial capillaries in the GASH/Sal might underlie the abnormalities of the organ of Corti and cause

important disturbances in sound transduction. Our molecular study further revealed concomitant molecular disruptions in the expression of cochlear genes that are involved in the mechanotransduction. The reduced mRNA levels of prestin in the GASH/Sal suggests loss of OHC electromotility, which in turn might affect cochlear amplification. Previous studies reported that absence of OHC electromotility in a prestin-knockout mice resulted in a loss of 40–60 dB in cochlear sensitivity (Liberman et al., 2002), and that uncoupling of hair-cell stereocilia from the tectorial membrane due to buckling of supporting cells may contribute for the loss of cochlear amplification (Flock et al., 1999; Nordmann et al., 2000). In line with that, our results showed that the GASH/Sal exhibited a greater than 40 dB cochlear sensitivity loss as well as defects of OHC stereocilia and alteration of Deiters' cells. The fact that the heads of Deiters' cells showed an increase of short microvilli might indicate that are sites of altered and intense metabolic exchange. Since Deiters' cells contribute to the micromechanics of the organ of Corti and to the control of hearing sensitivity (Laffon and Angelini, 1996; Flock et al., 1999), our results indicate that the surviving but dysfunctional package of OHCs and Deiters' cells in the GASH/Sal may negatively affect cochlear amplification. Interestingly, Penny et al. (1983) reported abnormal anatomical and functional associations of hair cells with the tectorial membrane in GEPR rats. It is noteworthy to highlight the similarity of the reticular lamina in both genetically AGS models. As occurs in GEPR rats (Penny et al., 1983), the hair cells of the GASH/Sal showed elongated stereocilia, non-parallel rows of OHCs as well as absence of normal "V-shaped" and "staircase" patterns of OHC stereocilia. The most plausible explanation is that the elongated and wavy stereocilia could represent a compensatory growth mechanism during development whereby hair cells attempt to contact the tectorial membrane for proper function (Penny et al., 1983). Normally, stereocilia growth during development requires actin polymerization to increase filament length that is precisely maintained during life by a slow turnover of actin at the apical tips (Narayanan et al., 2015). The elongation of stereocilia in the GASH/Sal therefore implies that the machinery for trafficking actin to the tips of stereocilia is still active, as being consistent with the presence of viable hair cells. It also suggests, however, an improper actin dynamics for controlling stereocilia length, which might negatively affect the normal mechanotransduction of the GASH/Sal hair cells. In addition, the signal transduction and role of the feedback mechanism in the sensitivity of the peripheral acoustic receptors might play a very important part of presumably pathological mechanisms of the AGS. In this regard, recent data from our laboratory has shown morphofunctional alterations in the olivocochlear efferent system of the GASH/Sal at naïve conditions, including absence of otoacoustic emissions in a wide range of frequencies and cell body shrinkage of olivocochlear neurons (Sánchez-Benito et al., 2017). Medial olivocochlear neurons innervate the OHCs modulating the cochlear amplifier gain (Warr and Beck, 1996; Cooper and Guinan, 2006; Gómez-Nieto et al., 2008a), therefore deficits in the olivocochlear efferent system of the GASH/Sal may contribute to an altered hearing sensitivity. Whether the molecular and morphological defects detected in the hair cells of the GASH/Sal were due to dysfunction of the olivocochlear efferent system, or vice versa, the olivocochlear neurons shrinkage were caused by an altered peripheral auditory system remains to be determined.

Our result showing decreased mRNA expression levels of *Cdh23* and *Pcdh15* genes also supports the existence of an abnormal mechanotransduction in the GASH/Sal cochlea. Thus, mice with mutations in the two genes, *Cdh23* and *Pcdh15*, showed disruption of hair-bundle morphology and aberrant transducer currents in the sensory hair cells (Alagramam et al., 2011). As reported in those mouse mutants, our electron microscopy analysis showed similar

structural alterations in the IHCs and OHCs, including loss of tip-links and disorganized hair bundles, suggesting an impaired cochlear transduction in the GASH/Sal. Interestingly, a case report has documented a patient harboring concomitant mutations in a DNA-repair gene (*PNKP*) and *Pcdh15* that caused early-onset seizures and congenital sensorineural hearing loss (Nakashima et al., 2014). As noted in this patient, GASH/Sal animals carry high-impact mutations in genes involved in DNA-repair processes (Díaz-Casado et al., 2020), and as our study shows, loss of *Pcdh15* mRNA expression that can be the result of genetic lesions. Given that partially shared phenotypes and underlying genetic alterations hint at a common disease, it is worthwhile to compare genetic variations and global patterns of gene expression (transcriptome) not only between different genetic AGS models (Damasceno et al., 2020), but also between human and model organisms with inherited propensity for developing seizures (Díaz-Casado et al., 2020).

An intriguing controversy that arise from our results is that the reduced mechanosensitivity in the GASH/Sal cochlea seems to be opposed to the hyperexcitability required for its AGS susceptibility. As definite possibility is that GASH/Sal animals have concomitant audiogenic susceptibility and age-related sensorineural hearing loss, wherein these two disease processes might course both dependently or independently of one another. If so, the relationship of these overlapping hearing pathologies with their corresponding molecular and morphofunctional correlates in the cochlea and auditory pathway might be not simple. As in other genetically AGS models, the innate susceptibility of the GASH/Sal to seizures appears and declines with age, so convulsions highly correlated with the development and decline of auditory function (Henry, 1985; Misawa et al., 2002; Charizopoulou et al., 2011; Muñoz et al., 2017). Early studies in genetically AGS mice and primed AGS models with elevated high frequency thresholds support that susceptibility is associated to a certain degree of high frequency dysfunction or damage during cochlear development (Henry, 1985; Henry and Buzone, 1986). Furthermore, it has been suggested that AGS susceptibility after acoustic trauma in neonatal rats depend on derangements of topographic frequency representation in the inferior colliculus, which were probably due to abnormal tonotopic development of the cochlea (Pierson and Snyder-Keller, 1994; Garcia-Cairasco, 2002). Our electron microscopy results showing that changes in the GASH/Sal cochlea were more pronounced in the basal (high frequency) regions argued in favor of this hypothesis, but not the uniform loss of SGNs in all three regions of the cochlea. Studies in genetically AGS mice with specific mutations in cochlear genes further revealed that age-related hearing loss does not significantly contribute to the AGS susceptibility or the developmental regulation of seizures, suggesting that these two pathologies are independent (Misawa et al., 2002; Charizopoulou et al., 2011). With the advent of new molecular tools applied to the characterization of seizure susceptibility in genetically rodent strains (Bosque et al., 2019), a longitudinally study showing a correlation between the cochlear dysfunction causing upstream excitability and the sound-triggered seizures during the GASH/Sal lifespan might clarify the complex relationship between its sensorineural hearing loss and its AGS susceptibility.

4.3. Altered glutamate release in the GASH/Sal cochlear nucleus: relevance to audiogenic seizure susceptibility

Along with the molecular and morphological alterations in the organ of Corti and consistent with the loss of SGNs and auditory nerve deafferentation, our RT-qPCR analysis showed a reduction of *Vglut1* and *Vglut2* gene expression levels in the GASH/Sal cochlea. VGLUT1 and VGLUT2 are commonly used as markers for glutamate

release (Takamori, 2006) and are expressed in the SGNs, but not in the cochlear hair cells (Seal et al., 2008). Since type I auditory nerve fibers are the major source of excitation to the cochlear nucleus (Lorente de Nò, 1981), our results imply a decrease in glutamate concentrations in the GASH/Sal cochlear nucleus. However, apart from the primary auditory afferents, the cochlear nucleus receives glutamatergic inputs that are from intrinsic (i.e. parallel fibers from the granule cells) as well as other extrinsic sources (i.e. mossy fibers from somatosensory origin) (reviewed in Rubio, 2019). Then the question becomes, what are the effects of cochlear abnormalities on the glutamatergic signaling of the GASH/Sal cochlear nucleus? In an attempt to answer this question, our study determined the distribution of VGLUT2 puncta in all cochlear nucleus regions. In the cochlear nucleus, VGLUT1 is preferentially associated with auditory nerve terminals and VGLUT2 with non-auditory (somatosensory) terminals (Zhou et al., 2007; Gómez-Nieto and Rubio, 2009). In the GASH/Sal, our immunostaining results showed increases of VGLUT2 density in the magnocellular core of the PVCN and AVCN as compared to controls. PVCN and AVCN represents the beginning of the binaural pathway through its projections to the superior olfactory complex as well as the monaural pathway through direct projections to the inferior colliculus, conveying the incoming signals from the cochlear afferents in an accurate and timely manner (Oliver et al., 1999; reviewed in Malmierca, 2003). Thus, the increased VGLUT2-puncta density in the PVCN and AVCN of the GASH/Sal, possibly derived from somatosensory projections to the cochlear nucleus, might be a compensatory mechanism to solve lack of glutamatergic input from the auditory nerve, but in turn might contribute to aberrant neural activity in the inferior colliculus. In support of this argument, it has been suggested that divergent multiple-contact synapses of cochlear and non-cochlear inputs on bushy cells' clusters underlie the morphological substrate for the enhanced synchronization of bushy cells firing (Gómez-Nieto and Rubio, 2009). Therefore, a higher number of VGLUT2 puncta in the bushy cell network of the GASH/Sal might adversely affect the output signal of the ventral cochlear nucleus. In addition, elevated spontaneous rates in neurons of the ventral cochlear nucleus, in compensatory response to deafening, were correlated to the hyperactivity developed in the inferior colliculus after cochlear trauma (Vogler et al., 2011). The results of this study, along with others, suggested that tinnitus and hyperacusis are associated with cochlear deafferentation or neuropathy as well as elevated hyperactivity, enhanced synchrony and altered balance between auditory nerve and somatosensory inputs in the ventral cochlear nucleus (Zeng et al., 2009; Vogler et al., 2011; Liberman and Kujawa, 2017; Heeringa et al., 2018). Whether these perceptual abnormalities are also present in the GASH/Sal remains to be elucidated. On the other hand, our study indicated the opposite VGLUT2-immunolabeled pattern in the GCD, showing a reduced density of VGLUT2 puncta in GASH/Sal animals as compared to controls. The GCD is not a major target of type I auditory nerve fibers, but on the contrary receives type II auditory nerve inputs as well as a variety of descending auditory inputs and non-auditory projections from somatosensory nuclei (Malmierca, 2003; Rubio, 2019). This unique set of afferent projections might explain the opposed results in VGLUT2 densities between the GCD and the magnocellular regions in the GASH/Sal. Remarkably, changes in VGLUT1 and VGLUT2-immunoreactivity were also reported in the cochlear nucleus after cochlear damage by intracochlear injections of kanamycin (Zeng et al., 2009). Zeng et al. (2009) showed reductions in VGLUT1-immunoreactivity in magnocellular regions of the cochlear nucleus and increases in VGLUT2-immunoreactivity in all regions of the cochlear nucleus, particularly those that received non-auditory inputs as the GCD (Heeringa et al., 2016). This altered VGLUT2-immunolabeling pattern after cochlear deafferentation is

partially at odds with those observed in the GASH/Sal, suggesting that the plasticity of somatosensory inputs to the GASH/Sal cochlear nucleus could be associated to audiogenic susceptibility rather than being mere correlates of cochlear deafferentation. In fact, the deep and fusiform cell layer of the DCN in control and GASH/Sal animals showed no significant differences in VGLUT2 density, while VGLUT2-immunoreactivity in those regions of the DCN were affected after the cochlear damage (Zeng et al., 2009). The DCN is the principal part of the monaural pathway to the central nucleus of the inferior colliculus (Oliver et al., 1999) and its glutamatergic afferent innervation also differs from other cochlear nucleus regions, including projections from a great variety of auditory and non-auditory sources (Malmierca, 2003; Rubio, 2019). Thus, our results indicated that the structural and molecular abnormalities in the GASH/Sal cochlea had differently effects on the glutamatergic system of each cochlear nucleus subdivisions, and hence the bottom-up pathways to the inferior colliculus might be affected in different degrees. In agreement with this hypothesis, our finding showing lower mRNA transcript levels of *Vglut1* and *Vglut2* in the cochlear nucleus suggests a presynaptic dysregulation of glutamate release in the inferior colliculus of the GASH/Sal. VGLUT1 and VGLUT2 differentiate complementary patterns of glutamatergic inputs into the inferior colliculus with VGLUT1 endings predominantly on the dendrites and VGLUT2 on both dendrites and somas (Altschuler et al., 2008). Since those neurons with flattened dendritic arbors constitutes the structural basis for the tonotopic organization of the inferior colliculus (Malmierca, 2003), the glutamate pathology derived from the GASH/Sal cochlear nucleus might affect a number of pre- and postsynaptic events in the inferior colliculus, that finally might be reflected in a tonotopic map disruption or hyperexcitability. In this regard, studies that mapped Fos-immunoreactivity in the inferior colliculus of AGS rodent models of genetic origin and after priming procedures (neonatal acoustic trauma) provided clear evidences that the deteriorations in tonotopic organization of the inferior colliculi underlie AGS susceptibility (Pierson and Snyder-Kelly, 1994; Klein et al., 2004). Glutamate receptors are also involved in AGS networks of the inferior colliculus, in which the mechanisms of initiation and propagation of seizures are differently controlled by different types of ionotropic glutamate receptors (Yasuda et al., 2000). Thus, presynaptic dysregulation of glutamate release in the GASH/Sal inferior colliculus might lead to postsynaptic strengthening or weakening of synapsis via changes in glutamate receptors, and that could eventually culminate in long-term changes in the seizure-free prone neural circuitry. Supporting this, recent physiological and behavioural experiments demonstrated that corruption of the neural synchronization in the inferior colliculus is involved in the AGS susceptibility of the WAR model under seizure-free conditions (Pinto et al., 2019). Future experiments are required to provide a clear picture of the role of the glutamate system in triggering shift in connectivity and synchronicity that contributes to ictogenesis in the inferior colliculus of the GASH/Sal.

5. Concluding remarks

The present work examined the morphofunctional and molecular abnormalities of the cochlea and cochlear nucleus in the genetically audiogenic seizure-prone hamster GASH/Sal by comparison to control animals. In the Syrian golden hamster, the ABR waveforms, the reticular lamina, the cochlear gene expression profiles as well as the VGLUT2-immunolabeling pattern and anatomical characteristics of the cochlear nucleus subdivisions are equivalent to other rodent species. As compared to the wild-type golden hamster, the cochlear histopathology of the GASH/Sal

showed preservation of the sensory hair cells, but a significant loss of SGNs and mild atrophy of the SV in all cochlear turns. At the electron microscopy level, the reticular lamina of the GASH/Sal exhibited disarray of stereociliary tufts, blebs, and elongated stereocilia in the IHCs and OHCs. Loss of stereocilia tufts and tip-links in the OHCs were particularly more pronounced in the basal turn of the cochlea and caused absence of the normal bundle morphology. Non-parallel rows of OHCs were also detected, presumably due to distortion of the Deiters' cells. Consistently with those morphological manifestations, the GASH/Sal cochlea showed abnormal gene expression patterns of *prestin*, *Cdh23*, *Pcdh15*, *Vglut1* and *Vglut2*, suggesting that the mechanotransduction mechanism in the sensory hair cells is markedly altered. All these morphological and molecular defects in the GASH/Sal cochlea correlated to ABR waveform I alterations and elevated auditory thresholds. Crucially, these findings indicated that the GASH/Sal has a complex hearing impairment with severe hearing loss and cochlear neuropathy, in which acoustic cues are not faithfully transmitted from the inner ear to the cochlear nucleus. In fact, the distribution of VGLUT2 axon terminals was differently affected in each cochlear nucleus subdivision of the GASH/Sal. A significant increase in VGLUT2-puncta density were found in magnocellular regions of the PVCN and AVCN, whereas a drastic reduction was observed in the GCD. The deep and fusiform cell layer of the GASH/Sal DCN were unaffected. These results indicated a reorganization of glutamatergic projections from non-auditory sources to the GASH/Sal cochlear nucleus, which could be a compensatory mechanism of the cochlear neuropathy, but in turn contributes to either desynchronization or enhanced synchrony of cochlear nucleus neurons. In correlation with this finding, our molecular study showed a disruption in the gene expression of *Vglut1* and *Vglut2* in the GASH/Sal cochlear nucleus, suggesting aberrant glutamatergic release in the epileptogenic focus. Since our experiments were conducted in a genetically AGS model under seizure-free conditions, the alterations at the morphological and molecular connectome level of the primary acoustic pathway form part of the GASH/Sal seizure-prone neural network and represent the manifestations of genetic and developmental defects of its seizure susceptibility.

Declaration of competing interest

The authors declare no competing interests.

CRediT authorship contribution statement

David Sánchez-Benito: Conceptualization, Formal analysis, Investigation, Visualization, Validation, Writing - review & editing. **Miguel A. Hypolito:** Investigation, Writing - review & editing. **Antonio J. Alvarez-Morujo:** Investigation, Writing - review & editing. **Dolores E. López:** Conceptualization, Formal analysis, Project administration, Funding acquisition, Supervision, Writing - review & editing. **Ricardo Gómez-Nieto:** Writing - original draft, Conceptualization, Methodology, Formal analysis, Investigation, Visualization, Validation, Project administration, Funding acquisition, Supervision, Writing - review & editing.

Acknowledgement

The authors wish to thank Rosa García Aparicio, Adriana Murashima, Elena Díaz-Casado, Marianny Pernia and Samara Damasco for excellent technical assistance. We thank Daniel Medeiros for providing the MATLAB script. This study was supported by a research grant from the Instituto de Salud Carlos III (ISCIII), co-financed with European Union FEDER funds (#PI19/01364, Pls: Dolores E. López and Ricardo Gómez-Nieto), the

Regional Government of Castilla y León (#SA070P17; PI: Dolores E. López) and the research fellowship grant (#EDU/346/2013; awarded to David Sánchez-Benito). We also thank the International Collaboration Agreement between the FAPESP and the University of Salamanca (#2019/16574–2; Pls: Dolores E. López and Norberto García-Cairasco).

Appendix A. Supplementary data

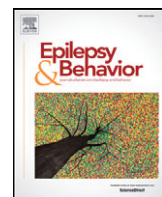
Supplementary data to this article can be found online at <https://doi.org/10.1016/j.heares.2020.107973>.

References

- Abercrombie, M., 1946. Estimation of nuclear population from microtome sections. *Anat. Rec.* 94, 239–247. <https://doi.org/10.1002/ar.1090940210>.
- Alagramam, K.N., Goodyear, R.J., Geng, R., Furness, D.N., van Aken, A.F., Marcotti, W., Kros, C.J., Richardson, G.P., 2011. Mutations in protocadherin 15 and cadherin 23 affect tip links and mechanotransduction in mammalian sensory hair cells. *PLoS One* 6 (4), e19183. <https://doi.org/10.1371/journal.pone.0019183>.
- Altschuler, R.A., Tong, L., Holt, A.G., Oliver, D.L., 2008. Immunolocalization of vesicular glutamate transporters 1 and 2 in the rat inferior colliculus. *Neuroscience* 154 (1), 226–232. <https://doi.org/10.1016/j.neuroscience.2008.03.036>.
- Barrera-Bailón, B., Oliveira, J.A.C., López, D.E., Muñoz de la Pascua, L.J., García-Cairasco, N., Sancho, C., 2013. Pharmacological and neuroethological study of three antiepileptic drugs in the genetic audiogenic seizure hamster (GASH:Sal). *Epilepsy Behav.* 28 (3), 413–425. <https://doi.org/10.1016/j.yebeh.2013.05.028>.
- Barrera-Bailón, B., Oliveira, J.A.C., López, D.E., Muñoz, L.J., García-Cairasco, N., Sancho, C., 2017. Pharmacological and neuroethological study of the acute and chronic effects of lamotrigine in the genetic audiogenic seizure hamster (GASH: Sal). *Epilepsy Behav.* 71 (Pt B), 207–217. <https://doi.org/10.1016/j.yebeh.2015.11.005>.
- Berglund, A.M., Ryugo, D.K., 1986. A monoclonal antibody labels type II neurons of the spiral ganglion. *Brain Res.* 383 (1–2), 327–332. [https://doi.org/10.1016/0006-8993\(86\)90034-X](https://doi.org/10.1016/0006-8993(86)90034-X).
- Berglund, A.M., Ryugo, D.K., 1991. Neurofilament antibodies and spiral ganglion neurons of the mammalian cochlea. *J. Comp. Neurol.* 306 (3), 393–408. <https://doi.org/10.1002/cne.903060304>, 1991 Apr 15.
- Bosque, J.R., Gómez-Nieto, R., Hormigo, S., Herrero-Turrión, M.J., Díaz-Casado, E., Sancho, C., López, D.E., 2019. Molecular tools for the characterization of seizure susceptibility in genetic rodent models of epilepsy. *Epilepsy Behav.* 1, 106594. <https://doi.org/10.1016/j.yebeh.2019.106594>.
- Browning, R.A., 1986. Neuroanatomical localization of structures responsible for seizures in the GEPR: lesion studies. *Life Sci.* 39 (10), 857–867. [https://doi.org/10.1016/0024-3205\(86\)90367-X](https://doi.org/10.1016/0024-3205(86)90367-X).
- Carballosa-González, M.M., Muñoz, L.J., López-Alburquerque, T., Pardal-Fernández, J.M., Nava, E., de Cabo, C., Sancho, C., López, D.E., 2013. EEG characterization of audiogenic seizures in the hamster strain GASH:Sal. *Epilepsy Res.* 106 (3), 318–325. <https://doi.org/10.1016/j.eplepsyres.2013.07.001>.
- Carlisle, L., Forge, A., 1989. The vessels of the stria vascularis: quantitative comparison of three rodent species. *Hear. Res.* 38 (1–2), 111–117. [https://doi.org/10.1016/0378-5955\(89\)90132-9](https://doi.org/10.1016/0378-5955(89)90132-9).
- Charizopoulos, N., Lelli, A., Schraders, M., Ray, K., Hildebrand, M.S., Ramesh, A., Srisailapathy, C.R., Oostrik, J., Admiraal, R.J., Neely, H.R., Latoche, J.R., Smith, R.J., Northup, J.K., Kremer, H., Holt, J.R., Noben-Trauth, K., 2011. Gipc3 mutations associated with audiogenic seizures and sensorineural hearing loss in mouse and human. *Nat. Commun.* 2, 201. <https://doi.org/10.1038/ncomms1200>.
- Church, M.W., Kaltenbach, J.A., 1993. The hamster's auditory brain stem response as a function of stimulus intensity, tone burst frequency, and hearing loss. *Ear Hear.* 14 (4), 249–257. <https://doi.org/10.1097/00003446-199308000-00004>.
- Colmenárez-Raga, A.C., Díaz, I., Pernia, M., Pérez-González, D., Delgado-García, J.M., Carro, J., Plaza, I., Merchán, M.A., 2019. Reversible functional changes evoked by anodal epidural direct current electrical stimulation of the rat auditory cortex. *Front. Neurosci.* 13, 356. <https://doi.org/10.3389/fnins.2019.00356>.
- Cooper, N.P., Guinan Jr., J.J., 2006. Efferent-mediated control of basilar membrane motion. *J. Physiol.* 576 (Pt 1), 49–54. <https://doi.org/10.1111/j.physiol.2006.114991>.
- Damasceno, S., Gómez-Nieto, R., García-Cairasco, N., Herrero-Turrión, M.J., Marín, F., López, D.E., 2020. Top common differentially expressed genes in the epileptogenic nucleus of two strains of rodents susceptible to audiogenic seizures: WAR and GASH/sal. *Front. Neurosci.* 11, 33. <https://doi.org/10.3389/fnneur.2020.00033>.
- De Sarro, G., Russo, E., Citraro, R., Meldrum, B.S., 2017. Genetically epilepsy-prone rats (GEPRs) and DBA/2 mice: two animal models of audiogenic reflex epilepsy for the evaluation of new generation AEDs. *Epilepsy Behav.* 71 (Pt B), 165–173. <https://doi.org/10.1016/j.yebeh.2015.06.030>.
- Díaz-Casado, E., Gómez-Nieto, R., Pereda, J.M., Muñoz, L.J., Jara, M., López, D.E., 2020. Analysis of gene variants in the GASH/Sal model of epilepsy. *PLoS ONE* 15 (3), e0229953. <https://doi.org/10.1371/journal.pone.0229953>.
- Doretto, M.C., Fonseca, C.G., Lobo, R.B., Terra, V.C., Oliveira, J.A., García-Cairasco, N., 2003. Quantitative study of the response to genetic selection of the Wistar

- audiogenic rat strain (WAR). *Behav. Genet.* 33 (1), 33–42. <https://doi.org/10.1023/a:1021099432759>.
- Faingold, C.L., Naritoku, D.K., Copley, C.A., Randall, M.E., Riaz, A., Anderson, C.A., Arneric, S.P., 1992. Glutamate in the inferior colliculus plays a critical role in audiogenic seizure initiation. *Epilepsy Res.* 13 (2), 95–105. [https://doi.org/10.1016/0920-1211\(92\)90064-Z](https://doi.org/10.1016/0920-1211(92)90064-Z).
- Flock, A., Flock, B., Fridberger, A., Scarfone, E., Ulfendahl, M., 1999. Supporting cells contribute to control of hearing sensitivity. *J. Neurosci.* 19 (11), 4498–4507. <https://doi.org/10.1523/JNEUROSCI.19-11-04498.1999>.
- Fremeau Jr, R.T., Troyer, M.D., Pahner, I., Nygaard, G.O., Tran, C.H., Reimer, R.J., Bellocchio, E.E., Fortin, D., Storm-Mathisen, J., Edwards, R.H., 2001. The expression of vesicular glutamate transporters defines two classes of excitatory synapse. *Neuron* 31 (2), 247–260. [https://doi.org/10.1016/s0896-6273\(01\)00344-0](https://doi.org/10.1016/s0896-6273(01)00344-0).
- Fuentes-Santamaría, V., Cantos, R., Alvarado, J.C., García-Atarés, N., López, D.E., 2005. Morphologic and neurochemical abnormalities in the auditory brainstem of the genetically epilepsy-prone hamster (GPG/Vall). *Epilepsia* 46 (7), 1027–1045. <https://doi.org/10.1111/j.1528-1167.2005.68104.x>.
- Furness, D.N., Lawton, D.M., 2003. Comparative distribution of glutamate transporters and receptors in relation to afferent innervation density in the mammalian cochlea. *J. Neurosci.* 23 (36), 11296–11304. <https://doi.org/10.1523/JNEUROSCI.23-36-11296.2003>. In press.
- García-Cairasco, N., 2002. A critical review on the participation of inferior colliculus in acoustic-motor and acoustic-limbic networks involved in the expression of acute and kindled audiogenic seizures. *Hear. Res.* 168 (1–2), 208–222. [https://doi.org/10.1016/s0378-5955\(02\)00371-4](https://doi.org/10.1016/s0378-5955(02)00371-4). 2002 Jun.
- Godfrey, D.A., Lee, A.C., Hamilton, W.D., Benjamin 3rd, L.C., Vishwanath, S., Simo, H., Godfrey, L.M., Mustapha, A.I., Heffner, R.S., 2016. Volumes of cochlear nucleus regions in rodents. *Hear. Res.* 339, 161–174. <https://doi.org/10.1016/j.heares.2016.07.003>.
- Gómez-Nieto, R., Rubio, M.E., López, D.E., 2008a. Cholinergic input from the ventral nucleus of the trapezoid body to cochlear root neurons in rats. *J. Comp. Neurol.* 506 (3), 452–468. <https://doi.org/10.1002/cne.21554>.
- Gómez-Nieto, R., Horta-Junior, J.A., Castellano, O., Herrero-Turrión, M.J., Rubio, M.E., López, D.E., 2008b. Neurochemistry of the afferents to the rat cochlear root nucleus: possible synaptic modulation of the acoustic startle. *Neuroscience* 154 (1), 51–64. <https://doi.org/10.1016/j.neuroscience.2008.01.079>.
- Gómez-Nieto, R., Rubio, M.E., 2009. A bushy cell network in the rat ventral cochlear nucleus. *J. Comp. Neurol.* 516 (4), 241–263. <https://doi.org/10.1002/cne.22139>.
- Gómez-Nieto, R., Rubio, M.E., 2011. Ultrastructure, synaptic organization, and molecular components of bushy cell networks in the anteroventral cochlear nucleus of the rhesus monkey. *Neuroscience* 179, 188–207. <https://doi.org/10.1016/j.neuroscience.2011.01.058>.
- Gómez-Nieto, R., Horta-Júnior, J.de A., Castellano, O., Millian-Morell, L., Rubio, M.E., López, D.E., 2014. Origin and function of short-latency inputs to the neural substrates underlying the acoustic startle reflex. *Front. Neurosci.* 8, 216. <https://doi.org/10.3389/fnins.2014.00216>.
- Gratton, M.A., Schulte, B.A., 1995. Alterations in microvasculature are associated with atrophy of the stria vascularis in quiet-aged gerbils. *Hear. Res.* 82, 44–52. [https://doi.org/10.1016/0378-5955\(94\)00161-I](https://doi.org/10.1016/0378-5955(94)00161-I).
- Grone, B.P., Baraban, S.C., 2015. Animal models in epilepsy research: legacies and new directions. *Nat. Neurosci.* 18 (3), 339–343. <https://doi.org/10.1038/nn.3934>.
- Heeringa, A.N., Stefanescu, R.A., Raphael, Y., Shore, S.E., 2016. Altered vesicular glutamate transporter distributions in the mouse cochlear nucleus following cochlear insult. *Neuroscience* 315, 114–124. <https://doi.org/10.1016/j.neuroscience.2015.12.009>.
- Heeringa, A.N., Wu, C., Chung, C., West, M., Martel, D., Liberman, L., Liberman, M.C., Shore, S.E., 2018. Glutamatergic projections to the cochlear nucleus are redistributed in tinnitus. *Neuroscience* 391, 91–103. <https://doi.org/10.1016/j.neuroscience.2018.09.008>.
- Henry, K.R., 1985. Cochlear function and audiogenic seizures: developmental covariance in the LP/J mouse. *Dev. Psychobiol.* 18 (6), 461–466. <https://doi.org/10.1002/dev.420180603>.
- Henry, K.R., Buzzone, R., 1986. Auditory physiology and behavior in RB/1bg, RB/3bg, and their F1 hybrid mice (*Mus musculus*): influence of genetics, age, and acoustic variables on audiogenic seizure thresholds and cochlear functions. *J. Comp. Psychol.* 100 (1), 46–51. <https://doi.org/10.1037/0735-7036.100.1.46>.
- Hioki, H., Fujiyama, F., Taki, K., Tomioka, R., Furuta, T., Tamamaki, N., Kaneko, T., 2003. Differential distribution of vesicular glutamate transporters in the rat cerebellar cortex. *Neuroscience* 117 (1), 1–6. [https://doi.org/10.1016/s0306-4522\(02\)00943-0](https://doi.org/10.1016/s0306-4522(02)00943-0).
- Kaltenbach, J.A., Falzarano, P.R., 1994. Postnatal development of the hamster cochlea. I. Growth of hair cells and the organ of Corti. *J. Comp. Neurol.* 340 (1), 87–97. <https://doi.org/10.1002/cne.903400107>.
- Kaltenbach, J.A., Falzarano, P.R., Simpson, T.H., 1994. Postnatal development of the hamster cochlea. II. Growth and differentiation of stereocilia bundles. *J. Comp. Neurol.* 350 (2), 187–198. <https://doi.org/10.1002/cne.903500204>.
- Kandratavicius, L., Balista, P.A., Lopes-Aguiar, C., Ruggiero, R.N., Umeoka, E.H., García-Cairasco, N., Bueno-Junior, L.S., Leite, J.P., 2014. Animal models of epilepsy: use and limitations. *Neuropsychiatric Dis. Treat.* 10, 1693–1705. <https://doi.org/10.2147/NDT.S50371>.
- Kazmierczak, P., Sakaguchi, H., Tokita, J., Wilson-Kubalek, E.M., Milligan, R.A., Müller, U., Kachar, B., 2007. Cadherin 23 and protocadherin 15 interact to form tip-link filaments in sensory hair cells. *Nature* 449 (7158), 87–91. <https://doi.org/10.1038/nature06091>, 2007 Sep. 6.
- Keithley, E.M., Feldman, M.L., 1979. Spiral ganglion cell counts in an age-graded series of rat cochleas. *J. Comp. Neurol.* 188 (3), 429–442. <https://doi.org/10.1002/cne.901880306>. 1979 Dec 1.
- Keithley, E.M., Canto, C., Zheng, Q.Y., Wang, X., Fischel-Ghodsian, N., Johnson, K.R., 2005. Cu/Zn superoxide dismutase and age-related hearing loss. *Hear. Res.* 209 (1–2), 76–85. <https://doi.org/10.1016/j.heares.2005.06.009>. 2005 Nov.
- Klein, B.D., Fu, Y.H., Ptacek, L.J., White, H.S., 2004. c-Fos immunohistochemical mapping of the audiogenic seizure network and tonotopic neuronal hyperexcitability in the inferior colliculus of the Frings mouse. *Epilepsy Res.* 62 (1), 13–25. <https://doi.org/10.1016/j.epilepsires.2004.06.007>.
- Laffon, E., Angelini, E., 1996. On the Deiters cell contribution to the micromechanics of the organ of Corti. *Hear. Res.* 99 (1–2), 106–109. [https://doi.org/10.1016/s0378-5955\(96\)00089-5](https://doi.org/10.1016/s0378-5955(96)00089-5).
- Liberman, M.C., Gao, J., He, D.Z., Wu, X., Jia, S., Zuo, J., 2002. Prestin is required for electromotility of the outer hair cell and for the cochlear amplifier. *Nature* 419 (6904), 300–304. <https://doi.org/10.1038/nature01059>.
- Liberman, M.C., Kujawa, S.G., 2017. Cochlear synaptopathy in acquired sensorineural hearing loss: manifestations and mechanisms. *Hear. Res.* 349, 138–147. <https://doi.org/10.1016/j.heares.2017.01.003>.
- López-López, D., Gómez-Nieto, R., Herrero-Turrión, M.J., García-Cairasco, N., Sánchez-Benito, D., Ludeña, M.D., López, D.E., 2017. Overexpression of the immediate-early genes Egr1, Egr2, and Egr3 in two strains of rodents susceptible to audiogenic seizures. *Epilepsy Behav.* 71 (Pt B), 226–237. <https://doi.org/10.1016/j.yebeh.2015.12.020>.
- Lorente de Nò, R., 1981. *The Primary Acoustic Nuclei*. Raven Press, New York, NY.
- Loscher, W., 2011. Critical review of current animal models of seizures and epilepsy used in the discovery and development of new antiepileptic drugs. *Seizure* 20, 359–368. <https://doi.org/10.1016/j.nn.3934>.
- Malmierca, M.S., 2003. The structure and physiology of the rat auditory system: an overview. *Int. Rev. Neurobiol.* 56, 147–211. [https://doi.org/10.1016/S0074-7742\(03\)56005-6](https://doi.org/10.1016/S0074-7742(03)56005-6).
- Milloy, V., Fournier, P., Benoit, D., Noreña, A., Koravand, A., 2017. Auditory brainstem responses in tinnitus: a review of who, how, and what? *Front. Aging Neurosci.* 9, 237. <https://doi.org/10.3389/fnagi.2017.00237>.
- Misawa, H., Sherr, E.H., Lee, D.J., Chetkovich, D.M., Tan, A., Schreiner, C.E., Bredt, D.S., 2002. Identification of a monogenic locus (jams1) causing juvenile audiogenic seizures in mice. *J. Neurosci.* 22 (23), 10088–10093. <https://doi.org/10.1016/j.jneurosci.2002.09.088>.
- Miyazaki, T., Fukaya, M., Shimizu, H., Watanabe, M., 2003. Subtype switching of vesicular glutamate transporters at parallel fibre-Purkinje cell synapses in developing mouse cerebellum. *Eur. J. Neurosci.* 17 (12), 2563–2572. <https://doi.org/10.1046/j.1460-9568.2003.02698.x>.
- Mulders, W.H., Ding, D., Salvi, R., Robertson, D., 2011. Relationship between auditory thresholds, central spontaneous activity, and hair cell loss after acoustic trauma. *J. Comp. Neurol.* 519 (13), 2637–2647. <https://doi.org/10.1002/cne.22644>.
- Muñoz, L.J., Carballo-Gautam, M.M., Yanowsky, K., García-Atarés, N., López, D.E., 2017. The genetic audiogenic seizure hamster from Salamanca: the GASH:Sal. *Epilepsy Behav.* 71 (Pt B), 181–192. <https://doi.org/10.1016/j.yebeh.2016.03.002>.
- Nadol Jr, J.B., 1988. Quantification of human spiral ganglion cells by serial section reconstruction and segmental density estimates. *Am. J. Otolaryngol.* 9 (2), 47–51. [https://doi.org/10.1016/s0196-0709\(88\)80007-3](https://doi.org/10.1016/s0196-0709(88)80007-3).
- Narayanan, P., Chatterton, P., Ikeda, A., Ikeda, S., Corey, D.P., Ervasti, J.M., Perrin, B.J., 2015. Length regulation of mechanosensitive stereocilia depends on very slow actin dynamics and filament-severing proteins. *Nat. Commun.* 6, 6855. <https://doi.org/10.1038/ncomms7855>.
- N'Gouemo, P., Faingold, C.L., Morad, M., 2009. Calcium channel dysfunction in inferior colliculus neurons of the genetically epilepsy-prone rat. *Neuropharmacology* 56 (3), 65–75. <https://doi.org/10.1016/j.neuropharm.2008.11.005>.
- Nakashima, M., Takano, K., Osaka, H., Aida, N., Tsurusaki, Y., Miyake, N., Saitsu, H., Matsumoto, N., 2014. Causative novel PNKP mutations and concomitant PCDH15 mutations in a patient with microcephaly with early-onset seizures and developmental delay syndrome and hearing loss. *J. Hum. Genet.* 59 (8), 471–474. <https://doi.org/10.1038/jhg.2014.51>.
- Nordmann, A.S., Bohne, B.A., Harding, G.W., 2000. Histopathological differences between temporary and permanent threshold shift. *Hear. Res.* 139 (1–2), 13–30. [https://doi.org/10.1016/s0378-5955\(99\)00163-x](https://doi.org/10.1016/s0378-5955(99)00163-x).
- Oliver, D.L., Ostapoff, E.M., Beckius, G.E., 1999. Direct innervation of identified pretectal thalamic neurons in the inferior colliculus by axons from the cochlear nucleus. *Neuroscience* 93 (2), 643–658. [https://doi.org/10.1016/s0306-4522\(99\)00143-8](https://doi.org/10.1016/s0306-4522(99)00143-8).
- Patuzzi, R., 2011. Ion flow in stria vascularis and the production and regulation of cochlear endolymph and the endolymphatic potential. *Hear. Res.* 277, 4–19. <https://doi.org/10.1016/j.heares.2011.01.010>.
- Penny, J.E., Brown, R.D., Hodges, K.B., Kupetz, S.A., Glenn, D.W., Jobe, P.C., 1983. Cochlear morphology of the audiogenic-seizure susceptible (AGS) or genetically epileptic prone rat (GEPR). *Acta Otolaryngol.* 95 (1–2), 1–12. <https://doi.org/10.3109/00016488309130909>. 1983 Jan-Feb.
- Pierson, M., Snyder-Keller, A., 1994. Development of frequency-selective domains in inferior colliculus of normal and neonatally noise-exposed rats. *Brain Res.* 636 (1), 55–67. [https://doi.org/10.1016/0006-8993\(94\)90175-9](https://doi.org/10.1016/0006-8993(94)90175-9).
- Pinto, H.P.P., Oliveira Lucas, E.L., Carvalho, V.R., Mourão, F.A.G., Guarneri, L.O., Mendes, E.M.A.M., Medeiros, D.C., Moraes, M.F.D., 2019. Seizure susceptibility corrupts inferior colliculus acoustic integration. *Front. Syst. Neurosci.* 13, 63. <https://doi.org/10.3389/fnsys.2019.00063>.
- Prieto-Martín, A.I., Aroca-Aguilar, J.D., Sánchez-Sánchez, F., Muñoz, L.J., López, D.E.,

- Escribano, J., de Cabo, C., 2017. Molecular and neurochemical substrates of the audiogenic seizure strains: the GASH:Sal model. *Epilepsy Behav.* 71 (Pt B), 218–225. <https://doi.org/10.1016/j.yebeh.2015.05.025>.
- Pujol, R., Abonnenc, M., 1977. Receptor maturation and synaptogenesis in the golden hamster cochlea. *Arch. Oto-Rhino-Laryngol.* 217 (1), 1–12. <https://doi.org/10.1007/bf00453886>.
- Rachel, J.D., Kaltenbach, J.A., Janisse, J., 2002. Increases in spontaneous neural activity in the hamster dorsal cochlear nucleus following cisplatin treatment: a possible basis for cisplatin-induced tinnitus. *Hear. Res.* 164 (1–2), 206–214. [https://doi.org/10.1016/s0378-5955\(02\)00287-3](https://doi.org/10.1016/s0378-5955(02)00287-3).
- Reigel, C.E., Dailey, J.W., Jobe, P.C., 1986. The genetically epilepsy-prone rat: an overview of seizure-prone characteristics and responsiveness to anticonvulsant drugs. *Life Sci.* 39 (9), 763–767. [https://doi.org/10.1016/0024-3205\(86\)90454-6](https://doi.org/10.1016/0024-3205(86)90454-6).
- Ross, K.C., Coleman, J.R., 2000. Developmental and genetic audiogenic seizure models: behavior and biological substrates. *Neurosci. Biobehav. Rev.* 24 (6), 639–653. [https://doi.org/10.1016/s0149-7634\(00\)00029-4](https://doi.org/10.1016/s0149-7634(00)00029-4) submitted for publication.
- Rubio, M.E., 2019. Molecular and structural changes in the cochlear nucleus in response to hearing loss. In: Kandler, Karl (Ed.), *The Oxford Handbook of the Auditory Brainstem*. <https://doi.org/10.1093/oxfordhb/9780190849061.013.7>.
- Salvi, R.J., Wang, J., Ding, D., 2000. Auditory plasticity and hyperactivity following cochlear damage. *Hear. Res.* 147 (1–2), 261–274. [https://doi.org/10.1016/s0378-5955\(00\)00136-2](https://doi.org/10.1016/s0378-5955(00)00136-2), 2000 Sep.
- Sánchez-Benito, D., Gómez-Nieto, R., Hernández-Noriega, S., Murashima, A.A.B., de Oliveira, J.A.C., García-Cairasco, N., López, D.E., Hypolito, M.A., 2017. Morphofunctional alterations in the olivocochlear efferent system of the genetic audiogenic seizure-prone hamster GASH:Sal. *Epilepsy Behav.* 71 (Pt B), 193–206. <https://doi.org/10.1016/j.yebeh.2016.05.040>.
- Seal, R.P., Akil, O., Yi, E., Weber, C.M., Grant, L., Yoo, J., Clause, A., Kandler, K., Noebels, J.L., Glowatzki, E., Lustig, L.R., Edwards, R.H., 2008. Sensorineural deafness and seizures in mice lacking vesicular glutamate transporter 3. *Neuron* 57 (2), 263–275. <https://doi.org/10.1016/j.neuron.2007.11.032>.
- Sievers, F., Higgins, D.G., 2018. Clustal Omega for making accurate alignments of many protein sequences. *Protein Sci.* 27 (1), 135–145. <https://doi.org/10.1002/pro.3290>.
- Simmons, D.D., Manson-Gieseke, L., Hendrix, T.W., Morris, K., Williams, S.J., 1991. Postnatal maturation of spiral ganglion neurons: a horseradish peroxidase study. *Hear. Res.* 55 (1), 81–91. [https://doi.org/10.1016/0378-5955\(91\)90094-P](https://doi.org/10.1016/0378-5955(91)90094-P).
- Simmons, D.D., Rogers, M.S., Woody, D., 1994. Acute effects of capsaicin on the postnatal spiral ganglion. *Int. J. Dev. Neurosci.* 12 (5), 517–525. [https://doi.org/10.1016/0736-5748\(94\)90036-1](https://doi.org/10.1016/0736-5748(94)90036-1).
- Schaette, R., McAlpine, D., 2011. Tinnitus with a normal audiogram: physiological evidence for hidden hearing loss and computational model. *J. Neurosci.* 31 (38), 13452–13457. <https://doi.org/10.1523/JNEUROSCI.2156-11.2011>.
- Schuknecht, H.F., Watanuki, K., Takahashi, T., Belal Jr., A.A., Kimura, R.S., Jones, D.D., Ota, C.Y., 1974. Atrophy of the stria vascularis, a common cause for hearing loss. *Laryngoscope* 84 (10), 1777–1821. <https://doi.org/10.1288/00005537-197410000-00012>.
- Skradski, S.L., Clark, A.M., Jiang, H., White, H.S., Fu, Y.H., Ptacek, L.J., 2001. A novel gene causing a mendelian audiogenic mouse epilepsy. *Neuron* 31, 537–544. [https://doi.org/10.1016/s0896-6273\(01\)00397-X](https://doi.org/10.1016/s0896-6273(01)00397-X).
- Takamori, S., 2006. VGLUTs: 'exciting' times for glutamatergic research? *Neurosci. Res.* 55 (4), 343–351. <https://doi.org/10.1016/j.neures.2006.04.016>.
- Takamori, S., Rhee, J.S., Rosenmund, C., Jahn, R., 2001. Identification of differentiation-associated brain-specific phosphate transporter as a second vesicular glutamate transporter (VGLUT2). *J. Neurosci.* 21 (22), RC182. <https://doi.org/10.1523/JNEUROSCI.21-22-j0002.2001>.
- Vogler, D.P., Robertson, D., Mulders, W.H., 2011. Hyperactivity in the ventral cochlear nucleus after cochlear trauma. *J. Neurosci.* 31 (18), 6639–6645. <https://doi.org/10.1523/JNEUROSCI.6538-10.2011>.
- Wallén-Mackenzie, A., Wootz, H., Englund, H., 2010. Genetic inactivation of the vesicular glutamate transporter 2 (VGLUT2) in the mouse: what have we learnt about functional glutamatergic neurotransmission? *Ups. J. Med. Sci.* 115 (1), 11–20. <https://doi.org/10.3109/03009730903572073>.
- Warr, W.B., Beck, J.E., 1996. Multiple projections from the ventral nucleus of the trapezoid body in the rat, vol. 93, pp. 83–101. [https://doi.org/10.1016/0378-5955\(95\)00198-0](https://doi.org/10.1016/0378-5955(95)00198-0) (1–2).
- Werner, F.M., Coveñas, R., 2017. Classical neurotransmitters and neuropeptides involved in generalized epilepsy in a multi-neurotransmitter system: how to improve the antiepileptic effect? *Epilepsy Behav.* 71 (Pt B), 124–129. <https://doi.org/10.1016/j.yebeh.2015.01.038>.
- Xia, A., Song, Y., Wang, R., Gao, S.S., Clifton, W., Raphael, P., Chao, S.I., Pereira, F.A., Groves, A.K., Oghalai, J.S., 2013. Prestin regulation and function in residual outer hair cells after noise-induced hearing loss. *PLoS One* 8 (12), e82602. <https://doi.org/10.1371/journal.pone.0082602>.
- Yasuda, S., Ishida, N., Higashiyama, A., Morinobu, S., Kato, N., 2000. Characterization of audiogenic-like seizures in naive rats evoked by activation of AMPA and NMDA receptors in the inferior colliculus. *Exp. Neurol.* 164 (2), 396–406. <https://doi.org/10.1006/exnr.2000.7401>.
- Zeng, C., Nannapaneni, N., Zhou, J., Hughes, L.F., Shore, S., 2009. Cochlear damage changes the distribution of vesicular glutamate transporters associated with auditory and nonauditory inputs to the cochlear nucleus. *J. Neurosci.* 29 (13), 4210–4217. <https://doi.org/10.1523/JNEUROSCI.0208-09.2009>.
- Zhou, J., Nannapaneni, N., Shore, S., 2007. Vesicular glutamate transporters 1 and 2 are differentially associated with auditory nerve and spinal trigeminal inputs to the cochlear nucleus. *J. Comp. Neurol.* 500 (4), 777–787. <https://doi.org/10.1002/cne.21208>.



Morphofunctional alterations in the olivocochlear efferent system of the genetic audiogenic seizure-prone hamster GASH:Sal



David Sánchez-Benito ^{a,b,c}, Ricardo Gómez-Nieto ^{a,b,c}, Sonia Hernández-Noriega ^{a,b}, Adriana Andrade Batista Murashima ^d, José Antonio Cortes de Oliveira ^e, Norberto García-Cairasco ^e, Dolores E. López ^{a,b,c,*}, Miguel Angelo Hyppolito ^d

^a Institute of Neuroscience of Castilla y León (INCYL), University of Salamanca, Salamanca, Spain

^b Institute of Biomedical Research of Salamanca (IBSAL), University of Salamanca, Salamanca, Spain

^c Department of Cell Biology and Pathology, Faculty of Medicine, University of Salamanca, Salamanca, Spain

^d Laboratory of Neurobiology of Hearing, Ribeirão Preto Medical School, University of São Paulo, São Paulo, Brazil

^e Neurophysiology and Experimental Neuroethology Laboratory, Ribeirão Preto Medical School, University of São Paulo, São Paulo, Brazil

ARTICLE INFO

Article history:

Received 9 December 2015

Revised 13 May 2016

Accepted 31 May 2016

Available online 1 August 2016

Keywords:

Animal models of epilepsy
Reflex seizures
Distortion-product otoacoustic emission (DPOAE)
Hair cell
Olivocochlear neurons
Pathogenesis of epilepsy
Scanning electron microscopy

ABSTRACT

The genetic audiogenic seizure hamster (GASH:Sal) is a model of a form of reflex epilepsy that is manifested as generalized tonic-clonic seizures induced by external acoustic stimulation. The morphofunctional alterations in the auditory system of the GASH:Sal that may contribute to seizure susceptibility have not been thoroughly determined. In this study, we analyzed the olivocochlear efferent system of the GASH:Sal from the organ of Corti, including outer and inner hair cells, to the olivocochlear neurons, including shell, lateral, and medial olivocochlear (LOC and MOC) neurons that innervate the cochlear receptor. To achieve this, we carried out a multi-technical approach that combined auditory hearing screenings, scanning electron microscopy, morphometric analysis of labeled LOC and MOC neurons after unilateral Fluoro-Gold injections into the cochlea, and 3D reconstruction of the lateral superior olive (LSO). Our results showed that the GASH:Sal exhibited higher auditory brain response (ABR) thresholds than their controls, as well as absence of distortion-product of otoacoustic emissions (DPOAEs) in a wide range of frequencies. The ABR and DPOAE results also showed differences between the left and right ears, indicating asymmetrical hearing alterations in the GASH:Sal. These alterations in the peripheral auditory activity correlated with morphological alterations. At the cochlear level, the scanning electron microscopy analysis showed marked distortions of the stereocilia from basal to apical cochlear turns in the GASH:Sal, which were not observed in the control hamsters. At the brainstem level, MOC, LOC, and shell neurons had reduced soma areas compared with control animals. This LOC neuron shrinkage contributed to reduction in the LSO volume of the GASH:Sal as shown in the 3D reconstruction analysis. Our study demonstrated that the morphofunctional alterations of the olivocochlear efferent system are innate components of the GASH:Sal, which might contribute to their susceptibility to audiogenic seizures.

This article is part of a Special Issue entitled “Genetic and Reflex Epilepsies, Audiogenic Seizures and Strains: From Experimental Models to the Clinic”.

© 2016 Elsevier Inc. All rights reserved.

1. Introduction

The genetic audiogenic seizure hamster (GASH:Sal), in which exposure to intense acoustic stimulation induces generalized convulsive audiogenic seizures, is a strain of Syrian hamster inbred at the University of Salamanca [1]. Recent studies have supported the GASH:Sal as a

promising animal model to study the development of epileptic seizures [2–4] and the characterization of antiepileptic drugs [5,6]. Functional, electrophysiological, and structural characterization of the auditory pathways in the GASH:Sal might be a further step towards understanding the pathophysiological mechanisms involved in different types of seizures including focal and generalized tonic-clonic seizures. In fact, several studies reported that the hyperactivity of an important midbrain auditory structure, the inferior colliculus (IC), is implicated in the initiation and propagation of audiogenic seizures [7].

Several audiogenic seizure-susceptible strains have been genetically selected worldwide [8,9]. The GASH:Sal was originated at the University

* Corresponding author at: Institute for Neuroscience of Castilla y León (INCYL), Laboratory 12, C/ Pintor Fernando Gallego 1., 37007 Salamanca, Spain. Tel.: +34 923294400x1868.

E-mail address: lopezde@usal.es (D.E. López).

of Salamanca [1] and exhibits epileptic seizures in response to sounds [3,4]. After acoustic stimulation, the seizure appears within seconds and lasts for approximately 5 min, following a sequence of behavioral phases: wild running, tonic-clonic seizures, and a comatose postictal phase with subsequent recovery. The GASH:Sal hamsters exhibit their maximum susceptibility to seizures from 1 to 4 months of age, but this condition gradually disappears around the age of 1 year, showing the running phase without the convulsive phase [4,5].

Experimental models of epilepsy are necessary for understanding the neural substrates and neurochemical mechanisms involved in epileptogenesis, as well as for determining the mechanisms of drug action in clinical practice and selection of new anticonvulsant agents. Each model has specific characteristics regarding motor expression, electroencephalography, and response to different antiepileptic drugs. The rodent models (usually rats and mice) of electrically [10] and acoustically induced acute and chronic seizures have been associated with partial and generalized tonic-clonic seizures, with selective involvement of brainstem and limbic structures [11]. The IC, deep layers of superior colliculus, reticular formation, substantia nigra pars reticulata, and periaqueductal gray matter are implicated in the pathophysiological aspects of audiogenic seizures [11–13].

The possible morphofunctional alterations in the auditory system of the GASH:Sal, including the superior olfactory complex (SOC) and the cochlear receptor, which might be involved in the expression of their audiogenic seizures, have not been thoroughly studied. The SOC, a collection of brainstem nuclei that participate in multiple aspects of hearing, contains the source of the olivocochlear system that innervates the cochlea. In mammals, the olivocochlear neurons form a dense bundle of fibers which projects bilaterally from the SOC to the organ of Corti. This olivocochlear bundle is divided into two efferent systems based on the cell bodies' site of origin and the projection pattern: 1) the lateral superior olive (LSO), a distinct group of neurons located in the lateral part of the SOC that forms the lateral olivocochlear (LOC) system, and 2) the ventral nucleus of the trapezoid body (VNTB), a diffuse and heterogeneous group of neurons located ventrally within the complex that forms the medial olivocochlear (MOC) system. Lateral olivocochlear neurons send unmyelinated axons to project beneath the inner hair cells (IHCs) of the cochlea, with a clear ipsilateral preference. On the contrary, MOC neurons send their myelinated axons to innervate the outer hair cells (OHCs) of the cochlea with a contralateral preference [14]. Afferent inputs to LOC neurons originate almost exclusively from the ipsilateral cochlear nucleus. Those to MOC neurons are somewhat more complex and include predominantly contralateral projections from the cochlear nuclei, as well as descending fibers from the IC and the auditory cortex [15,16].

The inputs descending from higher levels are thought to underlie the possible involvement of the MOC system in selective attention [17–20]. In addition to these classically defined LOC and MOC neurons, neuronal tract-tracing studies revealed a third class of olivocochlear neurons, called "shell neurons", which surround the LSO [21]. Lateral olivocochlear neurons have round spherical cell bodies that are located within the LSO, and hence, they are referred to as intrinsic LOC neurons. In contrast, shell neurons are referred to as extrinsic because they are located surrounding the LSO. Shell neurons project mainly to the ipsilateral cochlea, they are larger than intrinsic LOC neurons, and their somata are morphologically similar to MOC neurons, which have large multipolar cell bodies. Lateral olivocochlear neurons are tonotopically organized within the LSO with high-to-low frequencies represented from medial to lateral. Although this organization within the nucleus is not that clear for MOC neurons, their afferent and efferent projections are organized in a tonotopic fashion. The functional role of the MOC and LOC systems is, in general, to reflexively modulate the sensitivity of receptor mechanisms operating in relation to each type of hair cell within the organ of Corti [22–25]. Evidence of the action of the medial olivocochlear efferent system has been obtained by the suppression of

the so-called distortion-product of otoacoustic emissions (DPOAEs), following acoustic stimulation.

Therefore, hearing evaluation using DPOAEs and auditory brainstem responses (ABRs) provides valuable information on functional, morphological, and electrophysiological aspects of the auditory system and particularly on the olivocochlear efferent pathway and the cochlear status, giving information about hair cell function. In fact, DPOAEs measure the feedback of biomechanical energy to the contraction of the outer hair cells [26]. The ABR measures the bioelectrical phenomena triggered by the sound stimulus through the auditory brainstem. This electrical activity can be filtered and captured by surface electrodes and is represented by 5 to 7 waves (I, II, III, IV, V, VI, and VII), each one of them referring to a specific location of the central auditory pathway. In rodents, the elicited waveform response has the following correlation: wave I, auditory nerve; wave II, cochlear nuclei; wave III, superior olfactory complex; wave IV, lateral lemniscus and IC; and wave V, medial geniculate body and thalamocortical auditory radiation. The present study aimed to determine whether the olivocochlear system of the GASH:Sal has functional and morphological alterations that might explain its susceptibility to audiogenic seizures. Thus, functional assessment of the olivocochlear system was carried out using DPOAE and ABR tests in the GASH:Sal. Furthermore, in order to assess possible morphological alterations, we performed a morphometric analysis of MOC, LOC, and shell neurons as well as a 3D reconstruction analysis of the LSO. Since olivocochlear alterations might lead to cilia malfunctioning, we further studied the organ of Corti by employing the scanning electron microscopy in order to determine any derangement or distortion of cilia. All these morphological studies in the GASH:Sal were compared to control animals and correlated to the electrophysiological examinations. Our data represent the first link of functional and morphological alterations in the auditory system of the GASH:Sal hamsters that might contribute to their audiogenic seizure susceptibility.

2. Material and methods

2.1. Experimental animals

In total, 9 control hamsters (*Mesocricetus auratus*) from Charles River Labs (Barcelona, Spain) and 16 hamsters of the GASH:Sal strain from the animal's facility of the University of Salamanca (Salamanca, Spain), 4 months of age, were used in this study. All the GASH:Sal hamsters were naïve without receiving any acoustic stimulation to trigger audiogenic seizures. The experiments were conducted in compliance with the guidelines for the use and care of laboratory animals of the European Communities Council Directive (2010/63/EU), with the current Spanish legislation (RD 1201/05), and with those established by the Institutional Bioethics Committee. All efforts were made to minimize the number of animals and their suffering. The animals were maintained under normal conditions of lighting (12-h light/dark cycle) and constant temperature with ad libitum access to food and water.

2.2. DPOAE and ABR tests

For the functional and electrophysiological auditory assessment, 8 GASH:Sal and 3 control hamsters were evaluated for DPOAE and ABR tests under anesthesia with ketamine hydrochloride (40 mg/kg) and xylazine (10 mg/kg) via intramuscular administration. Studies were performed with the Smart EP-DPOAE equipment manufactured by Intelligent Hearing Systems (Miami, FL, USA) and calibrated by the manufacturer. Analysis of DPOAE was performed following the relationship of frequencies of $2f_1-f_2$ with $f_1:f_2 = 1.22$, two points per octave resolution (DPGRAM). The DPOAEs were 55-dB SPL less intense than the stimulus.

The DPGram provides information about function of the cochlear outer hair cells that were responsible for the analyzed frequencies. For evaluation of the auditory threshold, the ABR test was performed.

Surface electrodes were positioned as follows: a positive electrode on the cranial vertex, two negative electrodes in the posterior portion of the pinna, and a reference electrode (ground) on the forehead, between the orbits. These electrodes were placed with interposition of electrolytic paste, for better conductivity of electrical signal and reduction of artifacts. For sound stimulation, inserted headphones were placed in the external auditory canal. The stimulus used was the alternated click, with 27.7 stimuli per second and a duration of 0.1 ms. Fundamental frequency was 2000–4000 Hz, using the intensity of 90-dB nHL. The signal picked up by electrodes was pass filtered – high and low of 150 and 3000 Hz, respectively. The filtered and amplified signal was the average of 1024 ABR recordings, with a window of 12 ms. The final result was provided in the form of waves of electric potential. The research of the auditory threshold was performed by means of sound stimulus which was decreased by 10 dB until the approximate threshold. The threshold was considered as the lowest intensity in which the first wave of auditory potential was obtained. For the ABR tests, we used Smart EP–Intelligent Hearing Systems (Miami, FL, USA), calibrated by the manufacturer. The latency of each ABR component was measured at an intensity of 90 dB.

2.3. Scanning electron microscopy study

For the scanning electron microscopy study of the cochlear hair cells, 1 control and 3 GASH:Sal hamsters were used. The tissue was obtained by perfusion of each animal after anesthesia with sodium thiopental (Abbott) (69 mg/kg). Animals were perfused transcardially with 0.1-M phosphate buffer solution, followed by 4% paraformaldehyde and 0.1% glutaraldehyde in 0.1 M of phosphate buffer (pH = 7.4) using a speed-controlled pump perfusion Masterflex® (Paste, Parmer). Then, a craniotomy was performed to quickly remove the brain and the tympanic bulla. The bulla was opened, and the cochlea was dissected under the microscope and perfused in 4% paraformaldehyde solution and subsequently maintained in the same fixative solution for 4 h.

Cochleae were processed for scanning electron microscopy, washed three times for 5 min with 0.1 M phosphate buffer (pH = 7.4). After these procedures, cochleae were fixed in 1% osmium tetroxide solution in 0.1-M phosphate buffer (pH = 7.4), for 2 h at 4 °C, washed with phosphate buffer solution 0.1-M (pH = 7.4), and dehydrated at room temperature in graded concentrations of ethanol (50%, 70%, 90%, and 95% – once for 10 min at each concentration) and absolute ethanol three times for 15 min. Completed dehydration was performed following the drying method of critical point in CO₂, using the equipment BAL-TEC CPD 030® (Critical Point Dryers), in which after successive baths in liquid CO₂ at 4 °C, the ethanol was removed. Then, the material was subjected to an increase in temperature to 40 °C in order to pass CO₂ from liquid to gaseous state. The material was fixed in a metal support, being coated in a vacuum chamber BAL-TEC SCD 050 with vapors of gold. After this tissue preparation procedure, the cochleae were electrically conductive. The observation and analysis of the cochlear hair cells were carried out with an Electron Microscope JEOL SCANNING MICROSCOPE – JSM 5200.

2.4. Injection of Fluoro-Gold

For the morphological study of the olivocochlear neurons, 3 control and 3 GASH:Sal hamsters received unilateral injections of the retrograde tracer Fluoro-Gold® (FG – Fluorochrome, Denver, CO, USA), diluted in 4% in saline solution, into the left cochlea. Animals were prepared under deep anesthesia with ketamine (200 mg/kg) and xylazine (10 mg/kg), and when necessary, anesthetic complementation with 1/5 of the initial dose was injected during the surgery. In addition, local anesthetic (2% lidocaine with epinephrine 1:200,000) was administered before surgery. After a skin incision and removal of adipose tissue in the postauricular region, the tympanic bulla was exposed. Then, the bulla was opened with a diamond drill, and the round window of the cochlea was visualized. The FG was injected by

pressure into the cochlea through the round window using a micropipette of glass with a diameter of 50–60 µm. After the injection, the bulla was sealed with bone wax, and the incision was sutured. Animals recovered from surgery, following a postinjection survival time of 10 days, and immediately after that, they were processed for histology. Under deep anesthesia with sodium pentobarbital, hamsters were perfused transcardially with a Ringer's solution (37 °C, pH 6.9), followed by 4% paraformaldehyde. The brains were removed and cryoprotected for 48–72 h at 4 °C in a solution containing 30% sucrose. Serial coronal brainstem sections of 40-µm thickness were obtained in a freezing microtome. The FG was visualized following the immunohistochemical procedure described by Gómez-Nieto et al. [27]. All sections were incubated with a rabbit anti-FG antibody (dilution 1:2000), followed by a goat biotinylated secondary antibody anti-rabbit (dilution 1:200). Then, the sections were incubated in the avidin–biotin–peroxidase complex, developed for peroxidase reaction, mounted on slides, dehydrated in ethanol, and coverslipped as described by Gómez-Nieto et al. [27].

2.5. 3D reconstruction

Four animals, 2 control and 2 GASH:Sal hamsters, were employed to generate 3D reconstructions of the LSO using Neurolucida (version 10) and NeuroExplorer (version 3) software applications from MicroBrightField Bioscience, (Williston, VT, USA) following the procedure described elsewhere [28]. After perfusion of the animal, the brain was collected, and a hole was made by the passage of a surgical needle throughout the rostrocaudal plane of the left brainstem, and serial brain sections were obtained as described above. Then, alternate serial sections were processed for immunohistochemical visualization of the calcium-binding protein, calbindin D-28k (CaBP), using an identical procedure to the one used by Gómez-Nieto et al. [27]. For each brain, all sections were mounted on slides, and alternate series without immunohistochemistry for CaBP were counterstained with cresyl violet to highlight cytoarchitectonic divisions; the other sections processed for CaBP immunohistochemistry were dehydrated in ethanol and coverslipped. The outline of CaBP and cresyl violet-stained coronal sections was viewed with the 5× objective lens of a Leica DMRB microscope and was drawn on the computer screen. Successive sections were aligned via rotation and translation of the drawing with the help of four reference points. The hole, created by the needle, was used for setting one of these reference points, and the other three were set using different anatomical landmarks as the edges of adjacent sections. All these structures were superimposed and matched in the two successive sections to achieve accurate alignment. After that, the contours of the LSO were manually traced using a 20× objective lens. The contours of the brainstem and the LSO were digitized with Neurolucida and metrically and topologically analyzed with NeuroExplorer. Images and movie documents from the 3D renderings were obtained using Neurolucida software.

2.6. Imaging and data analysis

The histological sections processed for light microscopy were examined using a Leica microscope DMLB, coupled to a drawing tube and a digital camera to obtain the images. Low magnification images were taken with the 4× and 10× objective lens, and high magnification images were taken with a 40× objective lens. Drawing schemes of brainstem sections were carried out using the camera Lucida and digitized with the Canvas software (version 14 Build 1618, ACD Systems of America, Inc.). The morphometric analysis of labeled olivocochlear neurons was carried out with ImageJ (version 1.42; Rasband, N.S., National Institutes of Health, Bethesda, Maryland, USA; <http://rsb.info.nih.gov/ij>). For the scanning electron microscopy study, images of the basal, medial, and apical cochlear turns were obtained at a magnification that ranged from 2000× to 3500×. All representative images shown in the figures were processed by minor modifications with regard to brightness

and contrast using ImageJ, and the final figures were composed with Canva 14.

Statistical analysis of the morphometric features such as area, perimeter, and roundness of labeled olivocochlear neurons, as well as the volume and area of the 3D reconstruction, was performed using the SPSS software, version 18.0 (SPSS Inc., Chicago, IL, USA). For each of the morphometric parameters in the labeled neurons, one factor analysis of variance test and post hoc analysis with Fisher's PLSD and Sheffe's test were applied. We considered six groups for the statistical comparisons between the control and GASH:Sal hamsters:

ipsilateral and contralateral intrinsic LOC neurons, ipsilateral and contralateral shell neurons, and ipsilateral and contralateral MOC neurons. All values were expressed as the mean \pm standard error of the mean.

3. Results

3.1. ABR and DPOAE evaluations in the GASH:Sal

We performed a hearing screening of the GASH:Sal at 4 months of age by combining the two existing hearing tests: (1) the ABR test and

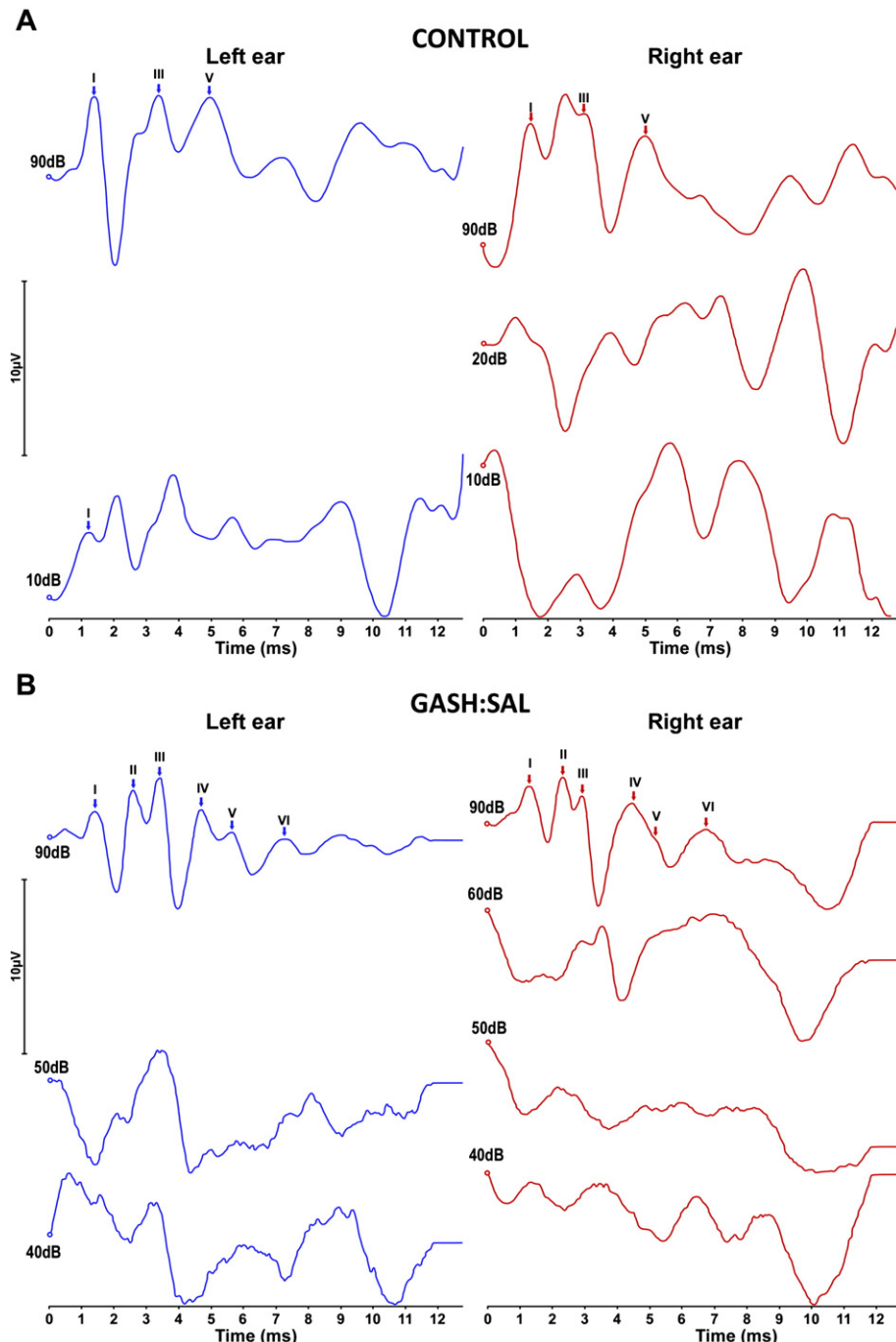


Fig. 1. Auditory brain response (ABR) evaluations in the control and GASH:Sal hamsters. A. Plots show ABR waveforms (amplitude in μ V) obtained from one control hamster after click stimulation on the left (in blue) and right (in red) ears. Notice that the ABR thresholds are 20 dB. B. Plots show ABRs (amplitude in μ V) obtained from one GASH:Sal hamster after click stimulation on the left (in blue) and right (in red) ears. Notice that thresholds of ABRs are 50 dB and 60 dB for the left and right ears, respectively. The plots showed representative ABR recordings at the smallest intensity of clicks which evoked visually detectable responses (ABR threshold) and the maximum intensity (90 dB), in which ABR waveforms were clearly visible. All responses displayed in the graphs were double-traced to confirm reproducibility (not shown in this figure).

(2) the DPOAE test. The ABR test showed that the lowest intensity in which the wave responses could be detected was 50 dB and 60 dB at 2–4 kHz for the left and right ears, respectively (Fig. 1). The identification of more appropriate latency–amplitude wave responses was observed at an intensity of 90 dB (Fig. 1). On the contrary, the control hamsters exhibited ABR thresholds of 20 dB, and hence, the ABR thresholds in the GASH:Sal were elevated approximately 30–40 dB more than in controls (see Fig. 1A–B for comparison).

A comparison of the ABR results between the right and left ears of the GASH:Sal showed an increase of approximately 0.5 to 1.3 ms in the latency of the left ear for each of the wave responses (Fig. 2). The latencies of the waves III, IV, and V were significantly higher for the left than for the right ear of the GASH:Sal. Such differences were not observed in the control hamster (see Fig. 2A–C for comparison). We further analyzed the ABR interpeak latencies of the wave's responses (Fig. 2). Thus, the GASH:Sal showed significantly higher interpeak latencies between the waves III and V as well as the waves I and V for the left than for the right ear stimulation (p value ≤ 0.05). By contrast, there were no statistically significant differences in the ABR latencies when comparing the left and right ears of the control hamsters (see Fig. 2B–D for comparison).

The DPOAE tests in the GASH:Sal showed that DPOAEs were absent in the low–middle frequency range from 500 to 6000 Hz in both ears. However, DPOAEs were observed at frequencies above 6000 Hz (Fig. 3). The DPOAEs at a frequency of 8000 Hz exhibited higher amplitude for the left than for the right ear, this difference being statistically significant (p value ≤ 0.001) (Fig. 3). On the contrary, the control hamsters exhibited normal DPOAEs for both ears at all frequencies (for comparison, see Fig. 3A–B and C–D).

3.2. Scanning electron microscopy study of the cochlear hair cells

The higher thresholds shown in the ABR tests of the GASH:Sal as well as the differences in the latency of ABRs and DPOAEs between the left and right ears led us to study the cochlear hair cells of the GASH:Sal with the scanning electron microscopy. Our results showed that the cochlea of control hamsters exhibited the ordered cellular mosaic pattern made of the apical domains of hair cells, as well as the supporting cells in the organ of Corti. The three rows of OHCs were separated from the single row of IHCs by the inner pillar cells (Fig. 4A). The OHCs and IHCs were characterized by tufts of stereocilia protruding from their apices. Stereocilia were observed as cylindrical protrusions morphologically similar to large microvilli. The stereocilia of IHCs formed straight or slightly curved bundles, while the stereocilia of the OHCs exhibited a V-shaped pattern (Fig. 4A). The organ of Corti of the GASH:Sal revealed a similar distribution of OHCs and IHCs than the one observed in the control hamster. The three rows of OHCs and a single row of IHCs were also present in the GASH:Sal, showing no differences in the number of cochlear hair cells between these two animal groups (Fig. 4). However, the stereociliary organization of the cochlear hair cells in the GASH:Sal was markedly different compared with that in the control hamsters. Such alterations in the stereocilia pattern were more noticeable in the basal turn of the cochlea. The majority of OHCs and IHCs showed disorganization of the tufts of stereocilia and loss of their links (Fig. 4B). Occasionally, these stereocilia appeared to be shortened and collapsed. In the medial turn of the cochlea, stereociliary distortion and disarrangement were frequently noticed in the OHCs, especially in the first row of OHCs, as well as in the IHCs (Fig. 4C). The apical turn of the cochlea in the GASH:Sal was the least altered of the three cochlear

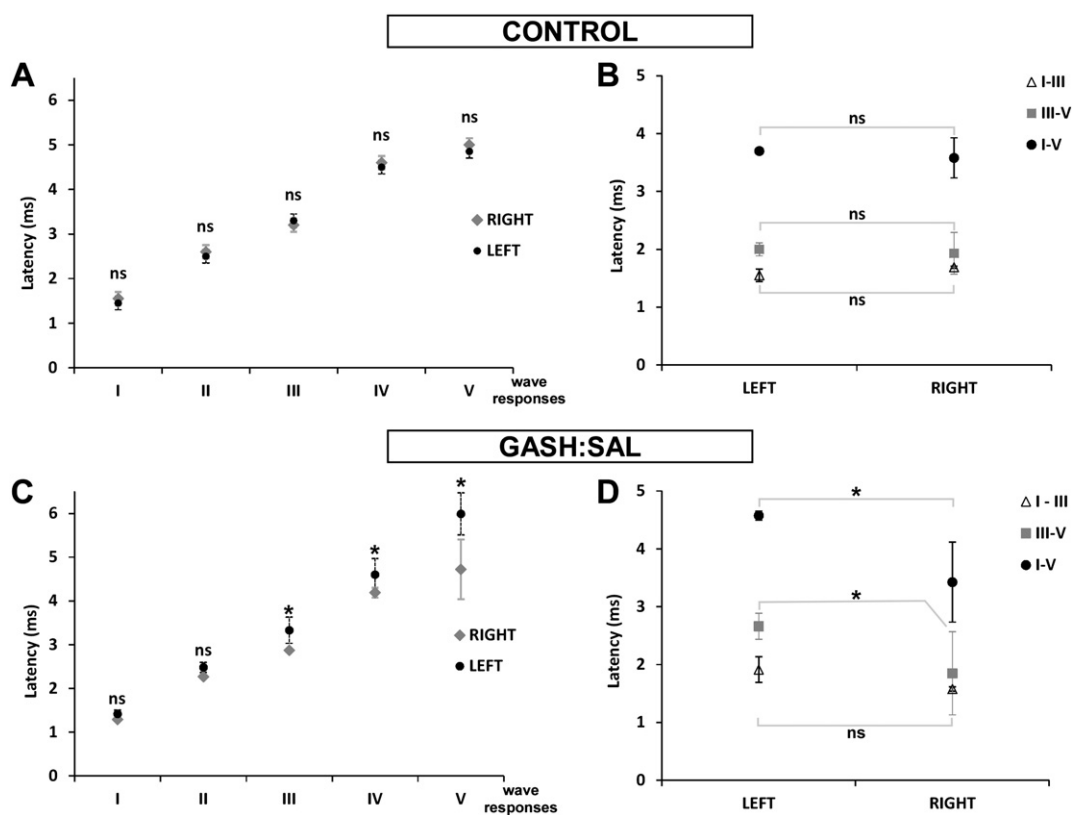


Fig. 2. Latencies of auditory brain responses (ABRs) in the control and GASH:Sal hamsters. A. Plot shows latencies for each waveform responses (I, II, III, IV, and V) in the left and right ears of the control hamsters. B. Plot shows interpeak latencies in the left and right ears of control hamsters. Notice that there were no significant differences between the left and right ears. C. Plot displays latencies for each waveform responses in the GASH:Sal. Notice significantly shorter latencies in the waves III, IV, and V for the right-ear stimulation. D. ABR interpeak latencies in the GASH:Sal hamsters, showing longer latency intervals for the left-ear stimulation. $^{**} = p$ value ≤ 0.05 . ns = nonsignificant.

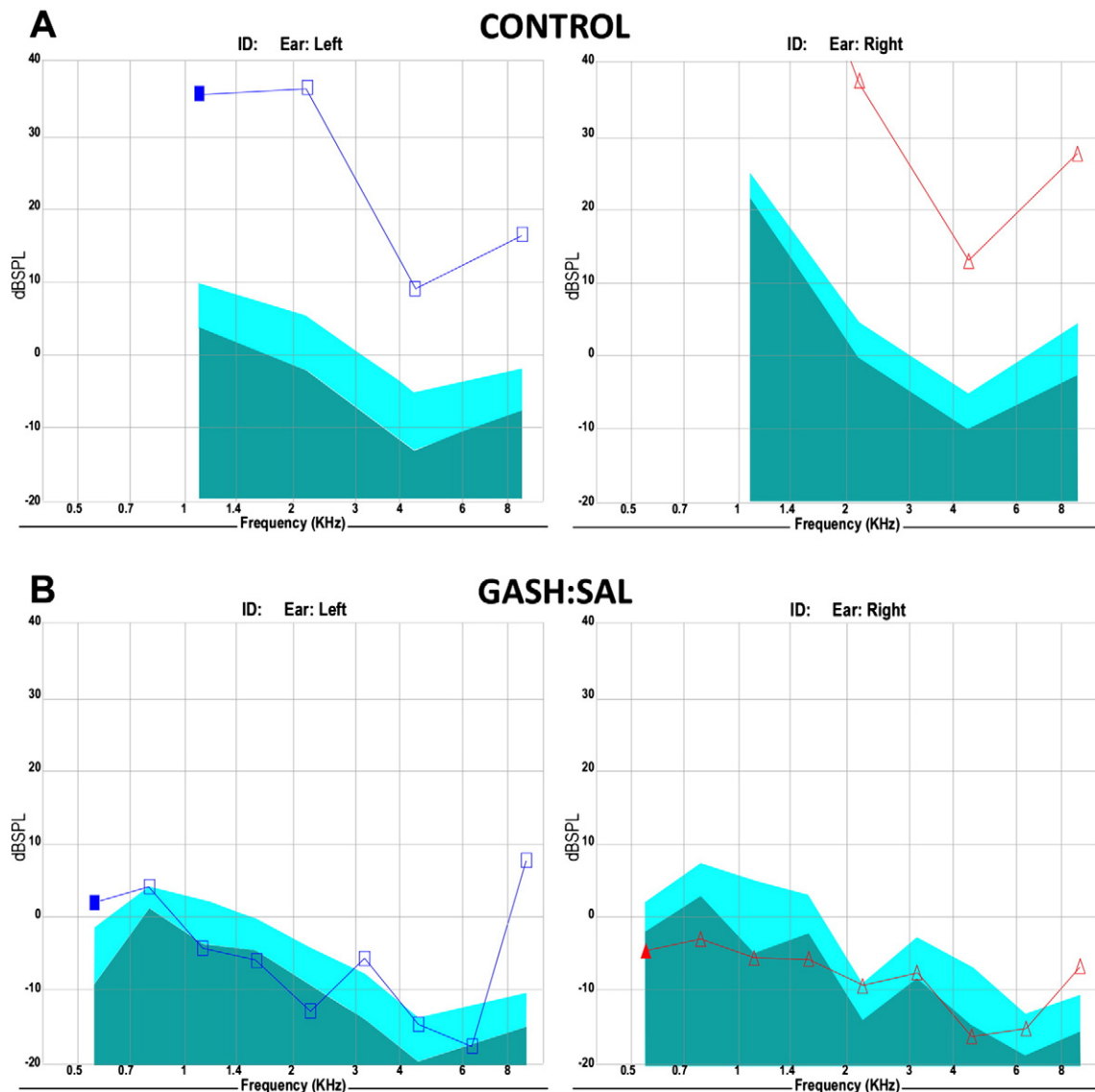


Fig. 3. Distortion-product of otoacoustic emissions (DPOAEs) in the left and right ears of the control and GASH:Sal hamsters. A. Histogram showing present and normal DPOAEs in the left and right ears from a control hamster. Both signal-to-noise ratio and absolute amplitude values are adequate and robust. B. Histogram showing a clearly absent DPOAEs in a GASH:Sal hamster. Notice that data points corresponding to the low–middle frequency range (from 500 to 6000 Hz) are embedded in the noise floor for both ears. Also, DPOAEs were significantly higher in the left than in the right ear at a frequency of 8000 Hz (p value ≤ 0.001). The DPOAEs are denoted with squares (blue line) and with triangles (red line) for the left and right ears, respectively.

turns, although several OHCs and IHCs showed distortion in their stereociliary pattern (Fig. 4D).

As shown in greater detail in Fig. 5, the scanning electron microscopy study indicated a distortion and disarrangement in the organization pattern, as well as an altered morphology of the stereocilia in the OHCs and IHCs of the GASH:Sal.

3.3. Morphology of the olivocochlear neurons in the GASH:Sal

The evaluation of cochlear structure in the scanning electron microscopy showed morphofunctional alterations of the OHCs and the IHCs in the GASH:Sal. Therefore, we further analyzed the olivocochlear efferent neurons that innervate the cochlear hair cells, in order to find whether there is any morphological deficit in olivocochlear neurons. To achieve this, we visualized the olivocochlear efferent neurons by injection of the retrograde tracer FG into the left cochlea of control and GASH:Sal hamsters. In both animals, these injections generated retrograde labeling in the VNTB and LSO, and no labeled neurons were observed in

any other auditory nuclei (Figs. 6 and 7), indicating that the injection sites were restricted to the cochlea.

Within the VNTB, we found labeled neurons that were identified as MOC neurons. They were large and multipolar neurons that distributed preferentially through the mediorstral extent of the VNTB with a clear contralateral preference. Thus, 80% of MOC neurons were found in the VTNB contralateral to the injection site, and 20% were ipsilateral (Fig. 7). Within the LSO and its surroundings, we found retrogradely labeled neurons that fit into the category of intrinsic and extrinsic LOC neurons, respectively. Intrinsic LSO neurons had an ovoid, fusiform shape and exhibited two or three primary dendrites (Fig. 8). In contrast, shell neurons were larger with a polygonal, globular, or elongated cell body and two or more dendrites that coursed along the edges of the LSO (Fig. 8). Intrinsic and extrinsic LOC neurons distributed mainly in the caudomedial extent of the LSO with a clear ipsilateral preference. Approximately, 90% of LOC and shell neurons were predominantly found ipsilateral to the side of the injection site (Fig. 7). A comparison between the control and the GASH:Sal hamsters showed that there

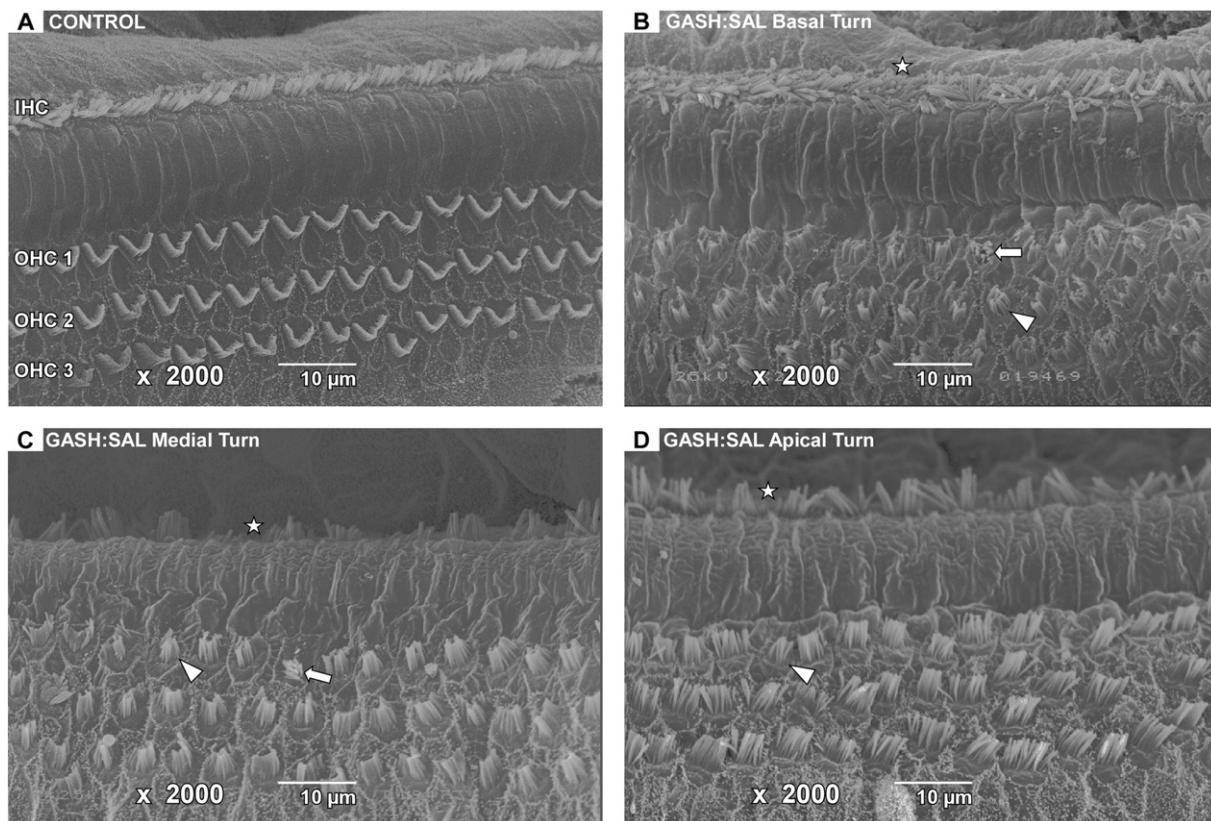


Fig. 4. Scanning electron microscopy of the organ of Corti in the control and GASH:Sal hamsters. A. Electron micrograph shows the organ of Corti in a control hamster. Notice normal distribution pattern of outer hair cells (OHCs) and inner hair cells (IHCs). Also, the stereocilia of the IHCs and OHCs exhibit the normal morphology, straight or slightly curved bundles for IHCs and V-shaped pattern for the three OHCs' rows (OHCs 1–3). B–D. Electron micrographs show the basal (B), medial (C), and apical (D) turns of the cochlea in the GASH:Sal. Notice the stereocilia distortion in the three rows of the OHCs and in the IHCs. Shortened stereocilia (arrows) as well as distortion and collapse of the stereociliary tufts (arrowheads) in the OHCs were frequently observed. V-like pattern of OHC stereocilia was absent in the corresponding three rows (OHCs 1–3). Stars indicate distortion of IHC stereocilia. Scale bars = 10 μm.

were no differences in the rostrocaudal distribution of MOC, LOC, and shell neurons (Fig. 7).

The difference in the number of intrinsic LOC and MOC neurons located ipsilateral vs. contralateral to the injected cochlea was statistically significant in control and GASH:Sal hamsters (p value ≤ 0.001 , Table 1). Although we found fewer labeled neurons in the GASH:Sal than in the

control hamster, this difference was not statistically significant (Fig. 9A and Table 1).

Regarding the size of the labeled olivocochlear neurons, we qualitatively observed that MOC, LOC, and shell neurons in the GASH:Sal had smaller cell bodies than that in the control hamster (Fig. 8).

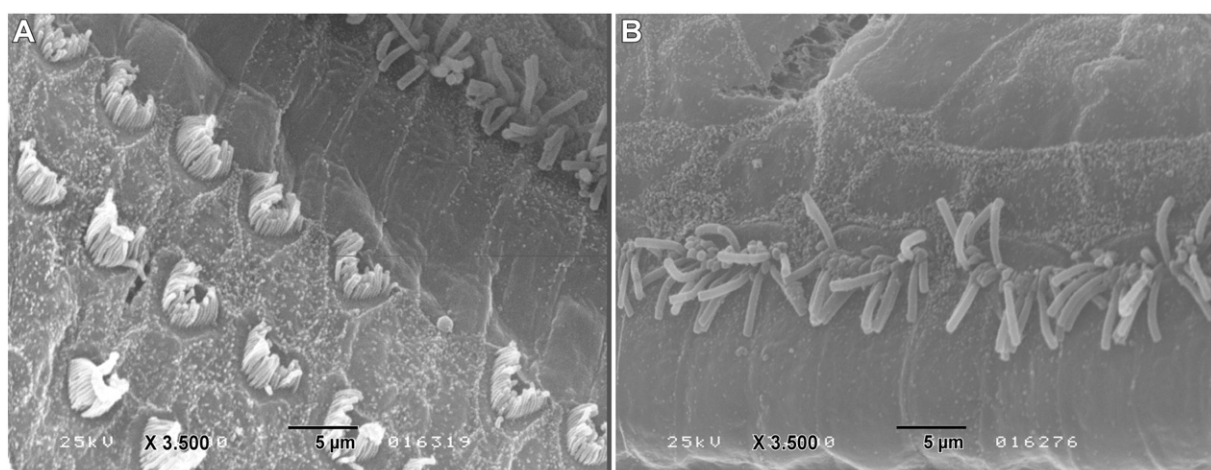


Fig. 5. Details of the stereocilia in the outer and inner hair cells (OHCs and IHCs) of the GASH:Sal. A. High magnification electron micrograph shows collapsed stereocilia in the OHCs. B. High magnification electron micrograph shows disrupted stereocilia pattern of the IHCs. Scale bars = 5 μm.

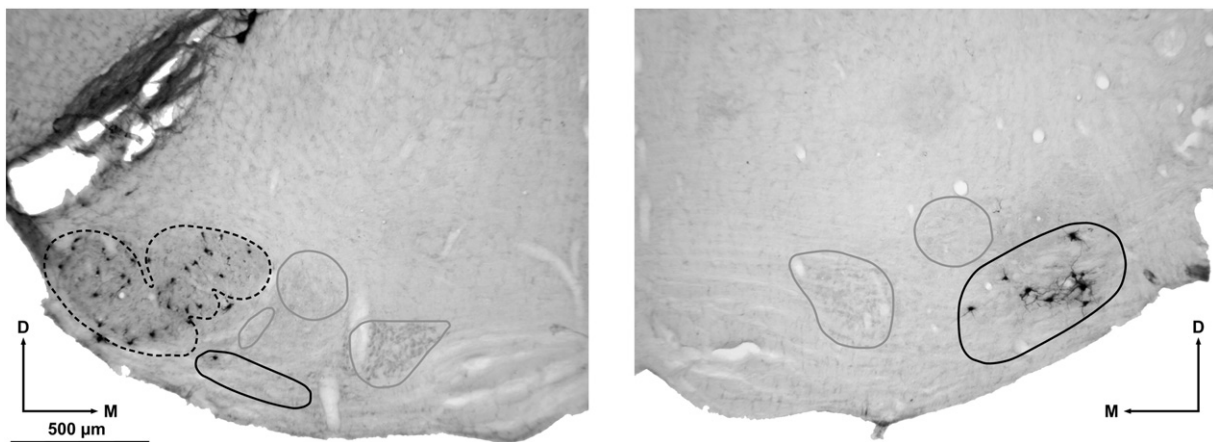


Fig. 6. Retrogradely labeled olivocochlear neurons after Fluoro-Gold injections into the left cochlea of the GASH:Sal. Micrographs show lateral olivocochlear (LOC) neurons in the ipsilateral lateral superior olive (LSO, denoted with dashed line) and medial olivocochlear (MOC) neurons in the contralateral ventral nucleus of the trapezoid body (VNTB, denoted with black solid line). Notice that no labeling was found in any other auditory nuclei (denoted in gray line). Scale bar = 500 μ m.

The morphometric analysis of the soma areas of LOC and shell neurons located in the ipsilateral side to the injected cochlea confirmed that those neurons were significantly smaller in the GASH:Sal than in the control hamster (Fig. 9B and Table 2). Also, the soma areas of MOC neurons were significantly smaller in the GASH:Sal than in the control hamster (Fig. 9B and Table 2). When comparing the soma areas of LOC, MOC, and shell neurons depending on their ipsi- vs. contralateral location, we found that the sizes of the olivocochlear neurons were statistically different in the GASH:Sal (Fig. 9B and Table 2). In the GASH:Sal, soma areas of intrinsic and extrinsic LOC neurons were significantly smaller in the ipsilateral than in the contralateral side, and the soma areas of the MOC neurons were larger in the ipsilateral than in the contralateral side (Fig. 9B and Table 2). Such differences in soma areas were not found in the control animals with the exception of the shell neurons (Fig. 9B and Table 2).

Furthermore, we analyzed the roundness of the olivocochlear neurons in the control and GASH:Sal hamsters. There were no significant differences in the soma roundness between the control and GASH:Sal hamsters, except for the MOC neurons that were located on the side contralateral to the injection site. These neurons exhibited significantly more circular cell bodies in the GASH:Sal than in the control hamster (Fig. 9C).

3.4. 3D reconstruction of the LSO

The morphometric analyses indicated differences in the soma areas of the LOC neurons between the control and GASH:Sal hamsters. To verify whether these neuronal soma differences contributed to differences in the volume of the LSO, we performed a 3D reconstruction of the LSO in the control and GASH:Sal hamsters. The 3D reconstruction showed the characteristic S-like shape of the LSO (Fig. 10). When we compared control versus GASH:Sal hamsters, we found a statistically significant reduction in the volume of the LSO in the GASH:Sal. The LSO had a volume of 147,380,000 μ m³ in the control hamster, whereas the GASH:Sal hamster had a total volume of 104,790,000 μ m³ in the LSO (Fig. 10B). Therefore, our data showed a reduction in the LSO volume of almost 30% in the GASH:Sal. Such reduction in volume was also evident in the LSO area that was significantly reduced in the GASH:Sal. Our results showed that the LSO area was 1,973,300 μ m² in the control hamster, while the LSO area in the GASH:Sal hamster was 1,411,655 μ m² (Fig. 10C). Although there was no statistically significant difference in the total perimeter of the LSO between the control and GASH:Sal hamster (Fig. 10D), the LSO perimeter in each of the analyzed sections through the rostrocaudal extent of the nucleus was significantly smaller in the GASH:Sal than in the control.

4. Discussion

The present study showed functional and morphological alterations in the olivocochlear efferent system of the GASH:Sal. The ABR screening test indicated that the GASH:Sal exhibited asymmetric hearing alterations with higher ABR thresholds than controls. Also, the DPOAE analysis showed an absence of DPOAEs in the low-middle frequency range in both ears. These alterations in the olivocochlear efferent function of the GASH:Sal were associated with morphological alterations in the organ of Corti, size of the olivocochlear neurons, and volume of the LSO. Since the olivocochlear efferent system modulates the cochlear gain improving the auditory afferent information [29–31], its malfunctioning might be involved in the initiation and propagation of audiogenic seizures in the GASH:Sal.

4.1. Alterations in the peripheral auditory activity of the GASH:Sal

Recent studies from our research group have reported differences in ABR thresholds between the control and GASH:Sal hamsters [4]. In those experiments, the ABRs were assessed by acoustic stimulation in open field, showing ABR thresholds of approximately 40 dB and 80 dB for the control and GASH:Sal hamsters, respectively. In the present study, we have further assessed the ABR in the GASH:Sal by acoustic stimulation through inserted earphones. Our results showed that the ABR thresholds in the GASH:Sal were 50 dB and 60 dB after acoustic stimulation in the left and right ears, respectively. These ABR thresholds were lower than those obtained by Muñoz et al. [4], probably because of the different stimulation method. Despite this methodological difference, our results were in accordance with that study, showing higher ABR thresholds in the GASH:Sal than in the control hamsters. The ABR thresholds in young adult hamsters have been previously studied and were about 32 dB in response to click stimulation [32,33]. The ABR thresholds in the GASH:Sal were 50–60 dB, and hence, they were elevated by approximately 30 dB when compared with those in Syrian hamsters. Thus, our study confirmed hearing deficits and alterations in the auditory thresholds of the GASH:Sal. We also found differences in ABR latencies between the left and right ears of the GASH:Sal, showing higher ABR latencies for the left ear. This was verified by analyzing the interpeak latencies, which were significantly longer in duration for the waves III–V and I–V for the left ear compared with those for the right ear. Altogether, these data suggest a delay in the left auditory brainstem processing of the GASH:Sal. Such difference between the left and right auditory processing was not observed in the control hamster. In the GASH:Sal, we also found no differences between the right and left ears for the absolute latencies to I (auditory nerve) and II (cochlear nuclei)

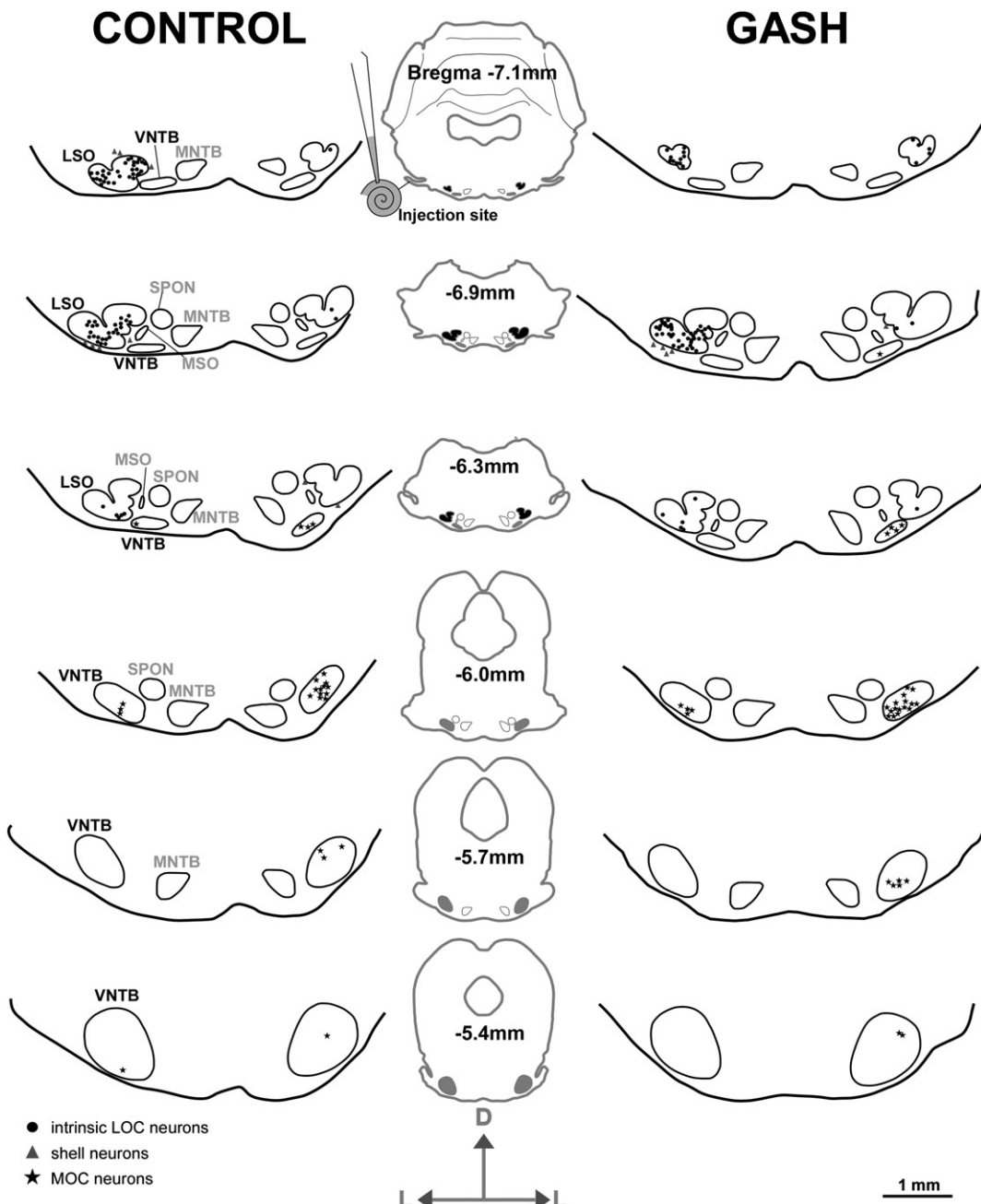


Fig. 7. Schematic drawings of coronal sections depicting the distribution of retrogradely labeled olivocochlear neurons after Fluoro-Gold injections into the left cochlea. Sections are arranged from caudal to rostral with distance relative to Bregma in mm. The center column shows the caudorostral distribution of the LSO (in black) and the VNTB (in gray). Notice the ipsi- vs. contralateral distribution of the lateral olivocochlear (LOC) and medial olivocochlear (MOC) neurons. LSO, lateral superior olive; MNTB, medial nucleus of the trapezoid body; MSO, medial superior olive; SPON, superior periolivary nucleus; VNTB, ventral nucleus of the trapezoid body. Symbols: circles = LOC neurons; triangles = shell neurons; stars = MOC neurons. Scale bar = 1 mm.

waves and interpeak symmetric latencies to ABR I-III waves. Thus, the auditory asymmetry in the auditory brainstem pathway occurs beyond the cochlear nucleus and includes the superior olfactory complex (wave III), the inferior colliculus (wave IV), and the medial geniculate body (wave V). At the cochlear level of the GASH:Sal, we also reported differences between left and right ears, showing higher left-ear DPOAE amplitudes at a frequency of 8 kHz. Also, our study showed an absence of DPOAEs in the low-middle frequency range of the GASH:Sal, while the control hamsters showed normal presence of DPOAEs without left-right auditory asymmetry. Supporting this, previous studies in control mice reported no differences between left and right ears in DPOAE amplitudes at 8 kHz [34].

In humans, it is known that the right ear is more sensitive than the left to simple sounds, the so-called peripheral right-ear advantage that became manifested in higher otoacoustic emission amplitudes for the right ear compared with those for the left ear [35]. Thus, our DPOAE evaluation showed that the GASH:Sal exhibited, contrary to our expectations, a lateralization in auditory brainstem processing with a left side-ear dominance. This lateralization might be a distinct auditory feature of the GASH:Sal that has to be considered for future investigations related to seizures. In humans, electrophysiological lateralization of auditory evoked potentials has been found in patients with temporal lobe epilepsy, showing significant reduction in amplitude over the left hemisphere [36]. The auditory pathway ends at the temporal lobe, and

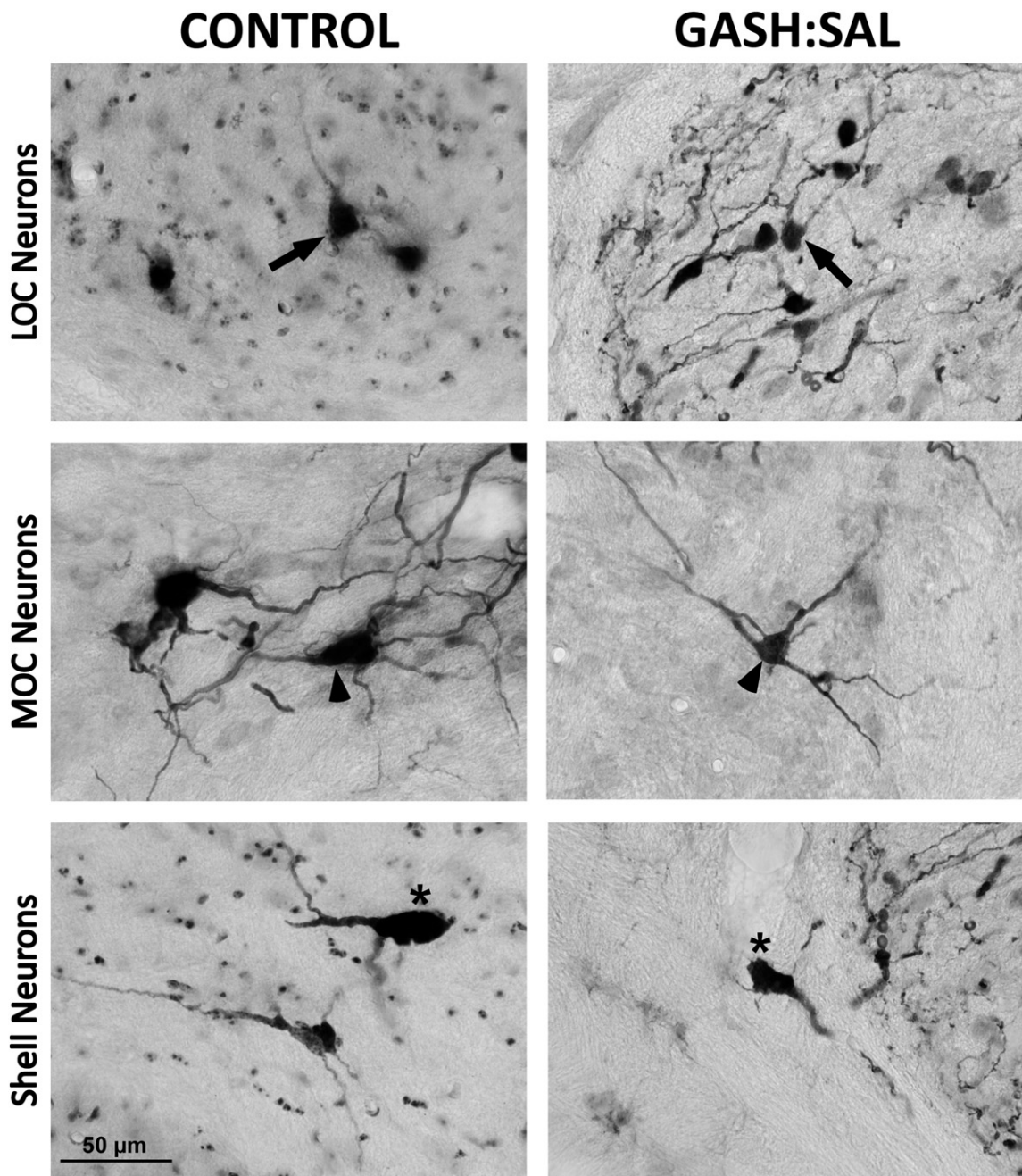


Fig. 8. Olivocochlear immunolabeled neurons after Fluoro-Gold injection into the left cochlea. LOC, MOC, and shell neurons are shown from upper to bottom panels, respectively. Notice that LOC neurons (denoted with arrows), MOC neurons (denoted with arrowheads), and shell neurons (denoted with asterisks) in the GASH:Sal (right panel) are smaller than in the control hamster (left panel). All microphotographs display the same magnification. Scale bar = 50 μ m. MOC, medial olivocochlear; LOC, lateral olivocochlear.

Table 1

Average number and percentage of olivocochlear neurons labeled with Fluoro-Gold in the control and GASH:Sal hamsters. Notice the difference in percentage of olivocochlear neurons based on the ipsi- vs. contralateral location.

	Control		GASH:Sal	
	n	%	n	%
Ipsi LOC	369	59.97%	294.33	53.03%
Ipsi Shell	27.67	4.5%	21.67	3.9%
Ipsi MOC	29.67	4.82%	45.67	8.23%
Contra LOC	44	7.15%	20.33	3.66%
Contra Shell	6	0.98%	3.33	0.6%
Contra MOC	139	22.59%	169.67	30.57%
Total	615.33	100	555	100

hence, patients with temporal lobe epilepsy had more deficits in auditory processing than those without cortical damage [37]. These asymmetrical hearing alterations are thought to be caused by the seizures that impair the anatomical and functional integrity of the auditory brainstem pathway [37]. Our ABR and DPOAE results indicated that the GASH:Sal also exhibited an asymmetrical hearing alteration, even though the GASH:Sal hamsters were naïve without having suffered epileptic seizures. Thus, our data suggest that the GASH:Sal has innate functional alterations in the olivocochlear efferent system that impair its auditory sensitivity, making it particularly susceptible to audiogenic seizures. The fact that we found an absence of DPOAEs in both ears is consistent with an altered medial olivocochlear function in the GASH:Sal. The medial olivocochlear system reduces the gain of the cochlear amplifier

through reflexive activation by sound, and the DPOAE test is used as an indicator of the status of the medial olivocochlear efferent system [31, 38]. Since the GASH:Sal exhibited an absence of the DPOAEs, the medial olivocochlear efferent system is not able to turn down the cochlear response to sound, and as a result, this might contribute to trigger audiogenic seizures. However, it could be argued that the deficits observed in the ABRs and DPOAEs of the GASH:Sal were caused by the anesthetic. The anesthetic used in our study was ketamine-xylazine that produced an adequate level of anesthesia without tissue damage and has been commonly used in rodents to assess the integrity of the auditory brainstem, without alterations on ABRs or DPOAEs [39–41]. Furthermore, and more importantly, our study demonstrated changes in the anatomy of the olivocochlear efferent system, including the organ of Corti and olivocochlear neurons, which correlated with the alterations shown in the ABRs and DPOAEs of the GASH:Sal.

4.2. Morphological alterations in the olivocochlear efferent system of the GASH:Sal

One of the main goals of the present study was to determine whether the functional alterations observed in the peripheral auditory activity of the GASH:Sal have their corresponding anatomical correlations. A considerable number of studies used ABR and DPOAE tests to assess damage in the cochlea and in the brainstem auditory pathway, as well as an indicator of OHC function and the status of the olivocochlear efferent system [42–44]. To further explore our ABR and DPOAE results in the GASH:Sal, we performed a morphological study of the efferent olivocochlear system using a multi-technical approach that included a scanning electron microscopic analysis of the organ of Corti, a morphometric analysis of the olivocochlear neurons, and a 3D reconstruction of the LSO. At the cochlear level, our electron microscopy results showed that the stereociliary organization of the cochlear hair cells in the GASH:Sal was drastically impaired when compared with that in the control hamsters. The distorted pattern of the IHC stereocilia might correlate with high ABR thresholds observed in the GASH:Sal. Furthermore, the GASH:Sal exhibited deficits in the organization of the OHC stereocilia from basal to apical cochlear turns, which is consistent with the absence of DPOAEs over a wide frequency range. At the auditory brainstem level, the morphometric analysis of olivocochlear neurons in the GASH:Sal revealed a significant reduction in cell body size compared with that in the control hamsters. This morphometric analysis was carried out in retrogradely labeled neurons after injections of FG into the cochlea. Consistently with previous track-tracing studies in rodents [21,44,45], our injections generated retrograde labeling of the three types of olivocochlear neurons: LOC, MOC, and shell neurons. We also obtained a distribution pattern of olivocochlear neurons at the ipsilateral and contralateral levels, in the GASH:Sal and control hamsters, which was similar to that reported in other rodents [21, 46–49]. In our material, the total number of olivocochlear neurons in the control and GASH:Sal hamsters was higher than that obtained in our previous study using FG injections into the hamster's cochlea [21]. In fact, our quantification was very similar to that obtained in the mouse [47]. This rather unexpected result might be explained by the differences in the injection procedure that leads to different efficiencies in the neuronal tracer uptake. Despite this difference in the total number of labeled neurons, the percentage of labeled neurons in the LSO and VNTB was very similar in both studies (our results; [21]). Interestingly, one would expect to find a reduction in the number of MOC neurons in the GASH:Sal compared with that in the controls, based on the DPOAE alterations of the GASH:Sal. However, we observed a tendency towards a reduction in the number of labeled olivocochlear neurons in the GASH:Sal that was not statistically significant when compared with that in the controls. This might be explained because deficits in ABRs and DPOAEs do not necessarily involve degeneration of olivocochlear neurons. Supporting this argument, a recent study using

ABR and DPOAE tests combined with FG injections in the cochlea indicated that, in acoustic trauma, LOC and MOC neurons remain intact despite hair cell dysfunction [44]. Our statistical comparative analysis of the soma area indicated that the MOC, LOC, and shell neurons of the ipsilateral side were significantly smaller in the GASH:Sal than in controls, as well as MOC neurons of the contralateral side. These results might be related to the asymmetrical hearing alteration found in our ABR and DPOAE results in the GASH:Sal. Although LOC and shell neurons of the contralateral side were also smaller in the GASH:Sal, we obtained no significant differences compared with those in controls. This lack of significant difference might be explained by the few LOC and shell neurons that were contralaterally labeled with FG, due to the fact that the lateral olivocochlear projection is predominantly ipsilateral [21]. To verify whether the neural size affected the size of the nucleus, we carried out a 3D reconstruction analysis of the LSO as a representative example. Our results confirmed that the area and volume of the LSO were significantly smaller in the GASH:Sal than in the control hamster. Supporting this, a previous study in other neuronal structures has also found that shrinkage of neurons contributes to the reduction of the nucleus' volume [50]. Further experiments are necessary to verify this reduction in the VNTB and to assess whether the differences in neuropil (dendrites and afferent and efferent axons) also contribute to the reduction of the LSO volume in the GASH:Sal. The LSO and VNTB send ascending inputs to the IC [51,52], which in turn, sends to a much lesser extent descending inputs to the LSO and VNTB [27,53]. Since the IC is a key structure in the initiation of audiogenic seizures [54–56], deficits in these reciprocal connections might contribute to the epileptogenesis in the IC of the GASH:Sal. Also, the descending olivocochlear pathway is influenced from higher auditory nuclei that adapt hearing function according to cortical analysis of the ascending auditory input [57]. Thus, alterations in the olivocochlear efferent system of the GASH:Sal might be due to malfunctioning of the feedback from higher auditory nuclei. One of the most intriguing questions regarding the epileptogenic process in the GASH:Sal is whether the seizures induced the morphological changes in the auditory system or, conversely, morphological alterations underlie the susceptibility of the GASH:Sal to audiogenic seizure. In our study, the GASH:Sal animals were nonstimulated and did not suffer any epileptic seizure. Therefore, the morphological alterations of the olivocochlear efferent system in the GASH:Sal are innate components of this animal model, and hence, it can be inferred that such alterations have genetic origin. The audiogenic seizure pathology in the GASH:Sal model is a form of reflex epilepsy, manifested as generalized tonic-clonic seizures after external acoustic stimulation [1,3,5]. In humans, the pathogenesis underlying acoustic reflex epilepsies is not clear, whether the seizure susceptibility originates in the central or peripheral auditory system. Our study provides important information with this respect and supports the GASH:Sal as a valuable animal model to investigate the links between the morphological alterations and the seizures, as well as for better understanding the cause of acoustic hypersensitivity.

5. Conclusions

The olivocochlear efferent system of the GASH:Sal has functional and morphological alterations. The GASH:Sal exhibited high ABR thresholds as well as an absence of DPOAEs in a wide range of frequencies and a clear lateralization in auditory brainstem processing. Since this left-right auditory asymmetry was not present in control hamsters, it might be a distinct auditory feature of the GASH:Sal.

Morphological alterations in the olivocochlear efferent system of the GASH:Sal were observed from the cochlear receptor to the SOC. At the cochlear level, there is a derangement and distortion of the cochlear stereocilia from basal to apical cochlear turns of the GASH:Sal that were not observed in the control hamster. At the brainstem level, the olivocochlear neurons, including MOC, LOC, and shell

neurons, have reduced soma areas compared with those of control animals. This neuron shrinkage contributes to the reduction of the LSO volume as shown in the 3D reconstruction analysis. The functional

alterations of the peripheral auditory activity were positively correlated with the morphological alterations of the olivocochlear efferent system.

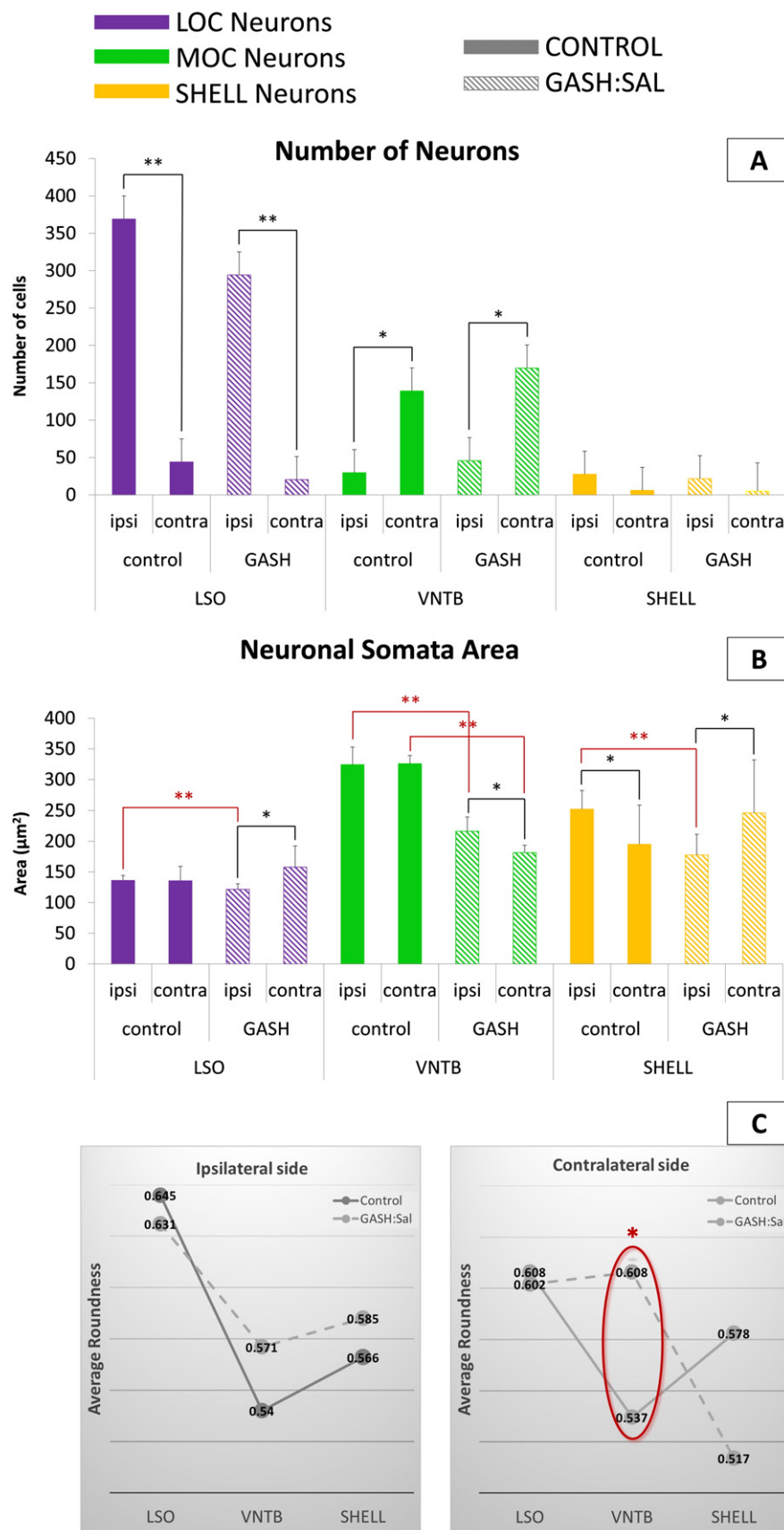


Table 2

Neuronal somata areas (in μm^2) of the three types of olivocochlear neurons (LOC, MOC, shell) in control and GASH:Sal hamsters.

	LOC		MOC		Shell	
	Ipsi-	Contra-	Ipsi-	Contra-	Ipsi-	Contra-
Control	136,079	135,476	324.21	325.78	252,354	195,112
GASH:Sal	121,632**	157,711	216,366**	181,588**	177,801**	246,367

** Significant difference with respect to control p value < 0.01 .

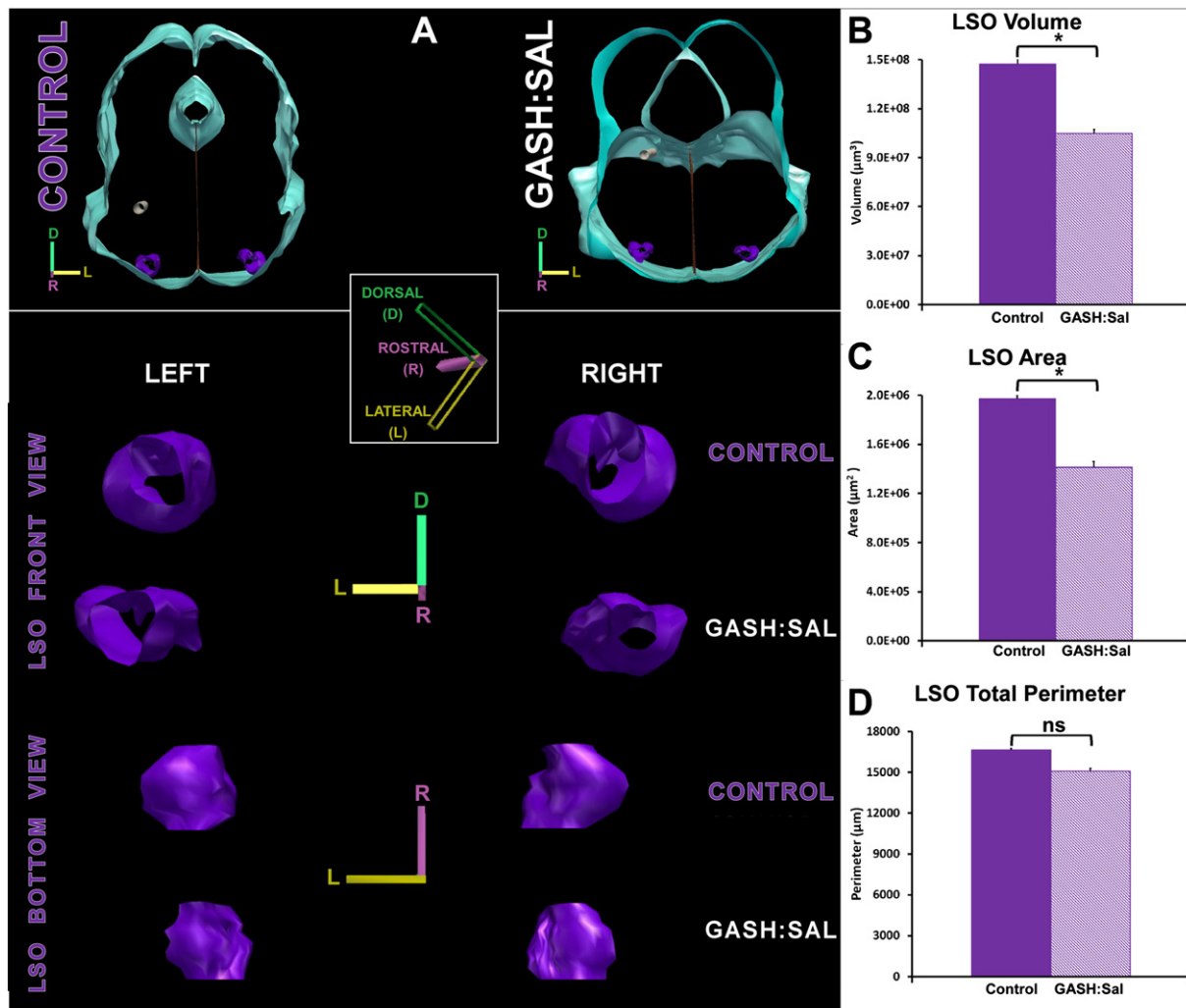


Fig. 10. Differences in the size of the lateral superior olive (LSO) between the control and GASH:Sal hamsters. A. 3D reconstruction of the LSO in the control and GASH:Sal hamsters. The upper panel shows the reconstruction of brainstem sections in which the LSO was found. The lower panel shows different views of the 3D reconstruction (front and bottom views) in the control and GASH:Sal hamsters. Each scale bar represents 500 μm . B–D. Histograms show the LSO volume (B), area (C), and perimeter (D) in the control and GASH:Sal hamsters. ** = p value ≤ 0.05 ; ns = nonsignificant.

The functional and morphological alterations in the olivocochlear efferent system are intrinsic and innate components of the GASH:Sal and might impair its auditory sensitivity, making them particularly susceptible to audiogenic seizures.

Acknowledgments

This study was supported by the Spanish JCyL (#SA023A12-2), the University of Salamanca Research grant to (GIR 2016-184092), and

Fig. 9. Morphometric analysis of the labeled olivocochlear neurons after Fluoro-Gold injection into the left cochlea. A. Histogram shows the number of olivocochlear neurons in the ipsi- and contralateral sides of control and GASH:Sal hamsters. B. Histogram shows the neuronal soma areas in the ipsi- and contralateral sides of control and GASH:Sal hamsters. For histograms A and B, LOC neurons are displayed in purple, MOC neurons in green, and shell neurons in yellow. Solid histogram bars are used for control hamsters and striped histogram bars for GASH:Sal. ** = p value ≤ 0.05 and *** = p value ≤ 0.01 . Black lines have been used for comparison between ipsi- and contralateral sides whereas red lines have been used for comparison between control and GASH:Sal hamsters. C. Plots show the soma roundness of olivocochlear neurons in the ipsi- (left plot) and contralateral sides (right plot) of control (solid line) and GASH:Sal (dashed line) hamsters. Notice that the roundness of MOC neurons of the VNTB was significantly different between the control and GASH:Sal hamsters (red oval). ** = p value ≤ 0.05 . LOC, lateral olivocochlear; LSO, lateral superior olive; MOC, medial olivocochlear; VNTB, ventral nucleus of the trapezoid body.

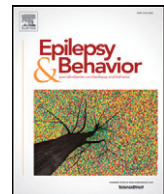
the University of São Paulo (USP)/University of Salamanca (USAL) Program for the Promotion of the Bilateral Cooperation in the Field of Research (#2011.1.23386.1.3; #2011.1.23386.1.3). Other financial support: FAPESP (#2007/50261-4), FAPESP-Cinapce (#2005/56447-7), CNPq, and CAPES-PROEX.

Conflict of interest

The authors certify that they have no affiliations with or involvement in any organization or entity with any financial interest (such as honoraria, educational grants, participation in speakers' bureaus, membership, employment, consultancies, stock ownership, or other equity interest or expert testimony or patent-licensing arrangements) or non-financial interest (such as personal or professional relationships, affiliations, knowledge, or beliefs) in the subject matter or materials discussed in this manuscript.

References

- [1] Muñoz de la Pascua L, López-García DE. In: Muñoz L, editor. Establecimiento y caracterización de una línea de hamsters sirios propensos a padecer convulsiones audiogénicas; 2004 [ISBN 13: 978-84-609-5027-1].
- [2] Prieto-Martín AI, Llorens S, Pardal-Fernández JM, Muñoz LJ, López DE, Escribano J, et al. Opposite caudal versus rostral brain nitric oxide synthase response to generalized seizures in a novel rodent model of reflex epilepsy. *Life Sci* 2012;90(13–14): 531–7.
- [3] Carballosa-Gonzalez MM, Muñoz LJ, López-Alburquerque T, Pardal-Fernández JM, Nava E, de Cabo C, et al. EEG characterization of audiogenic seizures in the hamster strain GASH:Sal. *Epilepsy Res* 2013;106(3):318–25.
- [4] Muñoz LJ, Carballosa-Gautam MM, Yanowsky K, García-Atarés N, López DE. The genetic audiogenic seizure hamster from Salamanca: The GASH:Sal. *Epilepsy Behav* 2017;71:181–92.
- [5] Barrera-Bailón B, Oliveira JA, López DE, Muñoz LJ, García-Cairasco N, Sancho C. Pharmacological and neuroethological studies of three antiepileptic drugs in the genetic audiogenic seizure hamster (GASH:Sal). *Epilepsy Behav* 2013;28(3):413–25.
- [6] Sancho C, Barrera-Bailón B, Oliveira JAC, López DE, Muñoz LJ, García-Cairasco N. Pharmacological validation of the genetic audiogenic seizure hamster (GASH:Sal) using several antiepileptics. *Epilepsy Behav* 2013;28(3):413–25.
- [7] Faingold CL. The role of the brain stem in generalized epileptic seizures. *Metab Brain Dis* 1987;2(2):81–112.
- [8] Moraes MF, García-Cairasco N. Real time mapping of rat midbrain neural circuitry using auditory evoked potentials. *Hear Res* 2001;161(1–2):35–44.
- [9] Kandratavicius L, Balista PA, Lopes-Aguiar C, Ruggiero RN, Umeoka EH, García-Cairasco N, et al. Animal models of epilepsy: use and limitations. *Neuropsychiatr Dis Treat* 2014;10:1693–705.
- [10] Racine RJ. Modification of seizure activity by electrical stimulation. *Electroencephalogr Clin Neurophysiol* 1972;32:281–7.
- [11] García-Cairasco N, Terra VC, Doretto MC. Midbrain substrates of audiogenic seizures in rats. *Behav Brain Res* 1993;58(1–2):57–67.
- [12] García-Cairasco N, Doretto MC, Ramalho MJ, Antunes-Rodrigues J, Nonaka KO. Audiogenic and audiogenic-like seizures: locus of induction and seizure severity determine postictal prolactin patterns. *Pharmacol Biochem Behav* 1996;53(3): 503–10.
- [13] Faingold CL. Neuronal networks in the genetically epilepsy-prone rat. *Adv Neurol* 1999;79:311–21.
- [14] Warr WB. Organization of olivocochlear efferent systems in mammals. In: Webster DB, Popper AN, Fay RR, editors. *The mammalian auditory pathway: neuroanatomy*. New York: Springer; 1992. p. 410–48.
- [15] Mulders WH, Robertson D. Morphological relationships of peptidergic and noradrenergic nerve terminals to olivocochlear neurons in the rat. *Hear Res* 2000; 144(1–2):53–64.
- [16] Xiao Z, Suga N. Modulation of cochlear hair cells by the auditory cortex in the mustached bat. *Nat Neurosci* 2002;5(1):57–63.
- [17] Mulders WH, Robertson D. Effects on cochlear responses of activation of descending pathways from the inferior colliculus. *Hear Res* 2000;149(1–2):11–23.
- [18] Dewson JH. Efferent olivocochlear bundle: some relationships to stimulus discrimination in noise. *J Neurophysiol* 1968;31:122–30.
- [19] Oatman LC, Anderson BW. Effects of visual attention on tone burst evoked auditory potentials. *Exp Neurol* 1977;57:200–11.
- [20] Scharf B, Magnan J, Chays A. On the role of the olivocochlear bundle in hearing: 16 case studies. *Hear Res* 1997;103(1–2):101–22.
- [21] Sánchez-González MA, Warr WB, López DE. Anatomy of olivocochlear neurons in the hamster studied with FluoroGold. *Hear Res* 2003;185(1–2):65–76.
- [22] Guinan Jr JJ. Physiology of olivocochlear efferents. In: Dallos P, Popper AN, Fay RR, editors. *The cochlea*. New York: Springer; 1996. p. 435–502.
- [23] Le Prell CG, Bledsoe Jr SC, Bobbin RP, Puel JL. Neurotransmission in the inner ear: functional and molecular analysis. In: Santos-Sacchi J, Jahn AF, editors. *Physiology of the ear*. New York: Singular Publishing; 2001. p. 575–611.
- [24] Glowatzki E, Fuchs PA. Cholinergic synaptic inhibition of inner hair cells in the neonatal mammalian cochlea. *Science* 2000;288(5475):2366–8.
- [25] Puel JL, Ruel J, Guitton M, Wang J, Pujol R. The inner hair cell synaptic complex: physiology, pharmacology and new therapeutic strategies. *Audiol Neurotol* 2002; 7(1):49–54.
- [26] De Freitas MR, Figueiredo AA, Brito GA, Leitao RF, Carvalho Junior JV, Gomes Junior RM, et al. The role of apoptosis in cisplatin-induced ototoxicity in rats. *Braz J Otorhinolaryngol* 2009;75(5):745–52.
- [27] Gómez-Nieto R, Rubio ME, López DE. Cholinergic input from the ventral nucleus of the trapezoid body to cochlear root neurons in rats. *J Comp Neurol* 2008;506(3): 452–68.
- [28] Hormigo S, Gómez-Nieto R, Castellano O, Herrero-Turrión MJ, López DE, de Anchieto de Castro e Horta-Júnior J. The noradrenergic projection from the locus coeruleus to the cochlear root neurons in rats. *Brain Struct Funct* 2015;220(3):1477–96.
- [29] Warr WB, Guinan Jr JJ. Efferent innervation of the organ of corti: two separate systems. *Brain Res Sep 7* 1979;173(1):152–5.
- [30] Liberman MC, Puria S, Guinan Jr JJ. The ipsilaterally evoked olivocochlear reflex causes rapid adaptation of the 2f1–f2 distortion product otoacoustic emission. *J Acoust Soc Am* 1996;99(6):3572–84.
- [31] Puria S, Guinan Jr JJ, Liberman MC. Olivocochlear reflex assays: effects of contralateral sound on compound action potentials versus ear-canal distortion products. *J Acoust Soc Am* 1996;99(1):500–7.
- [32] Church MW, Kaltenbach JA. The hamster's auditory brain stem response as a function of stimulus intensity, tone burst frequency, and hearing loss. *Ear Hear* 1993; 14(4):249–57.
- [33] Heffner HE, Harrington IA. Tinnitus in hamsters following exposure to intense sound. *Hear Res* 2002;170(1–2):83–95.
- [34] Larsen E, Liberman MC. Contralateral cochlear effects of ipsilateral damage: no evidence for interaural coupling. *Hear Res* 2010;260(1–2):70–80.
- [35] Khalifa S, Collet L. Functional asymmetry of medial olivocochlear system in humans. Towards a peripheral auditory lateralization. *Neuroreport* 1996;7(5):993–6.
- [36] Brodtkorb E, Steinlein OK, Sand T. Asymmetry of long-latency auditory evoked potentials in LGI1-related autosomal dominant lateral temporal lobe epilepsy. *Epilepsia* 2005;46(10):1692–4.
- [37] Meneguello J, Leonhardt FD, Pereira LD. Auditory processing in patients with temporal lobe epilepsy. *Braz J Otorhinolaryngol* 2006;72(4):496–504.
- [38] Cooper NP, Guinan Jr JJ. Efferent-mediated control of basilar membrane motion. *J Physiol* 2006;576(Pt 1):49–54.
- [39] Payton AJ, Forsythe DB, Dixon D, Myers PH, Clark JA, Snipe JR. Evaluation of ketamine–xyazine in Syrian hamsters. *Cornell Vet* 1993;83(2):153–61.
- [40] Coomber B, Berger JJ, Kowalski VL, Shackleton TM, Palmer AR, Wallace MN. Neural changes accompanying tinnitus following unilateral acoustic trauma in the guinea pig. *Eur J Neurosci* 2014;40(2):2427–41.
- [41] Ruebhausen MR, Brozoski TJ, Bauer CA. A comparison of the effects of isoflurane and ketamine anesthesia on auditory brainstem response (ABR) thresholds in rats. *Hear Res* 2012;287(1–2):25–9.
- [42] Izquierdo MA, Gutierrez-Conde PM, Merchan MA, Malmierca MS. Non-plastic reorganization of frequency coding in the inferior colliculus of the rat following noise-induced hearing loss. *Neuroscience* 2008;154:355–69.
- [43] Charizopoulou N, Lelli A, Schraders M, Ray K, Hildebrand MS, Ramesh A, et al. Gipc3 mutations associated with audiogenic seizures and sensorineural hearing loss in mouse and human. *Nat Commun* 2011;2:201.
- [44] Reuss S, Closhen C, Riemann R, Jaumann M, Knipper M, Rüttiger L. Absence of early neuronal death in the olivocochlear system following acoustic overstimulation. *Anat Rec (Hoboken)* 2016;299(1):103–10.
- [45] Vetter DE, Mugnaini E. Distribution and dendritic features of three groups of rat olivocochlear neurons. A study with two retrograde cholera toxin tracers. *Anat Embryol (Berl)* 1992;185(1):1–16.
- [46] White JS, Warr WB. The dual origins of the olivocochlear bundle in the albino rat. *J Comp Neurol* 1983;219(2):203–14.
- [47] Campbell JP, Henson MM. Olivocochlear neurons in the brainstem of the mouse. *Hear Res* 1988;35(2–3):271–4.
- [48] Warr WB, Boche JB, Neely ST. Efferent innervation of the inner hair cell region: origins and terminations of two lateral olivocochlear systems. *Hear Res* 1997; 108(1–2):89–111.
- [49] Brown MC, Levine JL. Dendrites of medial olivocochlear neurons in mouse. *Neuroscience* 2008;154(1):147–59.
- [50] Loftus M, Knight RT, Amaral DG. An analysis of atrophy in the medial mammillary nucleus following hippocampal and fornix lesions in humans and nonhuman primates. *Exp Neurol* 2000;163(1):180–90.
- [51] Oliver DL. Ascending efferent projections of the superior olive complex. *Microsc Res Tech* 2000;51(4):355–63.
- [52] Warr WB, Beck JE. Multiple projections from the ventral nucleus of the trapezoid body in the rat. *Hear Res* 1996;93(1–2):83–101.
- [53] Faye-Lund H. Projection from the inferior colliculus to the superior olive complex in the albino rat. *Anat Embryol (Berl)* 1986;175(1):35–52.
- [54] García-Cairasco N, Sabbatini RM. Possible interaction between the inferior colliculus and the substantia nigra in audiogenic seizures in Wistar rats. *Physiol Behav* 1991; 50(2):421–7.
- [55] Kesner RP. Subcortical mechanisms of audiogenic seizures. *Exp Neurol* 1966;15(2): 192–205.
- [56] Wada JA, Terao A, Scholtmeyer H, Trapp WG. Reversible audiogenic seizure susceptibility induced by hyperbaric oxygenation. *Exp Neurol* 1970;29(3):400–4.
- [57] Khalifa S, Bougeard R, Morand N, Veillet E, Isnard J, Guenot M, et al. Evidence of peripheral auditory activity modulation by the auditory cortex in humans. *Neuroscience* 2001;104(2):347–58.



Overexpression of the immediate-early genes Egr1, Egr2, and Egr3 in two strains of rodents susceptible to audiogenic seizures



D. López-López ^{a,b}, R. Gómez-Nieto ^{a,b,c}, M.J. Herrero-Turrión ^a, N. García-Cairasco ^d, D. Sánchez-Benito ^{a,b}, M.D. Ludeña ^c, D.E. López ^{a,b,c,*}

^a Institute for Neuroscience of Castilla y León (INCYL), University of Salamanca, Salamanca, Spain

^b Salamanca Institute for Biomedical Research (IBSAL), Spain

^c Department of Cell Biology and Pathology, School of Medicine, University of Salamanca, Salamanca, Spain

^d Physiology Department, Ribeirão Preto School of Medicine, University of São Paulo, Ribeirão Preto, Brazil

ARTICLE INFO

Article history:

Revised 10 December 2015

Accepted 12 December 2015

Available online 14 January 2016

Keywords:

Audiogenic epilepsy

Early growth response

GASH:Sal

Seizure-induced transcriptome

Microarray

WAR

ABSTRACT

Genetic animal models of epilepsy are an important tool for further understanding the basic cellular mechanisms underlying epileptogenesis and for developing novel antiepileptic drugs. We conducted a comparative study of gene expression in the inferior colliculus, a nucleus that triggers audiogenic seizures, using two animal models, the Wistar audiogenic rat (WAR) and the genetic audiogenic seizure hamster (GASH:Sal). For this purpose, both models were exposed to high intensity auditory stimulation, and 60 min later, the inferior colliculi were collected. As controls, intact Wistar rats and Syrian hamsters were subjected to stimulation and tissue preparation protocols identical to those performed on the experimental animals. Ribonucleic acid was isolated, and microarray analysis comparing the stimulated Wistar and WAR rats showed that the genomic profile of these animals displayed significant (fold change, $|FC| \geq 2.0$ and $p < 0.05$) upregulation of 38 genes and downregulation of 47 genes. Comparison of gene expression profiles between stimulated control hamsters and stimulated GASH:Sal revealed the upregulation of 10 genes and the downregulation of 5 genes.

Among the common genes that were altered in both models, we identified the zinc finger immediate-early growth response gene *Egr3*. The *Egr3* protein is a transcription factor that is induced by distinct stress-elicited factors. Based on immunohistochemistry, this protein was expressed in the cochlear nucleus complex, the inferior colliculus, and the hippocampus of both animal models as well as in lymphoma tumors of the GASH:Sal. Our results support that the overexpression of the *Egr3* gene in both models might contribute to neuronal viability and development of lymphoma in response to stress associated with audiogenic seizures.

This article is part of a Special Issue entitled "Genetic and Reflex Epilepsies, Audiogenic Seizures and Strains: From Experimental Models to the Clinic".

© 2015 Elsevier Inc. All rights reserved.

1. Introduction

Epilepsy is a complex neurological disorder in terms of both its etiology and its cognitive, behavioral, electrophysiological, molecular, and cellular pathology [1–3]. Although enormous progress has been made in understanding the etiology of epilepsy, the current knowledge is very limited. The complexity of this neurological disorder requires intense interdisciplinary research. Thus, at the moment, a variety of models are available for exploring different aspects of epilepsy such as *in silico* [4], *in vivo* [5], and *in vitro* [6].

Some *in vivo* models represent the natural association between genetic predisposition and external events that trigger seizures [7]. Among the most used and well-characterized *in vivo* genetic models of epilepsy are audiogenic seizures, which are triggered by high intensity acoustic stimulation. The substantial characterization of their neural substrates, as well as their behavioral, cellular, and molecular alterations, combined with pharmacologically- or electrically-induced seizures, potentiates their usefulness in the elucidation of epileptogenesis and preclinical development of new antiepileptic drugs [8,9].

The present study focused on two animal strains that are categorized as audiogenic seizure models, the Wistar audiogenic rat (WAR) and the genetic audiogenic seizure hamster (GASH:Sal).

The WAR is a genetically selected strain susceptible to audiogenic seizures that was inbred at the School of Medicine of Ribeirão Preto (Brazil) beginning in 1990. This strain is a model of audiogenic idiopathic epilepsy that develops tonic–clonic generalized seizures [10,11].

* Corresponding author at: Institute for Neuroscience of Castilla y León (INCYL), Laboratory 12, C/Pintor Fernando Gallego 1, 37007 Salamanca, Spain. Tel.: +34 923294400x1868.

E-mail address: lopezde@usal.es (D.E. López).

The GASH:Sal, a hamster strain developed at the University of Salamanca, exhibits genetic audiogenic epilepsy similar to human tonic-clonic seizures [12]. The GASH:Sal shows an autosomal recessive inheritance for susceptibility to audiogenic seizures, which manifests more severely in young animals; the seizure severity progressively declines with age [13].

Similar to other animal models of audiogenic seizures [14–16], those with brainstem origin occur as a result of intense auditory stimulation [13,17]. Activation of auditory pathways is crucial for expression of the audiogenic seizure phenotype, and the inferior colliculus, in the auditory midbrain, plays a key role in its initiation [15,16]. Thus, bilateral lesions in the central nucleus of the IC permanently block audiogenic seizures [14,18–20], and lesions in the dorsal and external cortices of the IC partially attenuate the audiogenic seizures [14,21].

To find common molecular processes between these two models of audiogenic seizures, we have conducted a comparative analysis of the profiles of gene expression in the inferior colliculus (IC), a nucleus that triggers audiogenic seizures. Of all the possible comparisons, we have selected stimulated controls for comparison with the stimulated audiogenic strains, either GASH:Sal or WAR, to avoid bias related to sound-induced gene expression. Some of the deregulated genes detected via microarray analysis were validated by quantitative reverse transcription real-time PCR (RT-qPCR).

The present study might contribute toward understanding basic mechanisms associating genetic predisposition to epilepsy, early gene expression after seizures, and the recognition of new targets that could be consequently tested in the development of antiepileptic drugs.

Briefly, our results are important for the identification, in this particular case, of early genes induced by seizures and suggest molecular processes with potential implications for human epilepsy.

2. Material and methods

2.1. Experimental animals

A total of 51 animals were used in this study according to the following distribution: 17 male WAR and 6 male control rats (*Rattus norvegicus*, Wistar albino, Charles River Laboratories) at 12 weeks of age and a body weight of approximately 230 g. In the case of the hamsters, we used 12 control Syrian hamsters (*Mesocricetus auratus*) and 16 GASH:Sal at 16 weeks of age, weighing approximately 60 g. The WAR and GASH:Sal animals did not suffer any audiogenic seizure prior to the experiments. All animals were free of ear infection. To rapidly confirm normal hearing, we used the bilateral finger friction test in all cases.

The animals were exposed to auditory stimulation within an acrylic cylinder. The acoustic stimulus was recorded using a high-pass filter (>500 Hz; microphone Brüel & Kjaer #4134 and preamplifier Brüel & Kjaer #2619), digitized above 4 kHz, and reproduced by a computer coupled to an amplifier (Fonestar MA-25T, Revilla de Camargo, Spain) and a tweeter (Beyma T2010, Valencia, Spain) in the upper portion of the arena. The delivered sound was a semirandom acoustic stimulus of 0–18 kHz with an intensity of 115 to 120 dB. For more information see [10,22]. Sixty minutes after the seizures, we harvested the IC for all gene expression analyses. As controls, normal Wistar rats and Syrian hamsters were exposed to the same stimulation according to the identical procedure.

For each gene microarray (Rat Gene 1.0 ST & Microarray MoGene 1.0 ST), the rats or hamsters were randomly divided into four groups, and we used the right and left inferior colliculi from each animal (Table 1). For the transcriptomic analyses, we compared only stimulated Syrian hamsters and stimulated GASH:Sal, using four animals of each strain. For RT-qPCR, 3 to 8 of the replicates from each group were randomly selected and performed in triplicate on two separate occasions for each gene product examined.

Table 1

Number of animals used in this study in the different experimental approaches.

N	Microarray Rat Gene 1.0 ST	RT-qPCR	Histology
Wistar rat	4	3	N/A
Stimulated Wistar rat	3	3	N/A
WAR	6	6	2
Stimulated WAR	7	6	2

N	Microarray MoGene 1.0 ST	RT-qPCR	Histology	Transcriptome
Syrian hamster	6	3 (6 I.C.)	N/A	N/A
Stimulated Syrian hamster	6	3 (6 I.C.)	N/A	4 (7 I.C.)
GASH:Sal	6	4 (8 I.C.)	2	N/A
Stimulated GASH:Sal	6	3 (6 I.C.)	2	4 (8 I.C.)

2.2. Ethics statement

All procedures and experimental protocols were performed according to the guidelines of the European Community's Council Directive (2010/63/CE) and Brazilian legislation for the care and use of laboratory animals.

The experiments were performed at both the Neuroscience Institute of Castilla y León at the University of Salamanca and the Ribeirão Preto School of Medicine at the University of São Paulo, with the approval of the Animal Care and Ethics Committees of those institutions.

2.3. Tissue sampling

After anesthetizing the animals with an overdose of sodium pentobarbital, the IC was isolated, surgically removed, and placed in TRIzol® (Gibco BRL, Gaithersburg, MD, USA) for transcription analysis. For immunohistological studies, the protocols used for tissue preparation, including perfusion of the animals, brain dissection, and tissue slicing, were identical to those used elsewhere [23,24].

2.4. RNA isolation

Total RNA was purified using TRIzol®, followed by further RNA purification using an RNeasy Mini Kit for RNA cleanup (Qiagen Sciences, Germantown, Maryland, USA). Ribonucleic acid quantity and quality were then assessed using an Agilent 2100 Bioanalyzer (Agilent Technologies, Palo Alto, CA, USA) to test the integrity of the 18S and 28S ribosomal RNA (rRNA) bands, and samples displaying an RNA integrity number (RIN) > 8.0 were used.

2.5. Microarray hybridization data analysis: normalization, differential gene expression, and ontological analysis

Microarray analysis was performed at the Cancer Research Center of Salamanca according to standard procedures. Labeling and hybridization were performed according to protocols from Affymetrix. Briefly, 100–300 ng of total RNA was amplified and labeled using the WT Sense Target labeling and control reagents kit (Affymetrix Inc., Santa Clara, CA, USA) and was then hybridized to rat (Gene 1.0 ST Array) or mouse (GeneChip® Mouse Gene ST Array) microarrays, as appropriate. Washing and scanning were performed using the Affymetrix GeneChip system (GeneChip Hybridization Oven 640, GeneChip Fluidics Station 450, and GeneChip Scanner 7G).

Following image analysis, the microarray data were imported into GeneSpring GX7.3 (Agilent Technologies). The robust multiarray analysis (RMA) algorithm [25] was used for background correction and normalization of fluorescent hybridization signals of the microarrays at both the internal (intramicroarrays) and the comparative (intermicroarrays) levels. This algorithm was selected over other

available algorithms such as the MAS5 or MBEI [26] because it was deemed to provide the best precision in signal detection to achieve adequate multiple-chip normalization [27], especially in cases of low-level gene expression [25,28,29], by producing efficient quantile normalization of the distribution of probe intensities from each array in the context of a complete set of arrays.

We used Bioconductor and R as computational tools (www.bioconductor.org) to apply RMA to the dataset of microarray hybridizations including 3 to 6 different biological replicates corresponding to each of the experimental groups in the study (Wistar rat or Syrian hamster control, stimulated Wistar rat or Syrian hamster, WAR or GASH:Sal control, and stimulated WAR or GASH:Sal).

After quantitation of the expression level of each probe set in all analyzed Rat Gene 1.0 ST microarrays, the significance analysis of microarrays (SAM) algorithm [30] was used to identify probe sets displaying significant differential expression when comparing the experimental samples to their controls. This algorithm performs statistical discrimination analysis using permutations to check the stability of variables fulfilling the 'alternative hypothesis'. This method calculates the type I error, or the number of expected false positives, by calculating the false discovery rate (FDR) [31]. In this report, genes displaying an FDR of 6% or less were considered as significant. We selected the genes that vary in a range (fold change, $|FC| \geq 2$) among other genes and used different databases to determine their function.

In the case of the MoGene 1.0 ST microarrays, we compared the experimental groups corresponding to the stimulated hamster control and the stimulated GASH:Sal; all of our samples passed a stringent data quality control test and showed high intragroup homogeneity [32].

Potential differential expression was determined via one-way analysis of variance (ANOVA) (variances not assumed to be equal). Subsequently, an unpaired *t*-test ($p < 0.05$, filtered at 1.5 fold) was performed to search for the genes exhibiting differential expression (the levels in the control samples were considered as the basal levels) [32].

The data obtained and discussed in this publication have been deposited in the NCBI's Gene Expression Omnibus [33] at GEO Series accession numbers GSE74150 (<http://www.ncbi.nlm.nih.gov/geo/query/acc.cgi?acc=GSE74150>) for the WAR arrays and GSE74043 (<http://www.ncbi.nlm.nih.gov/geo/query/acc.cgi?acc=GSE74043>) for the GASH:Sal arrays.

Further processing, including functional analysis and overrepresentation calculations based on the Gene Ontology (GO) Annotation Tool and published data from the Database for Annotation, Visualization, and Integrated Discovery, was performed using GeneSpring GX 7.3 and DAVID Bioinformatics Resources 6.7 (<http://david.abcc.ncifcrf.gov/>) [34].

2.6. Transcriptome of the inferior colliculus, RNASeq library generation, sequencing, and bioinformatic analysis

The analysis was performed using 15 biological samples of the left or right IC, which were obtained from male GASH:Sal and control hamsters (HdsHan®:AURA). Specifically, 8 IC samples were obtained from the controls (4 from the left and 4 from the right IC), and 7 IC samples were obtained from GASH:Sal (4 from the left and 3 from the right IC).

The pool of isolated and precipitated RNAs was generated using 3 samples from each animal type, taking 1 µg of RNA from each animal, and 3 µg of the pooled RNA was used for the creation of RNASeq libraries using the TruSeq RNA Sample Prep Kit v2 (Illumina) after the removal of rRNA. Both obtained libraries were validated using the 2100 Agilent Bioanalyzer and were quantified via RT-qPCR analysis.

Sequencing of both libraries was conducted using an Ilx genome analyzer (Illumina) using the single read format, and the sequences that did not meet the purity criteria in the software were discarded. Quality values were associated with a value of 30 or greater on the Phred scale (0–40) for 25066143 reads PF (pass filter) considering a medium length

of 76 bp from the controls and 27848979 reads PF considering the same medium length from GASH:Sal.

After quality control, normalization of the libraries, and detection of no significant deviation between the differential expression and the average expression, we began analyzing the great quantity of data obtained. One of the most interesting means of analysis is the examination of the table containing all of the information about the differentially expressed genes. This information not only provides the biological processes, molecular functions, cellular components, and phenotypes associated with many genes according to their annotation but also describes whether the genes are upregulated or downregulated $|FC|$ and whether the results from a statistical perspective were significant (*p* value).

The data obtained and discussed in this publication have also been deposited in the NCBI BioProject at accession number 230618.

2.7. Quantitative reverse transcription real-time PCR (RT-qPCR)

Total RNA (2 µg), reacted with oligo-dT and random hexamer primers, was reverse transcribed into cDNA at 37 °C for 2 h using the First Strand cDNA Synthesis Kit (Promega Corporation, Madison, WI, USA). In all cases, a reverse transcriptase negative control was used to test genomic DNA contamination.

Quantitative RT-qPCR was performed using the SYBR Green method with a $2 \times$ Master Mix (Applied Biosystems). Each reaction contained 10 µl of Master Mix, 0.4 µl of each pair of primers, 3 µl of each cDNA sample in a different serial cDNA quantity for each gene, and MilliQ water up to 20 µl. The amplification reaction was performed in an ABI Prism 7000 detection system (Applied Biosystems) under the following conditions: 10 min at 95 °C followed by 40 cycles of 15 s at 95 °C and 1 min at 60 °C depending on each pair of primers. Quantitative reverse transcription real-time PCR experiments were performed in replicates of 3 to 8 samples and conducted in triplicate for each gene product examined. The list of primers used is provided in Table 2. β-actin was used as the housekeeping gene.

To choose the most stable genes as internal references for RT-qPCR data normalization, two candidates [β -actin and glyceraldehyde 3-phosphate dehydrogenase (*Gapdh*)] were selected according to their expression levels detected in the microarray studied. The expression of these two genes was also measured by RT-qPCR. NormFinder software [35] was used to calculate the intra- and intergroup variations in gene expression. Our results indicated that β -actin is the most stable gene, whereas *Gapdh* is less stable (data not shown). Thus, the mean threshold cycle (*Ct*) value and primer efficiency value of β -actin were used for normalization.

The comparative *Ct* method was used for presenting quantitative data [36]. Following the removal of outliers [37], raw fluorescence data were used to determine the PCR amplification efficiency (E) according to the formula $E = [10^{(-1/\text{slope})} - 1] * 100$. All amplifications had an E value of $100 \pm 10\%$, and an E value near 100% indicated efficient amplification. The relative gene expression value (FC) for each transcript was calculated according to the formula $2^{-(\Delta Ct \text{ "condition 1"} - \Delta Ct \text{ "condition 2"})}$, where "condition 1" corresponds to the experimental sample, "condition 2" to the sample from the control animal, and ΔCt of each "condition" is $Ct_{\text{experimental gene}} - Ct_{\text{endogenous gene}}$ [36]. The standard error for each relative gene expression value was calculated as a measure of data variation. The significance of the qPCR analysis results was determined using a one-tailed *t*-test for each gene, considering $|FC| > 1$ as significant ($p < 0.05$).

2.8. Immunostaining

The control animals and the animals exposed to auditory stimulation of both species were euthanized with pentobarbital (60 mg/kg) and perfused transcardially with 0.9% saline wash solution followed by 4% paraformaldehyde fixative solution (Table 1). The time between audio-genic stimulation and sacrifice was 60 min. After the fixative perfusion,

Table 2
Oligonucleotide primers employed.

Target protein	GenBank number ^a	Primer forward	cDNA forward ^a	Primer reverse	cDNA reverse ^a	Size of products	E ^b
Egr1	NM_012551.2 <i>Rattus norvegicus</i> XM_005065288.1 <i>Mesocricetus auratus</i> XM_007636101.1 <i>Cricetulus griseus</i>	CAGC(A/G)GCGC(T/C)TTCAATCCCTC	162–181 502–521 265–284	GTTGGTCAGGTGCTCGTAGGG	202–221 542–561 305–324	60	2.04
Egr2	XM_003515916.1 <i>Cricetulus griseus</i> XM_005070807.1 XM_005070806.1 <i>Mesocricetus auratus</i> AB264614.1 <i>Rattus norvegicus</i>	AGGCCCTTGGATCTCCATA	31–50 347–363 559–575 27–46	CAGCTGGACCAGGGTACTG	127–146 443–462 655–674 123–142	116	2.00
Egr3	XM_006252240.1 XM_006252239.1 <i>Rattus norvegicus</i> XM_005071015.1 XM_005071014.1 XM_005071013.1 <i>Mesocricetus auratus</i> XM_003496195.1 <i>Cricetulus griseus</i>	CCACAAGCCCTTCAGTGTC	1198–1217 1019–1038 789–808 955–975 1154–1173 780–799	GTGCGGATGTGAGTGCTGAG	1253–1273 1074–1094 844–860 1010–1026 1209–1225 835–855	75	1.98
Gabra4	XM_008770135.1 <i>Rattus norvegicus</i> XM_003507783.2 XM_007634147.1 XM_007634149.1 XM_007634150.1 <i>Cricetulus griseus</i> XM_005080795.1 XM_005080796.1 XM_005080797.1 <i>Mesocricetus auratus</i>	CACCAT(A/C)AGTCGGAGTGTC	1276–1295 498–517 498–517 441–460 441–460 605–624 441–460 441–460	ATTTCAAAGGGCAGGCATGA	1327–1346 549–568 549–568 492–511 492–511 656–675 492–511 492–511	71	1.98
Gapdh	NM_017008.4 <i>Rattus norvegicus</i> NM_001244854.2 <i>Cricetulus griseus</i>	ACATGCCGCCTGGAGAACCT	805–824 802–821	GCCCAGGATGCCCTTAGTGG	874–894 871–891	90	2.00
β-actin	XM_006248886.1 XM_006248885.1 <i>Rattus norvegicus</i> XM_007648665.1 <i>Cricetulus griseus</i> NM_001281595.1 <i>Mesocricetus auratus</i>	AGCCATGTACGTAGCCATCC	240–259 415–434 489–506 390–407	ACCCTCATAGATGGCACAG	335–354 510–529 584–602 485–503	115	2.03

^a The primer location in the corresponding GenBank sequences of rat and hamster origin is indicated.

^b qPCR primer efficiency (E) was calculated according to the following equation: E = 10^(-1/slope).

the brains were removed from the skulls and cryoprotected for 48 h at 4 °C in 30% sucrose in phosphate buffer (PB). Coronal brain sections at 40-μm thickness were generated using a freezing sliding microtome. All sections were processed for immunohistochemistry using similar procedures to those used in our previous studies of rats [24] and hamsters [23]. Briefly, the sections were washed and incubated in a rabbit anti-EGR3 primary antibody solution (1:500, #HPA006206, Sigma-Aldrich) diluted in TBS (Tris-buffered saline) for 24 h at 4 °C. The tissue was then washed and incubated with a goat biotinylated secondary antibody anti-rabbit (1:200, #BA-1000, Vector Labs) for 2 h at room temperature and finally visualized with the avidin–biotin–peroxidase complex procedure (Vectastain, Vector Labs) and histochemistry for peroxidase without heavy metal intensification. For each brain, all sections were mounted on slides, dehydrated, and coverslipped. Brain specimens taken from control animals, as well as from WAR and GASH:Sal animals, were processed simultaneously using the same batch of solutions and incubation times in order to minimize the variability in the visualization of immunoreactivity and DAB reaction product. For immunolocalization of markers in the lymphoma-derived tissue samples, the fixed tissues were processed in a commercial histological processor (Technicon, Assens Llofriu, Madrid, Spain), and the resulting paraffin blocks were cut into 3-μm sections. We used a Bond Polymer Refine Detection system (DS9800, Vision BioSystems, Newcastle, UK) (Leica Bond III), which included a polymeric horseradish peroxidase (HRP)-linked antibody for the detection of the secondary antibody,

according to the instructions of the manufacturer using the same concentration as cited above.

The primary antibody used was anti-Egr3 (1:500, #HPA006206, Sigma-Aldrich), a polyclonal antibody generated in rabbits against the recombinant early growth response 3 protein epitope signature tag (PrEST) (see details in the manufacturer's technical information).

Negative controls were not treated with primary antibodies, and this resulted in the complete absence of immunolabeling.

The histological sections were thoroughly examined under a microscope (DMLB, Leica), and images were captured using a digital camera (DP50, Olympus) adapted to the microscope.

3. Results

3.1. Microarray analysis

3.1.1. Gene expression arrays of the IC in the control vs. GASH:Sal hamsters after acoustic stimulation

From the full list of genetic analyses obtained from the MoGene 1.0 ST expression arrays of all samples, the analysis of sound-stimulated control hamsters and GASH:Sal was composed of 28,814 entries (26,293 of which were identifiable). The differences between the stimulated controls and stimulated GASH:Sal were analyzed. We identified a total of 82 genes that changed in expression when comparing stimulated controls to stimulated GASH:Sal (see complete list of differentially

expressed genes in Supplemental File 1). Of these 82 genes, we specifically identified 15 genes showing significant fold change ($|FC| \geq 1.5$) differences in gene expression. Thus, we found upregulation of 10 genes and downregulation of 5 genes in the stimulated GASH:Sal compared to stimulated control hamsters.

No relationships at the metabolic, structural, or functional level among the 15 genes were observed. Most of the genes were transcription factors (early growth response 2 [*Egr2*], early growth response 3 [*Egr3*], neuronal PAS domain protein 4 [*Npas4*], RAS protein-specific guanine nucleotide-releasing factor 2 [*Rasgrf2*], sterile alpha motif domain-containing 9-like [*Samd9l*]), some of which were related to signaling pathways associated with Rho or Ras proteins (*Rasgrf2*, *Samd9l*). There were also genes related to calcium ion metabolism (ATPase, Ca^{++} transporting, ubiquitous [*Atp2a3*], triadin [*Trdn*]), epigenesis (jumonji, AT-rich interactive domain 1D [*Jarid1d*]), ubiquitously transcribed tetratricopeptide repeat gene, Y chromosome [*Uty*]), translation processes (prostaglandin E synthase 3 (cytosolic)-like [*Ptges3l*]), or several biological processes (ADP-ribosylation factor-like 15 [*Arl15*], calcyclin-binding protein [*Cacybp*], cyclic nucleotide-binding domain-containing 1 [*Cnbd1*]). Interestingly, two of the genes encode transcription factors that belong to the family of early growth response genes, *Egr2* and

Egr3. The Gene Ontology (GO) annotations related to those genes include sequence-specific DNA binding transcription factor activity and transcription regulatory region DNA binding.

The functional analysis and overrepresentation calculations based on the GO Annotation Tool are shown in Fig. 1A.

3.1.2. Gene expression arrays of the IC in the Wistar vs. WAR rats after acoustic stimulation

Analysis of the differential expression between samples of the IC from stimulated Wistar and WAR rats provided a list of 297 genes. We reduced that list by choosing the most representative genes according to a cutoff absolute fold change of 2 or greater ($|FC| \geq 2$).

Comparative analysis of the microarray results between sound-stimulated Wistar and WAR rats showed that the genomic profile of these animals was significantly affected (displaying a $|FC| \geq 2$ and $p < 0.05$) in 39 upregulated genes and 32 downregulated genes.

To enhance the biological interpretation of the differentially expressed genes from our microarray studies, we determined whether any of the biological processes or molecular functions were overrepresented among the differentially expressed genes. The functional interpretation of the experimental data in the rat microarrays was performed using the GO

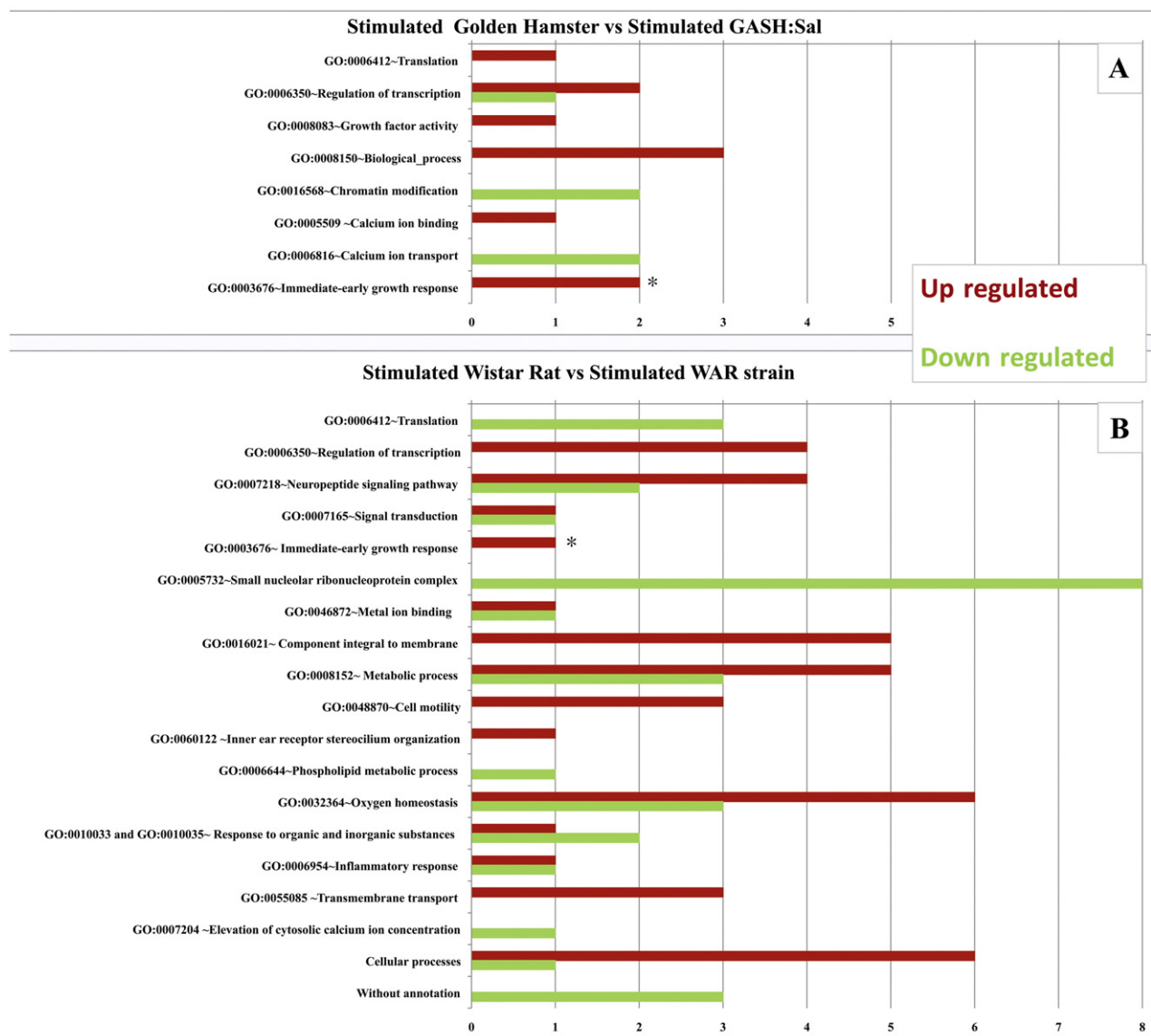


Fig. 1. Functional analysis of the genes in the most representative functional categories based on the Gene Ontology (GO) annotation. The bar graph shows the number of genes up- and downregulated in the IC after sound stimulation in the GASH:Sal (A) and WAR (B) models relative to their respective controls subjected to the same experimental conditions.

annotations (Fig. 1B). Our results indicated that although there were many overrepresented biological function categories, the majority of genes were related to a few function categories. We found certain functions that only corresponded to upregulated genes and other functions that corresponded to only downregulated genes or both up- and downregulated genes (Fig. 1B). In our study, the most relevant function categories included genes involved in responses to different stimuli (epoxide hydrolase 2, cytoplasmic [*Ephx2*], regulator of G-protein signaling 2 [*Rgs2*], regulator of G-protein signaling 5 [*Rgs5*], succinate receptor 1 [*Sucnr1*]), oxygen homeostasis (ATP-binding cassette, subfamily B (MDR/TAP), member 1 [*Abcb1a*], lecithin–cholesterol acyltransferase [*Lcat*], farnesyl diphosphate synthetase [*Fdps*]), metabolic process (DOPA decarboxylase [*Ddc*], phospholysine phosphohistidine inorganic pyrophosphate phosphatase [*Lhpp*]), phosphoribosyl pyrophosphate synthetase 1 [*Prps1*], transthyretin [*Ttr*]), translation process (60S ribosomal protein L12 [*LOC499782*]), transcription factors (nitric oxide synthase trafficking [*Nostrin*]), polymerase (RNA) III (DNA-directed) polypeptide K [*Polr3k*], SCAN domain-containing 1 [*Scand1*], U2 spliceosomal RNA [*U2*]), neuropeptide signaling pathway (EGF, latrophilin and seven transmembrane domain-containing protein 1 precursor [*ADGRF5*]), adhesion G-protein-coupled receptor F5 [*Gpr116*], G-protein-coupled receptor 126 gene [*Gpr126*]), 5-hydroxytryptamine receptor 3A [*Htr3a*], neuropeptide Y precursor [*NPY*], tachykinin, precursor 1 [*Tac1*]), calcium metabolism (mitochondrial fission 1 protein [*Fis1*]), and immediate-early growth response (*Egr3*), among other categories (Fig. 1B). Supplemental File 1 shows the complete list of differentially expressed genes.

The comparison between the gene expression profiles of the two seizure animal models using the microarray data showed only one common gene, the *Egr3*, which was upregulated in both cases.

3.2. Quantitative reverse transcription real-time PCR

We performed RT-qPCR analyses to validate the data obtained in the microarrays of the IC corresponding to the sound-stimulated audiogenic strains and their sound-stimulated controls. This included the overexpression of the *Egr3* in the experimental samples compared to the controls for both microarrays used in the present study. Moreover, we checked the expression of other deregulated genes in our microarrays and those belonging to the *Egr* family (*Egr1* and *Egr2*). The results of this set of experiments are shown in Fig. 2 and Table 3.

The three early growth response genes *Egr1*, *Egr2*, and *Egr3* were significantly overexpressed in both stimulated GASH:Sal and WAR compared to their respective stimulated controls (Fig. 2A and B). The value of *Egr3* and *Egr2* expression between stimulated Wistar and WAR rats was extraordinarily high (Fig. 2B), 10 fold higher than that observed for the comparison between stimulated control and GASH:Sal hamsters (Fig. 2A).

Furthermore, we determined the effect of sound stimulation in the IC gene expression, analyzing the expression of the *Egr* genes in the two strains with or without auditory stimulation by RT-qPCR. Thus, the gene expression of the IC in the baseline controls was compared with that in the sound-stimulated audiogenic strains (Fig. 2C and D).

The comparison of gene expression between nonstimulated GASH:Sal and stimulated GASH:Sal indicated that the expression of the three *Egr* genes was significantly higher in the stimulated GASH:Sal (100 fold higher than in the nonstimulated GASH:Sal) (Fig. 2C).

By comparing the nonstimulated WAR with the stimulated WAR, we found that the three *Egr* genes were significantly overexpressed in the stimulated WAR (Fig. 2D). The *Egr1* and *Egr3* expression results were similar to those found in the comparison of the GASH:Sal; alternatively,

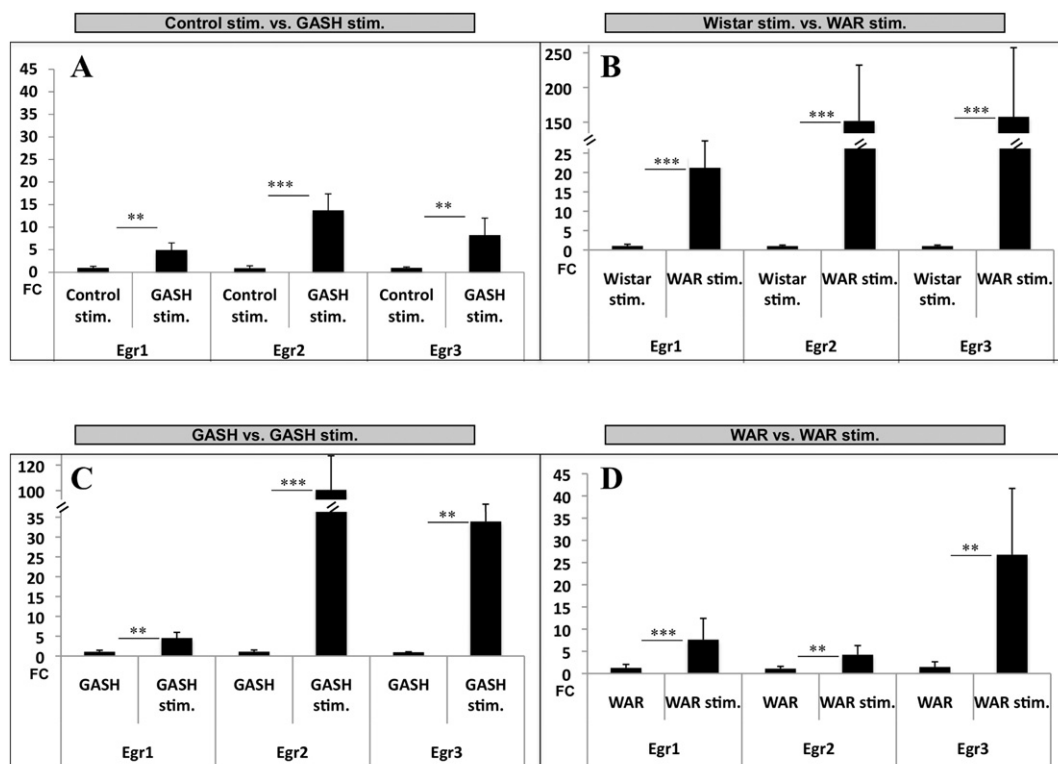


Fig. 2. The fold changes in *Egr* transcript expression in the IC of GASH:Sal and WAR models and their respective controls were measured via RT-qPCR. The expression of the three *Egr* genes was significantly increased in both audiogenic seizure models in comparison to their respective stimulated controls and in comparison with their basal levels. Error bars indicate hemistandard deviation (SD). The housekeeping gene used was β -actin. All the RT-qPCR primers are described in Table 1. Significant differences are indicated as $p < 0.01$ (**) or $p < 0.001$ (***)�. Abbreviation: FC, fold change (relative mRNA levels).

Table 3

The fold changes in GABRA4 transcript expression in the IC of the GASH:Sal and WAR models and their respective controls were measured via RT-qPCR. In red, upregulated; in green, downregulated. The housekeeping gene used was β -actin. All the RT-qPCR primers are described in Table 1. The significant differences are indicated as $p < 0.001$ (**); NS, not significant ($p > 0.05$).

Gene description	Gene symbol	Control stim. vs. GASH stim.		RT-qPCR <i>p</i> value	GASH vs. GASH stim.		RT-qPCR <i>p</i> value		
		RT-qPCR			RT-qPCR				
		Control stim.	GASH stim.		GASH	GASH stim.			
Gamma-aminobutyric acid (GABA) A receptor α 4 subunit	GABRA4	1.02 ± 0.27	0.79 ± 0.20	NS	1.10 ± 0.39	0.94 ± 0.24	NS		
Gene description	Gene symbol	Wistar stim. vs. WAR stim.		RT-qPCR <i>p</i> value	WAR vs. WAR stim.		RT-qPCR <i>p</i> value		
		RT-qPCR			RT-qPCR				
		Wistar stim.	WAR stim.		WAR	WAR stim.			
Gamma-aminobutyric acid (GABA) A receptor α 4 subunit	GABRA4	1.01 ± 0.19	4.56 ± 1.29	< 0.001 (***)	1.13 ± 0.70	1.42 ± 0.89	NS		

Egr2 expression was slightly higher in the stimulated WAR than in the nonstimulated WAR, although not to the extent observed in GASH:Sal.

Finally, we performed RT-qPCR analysis on other genes related to the function of the *Egr3*, such as the gene encoding the gamma-aminobutyric acid (GABA) A receptor, alpha 4 (*GABRA4*), despite not having been detected as deregulated in our microarray analysis. In our study, the expression of the gene encoding the alpha 4 subunit of GABA receptor was not significantly changed in the IC of the GASH:Sal under any of the conditions studied (Fig. 2A and C). Alternatively, *GABRA4* expression was significantly different in the IC of the sound-stimulated WAR compared to the sound-stimulated controls (Table 3).

3.3. Immunohistochemistry

Since *Egr3* was upregulated in the IC of both audiogenic strains, we studied the distribution of the *Egr3* protein in the nervous system under basal conditions and after sound stimulation. Using immunohistochemistry to detect *Egr3*, we found a similar immunostaining pattern between the two species (Figs. 3 and 4). Early growth response 3 immunopositive neurons were found in the auditory pathway of the stimulated animals and nonstimulated animals. In WAR and GASH:Sal animals, *Egr3* immunolabeled neurons were present in all the three divisions of the IC. The majority of *Egr3* immunolabeled neurons were found in the dorsal and external cortices of the IC, while weakly stained neurons were found in the central nucleus of the IC (Figs. 3 and 4). Also, *Egr3* immunostaining was present in the cochlear nucleus complex (Figs. 3 and 4). Outside the auditory pathway, we found *Egr3* immunoreactivity in the hippocampus (Figs. 3 and 4).

Because of the close relationship between *Egr3* expression and the proliferation of B and T lymphocytes [38], we examined the presence of this protein in lymphoma cells sporadically observed in the colony of GASH:Sal [39]. We found immunoreactivity for the *Egr3* protein in Burkitt-type non-Hodgkin neoplastic lymphoma tissue, which was previously observed in the GASH:Sal [39]. Early growth response 3 immunostaining revealed focal expression in the lymphoid cells localized to the cytoplasm (Fig. 5).

3.4. Transcriptome comparison

We used the mouse probes for the microarray analyses of gene expression in hamsters as the Syrian hamster probes were not currently available. To confirm these results, we employed Chinese hamster

probes (*Cricetulus griseus*) via transcriptomic analysis, comparing the stimulated controls with the stimulated GASH:Sal. The data are available in a database at NCBI under the project number PRJNA230618 (<https://submit.ncbi.nlm.nih.gov/ft/byid/bq7rg36z/gashsubmission.sqn>). Upon using these probes, the number of differentially expressed genes between stimulated GASH:Sal and the stimulated controls was increased. In the present study, we focused only on the results related to the *Egr* genes. The expression values from RT-qPCR and transcriptomic analyses showed significantly increased values of the early expression genes *Egr1*, *Egr2*, and *Egr3*. In the microarray analysis, we found upregulation of the *Egr2* and *Egr3* genes, but we did not detect upregulation of the *Egr1* (Fig. 6).

4. Discussion

Genetic animal models of epilepsy provide important tools for further understanding the basic cellular mechanisms underlying epileptogenesis and identifying new targets for antiepileptic drugs. They are also used to determine the genetic factors that induce seizures to discover molecular mechanisms in common with human epilepsy.

In the present study, using microarrays, we analyzed the changes in gene expression in two strains with audiogenic epilepsy after a seizure event, compared with controls under the same conditions. The comparison of the gene expression profiles between the two animal models using the microarray data showed only one common gene, *Egr3*, which was upregulated in both cases. On the other hand, using RT-qPCR studies, we confirmed the differential expression of this gene and two other early response genes, *Egr1* and *Egr2*, which were also upregulated in both species. Differences between microarray and RT-qPCR data occur for several reasons, including the fact that different probes are used for the microarray and RT-qPCR experiments (which can capture differential expression in splice variants), differences in the methods for normalization of expression data, and possible false-positive expression changes. In addition, lower correlations between RT-qPCR and microarray results were consistently reported for genes exhibiting small degrees of changes [40].

4.1. Methodological considerations

In our study, the time between the induced seizures and the tissue sampling for the RNA study was 60 min. Since it has been reported that the expression of *Egr2* and *Egr3* is dramatically induced 30 min

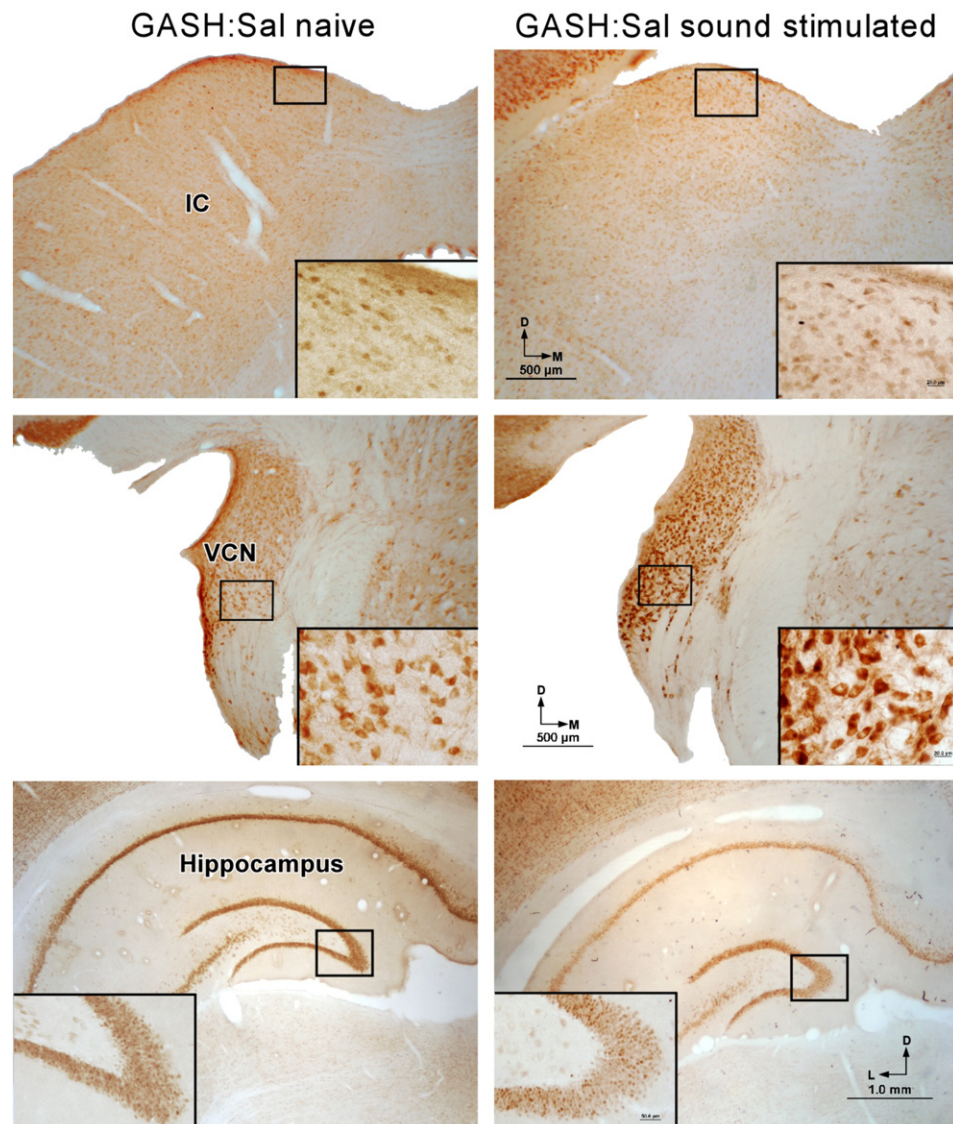


Fig. 3. Coronal sections of GASH:Sal were immunostained to visualize Egr3 protein expression. The inset shows a magnification of the boxed area. Abbreviations: IC, inferior colliculus; VCN, ventral cochlear nucleus.

after the onset of seizures induced by kainic acid [41], we set 60 min as a period of time sufficient to detect *Egr* gene expression. Microarray analysis enables global transcriptomic studies of the changes in gene expression because it enables the simultaneous analysis of thousands of genes in a single experiment. Briefly, after performing the hybridization arrays and after quantitation of the expression level of each probe set in all microarrays, we used a different algorithm to identify probe sets displaying significant differential expression by comparing the samples from audiogenic strains with their respective controls. We selected the genes that varied in a range (fold change) among other genes and used different databases to identify their function. Only genes displaying a $|FC| > 2$ (up- or downregulated) were considered for analysis. For the GASH:Sal, we have chosen a less restrictive criterion, $|FC| > 1.5$, because the probes used were not the most appropriate and did not allow us to detect many changes. Moreover, because a limited number of genes were differentially expressed, few genes fulfilled such a restrictive criterion. On the other hand, we used commercial mouse microarrays to study gene expression in hamsters because the genome of this species has not been described, and therefore, no specific arrays have been developed. Furthermore, it is well known that these two species (*M. auratus* and *Mus musculus*) are phylogenetically very close [42].

Genotyping of *M. auratus* is currently underway at the Broad Institute (NCBI-BioProject accession: PRJNA77669) but is not published yet. Therefore, to confirm the results of our gene expression analysis, we used the cDNA sequences of the Chinese hamster, *C. griseus*, for a comparative analysis of the transcriptomic profiles in the IC from GASH:Sal and control Syrian hamsters, both of which were stimulated with sound. The Chinese hamster genome was recently published [43], and this species displays greater similarity to the Syrian hamster than to the mouse [44].

4.2. Early growth response genes

The *Egr1*, *Egr2*, and *Egr3* genes are immediate-early genes; this term refers to genes whose transcription can be rapidly and transiently induced by a broad range of cellular stimuli (environmental, physiological, and pathological stimuli) [45,46]. These genes encode the EGR family of zinc-finger proteins, which bind to DNA, RNA, or proteins [47,48].

The factors that induce the expression of these genes in mammalian cells include stress [49], which may be induced by chemical and physical external stressors [50] or internal stressors, such as cardiac stress [51], which elevates the *Egr* mRNA level. The increased transcription of *Egr* due to stress occurs in tissues as variant as the adrenal glands [52] and

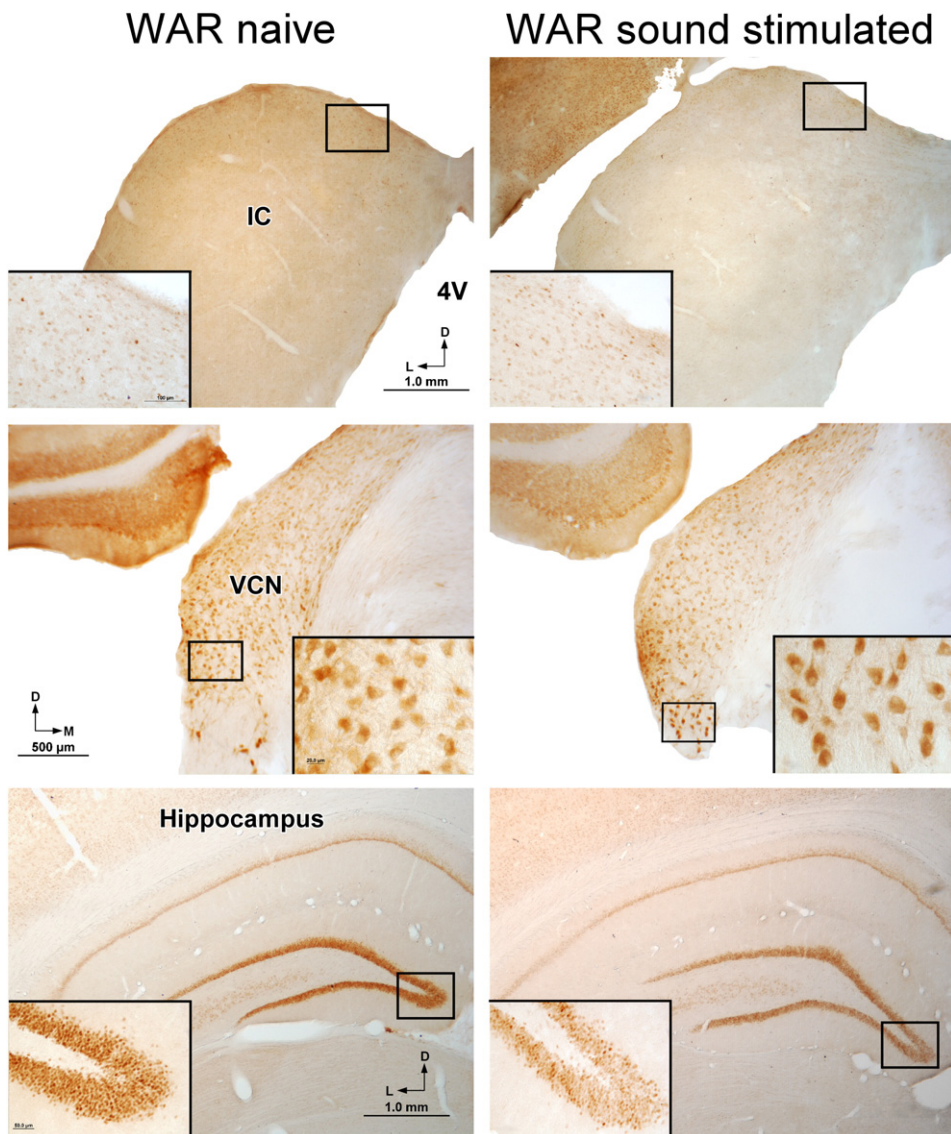


Fig. 4. Coronal sections of WAR were immunostained to visualize Egr3 protein expression. The inset shows a magnification of the boxed area. Abbreviations: 4v, fourth ventricle; IC, inferior colliculus; VCN, ventral cochlear nucleus.

the hippocampus [53]. It has been reported that Egr1 has a clear role in mediating gene expression required for some learning and memory processes [54,55], and Egr3 is associated with neuronal plasticity in response to stress and novelty [56]. In fact, the proteins expressed by the activity-regulated cytoskeletal-related (Arc) gene are directly regulated by Egr1 and Egr3, which can indirectly modulate synaptic plasticity by directly regulating Arc [57].

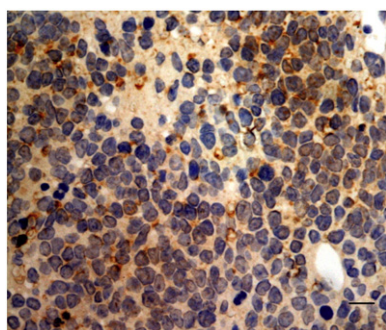


Fig. 5. Egr3 immunopositivity in lymphoid cells of GASH:Sal lymphoma tissue. Scale bar, 10 μ m.

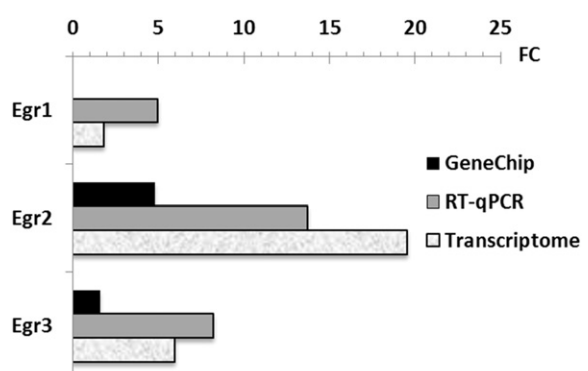


Fig. 6. Confirmation of the results for selected genes at the gene expression level. The fold changes in the expression levels of the three Egr transcripts in the IC of the sound-stimulated GASH:Sal compared to the sound-stimulated Syrian hamster controls were obtained by microarray, RT-qPCR, and transcriptomic analyses. Abbreviations: FC, fold change (relative mRNA levels).

The early growth response genes *Egr1*, *Egr2*, and *Egr3* mediate adaptation to novel stimuli and novelty [58]. This result from our material would explain their presence in the auditory nuclei, where cells respond to the sound. Exposure to novelty resulted in long-term depression (LTD), and *Egr3* has been associated with LTD processes [56], which are also mediated by the serum factor response (SRF) gene [59]; this gene was overexpressed in the GASH:Sal transcriptome (data not shown). Mice knocked out for this gene (*Egr3*^{-/-}) show abnormal adaptation to novelty and stress, deficits in startle habituation, and deficits in synaptic plasticity [56]. Based on immunohistochemistry, we found this protein in the hippocampus of WAR and GASH:Sal, in both animals subjected to auditory stimulation and naïve animals. Although we have not quantified the levels of this protein, it does not appear that its expression is increased in the hippocampus of the stimulated animals, and such a result would support its function. However, because the brains were collected 60 min after audiogenic stimulation, it is possible that insufficient time or number of stimulations was responsible for the inability to detect *Egr3*-immunolabeled differences in the hippocampus.

Different processes that contribute to neuronal hyperexcitability, such as the hyperexcitability produced by ethanol withdrawal [60] and induced seizures [61], resulted in overexpression of these *Egr* genes. Following seizures induced by kainic acid, it was possible to detect the expression pattern of these immediate-early genes (IEGs), especially in the hippocampus, the cortex, and the amygdala [61]. It has been previously reported that the *Egr3* expression is increased in the hippocampus of humans with temporal lobe epilepsy as well as in animal models of temporal lobe epilepsy [62]. On the contrary, Lgi1L385R/+ rats, which showed generalized tonic-clonic seizures in response to acoustic stimuli, have the opposite effect – a downregulation of *Egr2* after sound stimulation [63]. In humans, it has been reported as a common pattern of persistent gene activation in neocortical epileptic foci, including the *Egr1* and the *Egr2* [64] but not the *Egr3*. As far as we know, up to the present, there is no information in the literature regarding the upregulation of these genes and the increment of the corresponding proteins in the IC after the audiogenic seizures in animal models.

Sustained IEG expression might represent either a stress response by which the neurons are trying to protect themselves or an early indicator that these cells are initiating a pathway leading to programmed

cell death. In our case, the overexpression of *Egr3* following stimulation in both the WAR and GASH:Sal models could be explained by the essential role of *Egr3* in regulating gene expression to promote fusimotor innervation homeostasis [65], which changes with increased motor activity, as observed for ictal events. Along these lines, it has recently been reported that *Egr3* is a target of critical cocaine-mediated signaling pathways, which are responsible for the induction of locomotor activity [66].

The early growth response 3 gene has also been associated with changes in *GABRA4* expression after status epilepticus [67]. This gene encodes a subunit of the GABA_A receptor, an ion channel that mediates the majority of inhibition in the central nervous system. Seizure induced transcriptional upregulation of the $\alpha 4$ subunit gene (*GABRA4*) of this receptor [68] may play an important role in the etiology of temporal lobe epilepsy [67]. In our study, we have found this correlation only in the IC of WAR, which displayed upregulation of the *GABRA4* gene after the ictal event but not in that of GASH:Sal. Perhaps, in the latter model of epilepsy, excitotoxic mechanisms were unrelated to modifications of the expression of the $\alpha 4$ subunit of the GABA receptor but rather were related to modifications in the expression of other subunits ($\beta 2$) of this receptor, resulting in its dysfunction [69].

Another feature attributable to *Egr* genes, specifically *Egr3*, is that they play an essential role in the conversion of mitogenic signals by epidermal growth factor into a proliferative response to regulate sympathetic neuronal dendrite morphology and terminal axon branching; these processes are essential for normal sympathetic nervous system development [70]. Together with *Egr2*, *Egr3* performs critical functions in the myelination of the peripheral nervous system (Fig. 7) [71].

These transcription factors (*Egr2* and *Egr3*) are also involved in the control of inflammation [67] and in the proliferation of B and T lymphocytes [38,72,73]. Interestingly, we found immunoreactivity for the *Egr3* protein in Burkitt-type non-Hodgkin neoplastic lymphoma cells, which were previously observed in the GASH:Sal and in human Burkitt-type B lymphoma [39]. Early growth response 3 is also highly overexpressed in other types of cancer, such as prostate cancer [74] or breast cancer [75]. This relationship between *Egr3* and cancer has not been found for other *Egr* genes, for which the opposite relationship was described. For instance, numerous studies have detailed the

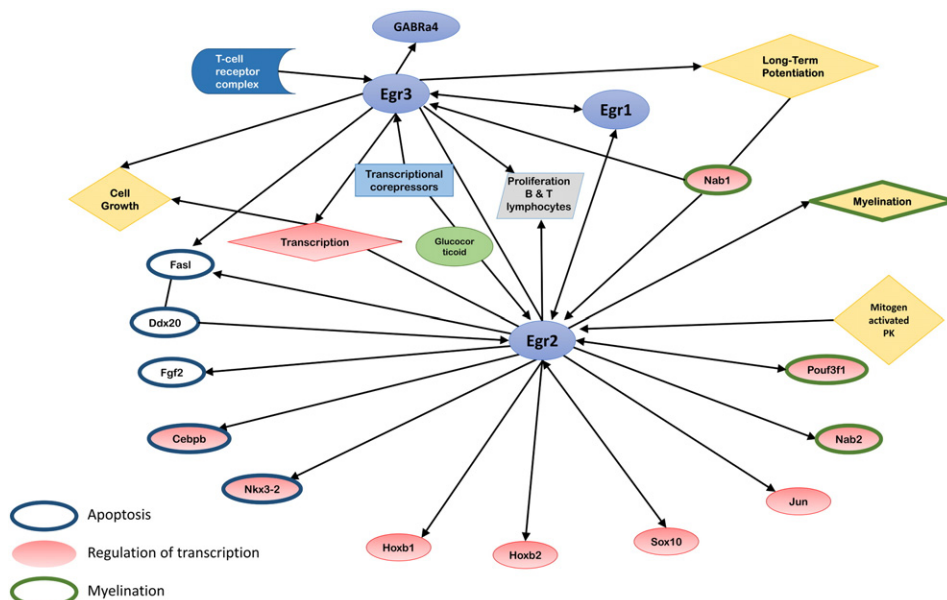


Fig. 7. Schematic relationship between the three *Egr* genes that were upregulated in the inferior colliculus after audiogenic stimulation in the WAR and GASH:Sal audiogenic seizure models. This figure summarizes the relationship between *Egr* genes associated with processes of cell growth, apoptosis, LTD, corticosteroid signaling, myelination, and transcriptional regulatory genes. These interconnections indicate that *Egr* proteins act as nuclear effectors of different signals.

tumor suppressor functions of *Egr1* and, consequently, its downregulation in breast, lung, and glial cancers [76–78]. In the near future, we plan to perform further research to determine whether *Egr3* can serve as a predictive marker of lymphoma and other cancer types.

5. Conclusions

Ictal events in strains susceptible to audiogenic seizures, specifically WAR and GASH:Sal, cause gene deregulation in the IC.

The technical limitations of the microarray analyses require the validation of the microarray data with real-time RT-PCR. The WAR and GASH:Sal exhibited overexpression of the early growth response genes *Egr1*, *Egr2*, and *Egr3*, presumably as an effect of the stress associated with seizures. The overexpression of these genes was higher in the WAR model than in the GASH:Sal model. These genes are transcription factors, and their activation precedes further transcriptional responses related to myelination processes, cell growth, apoptosis, LTD, and activation of transcriptional regulatory genes. Fig. 7 and Supplemental File 2 summarize the relationship between the *Egr* genes that were upregulated after an ictal event in the two models of audiogenic epilepsy studied, as well as their interconnection with other genes and cellular processes.

The present study showed for the first time upregulation of the early growth response genes *Egr1*, *Egr2*, and *Egr3* in the inferior colliculus (an epileptogenic focus) of the WAR and GASH:Sal strains.

Supplementary data to this article can be found online at <http://dx.doi.org/10.1016/j.yebeh.2015.12.020>.

Acknowledgments

This study was supported by the Spanish JCyL (#SA023A12-2), University of Salamanca Research Support Grant 2015 (#P1) (to Dr. Dolores E. López), USP/USAL Program for the Promotion of the Bilateral Cooperation in the Field of Research (#2011.1.23386.1.3), USP/USAL (2011.1.23386.81.3), and FAPESP (07/50261-4) (to Norberto García-Cairasco). Norberto García-Cairasco holds a CNPq research fellowship.

Conflict of interest

The authors declare no conflict of interest.

References

- [1] García-Cairasco N. Puzzling challenges in contemporary neuroscience: insights from complexity and emergence in epileptogenic circuits. *Epilepsy Behav* 2009;14(Suppl. 1):54–63.
- [2] García-Cairasco N. Learning about brain physiology and complexity from the study of the epilepsies. *Braz J Med Biol Res* 2009;42:76–86.
- [3] Tejada J, Costa KM, Beretti P, García-Cairasco N. The epilepsies: complex challenges needing complex solutions. *Epilepsy Behav* 2013;26:212–28.
- [4] Fisher L, Chaban G, Hertz E. Abnormal metabolic response to excess potassium in astrocytes from the Jimpy mouse, a convulsing neurological mutant. *Brain Res* 1980;181:482–7.
- [5] Fisher RS. Animal models of the epilepsies. *Brain Res Rev* 1989;14:245–78.
- [6] Case M, Solesz I. Computational modeling of epilepsy. *Epilepsia* 2011;52:12–5.
- [7] Engel J. Concepts of epilepsy. *Epilepsia* 1995;36(Suppl. 1):S23–9.
- [8] Kandratavicius L, Balista PA, Lopes-Aguilar C, Ruggiero RN, Umeoka EH, García-Cairasco N, et al. Animal models of epilepsy: use and limitations. *Neuropsychiatr Dis Treat* 2014;10:1693–705.
- [9] Serikawa T, Mashimo T, Kuramoto T, Voigt B, Ohno Y, Sasa M. Advances on genetic rat models of epilepsy. *Exp Anim* 2015;64(1):1–17.
- [10] García-Cairasco N, Wakamatsu H, Oliveira JAC, Gomes ELT, Del Bel EA, Mello LEAM. Neuroethological and morphological (Neo-Timm staining) correlates of limbic recruitment during the development of audiogenic kindling in seizure susceptible Wistar rats. *Epilepsia* 1996;26:177–92.
- [11] Doretto MC, Fonseca CG, Lobo RB, Terra VC, Oliveira JA, García-Cairasco N. Quantitative study of the response to genetic selection of the Wistar audiogenic rat strain (WAR). *Behav Genet* 2003;33(1):33–42.
- [12] Carballosa-Gonzalez MM, Muñoz LJ, Sancho C, López-Alburquerque T, Pardal-Fernández MJ, Nava E, et al. EEG characterization of audiogenic seizures in the hamster strain GASH:Sal. *Epilepsy Res* 2013;106:318–25.
- [13] Muñoz LJ, Carballosa-Gautam MM, Yanowsky K, García-Atarés N, López DE. The GASH:Sal. Where do we stand and where we're going. *Epilepsy Behav* 2016 [in press].
- [14] Willott JF, Lu SM. Midbrain pathways of audiogenic seizures in DBA/2 mice. *Exp Neurol* 1980;70(2):288–99.
- [15] Ross KC, Coleman JR. Developmental and genetic audiogenic seizure models: behavior and biological substrates. *Neurosci Biobehav Rev* 2000;24(6):639–53.
- [16] Faingold CL. Emergent properties of CNS neuronal networks as targets for pharmacology: application to anticonvulsant drug action. *Prog Neurobiol* 2004;72(1):55–85.
- [17] García-Cairasco N, Terra VC, Doretto MC. Midbrain substrates of audiogenic seizures in rats. *Behav Brain Res* 1993;58(1–2):57–67.
- [18] García-Cairasco N, Sabbatini RM. Possible interaction between the inferior colliculus and the substantia nigra in audiogenic seizures in Wistar rats. *Physiol Behav* 1991;50(2):421–7.
- [19] Kesner RP. Subcortical mechanisms of audiogenic seizures. *Exp Neurol* 1966;15(2):192–205.
- [20] Wada JA, Terao A, White B, Jung E. Inferior colliculus lesion and audiogenic seizure susceptibility. *Exp Neurol* 1970;28(2):326–32.
- [21] Ross KC, Coleman JR. Audiogenic seizures in the developmentally primed Long-Evans rat. *Dev Psychobiol* 1999;34(4):303–13.
- [22] Barrera-Bailón B, Oliveira JAC, López DE, Muñoz LJ, García-Cairasco N, Sancho C. Pharmacological and neuroethological study of three antiepileptic drugs in the genetic audiogenic seizure hamster (GASH:Sal). *Epilepsy Behav* 2013;28(3):413–25.
- [23] Fuentes-Santamaría V, Cantos R, Alvarado JC, García-Atarés N, López DE. Morphological and neurochemical abnormalities in the auditory brainstem of the genetically epilepsy-prone hamster (GPG/Vall). *Epilepsia* 2005;46(7):1027–46.
- [24] Gómez-Nieto R, Rubio ME, López DE. Cholinergic input from the ventral nucleus of the trapezoid body to cochlear nucleus of the trapezoid to cochlear root neurons in rats. *J Comp Neurol* 2008;506:452–68.
- [25] Irizarry RA, Hobbs B, Collin F, Beazer-Barclay YD, Antonellis KJ, Scherf U, et al. Exploration, normalization, and summaries of high density oligonucleotide array probe level data. *Biostatistics* 2003;4(2):249–64.
- [26] Li C, Wong WH. Model-based analysis of oligonucleotide arrays: expression index computation and outlier detection. *Proc Natl Acad Sci U S A* 2001;98(1):31–6.
- [27] Bolstad BM, Irizarry RA, Astrand M, Speed TP. A comparison of normalization methods for high density oligonucleotide array data based on variance and bias. *Bioinformatics* 2003;19(2):185–93.
- [28] Irizarry RA, Bolstad BM, Collin F, Cope LM, Hobbs B, Speed TP. Summaries of Affymetrix GeneChip probe level data. *Nucleic Acids Res* 2003;31(4):e15.
- [29] Barash Y, Dehan E, Krupsky M, Franklin W, Geraci M, Friedman N, et al. Comparative analysis of algorithms for signal quantitation from oligonucleotide microarrays. *Bioinformatics* 2004;20(6):839–46.
- [30] Tusher VG, Tibshirani R, Chu G. Significance analysis of microarrays applied to the ionizing radiation response. *Proc Natl Acad Sci U S A* 2001;98(9):5116–21.
- [31] Benjamini Y, Draai D, Elmer G, Kalfaki N, Golani I. Controlling the false discovery rate in behavior genetics research. *Behav Brain Res* 2001;125(1–2):279–84.
- [32] Storey JD, Tibshirani R. Statistical significance for genome wide studies. *Proc Natl Acad Sci U S A* 2003;100(16):9440–5.
- [33] Edgar R, Domrachev M, Lash AE. Gene Expression Omnibus: NCBI gene expression and hybridization array data repository. *Nucleic Acids Res* 2002;30:207–10.
- [34] Huang da W, Sherman BT, Lempicki RA. Systematic and integrative analysis of large gene lists using DAVID bioinformatics resources. *Nat Protoc* 2009;4(1):44–57.
- [35] Andersen CL, Jensen JL, Orntoft TF. Normalization of real-time quantitative reverse transcription-PCR data: a model-based variance estimation approach to identify genes suited for normalization, applied to bladder and colon cancer data sets. *Cancer Res* 2004;64(15):5245–50.
- [36] Schmittgen TD, Livak KJ. Analyzing real-time PCR data by the comparative CT method. *Nat Protoc* 2008;3(6):1101–8.
- [37] Burns MJ, Nixon CJ, Foy CA, Harris N. Standardisation of data from real-time quantitative PCR methods – evaluation of outliers and comparison of calibration curves. *BMC Biotechnol* 2005;5:31.
- [38] Li S, Miao T, Sebastian M, Bhullar P, Ghaffari E, Liu M, et al. The transcription factors *Egr2* and *Egr3* are essential for the control of inflammation and antigen-induced proliferation of B and T cells. *Immunity* 2012;37(4):685–96.
- [39] Muñoz LJ, Ludeña D, Gedvilaitė A, Zvirbliene A, Jandrig B, Voronkova T, et al. Lymphoma outbreak in the hamster GASH:Sal strain. *Arch Virol* 2013;150:2255–65.
- [40] Morey JS, Ryan JC, Van Dolah FM. Microarray validation: factors influencing correlation between oligonucleotide microarrays and real-time PCR. *Biol Proced Online* 2006;8:175–93.
- [41] Honkanen J, Sharp FR. Prolonged expression of zinc finger immediate-early gene mRNAs and decreased protein synthesis following kainic acid induced seizures. *J Neurosci* 1999;19(1):10–7.
- [42] Fabre PH, Hautier L, Dimitar Dimitrov D, Douzery EJP. A glimpse on the pattern of rodent diversification: a phylogenetic approach. *BMC Evol Biol* 2012;12:88.
- [43] Lewis NE, Liu X, Li Y, Nagarajan H, Yerganian G, O'Brien E, et al. Genomic landscapes of Chinese hamster ovary cell lines as revealed by the *Cricetulus griseus* draft genome. *Nat Biotechnol* 2013;31(8):759–65.
- [44] Tchitchek N, Safronetz D, Rasmussen AL, Martens C, Virtaneva K, Porcella SF, et al. Sequencing, annotation and analysis of the Syrian hamster (*Mesocricetus auratus*) transcriptome. *PLoS One* 2014;9(11):e112617.
- [45] Beckmann MA, Wilce PA. *Egr* transcription factors in the nervous system. *Neurochem Int* 1997;31:477–510.
- [46] Patwardhan S, Gashler A, Siegel MG, Chang LC, Joseph LJ, Shows TB, et al. EGR3, a novel member of the *Egr* family of genes encoding immediate-early transcription factors. *Oncogene* 1991;6:917–28.

- [47] Crosby SD, Puetz JJ, Simburger KS, Fahrner TJ, Milbrandt J. The early response gene NGFI-C encodes a zinc finger transcriptional activator and is a member of the GCGGGGCG (GSG) element-binding protein family. *Mol Cell Biol* 1991;11:3835–41.
- [48] O'Donovan KJ, Tourtellotte WG, Millbrandt J, Baraban JM. The EGR family of transcription-regulatory factors: progress at the interface of molecular and systems neuroscience. *Trends Neurosci* 1999;22:167–73.
- [49] Senba E, Ueyama T. Stress-induced expression of immediate early genes in the brain and peripheral organs of the rat. *Neurosci Res* 1997;29(3):183–207.
- [50] Ronkina N, Menon MB, Schwermann J, Arthur JSC, Legault H, Telliez J-B, et al. Stress induced gene expression: a direct role for MAPKAP kinases in transcriptional activation of immediate early genes. *Nucleic Acids Res* 2011;39(7):2503–18.
- [51] Shieh JTC, Huang Y, Gilmore J, Srivastava D. Elevated miR-499 levels blunt the cardiac stress response. *PLoS One* 2011;6(5):e19481.
- [52] Honkanen J, Zhang JS, Longo FM, Sharp FR. Stress induces zinc finger immediate early genes in the rat adrenal gland. *Brain Res* 2000;877(2):203–8.
- [53] Honkanen J, States BA, Weinstein PR, Espinoza J, Sharp FR. Global ischemia induces immediate early genes encoding zinc finger transcription factors. *J Cereb Blood Flow Metab* 1997;17:636–46.
- [54] Abraham WC, Dragunow M, Tate WP. The role of immediate early genes in the stabilization of long-term potentiation. *Mol Neurobiol* 1991;5:297–314.
- [55] Worley PF, Bhat RV, Baraban JM, Erickson CA, McNaughton BL, Barnes CA. Thresholds for synaptic activation of transcription factors in hippocampus: correlation with long-term enhancement. *J Neurosci* 1993;13:4776–86.
- [56] Gallitano-Mendel A, Izumi Y, Tokuda K, Zorumski CF, Howell MP, Muglia LJ, et al. The immediate early gene early growth response gene 3 mediates adaptation to stress and novelty. *Neuroscience* 2007;148:633–43.
- [57] Li L, Carter J, Gao X, Whitehead J, Tourtellotte WG. The neuroplasticity-associated arc gene is a direct transcriptional target of early growth response (Egr) transcription factors. *Mol Cell Biol* 2005;25(23):10286–300.
- [58] Poirier R, Cheval H, Mailhes C, Garel S, Charnay P, Davis S, et al. Distinct functions of Egr gene family members in cognitive processes. *Front Neurosci* 2008;2(1):47–55.
- [59] Lindecke A, Korte M, Zagrebelsky M, Horejschi V, Elvers M, Widera D, et al. Long-term depression activates transcription of immediate early transcription factor genes: involvement of serum response factor. *Eur J Neurosci* 2006;24:555–63.
- [60] Beckmann AM, Matsumoto I, Wilce PA. AP-1 and Egr DNA-binding activities are increased in rat brain during ethanol withdrawal. *J Neurochem* 1997;69(I):306–14.
- [61] Honkanen J, Sharp FR. Prolonged expression of zinc finger immediate-early gene mRNAs and decreased protein synthesis following kainic acid induced seizures. *Eur J Neurosci* 1999;11(1):10–7.
- [62] Roberts DS, Hu Y, Lund IV, Brooks-Kayal AR, Russek SJ. Brain-derived neurotrophic factor (BDNF)-induced synthesis of early growth response factor 3 (Egr3) controls the levels of type A GABA receptor α 4 subunits in hippocampal neurons. *J Biol Chem* 2006;281(40):29431–5.
- [63] Fumoto N, Mashimo T, Masui A, Ishida S, Mizuguchi Y, Minamimoto S, et al. Evaluation of seizure foci and genes in the Lgi1(L385R/+) mutant rat. *Neurosci Res* 2014;80:69–75.
- [64] Rakhae SN, Yao B, Ahmed S, Asano E, Beaumont TL, Shah AK, et al. A common pattern of persistent gene activation in human neocortical epileptic foci. *Ann Neurol* 2005;58:736–47.
- [65] Fernandes OM, Tourtellotte WG. Egr3-dependent muscle spindle stretch receptor intrafusal muscle fiber differentiation and fusimotor innervation homeostasis. *J Neurosci* 2015;35(14):5566–78.
- [66] Chandra R, Francis TC, Konkalmatt P, Amgalan A, Gancarz AM, Dietz DM, et al. Opposing role for Egr3 in nucleus accumbens cell subtypes in cocaine action. *J Neurosci* 2015;35(20):7927–37.
- [67] Grabenstatter HL, Russek SJ, Brooks-Kayal AR. Molecular pathways controlling inhibitory receptor expression. *Epilepsia* 2012;53(Suppl. 9):71–8.
- [68] Roberts DS, Raol YH, Bandyopadhyay S, Lund IV, Budreck EC, Passini MJ, et al. Egr3 stimulation of GABRA4 promoter activity as a mechanism for seizure-induced upregulation of GABA_A receptor α 4 subunit expression. *Proc Natl Acad Sci U S A* 2005;102(33):11894–9.
- [69] Prieto-Martín AI, Aroca-Aguilar JD, Sánchez-Sánchez F, Muñoz LJ, López DE, Escrivano J, et al. Molecular and neurochemical substrates of the audiogenic seizure strains: the GASH:Sal model. *Epilepsy Behav* 2017;71:218–25.
- [70] Quach DH, Oliveira-Fernandes M, Gruner KA, Tourtellotte WG. A sympathetic neuron autonomous role for Egr3-mediated gene regulation in dendrite morphogenesis and target tissue innervation. *J Neurosci* 2013;33(10):4570–83.
- [71] Tourtellotte WG, Milbrandt J. Sensory ataxia and muscle spindle agenesis in mice lacking the transcription factor Egr3. *Nat Genet* 1998;20:87–91.
- [72] Sumitomo S, Fujio K, Okamura T, Yamamoto K. Egr2 and Egr3 are the unique regulators for systemic autoimmunity. *JAKSTAT* 2013;2(2), e23952.
- [73] Lazarevic V, Zullo AJ, Schweitzer MN, Staton TL, Gallo EM, Crabtree GR, et al. The gene encoding early growth response 2, a target of the transcription factor NFAT, is required for the development and maturation of natural killer T cells. *Nat Immunol* 2009;10:306–13.
- [74] Pio R, Jia Z, Baron VT, Mercola D. Early growth response 3 (Egr3) is highly overexpressed in non-relapsing prostate cancer but not in relapsing prostate cancer. *PLoS One* 2013;8(1):e54096.
- [75] Inoue A, Omoto Y, Yamaguchi Y, Kiyama R, Hayashi SI. Transcription factor EGR3 is involved in the estrogen-signaling pathway in breast cancer cells. *J Mol Endocrinol* 2004;32:649–61.
- [76] Levin WJ, Casey G, Ramos JC, Arboleda MJ, Reissmann PT, Slamon DJ. Tumor suppressor and immediate early transcription factor genes in non-small cell lung cancer. *Chest* 1994;106:372S–6S.
- [77] Huang RP, Liu C, Fan Y, Mercola D, Adamson ED. Egr-1 negatively regulates human tumor cell growth via the DNA-binding domain. *Cancer Res* 1995;55:5054–62.
- [78] Calogero A, Arcella A, De Gregorio G, Porcellini A, Mercola D, Liu C, et al. The early growth response gene EGR-1 behaves as a suppressor gene that is down-regulated independent of ARF/Mdm2 but not p53 alterations in fresh human gliomas. *Clin Cancer Res* 2001;7:2788–96.